EXPERIMENTAL STUDY OF A MILLER CYCLE BASED APPROACH FOR AN EFFICIENT BOOSTED DOWNSIZED GASOLINE DI ENGINE

A thesis submitted for the degree of
Doctor of Philosophy

by

Yuanping Li

Department of Mechanical, Aerospace and Civil Engineering
College of Engineering, Design and Physical Sciences
Brunel University London
United Kingdom

September 2017

Abstract

Driven by the strict fuel consumption and CO_2 legislations in Europe and many countries, various technologies have been developed to improve the fuel economy of conventional internal combustion engines. Gasoline engine downsizing has become a popular and effective approach to reduce fleet CO_2 emissions of passenger cars. This is typically achieved in the form of boosted direct injection gasoline engines equipped with variable valve timing devices. Downsized gasoline engines reduce vehicle fuel consumption by making engine operate more at higher load to reduce pumping losses and also through reducing total engine friction losses. However, their compression ratio (CR) and efficiency are constrained by knocking combustion as well as the low speed pre-ignition phenomena. Miller cycle is typically achieved in an engine with reduced effective CR through Early Intake Valve Closure (EIVC) or Later Intake Valve Closure (LIVC). This technology has been adopted on modern gasoline engines to reduce in-cylinder charge temperature and enable a higher geometric CR to be used for better fuel economy.

The present work investigated the effectiveness and underlying process of a Miller cycle based approach for improving fuel consumption of a boosted downsized gasoline engine. A single cylinder direct injection gasoline engine and the testing facilities were set up and used for extensive engine experiments. Both EIVC and LIVC approaches were tested and compared to the conventional Otto cycle operation with a standard cam profile. Synergy between Miller cycle valve timings and different valve overlap period was analysed. Two pistons with different CRs were used in the Miller cycle engine testing to enable its full potential to be evaluated. The experimental study was carried out in a large engine operation area from idle to up to 4000rpm and 25.6bar NIMEP to determine the optimal Miller cycle strategy for improved engine fuel economy in real applications. In addition, the increased exhaust back pressure and friction losses corresponding to real world boosting devices were calculated to evaluate Miller cycle benefits at high loads in a production engine. The results have shown that EIVC combined with high CR can offer up to 11% reduction of fuel consumption in a downsized gasoline engine with simple setup and control strategy. At the end, this thesis presents an Miller cycle based approach for maximising fuel conversion efficiency of a gasoline engine by combining three-stage cam profiles switching and two-stage variable compression ratio.

Acknowledgements

First of all, I would like to express my deep gratitude to my supervisor, Professor Hua Zhao, for granting me the fully funded position to study in the great engine research group at Brunel University London, and also for his invaluable guidance on my research and learning, and for all the help given to make my life easier during these years.

I would like to acknowledge MAHLE Powertrain UK for all the support provided to this work. Particularly I am grateful to Mr Paul Freeland, Mr Dave OudeNijeweme and Dr Phil Stansfield for share of experience and knowledge and the warm help; and to Mr Tony Cains and Mr Justin Mape for their excellent technical supports on EMS system and engine rebuild.

I am thankful to my friends and colleagues in the group. Thanks to Dr Yan Zhang for lots of valuable help on both my study and life. Thanks to Dr Jun Ma, Dr Pin Lu, Dr Quan Liu and Mr Wei Guan for their friendship and help. Thanks to Mr Reza Golzari for his support and company in engine testing. Thanks to Mr Andy Selway, Mr Kenneth Anistiss, Mr Eamon Wyse and Mr Christopher Allan for their expertise and assistance to support the research work.

I also would like to thank all other friends met here for their company, help and encouragement. The life is much more joyful here thanks to all of you.

I am grateful to Ms Jady Wang and Professor Jianguo Lin for the peaceful and lovely place of accommodation and kindness in looking after my wife and me.

Finally, my most sincere gratitude goes to my family - my mother, my grandfather, my two sisters and brothers in law, for their endless and selfless love, encourage and support, which are the most important resources and powerful backing for me to pursue better life.

At the end of writing the thesis, particularly and most important, I must express my gratitude to my wife Ms Ming Wang - without your unconditional love and support and your endeavour, it would be not possible for me to overcome the difficulties and complete the study. Also thank my new born daughter Mira - you did so well and made so less trouble during my writing and your smile is the best gift spiriting me up.

Nomenclature

ABDC	After Bottom Dead Center
AFR	Air Fuel Ratio
ATDCF	After Firing Top Dead Center
ATDCNF	After Non-firing Top Dead Center
barA	Absolute Pressure in bar
BBDC	Before Bottom Dead Center
BDC	Bottom Dead Center
BLD	Borderline of Detonation
BSFC	Brake Specific Fuel Consumption
BTDCF	Before Firing Top Dead Center
BTDCNF	Before Non-firing Top Dead Center
CA10	Crank Angle at 10% Mass Fraction of Fuel Burnt
CA50	Crank Angle at 50% Mass Fraction of Fuel Burnt
CA90	Crank Angle at 90% Mass Fraction of Fuel Burnt
CAI	Controlled Auto-Ignition
cc	Cubic Centimetre
CO	Carbon Monoxide
CO2	Carbon Dioxide
COV	Coefficient of Variation
CPS	Cam Profile Switching
CR	Compression Ratio
CVVL	Continuously Variable Valve Timing and Lift
DAQ	Data Acquisition

dCA	Crank Angle Degree
degC (°C)	Celsius Temperature Degree
DI	Direct Injection
EBP	Exhaust Back Pressure
ECR	Effective Compression Ratio
ECU	Engine Control Unit
EGR	Exhaust Gas Re-circulation
EIVC	Early Intake Valve Closing
EMOP	Exhaust Cam Maximum Opening Point Timing
EMS	Engine Management System
EOI	End of Injection
EOI 2nd Injection	EOI of DI 2nd Injection
EOI2ndInj-spk	Gap between DI 2nd Injection and Spark
EVC	Exhaust Valve Closing at 0.5mm Lift
EVO	Exhaust Valve Opening at 0.5mm Lift
FMEP	Friction Mean Effective Pressure
FSN	Filter Smoke Number
GIMEP	Gross Indicated Mean Effective Pressure
GIMEP COV	Coefficient of Variation of GIMEP
GIMEP LNV	Lowest Normalized Value of GIMEP
GIMEP SD	Standard Deviation of GIMEP
HC	Total Hydrocarbon
HCCI	Homogeneous Charge Compression Ignition
HCR	High Compression Ratio
IEA	International Energy Agency

IEffg	Gross Indicated Fuel Conversion Efficiency
IEffn	Net Indicated Fuel Conversion Efficiency
IEffp	Pumping Indicated Fuel Conversion Efficiency
IMOP	Intake Cam Maximum Opening Point Timing
ISFCn	Net Indicated Specific Fuel Consumption
IVC	Intake Valve Closing at 0.5mm Lift
IVO	Intake Valve Opening at 0.5mm Lift
kPaA	Absolute Pressure in kPa
LCR	Low Compression Ratio
LHV	Low Heat Value
LIVC	Late Intake Valve Closing
LP	Low Pressure
LSPI	Low Speed Pre-Ignition
MCR	Miller Cycle Ratio
Misfire	Misfired Cycles with GIMEP LNV ≤ 0
MOP	Maximum Opening Point
NA	Naturally Aspirated
NEDC	New European Driving Cycle
NIMEP	Net Indicated Mean Effective Pressure
NOx	Nitrogen Oxides
OECD	Organisation for Economic Co-operation and Development
PFI	Port Fuel Injection
PM	Particle Mass
Pmax	Peak Cylinder Pressure
PMEP	Pumping Mean Effective Pressure

PN	Particle Number
ppm	Parts per Million
PRT	Platinum Resistance Thermometer
PW 2nd Injection	Pulsewidth of DI 2nd Injection
RDE	Real Driving Emission
RGF	Residual Gas Fraction
RON	Research Octane Number
rpm	Revolutions per Minute
Scavenging Pressure	Intake Port Absolute Pressure - Exhaust Port Absolute Pressure
SI	Spark Ignition
SOI	Start of Injection
Spark-CA10	Duration between Spark Timing and CA10
Std	Standard
TDC	Top Dead Center
TDCF	Firing (combustion) Top Dead Center
TDCNF	Non-firing (gas exchange) Top Dead Center
TGDI	Turbocharged Gasoline Direct Injection
TKE	Turbulence Kinetic Energy
TOR	Top of Ramp
UEGO	Universal Exhaust Gas Oxygen
UI	User Interface
VCR	Variable Compression Ratio
VCT/VCP	Variable Cam Timing/Phasing
Vol	Volume (Volumetric)
Vs	Engine Displacement Volume

VVL	Variable Valve Lift
VVT	Variable Valve Timing
WLTP/WLTC	World Harmonized Light Vehicle Test Procedure / Cycle
50% Partial Burn	Partial Burn Cycles with GIMEP LNV ≤ 50%

Contents

Abstract i

Acknowledgements ii

Nomenclature iii

List of Figures xi

List of Tables xvi

Chapter 1 Introduction 2

1.1 Introduction 2

1.2 Project Objectives 3

1.3 Thesis Outline 4

Chapter 2 Literature Review 6

2.1 Introduction 6

2.2 Technologies to Reduce Vehicle CO_2 9

2.3 Internal Combustion Engine Fuel Energy Conversion and Efficiency 10

2.4 Technologies for Improving Gasoline Engine Fuel Economy 15

2.4.1 Gasoline Direct Injection 15

2.4.2 Stratified Lean Combustion 15

2.4.3 CAI and HCCI 16

2.4.4 Gasoline DI Engines with Variable Cam Timing and Boosting (Downsizing) 17

2.4.5 Variable Valve Actuation and Air Intake 19

2.4.6 Variable Compression Ratio 20

2.4.7 Water Injection 21

2.4.8 Exhaust Gas Recirculation 21

2.5 Miller Cycle Technology Development and Application 22

2.5.1 Origin and Terminology 22

2.5.2 Development and Application of Miller Cycle for Passenger Car Gasoline Engines 23

2.6 Summary 39

Chapter 3 Experimental Setup and Methodology 42

3.1 Introduction 42

3.2 Research Design and Methodology 42

3.2.1 Details of Cam Profiles, Valve Timings and Effective Compression Ratios 44

3.2.2 Steady State Operation Points for Engine Testing 46

3.3 Single Cylinder Engine Testbed 47
3.3.1 Single Cylinder Engine 49
3.3.2 Oil System 50
3.3.3 Coolant System 51
3.3.4 Fuel System 52
3.3.5 Exhaust System 53
3.3.6 Intake System 55
3.4 Engine Management System 56
3.5 Data Acquisition System 57
3.5.1 DAQ Hardware 57
3.5.2 DAQ Software (Combustion Analyser) 59
3.5.3 TDC Determination 62
3.5.4 Pegging 64
3.6 Test Operation and Data Quality 65
3.6.1 Validation of Cam Timings 66
3.6.2 Validation of Indicate Pressure and Fuel Flow Measurements 66
3.6.3 Daily Checks 67
3.7 Summary 69
Chapter 4 Synergy between Boosting and Valve Timings with Miller Cycle Operation ... 71
4.1 Introduction 71
4.2 Overview of Optimised Valve Timings and Fuel Consumption Improvement 71
4.3 Impact of Exhaust Valve Timing 77
4.4 Impact of Valve Timings at Idle Operation 78
4.5 Impact of Valve Timings at Low Load Operation 85
4.6 Impact of Valve Timings at Mid Load Operation 95
4.7 Impact of Valve Timings at High Load Operation 107
4.8 Summary 118
Chapter 5 Synergy between High Compression Ratio and Miller Cycle Operation 122
5.1 Introduction 122
5.2 Overview of Optimised Valve Timings 122
5.3 Impact of High Compression Ratio with Standard Intake Cam 126
5.4 Impact of High Compression Ratio with LIVC Intake Cam 129
5.5 Impact of High Compression Ratio with EIVC Intake Cam 132
5.6 Comparison among Three Intake Cams at High Compression Ratio 135

5.7 Fuel Economy Improvement by combining Miller Cycle and High CR 137
5.8 Summary 139
Chapter 6 Injection Optimisation for Miller Cycle Operation 142
6.1 Introduction 142
6.2 Impact of Split Injection on Engine Fuel Consumption at Low Load 142
6.3 Impact of Split Injection on Engine Fuel Consumption at High Load 146
6.4 Impact of Split Injection on Engine Fuel Consumption at Full Load 150
6.5 Fuel Consumption Reduction through Split Injection 154
6.6 Lambda Strategy for Low Speed High Load Operation 156
6.7 Summary 157
Chapter 7 Impact of Boost Device on Miller Cycle Application 159
7.1 Introduction 159
7.2 Exhaust Back Pressure Impacts at High Load 159
7.3 Exhaust Back Pressure Impacts at Full Load 162
7.4 Compare ISFCn of Hardware Options at Equivalent EBP Condition 166
7.5 Impact of Supercharger Work Consumption 168
7.6 Systematic Balance for Miller Cycle Application 170
7.7 Fuel Consumption Benefits through Miller Cycle with CPS and VCR 171
7.8 Summary 172
Chapter 8 Conclusions and Recommendation for Future Work 175
8.1 Conclusions 175
8.2 Strategies for Miller Cycle Application and Potential Benefit 177
8.3 Recommendations for Future Work 178
References 179
Appendix 194
A.1 Fuel Flow Meter Validation 194

List of Figures

Figure 2.1 Toxic Emissions Standards for Passenger Cars [2] 6

Figure 2.2 Reduction of HC + NOx on Passenger Cars from Euro 0 to Euro 4 [4] 7

Figure 2.3 CO2 Emissions by Source [5] 8

Figure 2.4 Historical Fleet CO2 Emissions Performance and Current Standards (gCO2/km normalized to NEDC) for Passenger Cars [6] 9

Figure 2.5 WardsAuto Annual Survey: Technologies to Help Meet 2025 CAFE Standards [9] 10

Figure 2.6 Fuel Energy Conversion Process and Efficiencies in Internal Combustion Engines 11

Figure 2.7 BSFC Contour Map of a Turbocharged Gasoline DI Engine 13

Figure 2.8 Gasoline Direct Injection with Engine Boost (Source: Frost & Sullivan) [38] 18

Figure 3.1 Schematic of Engine Hardware and Controls Employed in the Research 42

Figure 3.2 LCR Piston (left) and HCR Piston (right) 43

Figure 3.3 Exhaust and Intake Cam Profiles and Phasing 44

Figure 3.4 IVC, IVC to BDC, Effective CR, MCR and Valve Overlap vs IMOP 46

Figure 3.5 Single Cylinder Engine Test Points and Engine Operation Area 47

Figure 3.6 Schematic of Single Cylinder Engine Testbed Setup 48

Figure 3.7 Single Cylinder Gasoline DI Engine on Testbed 50

Figure 3.8 Endress+Hauser Coriolis Mass Flow Meter 53

Figure 3.9 Kistler 4005BA10FA0 Piezoresistive Absolute Pressure Sensor 54

Figure 3.10 MAHLE Flexible ECU 56

Figure 3.11 DAQ Cards 58

Figure 3.12 Kistler 6041B Piezoelectric Pressure Transducer 59

Figure 3.13 Transient Combustion Analyser UI 60

Figure 3.14 p-V Diagrams of a Four-Stroke SI Engine [164] 61

Figure 3.15 Indicated Work and Fuel Conversion Efficiencies 62

Figure 3.16 Kistler 2629C TDC Sensor System 63

Figure 3.17 TDC Determination for Combustion Analyser TDC Setup 63

Figure 3.18 Log P-V Diagram from Engine Motoring 64

Figure 3.19 Cylinder Pressure Pegging (two examples) 65

Figure 3.20 Endress+Hauser Promass 83A01 DN01 Measurement Error 67

Figure 3.21 Track of Daily Motoring Logs (an example) 69

Figure 4.1 Optimised Cam Timings at Low CR 73

Figure 4.2 Valve Overlap, Scavenging Pressure and Miller Cycle Ratio at Optimised Cam Timings 74

Figure 4.3 ISFCn Improvement of LIVC / EIVC Cam compared to Standard Cam at Low CR 75

Figure 4.4 Differences between Indicated Efficiencies of LIVC / EIVC Cam and these of Standard Cam at Low CR 76

Figure 4.5 Cam Envelope Logs at Ten Test Points with Three Intake Cams 77

Figure 4.6 Exhaust Cam Timing Sweep and Related Cylinder Pressure Curve at 2000rpm 4.6bar 78

Figure 4.7 Cam Envelope Logs at 800rpm 2.0bar NIMEP with Three Intake Cams 79

Figure 4.8 Cam Envelope Results at 800rpm 2.0bar NIMEP with LCR LIVC Cam 80

Figure 4.9 Cam Envelope Results at 800rpm 2.0bar NIMEP with LCR EIVC Cam 82

Figure 4.10 Cam Envelope Results at 800rpm 2.0bar NIMEP with LCR Standard Cam 83

Figure 4.11 Comparison of the Optimised Results of Three Intake Cams at 800rpm 2.0bar NIMEP 84

Figure 4.12 P-V Diagrams of Three Intake Cams at 800rpm 2.0bar NIMEP with Optimised Cam Timings 85

Figure 4.13 Cam Envelope Results at 2000rpm 4.6bar NIMEP with LCR LIVC Cam 86

Figure 4.14 Contributions to IEffg at 2000rpm 4.6bar NIMEP with LCR LIVC Cam 87

Figure 4.15 Cam Envelope Results at 2000rpm 4.6bar NIMEP with LCR EIVC Cam 89

Figure 4.16 Contributions to IEffg at 2000rpm 4.6bar NIMEP with LCR EIVC Cam 90

Figure 4.17 Cam Envelope Results at 2000rpm 4.6bar NIMEP with LCR Standard Cam 91

Figure 4.18 Contributions to IEffg at 2000rpm 4.6bar NIMEP with LCR Standard Cam 92

Figure 4.19 P-V Diagrams of Three Intake Cams at 2000rpm 4.6bar NIMEP with Optimised Cam Timings 93

Figure 4.20 Gas Exchange Process of Three Intake Cams at 2000rpm 4.6bar NIMEP with Optimised Cam Timings 94

Figure 4.21 Comparison of the Optimised Results of Three Intake Cams at Low Load 95

Figure 4.22 Cam Envelope Results at 2000rpm 8.9bar NIMEP with LCR LIVC Cam 96
Figure 4.23 Contributions to IEffg at 2000rpm 8.9bar NIMEP with LCR LIVC Cam 97
Figure 4.24 Cam Envelope Results at 2000rpm 8.9bar NIMEP with LCR Standard Cam 98
Figure 4.25 Contributions to IEffg at 2000rpm 8.9bar NIMEP with LCR Standard Cam 99
Figure 4.26 Cam Envelope Results at 2000rpm 8.9bar NIMEP with LCR EIVC Cam 101
Figure 4.27 Contributions to IEffg at 2000rpm 8.9bar NIMEP with LCR EIVC Cam 102
Figure 4.28 Gas Exchange Process of Three Intake Cams at 2000rpm 8.9bar NIMEP with Maximum Valve Overlap 103
Figure 4.29 Gas Exchange Process of Three Intake Cams at 2000rpm 8.9bar NIMEP with Optimised Cam Timings 104
Figure 4.30 P-V Diagrams of Three Intake Cams at 2000rpm 8.9bar NIMEP with Optimised Cam Timings 105
Figure 4.31 Comparisons of the Optimised Results of Three Intake Cams at Mid Load 106
Figure 4.32 Cam Envelope Results at 2000rpm 16.0bar NIMEP with LCR LIVC Cam 108
Figure 4.33 Contributions to IEffg at 2000rpm 16.0bar NIMEP with LCR LIVC Cam 109
Figure 4.34 Cam Envelope Results at 2000rpm 16.0bar NIMEP with LCR Standard Cam 110
Figure 4.35 Scavenging Pressure and Volumetric Efficiency Changes along Cam Timing Envelope at 2000rpm 16.0bar NIMEP with LCR Standard Cam 111
Figure 4.36 Cam Envelope Results at 2000rpm 16.0bar NIMEP with LCR EIVC Cam 112
Figure 4.37 Contributions to IEffg at 2000rpm 16.0bar NIMEP with LCR EIVC Cam 113
Figure 4.38 Comparison of the Optimised Results of Three Intake Cams at 2000rpm 114
Figure 4.39 Entire P-V Diagrams of Three Intake Cams at 2000rpm 25.6bar NIMEP with Optimised Cam Timings 116
Figure 4.40 Low Pressure Loop in P-V Diagrams of Three Intake Cams at 2000rpm 25.6bar NIMEP with Optimised Cam Timings 117
Figure 4.41 Gas Exchange Process of Three Intake Cams at 2000rpm 25.6bar NIMEP with Optimised Cam Timings 118
Figure 5.1 Optimised Exhaust Cam Timings at Low CR vs at High CR 123

Figure 5.2 Optimised Intake Cam Timings at Low CR vs at High CR 124
Figure 5.3 Cam Envelope Results at 2000rpm 25.6bar NIMEP with HCR EIVC Cam 125
Figure 5.4 Differences of Indicated Efficiencies between HCR and LCR with Standard Cam 126
Figure 5.5 Comparison of Intake Pressure between HCR and LCR with Standard Cam 127
Figure 5.6 Comparisons of Spark Timing, Combustion Duration and Timing between HCR and LCR with Standard Cam 128
Figure 5.7 Differences of Indicated Efficiencies between HCR and LCR with LIVC Cam 129
Figure 5.8 Comparison of Intake Pressure between HCR and LCR with LIVC Cam 130
Figure 5.9 Comparisons of Spark Timing, Combustion Duration and Timing between HCR and LCR with LIVC Cam 131
Figure 5.10 Differences of Indicated Efficiencies between HCR and LCR with EIVC Cam 132
Figure 5.11 Comparison of Intake Pressure between HCR and LCR with EIVC Cam 133
Figure 5.12 Comparisons of Spark Timing, Combustion Duration and Timing between HCR and LCR with EIVC Cam 134
Figure 5.13 Differences between Indicated Efficiencies of LIVC / EIVC Cam and these of Standard Cam at High CR 136
Figure 5.14 ISFCn Improvement of LIVC / EIVC Cam with HCR compared to Standard Cam with LCR (baseline) 137
Figure 5.15 ISFCn Improvement of LIVC-EIVC Cam Switching with HCR compared to Standard Cam with LCR (baseline) 139
Figure 6.1 Split Injection Test Results with LCR LIVC Cam at 2000rpm 4.6bar NIMEP 143
Figure 6.2 Split Injection Test Results with LCR EIVC Cam at 2000rpm 4.6bar NIMEP 144
Figure 6.3 Split Injection Test Results with HCR EIVC Cam at 2000rpm 4.6bar NIMEP 146
Figure 6.4 Split Injection Test Results with LCR LIVC Cam at 2000rpm 16.0bar NIMEP 147
Figure 6.5 Split Injection Test Results with LCR EIVC Cam at 2000rpm 16.0bar NIMEP 148
Figure 6.6 Split Injection Test Results with HCR EIVC Cam at 2000rpm 16.0bar NIMEP 149
Figure 6.7 Split Injection Test Results with LCR LIVC Cam at 2000rpm 25.6bar NIMEP 151

Figure 6.8 Split Injection Test Results with LCR EIVC Cam at 2000rpm 25.6bar NIMEP 152

Figure 6.9 Split Injection Test Results with HCR EIVC Cam at 2000rpm 25.6bar NIMEP 153

Figure 6.10 ISFCn Improvement Achieved by Split Injection Compared to Single Injection at Different Load and Hardware 155

Figure 6.11 ISFCn Improvement of LIVC-EIVC Cam Switching with Split Injection and HCR compared to Standard Cam with LCR (baseline) 155

Figure 6.12 Exhaust Lambda Sweep at 2000rpm 16.0bar NIMEP with LCR EIVC Cam 156

Figure 7.1 EBP Sweep Test Results at 2000rpm 16.0bar NIMEP with LCR and Three Intake Cams 160

Figure 7.2 EBP Sweep Test Results at 2000rpm 16.0bar NIMEP with Standard and EIVC Cams at Different CRs 162

Figure 7.3 EBP Sweep Test Results at 2000rpm 25.6bar NIMEP with LCR and Three Intake Cams 163

Figure 7.4 EBP Sweep Pressure Traces at 2000rpm 25.6bar NIMEP with LCR and Three Intake Cams (arrows indicating increase of EBP) 164

Figure 7.5 EBP Sweep Test Results at 2000rpm 25.6bar NIMEP with Standard and EIVC Cams at Different CRs 166

Figure 7.6 ISFCn Comparison at Equivalent EBP Conditions 167

Figure 7.7 ISFCn and Corrected BSFC Comparison at 2000rpm 16.0bar NIMEP 169

Figure 7.8 ISFCn and Corrected BSFC Comparison at 2000rpm 25.6bar NIMEP 169

Figure 7.9 Factors Affecting Fuel Consumption of a Miller Cycle Engine 171

Figure 7.10 Maximise Efficiency of a Gasoline Engine through Miller Cycle Approach Combining CPS and VCR Technologies 172

Figure A.1 Flow Meter Measurement Linearity Check 195

List of Tables

Table 2.1 EU Emission Standards for Passenger Cars (Category M1*) [3] 7
Table 2.2 Key Aspects for Improving Gasoline Engine Efficiency 12
Table 2.3 Reasons for BSFC Increases in a Gasoline Engine Operation Map 14
Table 3.1 Exhaust and Intake Cam Specifications and Phasing 44
Table 3.2 Technical Specifications of the Test Engine 49
Table 3.3 ECU Inputs and Outputs Used 57
Table 3.4 High Speed Channels 58
Table 3.5 Test Operation and Boundary Conditions 65
Table 3.6 Test Conditions for Daily Checks 68
Table A.1 Flow Meter Measurement Compared to the Laboratory Scale 194

Chapter One

Introduction

Chapter 1 Introduction

1.1 Introduction

Automotive transportation has been changing the daily human life and the whole world. Usage of automobiles makes people's travel much easier hence extends the range of their movement, promotes the communication among different regions in the human-being society and widens people's vision and thoughts. Production and consumption of automotive products have become an essential part and sign of a country's industry and economy. However, in addition to these positive influences, mass utilisation of automobiles also brings some issues to the planet. The most critical one is the damage to environment. Pollutants like NOx, HC, CO and particulates from the emissions of cars, trucks, trains and ships are directly harmful to human health. Increased total CO_2 quantity due to human activity is contributing to the so-called "greenhouse effect" raising the global temperature and causing climate change. CO_2 produced by modern transport tools accounts for a considerable fraction of increase in CO_2 level. In order to protect the environment, many countries and areas have established strict regulations to limit the poisonous emissions and also the greenhouse gas CO_2 from automobiles.

Internal combustion engines are the main power source for modern transportation especially on passenger cars, light duty vehicles and trucks. Diesel engines and gasoline engines are the two main types of internal combustion engines used for the road transport. Gasoline engines have lower overall fuel conversion efficiency than diesel engines due to the part load pumping losses, lower compression ratio (CR) and relatively richer air fuel ratio. However gasoline engines remain the dominant propulsion unit for passenger cars in the world because of their higher power density, less complexity and cost, relatively simple exhaust after-treatment system. Therefore, improving fuel economy of gasoline engines plays a very important role in reduction of total CO_2 emission. As a result, many advanced technologies have been developed and applied on modern gasoline engines. Among them gasoline engine downsizing especially combined with fuel direct injection (DI) was already established as a proven technology to reduce fleet fuel consumption of passenger cars. However the downsizing level and CR on these engines are limited by irregular combustion phenomena mainly knocking and low speed pre-ignition, which

deteriorates the fuel economy benefits of this approach in the real world. There are many different technologies, which could be applied on downsized gasoline engines in order to improve their efficiency. One is to adopt the Miller cycle using shifted valve timing to reduce throttling losses in part load operation and reduce effective CR and consequent charge temperature at higher loads to optimise combustion phasing and enable a higher geometric CR.

In this work, the Miller cycle was achieved on a boosted highly downsized gasoline DI engine equipped with dual cam phasers. Miller cycle operating with Early Intake Valve Closing (EIVC), Late Intake Valve Closing (LIVC) cam profiles and optimised cam timings at low / high geometric CRs were investigated based on experimental studies carried out in a large engine speed and load area. Engine fuel conversion efficiencies were compared among different Miller cycle approaches and as well to the baseline engine configuration with low CR and standard cam profile. Impacts of injection strategy, exhaust back pressure (EBP) and friction loss of mechanical supercharger were also studied.

1.2 Project Objectives

The aim of the project is to investigate a Miller cycle based approach for improving fuel conversion efficiency on a boosted highly downsized gasoline DI engine. The best engine hardware structure and the optimal strategy need to be explored, with the potential of fuel consumption reduction to be assessed. The following aspects are considered and planned to ensure the objectives to be achieved:

(1) The single cylinder engine and its testing facility are set up and operated to allow precise control and accurate results to be obtained;

(2) Miller cycle via both LIVC and EIVC cams are tested and compared to the standard camshaft. LIVC cam features a long opening duration and standard valve lift and the EIVC cam has a short opening duration and low valve lift;

(3) Through independent intake and exhaust cam phasers, synergy between Miller cycle tended valve timings and different valve overlap periods is to be analysed;

(4) Both the normal CR and high CR are employed for Miller cycle operating to enable a full understanding of fuel economy benefits of this technical approach;

(5) A large engine operation area including high speed, full load and idle is tested supported by the high speed single cylinder crankcase and a high power boosting rig, which allows the optimisation of Miller cycle strategy to cover main operation regions that determine the engine overall fuel economy;

(6) Impact of potentially increased EBP and friction losses on automotive boosting systems are investigated and analysed, allowing the real world benefits of Miller cycle to be evaluated.

1.3 Thesis Outline

Following this introduction, Chapter-Two gives a review of literature related to this work, mainly the current development and application of Miller cycle on passenger car gasoline engines. In Chapter-Three, the experimental setup, methodology and test facilities are described in detail. This includes the single cylinder engine, dynamometer, fluids supply and conditioning systems, exhaust and intake systems, the external boosting rig and the data acquisition system. Chapter-Four presents the experimental results and findings through comparing EIVC, LIVC and standard cam profiles at optimised cam timings, low CR and ambient EBP conditions, while the impacts of swapping to high CR are discussed in Chapter-Five. Chapter-Six investigates split injection strategy and lean exhaust lambda and their effects on Miller cycle operation. The influences of increased EBP and friction losses related to real world boosting systems on Miller cycle engine fuel economy is discussed in Chapter-Seven. At the end, Chapter-Eight includes the conclusion and recommendation for future work.

Chapter Two

Literature Review

Chapter 2 Literature Review

2.1 Introduction

The performance and emissions of internal combustion engines have been improved greatly in the last two decades, which are mainly driven by the legislations establishing mandatory limits on pollutant emissions and CO_2 or fuel consumption of vehicles.

The history of emission standards can date back to the 1960s when California in the United States began to pursue a "technology-forcing" approach in setting up motor vehicle tailpipe emission standards [1]. From then related governmental agencies and emission regulations for environmental protection have been established in all main countries and regions worldwide. Figure 2.1 shows the timeline of toxic emissions standards of passenger cars in the main areas as for automotive manufacturing and also the markets [2]. The evolution of emission regulations includes the decrease in limits on toxic compositions in exhaust gas and upgrade of test cycles.

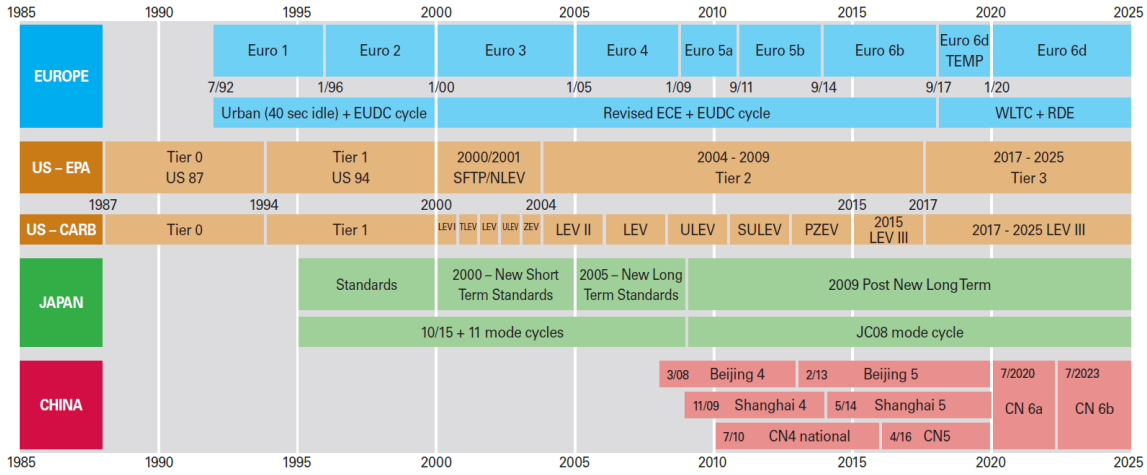

Figure 2.1 Toxic Emissions Standards for Passenger Cars [2]

In case of European emission regulations, they have been upgraded to the 6th stage in September 2014 since the 1st stage Euro emission standard was launched in July 1992. As shown in Table 2.1 [3], limits on all emission components have been reduced substantially. Limit on Particle Mass (PM) has been applied for gasoline engines from Euro 5. New limits on Particle Number (PN) have been brought in for diesel engine since

Euro 5b and also for gasoline engines in Euro 6 stage. The World Harmonized Light Vehicle Test Procedure / Cycle (WLTP/WLTC) and Real Driving Emission (RDE) test procedure have been developed to replace the New European Driving Cycle (NEDC) gradually from September 2017.

Table 2.1 EU Emission Standards for Passenger Cars (Category M_1*) [3]

Stage	Date	CO	HC	HC+NOx	NOx	PM	PN
		g/km					*#/km*
Compression Ignition (Diesel)							
Euro 1†	1992.07	2.72 (3.16)	-	0.97 (1.13)	-	0.14 (0.18)	-
Euro 2, IDI	1996.01	1.0	-	0.7	-	0.08	-
Euro 2, DI	1996.01[a]	1.0	-	0.9	-	0.10	-
Euro 3	2000.01	0.64	-	0.56	0.50	0.05	-
Euro 4	2005.01	0.50	-	0.30	0.25	0.025	-
Euro 5a	2009.09[b]	0.50	-	0.23	0.18	0.005[f]	-
Euro 5b	2011.09[c]	0.50	-	0.23	0.18	0.005[f]	6.0×10^{11}
Euro 6	2014.09	0.50	-	0.17	0.08	0.005[f]	6.0×10^{11}
Positive Ignition (Gasoline)							
Euro 1†	1992.07	2.72 (3.16)	-	0.97 (1.13)	-	-	-
Euro 2	1996.01	2.2	-	0.5	-	-	-
Euro 3	2000.01	2.30	0.20	-	0.15	-	-
Euro 4	2005.01	1.0	0.10	-	0.08	-	-
Euro 5	2009.09[b]	1.0	0.10[d]	-	0.06	0.005[e,f]	-
Euro 6	2014.09	1.0	0.10[d]	-	0.06	0.005[e,f]	6.0×10^{11} e,g

* At the Euro 1..4 stages, passenger vehicles > 2,500 kg were type approved as Category N_1 vehicles
† Values in brackets are conformity of production (COP) limits
a. until 1999.09.30 (after that date DI engines must meet the IDI limits)
b. 2011.01 for all models
c. 2013.01 for all models
d. and NMHC = 0.068 g/km
e. applicable only to vehicles using DI engines
f. 0.0045 g/km using the PMP measurement procedure
g. 6.0×10^{12} 1/km within first three years from Euro 6 effective dates

The establishment and evolution of emission standards was believed to significantly reduce vehicle tailpipe emissions as shown in Figure 2.2 [4]. In the meantime it promoted the development of new technologies like electronic control, fuel injection technology, combustion systems and aftertreatment devices.

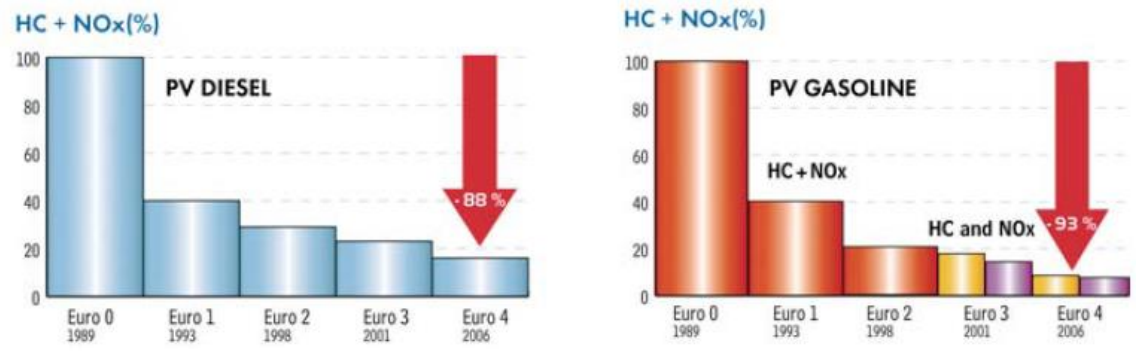

Figure 2.2 Reduction of HC + NOx on Passenger Cars from Euro 0 to Euro 4 [4]

Attention is increasingly turning to CO_2 emission in the last decade since it is widely agreed that the raised levels of CO_2 due mainly to human activity are contributing to the so-called "greenhouse effect", which has been raising the global temperatures and affecting climate [4]. CO_2 produced by cars undeniably accounts for a large fraction of CO_2 emissions generated by human, as shown in Figure 2.3 [5] which reveals the CO_2 emission sources in year 2015 in the UK. CO_2 in car exhaust comes from the complete burn of carbon-based fuels and there is no aftertreatment can be attached to a vehicle to filter it out. The most effective way to reduce CO_2 from cars is to use less fuel or change the fuel resource, which is the aim to introduce the CO_2 emission standards or fuel economy standards.

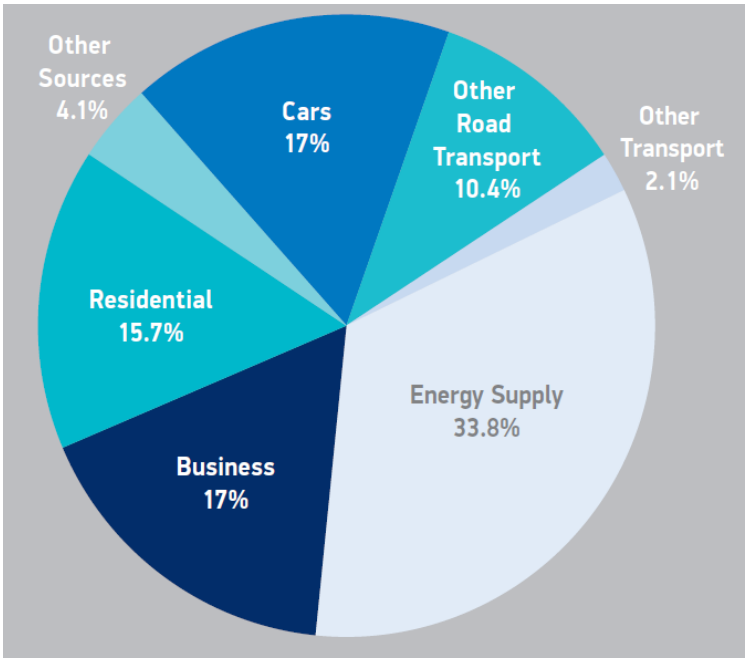

Figure 2.3 CO_2 Emissions by Source 2015 in the UK [5]

To deal with global climate change, ten governments among the top 15 vehicle markets worldwide - Brazil, Canada, China, the European Union, India, Japan, Mexico, Saudi Arabia, South Korea, and the United States - have established mandatory fuel economy or CO_2 emission standards for light duty vehicles [6]. And the fleet targets become increasingly strict as shown in Figure 2.4, which guarantees all the car makers have to take much more effort to develop and apply new technologies to reduce fuel consumption of cars.

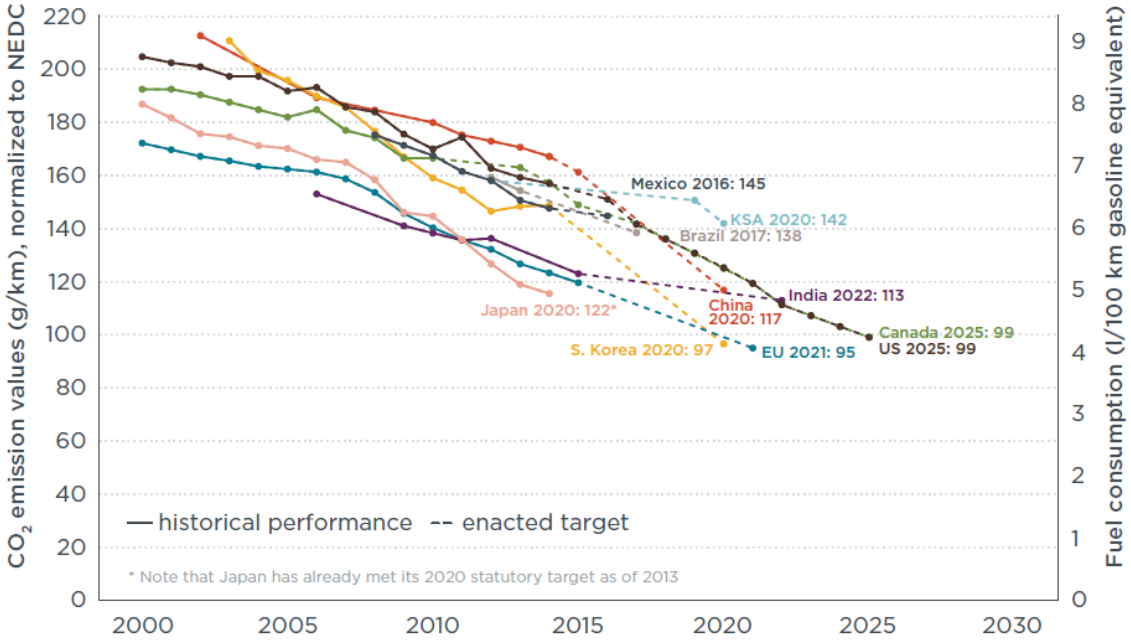

Figure 2.4 Historical Fleet CO_2 Emissions Performance and Current Standards (gCO_2/km normalized to NEDC) for Passenger Cars [6]

2.2 Technologies to Reduce Vehicle CO_2

In order to meet the fuel economy standards, technical development and design optimisation have to be applied to all systems which have impact on total fuel consumption of a vehicle [7], [8].

- Improve fuel conversion efficiency of traditional internal combustion engines
- Improve transmission efficiency and powertrain integration
- Intelligent thermal management
- Brake / kinetic energy recovery
- Exhaust / heat energy recovery
- Alternative fuels
- Propulsion electrification
- Improve aerodynamics and rolling resistance
- Light-weighting design and materials

The recent annual WardsAuto survey shows lightweighting and engine efficiency improvement remain the top focuses for automakers to meet future CO_2 standard, as shown in Figure 2.5 [9]. This research and thesis will focus on fuel economy of traditional Spark Ignition (SI) gasoline engines.

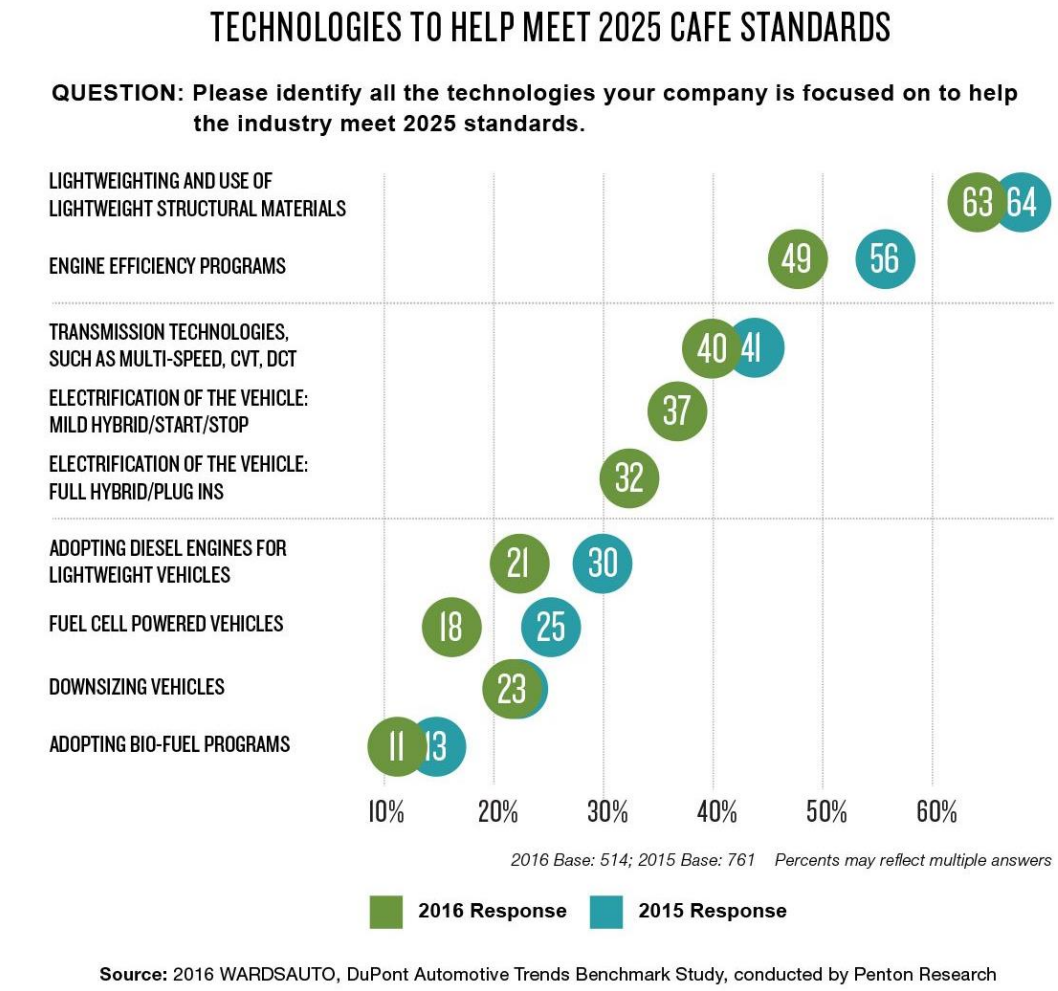

Figure 2.5 WardsAuto Annual Survey: Technologies to Help Meet 2025 CAFE Standards [9]

2.3 Internal Combustion Engine Fuel Energy Conversion and Efficiency

Improving fuel conversion efficiency of internal combustion engines is still the key area for reducing the fleet fuel consumption and CO_2 emission from passenger cars. There is a very complicated process for the chemical energy contained in the fuel being converted to the mechanical power output in an engine. It involves fluid dynamics, combustion, thermodynamics and mechanical movement hence there are unavoidable kinds of energy losses in each process. Percentage of the fuel chemical energy converted to the power output is defined as fuel conversion efficiency [10]. Principles of the energy conversion process and efficiencies have been extensively discussed in many books and articles [10]–[17], a summary by the author presented in Figure 2.6.

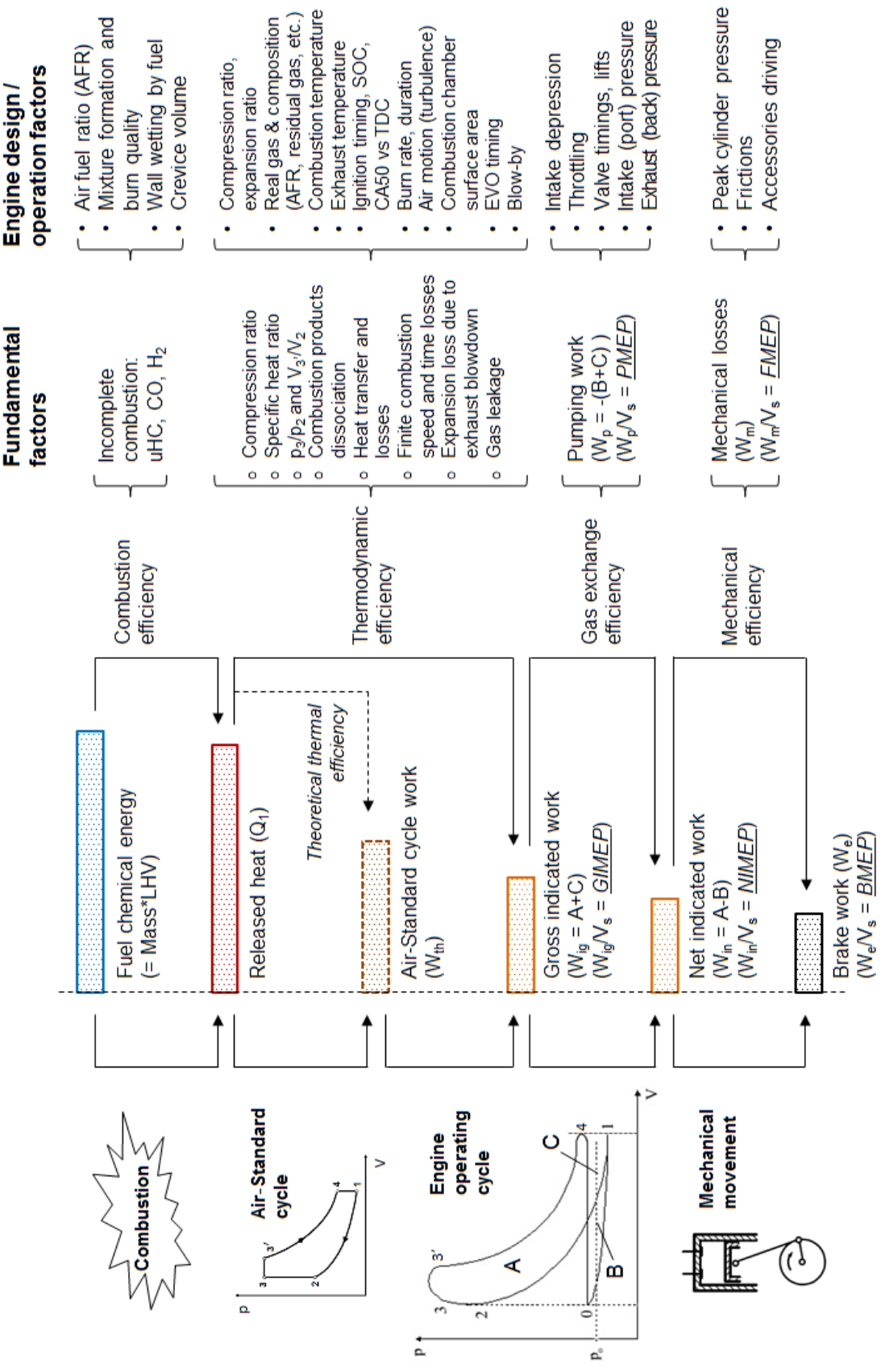

Figure 2.6 Fuel Energy Conversion Process and Efficiencies in Internal Combustion Engines

Gasoline engines remain the dominant propulsion unit for passenger cars in the world. IEA data has shown nearly 80% of light-duty vehicles used a gasoline engine in 2015. The percentage is a little lower in OECD countries but still close to 70% [18]. The overall fuel conversion efficiency of gasoline engines is worse than that of diesel engines. As a result, a large fraction of passenger cars in main European countries use diesel engines. Table 2.2 explains the key areas for gasoline engines to improve fuel economy and also the related main technical obstacles.

Table 2.2 Key Aspects for Improving Gasoline Engine Efficiency

Key objectives	Main obstacles and limitation in (SI) gasoline engine operation
Increase compression ratio	1) Abnormal combustion like knocking, low speed pre-ignition (LSPI); 2) Peak cylinder pressure limit from design side and also for reduction of friction.
Increase specific heat ratio	1) SI engine operates with stoichiometric Air/Fuel Ratio (AFR) mixture (relatively richer than diesel engine), due to the following requirements: i. Spark ignition and flame propagation are essential for gasoline engine combustion, which are greatly influenced by the AFR. AFR should be less than 20 for a typical SI engine; ii. SI engines apply three-way catalyst to reduce CO, HC and NOx emissions in exhaust gas. It requires the mixture to be near stoichiometric AFR. 2) Gasoline engine has higher combustion temperature than diesel engine mainly due to its stoichiometric combustion, which decreases specific heat ratio; 3) Gasoline engine has to use enriched mixture at high speed high load area to cool down exhaust temperature for exhaust components protection. It decreases both the combustion efficiency and specific heat ratio.
Reduce pumping loss	Gasoline engine normally uses throttling to reduce air intake mass at part load to control output meanwhile to maintain stoichiometric AFR. It causes decreased intake pressure and high pumping loss.

Optimise combustion time	1) Finite combustion speed causes combustion time losses in the gasoline engine. It will get worse when residual gas fraction increases (like at low load) or EGR increases, since they slows down the combustion; 2) Knocking at high load makes spark timing and CA50 retarded. It will make combustion phasing further away from optimum point.

When a gasoline engine changes the speed and load, the mechanisms influencing its fuel economy vary as well. As a result, the minimum BSFC is typically achieved at middle speed high load area, as shown in Figure 2.7. BSFC gets worse when engine speed goes lower or higher, and also when engine runs at very low load or at full load. The reasons of higher BSFC in these directions are explained in Table 2.3.

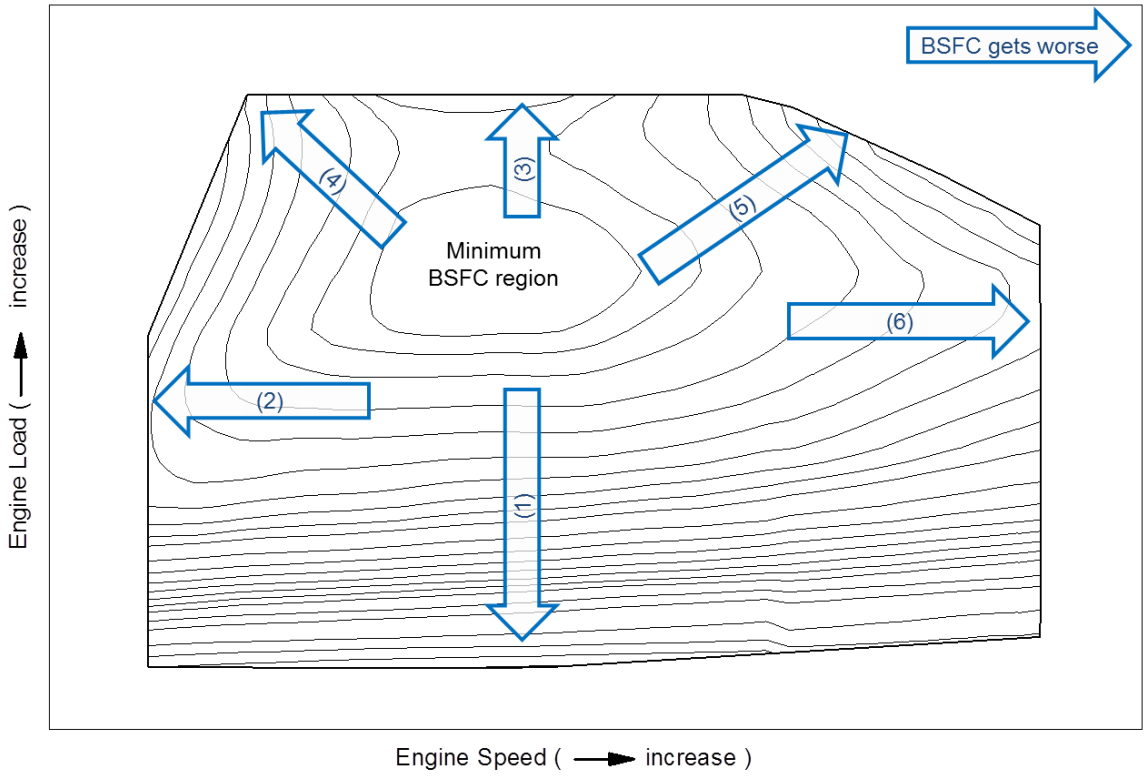

Figure 2.7 BSFC Contour Map of a Turbocharged Gasoline DI Engine

Table 2.3 Reasons for BSFC Increases in a Gasoline Engine Operation Map

BSFC increases	Main reasons
(1)	i. Intake pressure decreases because of throttling at lower load, causing higher pumping loss; ii. Low intake pressure also results in higher residual gas fraction. Meanwhile engine temperature is low at low load. These can slow down the combustion and cause combustion time loss increase.
(2)	i. Heat losses and gas leakage increase at low speed because of longer time for each cycle; ii. In cylinder charge motion and turbulence become weak as engine speed reduces, resulting in low burning rate and long combustion duration.
(3) & (4)	i. Pumping loss in gasoline engines decreases when engine load increases; However, ii. Gasoline SI engine has knocking combustion at high BMEP because of higher thermal load. Retard of spark timing is then demanded, resulting in later combustion timing and increase in combustion time loss; iii. The knocking tendency strengthens at low speed high load, due to slow combustion and high gas temperature. It requires more retard of spark timing and combustion timing • In a highly downsized gasoline engine, the LSPI issue may occur at low speed high load area. It cannot be eliminated simply by retarding the spark timing.
(5)	i. The knocking tendency reduces at high speed high load compared to at low speed; However, ii. Gasoline engine employs enriched AFR at high speed high load area to cool down exhaust temperature for protecting exhaust components; Enrichment might also be utilised for increasing the peak power, normally on Naturally Aspirated (NA) engines. The overfueling causes combustion efficiency and specific heat ratio deteriorated.
(6)	Mechanical losses increase as engine speed becomes high. Friction, power consumed to drive engine accessories and also pumping loss will all increase in this direction.

2.4 Technologies for Improving Gasoline Engine Fuel Economy

In the recent years, many advanced technologies have been developed and applied on gasoline engine products or become hot research areas for improving passenger cars fleet fuel economy. This section will briefly discuss some of the advanced technologies.

2.4.1 Gasoline Direct Injection

The modern gasoline direction injection (DI) technology was utilised on mass production gasoline engine by Mitsubishi in 1996 to realise stratified lean combustion. However the gasoline DI technology itself has two key advantages making it a revolutionary technology for gasoline engine development [13]–[15], [19], [20].

- The fuel is injected into combustion chamber and mainly evaporates in the air, which absorbs the heat from air providing so-called "cooling effect". It is desirable to increase compression ratio (CR) hence improving engine thermal efficiency. The decreased charge temperature can also reduce heat losses and improves engine volumetric efficiency therefore enhancing torque output.
- This technology is able to provide flexible injection strategy and accurate control of fuel injection mass. It improves AFR control during engine cold start and transient operation, which is beneficial to reduction of engine emissions and fuel consumption. This feature also makes gasoline DI technology very useful to collaborate with other technologies and to enable advanced combustion processes.

2.4.2 Stratified Lean Combustion

As discussed previously, pumping loss and low specific heat ratio are the main reasons for gasoline engines having worse fuel economy than diesel engines, both relating to the requirement of stoichiometric AFR control. There is a long history of study on lean combustion technology for reducing fuel consumption of gasoline engines [21]–[23]. Homogeneous lean combustion systems normally demand technologically advanced ignition system to ensure reliable ignition. Stratified lean combustion is able to reduce the requirements on spark ignition system since the rich mixture near spark plug can help the ignition core formation and flame propagation. However it is quite challenging to form ideal stratified charge with Port Fuel Injection (PFI). The flexibility of gasoline DI

including multiple injection capability makes stratified charge organization much easier. As a result, the first generation of mass production gasoline DI engines developed by Mitsubishi, Toyota, Nissan, VW/Audi, Honda, etc. in the 1990s were all stratified lean combustion systems [13], [24]. These engines used wall-guided or air-guided DI injection to form stratified/rich mixture nearby the spark plug. Mercedes-Benz and BMW brought a new generation of gasoline DI engines with spray-guided stratified combustion systems into the market in 2006 and 2007 [13].

The lean burn engines need lean NOx aftertreatment systems to meet emission standards, which are complex in technology and calibration, quite costly and also sensitive to fuel quality especially the sulphur content in fuel. High sulphur concentration in fuel can cause sulphur poisoning of NOx storage catalysts and also deteriorates the fuel economy benefits [25], [26]. Another challenging for these stratified combustion gasoline DI engines is the smoke and particle emissions [15]. As a result, most car makers have terminated this type of products. However the automotive industry still preserves the interests on this technology considering its great potential to meet future CO_2 standards. Mercedes-Benz continued the spray-guided stratified lean combustion system in the new 1.6l and 2.0l in-line four cylinder engines [27].

2.4.3 CAI and HCCI

Controlled Auto-Ignition (CAI) and Homogeneous Charge Compression Ignition (HCCI) combustion are radically different from the conventional spark ignition (SI) combustion in a gasoline engine and compression ignition (CI) diffusion combustion in a diesel engine [28]. CAI/HCCI combustion systems typically use highly diluted, lean and premixed fuel and air mixture. The CI method leads to multiple ignition sites throughout the combustion chamber. As a result, this technology is able to eliminate the high combustion temperature zones and prevents the production of soot particles, hence producing ultra-low NOx and particulate emissions. The use of lean air/fuel mixture with recycled burned gases permits unthrottled operation of a CAI/HCCI gasoline engine, thus yielding higher engine efficiency and better fuel economy than SI combustion.

The challenges for a CAI/HCCI gasoline engine include the combustion timing control and switching between CAI/HCCI and SI combustion modes, which obstructs the mass

production of this type of engines, though several companies like AVL, Mercedes-Benz, GM and Volkswagen have launched demonstrator engines even demonstration cars [29]–[32]. However, this situation may change in 2019 when Mazda debuts its first commercial HCCI gasoline engine product, which is reported to use a proprietary combustion method called Spark Controlled Compression Ignition (SPCCI) [33]–[35].

2.4.4 Gasoline DI Engines with Variable Cam Timing and Boosting (Downsizing)

In order to avoid the complex exhaust aftertreatment system on stratified combustion engines, many car makers started to develop and produce gasoline DI engines with homogenous stoichiometric combustion process early in this century. This type of engines only needs typical three-way catalyst as typical PFI engines for emission control. They still get the benefits provided by the "cooling effect" of gasoline DI including increase in CR and torque output. However the fuel saving level is limited since no improvement of pumping loss and specific heat ratio is achieved [13], [15], [20].

Boosting the SI engine by a turbocharger or supercharger is a technology which has traditionally been used to increase the maximum torque or power of an engine. In recent years, the technology has more become the synonymous with fuel consumption improvement through the advent of engine 'downsizing', which means to replace an existing NA engine by a boosted engine having a smaller displacement but offering at least the same performance [13], [36]. The downsized engines are enforced to run at a higher BMEP level to produce the same torque output compared with a larger NA engine, which helps the engine to operate more at an area with better efficiency due to less pumping loss as explained in Figure 2.7. Downsizing also benefits vehicle CO_2 emission by reducing the number of cylinders to lower the total friction and weight of engine, and improving cold start performance thanks to faster warming up [37].

Boosted downsized SI engines normally need to decrease the CR since they are prone to knocking combustion, hence deteriorating the improvement effects on fuel economy and performance. Gasoline DI is able to reduce charge temperature and consequent knocking tendency, which results in considerable synergy between gasoline DI and boosting. As a result, boosted/downsized DISI engine has become a mainstream in the newly developed

gasoline engines. The majority of gasoline engines will be turbocharged DI engines by 2018 in Europe, as reported in Figure 2.8 [38].

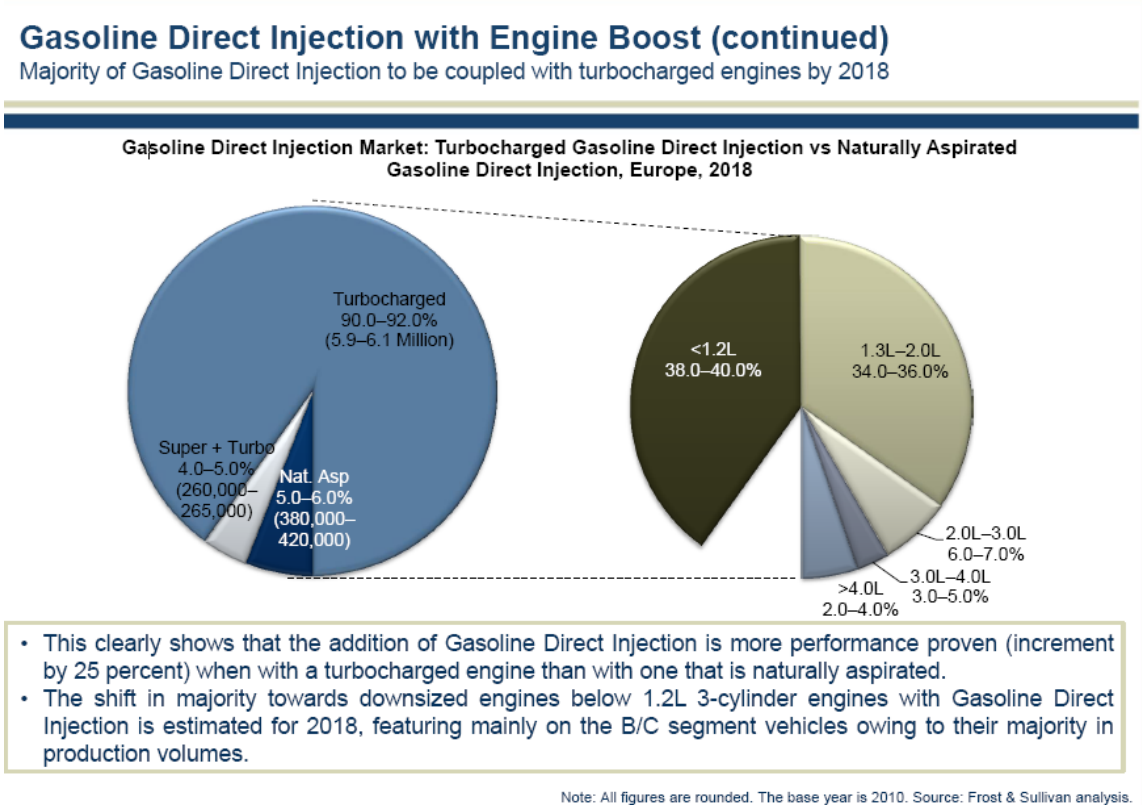

Figure 2.8 Gasoline Direct Injection with Engine Boost (Source: Frost & Sullivan) [38]

Variable Cam Timing (VCT) technology has been employed to improve SI engine performance since 1980s, which is able to rotate the camshaft from its initial orientation hence change the relative cam timing to engine crank timing. These devices enable engineers to optimise engine cam timings according to engine speed and load hence to reduce pumping loss and improve performance output. This technology has been proven to be great for boosted gasoline DI engines. It is beneficial for reducing engine pumping loss at low load and strengthening scavenging effect at low speed high load zone to improve peak torque. Gasoline DI approach separates the air intake and fuel injection, which provides more flexibility for applying variable cam timing strategies [15][39], [40]. Therefore, VCT devices have been utilised on almost all the modern gasoline DI engines [41].

2.4.5 Variable Valve Actuation and Air Intake

Since the gas exchange process has huge impact on the pumping and combustion processes on gasoline engines, lots of efforts have been spent by automotive industry and researchers to develop kinds of variable air intake mechanisms to provide the flexibility for optimising the gas exchange process. These devices can be classified into several categories providing 3% to 12% fuel consumption improvement [42]: Variable Intake Manifold, Variable Cam Timing / Phaser (VCT / VCP), 2-Step or 3-Step Cam Profile Switching (CPS) / Variable Valve Lift (VVL), Continuous Variable Valve Lift (CVVL), Camless Valvetrain and Variable Charge Motion.

Variable intake manifold optimises intake tuning effect for different engine speeds normally by step adjusting or continuous adjusting the manifold length. Engine torque / power can be optimised in the whole speed range due to the improved volumetric efficiency [43], [44].

VCT or VCP devices are commonly used on modern SI engines. These devices are able to advance or retard the camshaft timing in relative to crank timing hence change the valve opening and closing timings during engine operation. Mostly used products are hydraulically driven continuously adjustable VCT. Electronic VCT products become popular recently due to their faster response capability. It is quite common for current gasoline engines to use VCT at both intake and exhaust sides, which enables these engines to reduce the pumping losses at part load by optimising intake and exhaust valve opening/closing timings and to improve low speed peak torque through scavenging behaviour [39], [40], [45], [46].

VCT devices move the camshaft phasing hence have to change both the valve opening and closure timings parallel. Another limit of this type of systems is their inability to change the valve lift. Variable valvetrains have been developed to change the valve event and lift. Some can provide 2-step or 3-step valve lift adjustment by switching cam profiles, like Audi Valvelift System (AVS) and Honda VTEC. CVVL systems can provide continuous valve lift adjustment in a big range, like the BMW Valvetronic, Nissan VVEL, Toyota Valvematic and Mitsubishi MIVEC. VVL especially CVVL devices are able to reduce throttling even provide un-throttling operating on gasoline

engines hence significantly decrease the pumping loss. These mechanisms are also utilised to realise other engine concepts like cylinder deactivation, Atkinson cycle / Miller cycle operation and CAI/HCCI combustion [47]–[55]. Electronic and electro-hydraulic valvetrains also have been investigated for camless operation and more flexible control of valve actions. However, they are not widely applied on mass production engines due to their durability, cost and complexity.

There are also kinds of devices developed to adjust the intake charge motion. Some VW / Audi gasoline DI engines use a tumble flap fitted in the intake manifold, which are able to increase tumble motion at part loads by blocking the bottom half of intake ports [56], [57]. Another mechanism is to increase swirl motion by deactivating one of the two intake valves or adopting asymmetric intake valve profiles [23], [53], [58]. These systems are beneficial to air fuel mixing and also the combustion process by enhancing air charge motion and turbulence hence improve gasoline engine fuel consumption.

2.4.6 Variable Compression Ratio

Increase in CR leads to high theoretical efficiency. Low CR is one of the main reasons for gasoline engines having worse fuel conversion efficiency than diesel engines, which is due to the detonation limit at high load operating. This problem can be improved by a Variable Compression Ratio (VCR) mechanism, which allows the SI engine to use higher CR at low load area where there is no knocking combustion and reduces CR for high load operation. Many different types of VCR systems have been developed with 5% to 12% fuel economy improvement claimed [59]-[63]. The benefits can become much more if applying VCR with other technology like lean burn, CAI/HCCI, VVL, Atkinson/Miller cycle [59]–[63]. Durability, system complexity and cost are still quite challenging for most VCR technologies hence limit their application on mass production engines. However, this is a promising technology considering its great potential in reducing gasoline engine CO_2 emission. Nissan has introduced the VCR technology in their premium brand vehicles in 2016 [64], in which the varied CR was realised by seamlessly raising or lowering the height the pistons reach.

2.4.7 Water Injection

Knocking combustion at high load makes SI engines have to retard spark timing and cause further combustion timing loss. This becomes more intensive for downsizing engines therefore limits their benefits. Any technologies which are capable of reducing knocking tendency of SI engines are able to advance the combustion hence benefit the fuel economy.

Investigation of water injection for automotive gasoline engines can date back to 1970s when this technology was studied for reducing NOx emissions through cooling down combustion temperature [65]–[68]. This technology attracts the attention of automotive industry again in recent, since its potential to mitigate knocking combustion and decrease heat transfer loss consequently improve fuel conversion efficiency of downsized SI engines [69]–[72]. The main challenge is the requirement of additional storage and supply of distilled water.

2.4.8 Exhaust Gas Recirculation

There is a long history of more than 40 years for applying Exhaust Gas Recirculation (EGR) technology for improving emission and fuel consumption on gasoline engines. EGR is used to dilute the in-cylinder charge while maintaining stoichiometric AFR, which is capable of lowering the pumping loss and gas temperature in the combustion chamber. The latter effect leads to reduction in thermal losses and dissociation and suppressed tendency of knocking combustion [73]–[76]. More attention has been drawn nowadays by combining external cooled EGR with downsized gasoline DI engines due to its potential to reduce knocking hence to increase CR for better fuel economy [13], [77]–[79]. The use of EGR is also one of the key measures in the most efficient production SI engine produced by Toyota in their latest hybrid vehicles, with the highest thermal efficiency of 41% [80], [81]. There are two types of external EGR systems have been adopted in product gasoline engines depending on the location where exhaust gas is taken. High pressure EGR systems take exhaust gas upstream of the turbocharger, while a low pressure EGR system inducts exhaust gas downstream of the turbine.

2.5 Miller Cycle Technology Development and Application

2.5.1 Origin and Terminology

The nomenclature Miller cycle came from an American engineer, Ralph Miller, who patented his invention on internal combustion engine work process in 1954, 1956 and 1957 [82]–[84]. Main objects described in these patents included:

- An engine operating cycle shall decrease the thermal load and knocking / pre-ignition tendency of the engine and enable an increase of engine power through supercharging;
- Lower the charge temperature at the end of compression stroke through a reduced effective compression ratio (ECR) whilst still retaining the thermodynamic benefit of a high expansion ratio;
- Control auto-ignition with the correct AFR and enable operating at higher load and high expansion ratio / geometric compression ratio;
- The preferred embodiment was to use early intake valve closing (EIVC) and expand the charge to bottom dead-centre (BDC) reducing the initial temperature and pressure of compression. However, other methods for reducing the ECR were also referred to, including holding the exhaust valves, intake valves or a 'compression control valve' open for a short period of time during the compression stroke, which is obviously the late intake valve closing (LIVC) approach;
- Load control via intake valve control hence possible unthrottling to avoid the low efficiency pumping process;
- Improve scavenging due to high boost pressure and subsequent increased differential between the boost pressure and the exhaust back pressure;
- Different valve lifts could be applied for full load and light load operation;
- The preferred application is a supercharged / turbocharged engine, however the inventor claimed the process could be applied to a NA engine as well;
- The approach can work on gases, diesel and gasoline engines.

Another nomenclature Atkinson cycle has to be mentioned when discussing Miller cycle, which was named by the British engineer James Atkinson, who was the first one to

describe a four stroke internal combustion engine process with unequal compression stroke and expansion stroke. Atkinson initially presented this concept in his 1886 paten for an opposed piston engine [85]. Then he patented a four stroke engine realizing the process by a special crank mechanism in 1887 [86]. Due to the unique linkage design, the engine described in his invention has a power stroke longer than the compression stroke, i.e. expansion ratio greater than compression ratio. In addition, the engine completes the intake, compression, power and exhaust strokes in a single revolution of crankshaft.

Nowadays many internal combustion engines achieving a lower ECR than its expansion ratio via retarded intake valve closure were tagged with Atkinson cycle engine, which doesn't correspond well to the patents filed by Atkinson and Miller. This may be originated by Luria in 1982 [87], [88]. The paper described an engine working at a higher expansion ratio than ECR through an increased geometric CR and LIVC instead of Atkinson's complicated crank mechanism. Luria denoted this approach as 'Otto-Atkinson' cycle and claimed a 19% improvement of fuel consumption compared with the conventional Otto cycle engine.

However, all aspects of this cycle were anticipated 30 years earlier by Miller. Thus the author assert that any engine cycles where its ECR is reduced and less than the expansion ratio through either EIVC or LIVC are embodiments of the Miller cycle irrespective of boosted or naturally aspirated air induction. Only those engine concepts with increased expansion ratio realized by mechanical linkages should be catalogued as the Atkinson cycle, such as the Honda EXlink engine [89], the Otto-Atkinson engine with a novel crank linkage presented by Kentfield [90], [91], the variable displacement engine reported by Rosso [92], the engine with an alternative crankshaft mechanism by Boretti [93], and the ultra-downsizing engine by means of real Atkinson cycles using asymmetrical crank mechanisms as published by Gheorghiu [94].

2.5.2 Development and Application of Miller Cycle for Passenger Car Gasoline Engines

Miller cycle has been extensively studied since it was invented and also widely applied on kinds of industry products including gas engines, diesel engines and gasoline engines

because of its capability to improve engine fuel conversion efficiency. This study will focus its development and application on gasoline engines in passenger car.

(1) Ford Motor

Sherman and Blumberg of Ford Motor (1977) described an overall engine model for predicting the impact of induction and exhaust processes on SI engine emissions and fuel consumption. Non-conventional configurations such as engine load control by EIVC was referred to [95]. Blakey and Ma et al. (1991) established a prototype LIVC mechanism and investigated the so-called 'Otto-Atkinson' cycle on a Ford 2.0l I-4 16 valves gasoline engine with earlier model of electronic fuel injection [96]. It was concluded LIVC to be combined with throttling as for a load control strategy. Large reduction in pumping mean effective pressure (PMEP) was observed at 2000rpm when LIVC was used instead of throttling, however the improvement of PMEP became less at 3000rpm. LIVC strategy deteriorated the cylinder to cylinder fuel distribution due to outgoing charge returning to the manifold plenum and transporting into subsequent cylinders. As a result, reduction in pumping loss did not lead to fuel consumption improvement. This issue was improved by changes made to fuel supply device and intake manifold. Then a maximum 7% decrease in BSFC was achieved at light loads. A hydraulic VCR system was also described in the paper with the intention to use both LIVC and VCR for 'Atkinson' cycle operation, however no much results was obtained due to leaks of the system.

Boggs et al. of Ford Motor (1995) carried out simulation and engine tests on a modified 1.6l I-4 gasoline engine to investigate the effect of 'Otto-Atkinson' cycle on engine fuel economy and emissions [97]. The engine operated on Otto cycle at full load with a CR of 9:1 and on the 'Atkinson' cycle at part loads, which was realised by increasing the geometric CR to 16:1 and retarding the closing timing of the secondary intake valve by up to 80dCA. Exhaust cam was retarded at part loads as well to increase EGR level. The test results obtained at different loads at 1500rpm shown the reduction of PMEP, ISFC and BSFC at part loads <6bar BMEP by 'Atkinson' cycle operation. The maximum 15% improvement in BSFC was achieved at 2.62bar BMEP compared to the standard SI engine with 10% EGR. BSCO and BSNOx were decreased by 60% and 54% respectively at this point however with a 60% increase in BSHC. Idle assessment was conducted at 750rpm and 0.7bar BMEP with closure timing of the secondary intake valve retarded by

40dCA. BSFC at this point was reduced by 4% due to increased geometric CR and reduced pumping loss through 'Atkinson' cycle. The increased in-cylinder turbulence resulted from asymmetrical intake valve events also contributed to a 49% reduction in BSCO, better combustion stability and only a slight increase of burn duration. Hardware design for creating the 'Otto-Atkinson' engine was also described in the paper including a VCR piston and a coaxial camshaft enabling shifting of the secondary intake lobes.

Hasan et al. of Continental Automotive and Lorenz et al. of Ford-Werke (2015) presented charging technologies for engine CO_2 optimisation through 'Millerization' [98]. The 'Millerization' was achieved by increasing intake event length and increasing geometric CR from 10 to 12 based on a Ford 1.0l I-3 Turbocharged Gasoline DI (TGDI) engine. It claimed the fuel consumption under WLTC hot cycle was improved by 3.4% with the 'Millerization' approach. The authors also pointed out the concept should have adverse impact on engine transient performance and car driveability. Therefore, advanced charging technologies will be demanded.

(2) GM

Tuttle of GM (1980, 82) investigated the approaches to control engine load by LIVC and EIVC based on single cylinder SI engine experiments [47], [48]. Timings of Exhaust Valve Opening / Closure (EVO/EVC) and Intake Valve Opening (IVO) were fixed during engine testing. Three LIVC timings with 60, 80 and 96dCA delayed versus conventional IVC were realised by modified cam profiles. Another modified EIVC cam reduced the valve lift from 9.4mm to 3.2mm and advanced the IVC timing by 120dCA compared to conventional IVC and to 40dCA BBDC. Engine testing was carried out at 1600rpm and 35 to 100kPa absolute manifold pressure. It was concluded LIVC timing has to be limited at 96dCA delay to avoid large deterioration of indicated thermal efficiency, thus it needed to be combined with a throttle for full range of load control. With the original CR 8.4:1 used, LIVC lowered the engine indicated thermal efficiency at part load due to lower ECR and longer combustion duration. However the Net Indicated Specific Fuel Consumption (ISFCn) was still reduced by up to 6.5% thanks to the greatly decreased pumping loss. EIVC has the potential to regulate engine output without intake throttling however proper valve control mechanism is required. EIVC had a pumping loss 40% lower than the conventional engine at part load and also a higher

indicated thermal efficiency because of reduced heat loss, finally achieving a 10% improvement of ISFCn.

Anderson et al. (1998) compared a NA SI engine with LIVC Miller cycle to a conventionally-throttled engine using numerical simulation [99]. They also concluded LIVC requires supplemental throttling for very light load operation since it was only able to control engine output down to 35% of the maximum. LIVC engine had much hotter air intake due to reverse flow from cylinder, which led to more heat losses during induction stroke. However LIVC engine still could achieve up to 6.3% higher indicated thermal efficiency at part load.

He et al. (2016) assessed the performance of a Miller cycle demonstrator engine [100]. Both EIVC and LIVC approaches were tested on a 2.0l DISI engine with the CR increased from original 9.3:1 to 12.0:1. Two options of multi-stage boosting systems were also investigated, i.e. turbocharger-supercharger combination and a two-stage turbocharger. Engine testing was carried out at 2000rpm and 2~20bar BMEP and also at power curve from 1000rpm to 5500rpm. It was concluded longer-duration LIVC cam to be superior to the short-duration low-lift EIVC cam, because EIVC cam showed a worse combustion stability and BSFC at higher engine loads due to the reduced charge motion and poor mixing. Results in the paper also shown turbocharger-supercharger combination generated significantly more losses hence higher BSFC than two-stage turbocharger, however this could be caused by insufficient optimisation. Both EIVC and LIVC cam achieved around 20g/kWh BSFC reduction at part load up to 10bar BMEP. Final analysis based on experimental results indicated the Miller cycle engine can reduce the fuel consumption of a vehicle in typical city and highway driving cycles like WLTC by 3~4% and maintain the same torque performance as the baseline turbocharged engine. Li et al. (2014) conducted similar experimental investigations at 1000rpm 13.2bar BMEP and 2000rpm 4bar BMEP on the same 2.0l DISI engine and presented similar results [101]. They further pointed out improvement of pumping loss with EIVC was greater than with LIVC at low load.

He et al. (2017) reported the updates of the Miller cycle engine development [102]. The engine stroke increased from 86mm to 94.6mm, therefore the bore-to-stroke ratio reduced from 1.0 to 0.91 and engine displacement increased to 2.2l. The new Miller

cycle demonstrator engine focused on LIVC strategy and integrated with a twin-scroll single-stage turbocharger and low-pressure cooled external EGR. Maximum geometric CR changed to 12.5:1. It claimed a 3% improvement of BSFC at part load by LIVC cam compared to the baseline 2.2l turbocharged SI engine having 9.5:1 CR. Adding of the EGR provided an average of 3.2% additional fuel economy benefit. It reported the EGR also brought noticeable BSFC reduction in high load conditions and increased the maximum BMEP from 20.9bar to 22.5bar thanks to its capability of mitigating knocking combustion and pre-ignition.

(3) Nissan

Hara et al. of Nissan Motor (1985) studied the effects of different intake valve closing timings on pumping losses and the combustion process of a SI engine [103]. A significant reduction in pumping loss was achieved from both LIVC and EIVC, but an equivalent reduction in fuel consumption was not achieved. This was mainly due to a deterioration of combustion performance, with longer combustion durations and increased cyclic variation caused by the drop in cylinder gas temperature and pressure due to the decrease in the effective compression ratio.

Sugiyama et al. (2007) examined the potential benefits of a concept NA SI engine that combined the EIVC Miller cycle operating enabled by a CVVL system and a VCR mechanism [104]. The EIVC was proven to be able to reduce fuel consumption because of pumping benefits, however the benefit could be deteriorated at light load due to lowered in-cylinder temperature and consequent worsened combustion. This could be improved by high geometric CR enabled by VCR technology and increase of internal hot EGR provided by CVVL controls. Finally fuel consumption was reduced by 16.2% at 1600rpm and 2.5bar BMEP as reported. Increase of CR beyond 15:1 did not further improve fuel economy because of the poor surface to volume ratio of combustion chamber hence increase of heat transfer loss.

Nissan launched a 1.2l 3 cylinder supercharged gasoline DI engine in 2012, a 1.6l I-4 TGDI engine in 2014 and a 3.0l V6 twin-turbocharged gasoline DI engine in 2016 all with Mille cycle and EGR technologies applied [105]–[107]. Miller cycle was implemented by VCT devices therefore the LIVC approach on these engines. Internal

EGR was used in the 1.2l and 3.0l variants while additional cooled low-pressure external EGR was employed by the 1.6l engine. The 1.2l engine adopted a high CR at 13.0:1 and achieved 95g/km CO_2 level under NEDC cycle. The 1.6l and 3.0l engines had 10.5:1 CR and improved the fuel economy by 10% and 7% respectively compared to their predecessors thanks to the new technologies utilized as reported.

(4) Mazda

Kono of Mazda Motor (1988) studied the impacts of EIVC and LIVC timings on in-cylinder flow, gas temperature and combustion in SI engines by means of engine simulation and in-cylinder flow measurements using the hot wire method [108]. The inlet camshaft was phased relative to crankshaft through a gear for advanced or retarded IVC timings. Decrease of gas flow velocity and temperature with EIVC and LIVC was observed. The potential harm to thermal efficiency was considered to be resolved by increasing the swirl and turbulence.

Mazda Motor introduced a 2.3l V6 Miller cycle engine with LIVC feature and a Lysholm compressor in 1993 [109]–[112]. The engine had a CR at 10.0 and ECR could be reduced to 7.6 by a retarded IVC timing at 70dCA ABDC. A tumble port was designed and a mask was added to intake side of combustion chamber to strengthen the turbulence for combustion improvement. It reported the BSFC of this engine was about 10 to 15% lower in 20 to 60% of full load compared to a V6 3.3l NA baseline engine. Miller cycle reduced pumping loss at part load and lowered ECR for anti-knocking performance while keeping high expansion ratio. It was effective in increase of maximum BMEP hence enabling engine downsizing which decreased the engine friction loss.

In 2007, Mazda developed another mass production Miller cycle engine for the new Mazda2 passenger car, which was a 1.3l NA engine [113]. The limitedly released information shown this engine had a LIVC feature and helped the new Mazda2 reduce fuel consumption by 20% combined with a continuously variable transmission (CVT). Mazda introduced another NA gasoline engine with LIVC Miller cycle technology into market in 2011, which was the 2.0l SKYACTIV-G engine [114]. The engine adopted a very high CR at 14.0:1 and mitigated knocking and pre-ignition issue by ECR reduction through LIVC which was enabled by an electrically-driven cam phaser at intake side. A

hydraulic cam phaser was used at exhaust side to adjust the internal EGR level. Fuel economy of C/D-class vehicles equipped with this engine was reported to achieve a improvement by 15%, with 8% contribution from the increased geometric CR and pumping efficiency.

(5) Volkswagen / Audi

Haugen et al. of University of Minnesota and Esler of VW (1992) modified a 2.3l Quad 4 engine to permit LIVC operation [115]. The IVC timing was altered in a range of 50dCA to 153dCA ABDC and consequently the ECR was varied from 9.32 to 4.96. Engine tests were carried out at 1500rpm from 9bar to 3.5bar BMEP, with the largest 6.3% improvement of fuel economy obtained at light load through LIVC method compared to throttling.

VW/Audi group widely introduced the Miller cycle technology into their new generation of TFSI/TSI engine products in 2015/16 [116]–[120]. Both the new EA888 Gen.3B 2.0l TFSI and EA839 3.0l V6 TFSI engines utilised the Audi Valvelift System (AVS) at intake side for 2-step cam profiles switching. One cam featuring a short opening duration and low valve lift was used at part load for Miller cycle operation, while another cam profile had relatively long duration and standard valve lift which was for conventional Otto cycle operation at high load for desired power density. The requirement on turbocharger was balanced by the so-called “Right-sizing” strategy. CR was increased to 11.7 and 11.2 respectively for the 2.0l and 3.0l engine, which contributed to the improvement of fuel conversion efficiency. The new EA211 1.5l TSI engine adopted a different solution. It only had one intake cam profile with 150dCA valve opening duration and 7mm peak valve lift, however the intake cam phaser provided 70dCA adjustment range for the capability of altering the Miller cycle level and ECR, as a result the 12.5 CR was employed. The engine used an electrically actuated variable turbine geometry (VTG), a world first in volume-produced SI engines as claimed, in order to produce efficient boosting for achieving 200Nm peak torque and 96kW peak power. The 1.5l engine also combined the Miller cycle technology and cylinder deactivation for maximising the fuel economy at part load. Finally the new 2.0l engine achieved the minimum BSFC of 225g/kWh in a big region, the new 3.0l engine had the minimum BSFC at 224g/kWh and a BSFC of 230g/kWh in a big region and the new 1.5l engine

achieved the minimum BSFC of 222g/kWh at 3500rpm 12bar BMEP and a BSFC of 240g/kWh in a region equalling to almost 60% of the whole engine map as reported by the manufacturer.

(6) Honda

Urata et al. of Honda (1993) assessed a non-throttling SI engine with EIVC mechanism [49] on a prototype vehicle. A newly developed Hydraulic Variable-valve Train (HVT) provided full flexibility of intake valve lift control which enabled EIVC Miller cycle operation. The experimental results showed up to 80% reduction in pumping loss and about 7% improvement of vehicle fuel consumption. The engine had a normal CR of 9.5 therefore the reduced ECR lowered in cylinder gas temperature at low load and caused fluctuation in combustion. This issue was improved by enhancing charge motion through masking around intake-valve seat and the two spark plug configuration.

Akima et al. (2006) reported the Honda newly developed 1.8l i-VTEC NA gasoline engine with LIVC feature for low fuel consumption [121]. The i-VTEC valvetrain integrated at intake side allowed two cam profiles switching. Engine operated with LIVC cam in a region from around 1200rpm to 3500rpm and up to approximately 90% of WOT torque for optimal fuel economy. Another high output cam was utilised in other area for engine performance. Engine fuel efficiency was reduced by 6% against the previous generation due to the application of LIVC strategy. In 2013, the similar hardware and LIVC strategy was also applied on a new 2.0l gasoline engine for Accord Hybrid car. The engine fuel consumption was further optimised by an increased CR of 13.0 and cooled EGR [122].

Kuzuoka et al. (2014) carried out experimental study on performance improvement of high CR gasoline engines based on Miller cycle and ethanol fuel [123]. A fuel separation system was established to separate ethanol blended gasoline into high-concentration ethanol fuel and gasoline. A CPS mechanism at intake side allowed switching between short-duration low-lift cam profile for Miller cycle operation at part load and standard cam profile for Otto cycle running at high load conditions, where large quantities of ethanol injection was employed for knocking mitigation. This approach allowed CR up to 13.5 for NA engine and 13.5 to 12.5 for a turbocharged application. It claimed to be

able to improve vehicle fuel economy by up to 26.8% when applied in a downsized turbocharged gasoline engine.

Ikeya et al. (2015) investigated a package of technologies for thermal efficiency enhancement of a supercharged gasoline engine [124]. Increasing compression ratio and diluting by low-pressure EGR were considered as the main measurements. LIVC Miller cycle was adopted to reduce the ECR to 12.5 while a geometric CR of 17.0 was used. Optimisation of the combustion system were implemented to deal with the slow combustion and reduced ignitability due to Miller cycle operation and high EGR rate above 30%, which included increasing stroke-bore-ratio to 1.5, optimising combustion chamber geometry, developing a high tumble port and also applying a high energy ignition system. As a result, a brake thermal efficiency of 45% was demonstrated at 2000rpm 8bar BMEP.

(7) AVL

Wirth et al. (2000) and Kapus et al. (2000, 2002) discussed a AVL "CBR reverse Miller cycle" concept [125]–[127]. CBR means Controlled Burn Rate which was enabled by variable swirl motion control. One intake port was a tangential port for creating swirl flow and another neutral port could be shut-down or deactivated by a slider to further strengthen the swirl ratio when necessary. Reverse Miller cycle was actually the LIVC approach, which could be combined with EGR for improving fuel economy at part load or reduce ECR for applying high CR on a TGDI engine. The strengthened charge motion was proven to be beneficial for Miller cycle operation especially when combined with EGR. It was also believed the swirl flow was better than tumble flow for applying the 'reverse Miller cycle' on a stratified combustion system because of less impact on the stratified charge formation. However it can be less important for a homogenous gasoline DI engine.

Fraidl et al. (2015) discussed the strategy for gasoline engines to achieve the performance and BSFC targets of 200kW/l and 200g/kWh [128]. Technologies like Miller cycle, cooled EGR, VVL and VCR were discussed as the potential combination to achieve this target. The concept was embodied by Sorger et al. in 2016 by presenting a combination of a 2-stage VCR system and Miller cycle operation [129]. The VCR was realised by a

length adjustable connection rod, which enabled CR switching between 14 and 9.5 on a 2.0l VCR Miller test engine. The engine had a maximum BMEP of 25bar and demonstrated a minimum BSFC of 216g/kWh at 3000rpm 13bar BMEP, the 220g/kWh BSFC in a big operation region and 322g/kWh at 2000rpm 2bar.

(8) Toyota

Toyota had been using LIVC based 'Atkinson' cycle technology for high efficiency engine on hybrid cars quite early. The renewed I-4 engine series for Toyota Hybrid System (THS) was introduced in 2012 [130], which combined the high 13.0 CR, cooled EGR, 'Atkinson' cycle and electric water pump to optimise the overall benefits when integrated within the hybrid system. The Variable Valve Timing-intelligent (VVT-i) device was used to adjust IVC timing from 102dCA to 61dCA ABDC. Latest IVC timing and high EGR rate up to 30% were used at low load conditions for the lowest pumping loss and best BSFC. Moderate LIVC timing and high EGR rate were applied at high load condition for advancing spark timing and reducing BSFC. The cooled EGR was also employed at the maximum power output points above 5000rpm for reducing gas temperature to reduce knocking combustion and enable stoichiometric air-fuel ratio.

In addition to the THS applications, Toyota also widely applied 'Atkinson' cycle technology on its gasoline engines including the ESTEC (Economy with Superior Thermal Efficient Combustion) and TNGA (Toyota New Global Architecture) platforms [81], [131]–[133]. The 1.2l ESTEC TGDI engine had a moderate CR at 10.0 and used LIVC 'Atkinson' cycle mainly at part load to reduce pumping loss which was enabled by a VVT-i variant with mid-position lock system. The same VVT device was also applied on the new I-4 2.5l TNGA NA engine for enabling a 13.0 CR and improving pumping loss and fuel consumption at low load conditions through 'Atkinson' cycle. EGR is also employed on the 2.5l engine to make it the most efficient production SI engine in the world as claimed by Toyota, with the highest thermal efficiency of 41% in their latest hybrid vehicles and 40% when driving the gasoline vehicle solely.

(9) Mahle Powertrain

Cairns et al. of Mahle Powertrain (2009) investigated the benefits of replacing throttling through EIVC and internal EGR combination for both PFI and DI engines [134].

Independent cam phasers were utilised at both intake and exhaust side and a CVVL mechanism was applied at intake side for EIVC and internal EGR adjustment on a single cylinder research engine. It reported that EIVC operation allowed fuel consumption reductions of up to 8% at a typical part-load site of 1500rpm/3.2bar IMEP. The addition of inlet VCT allowed further savings of up to 3%. Exhaust VCT then provided additional small improvement of 2%. Increased valve overlap and consequent higher internal EGR rate was supportive to EIVC operation at low loads. It was observed the fuel economy benefit dropped when using EIVC and VVT on gasoline DI engine compared to the PFI platform.

Taylor et al. (2011) assessed the benefits of LIVC strategy on a turbocharged downsized gasoline engine through Mahle CamInCam technology [135]. The CamInCam camshaft was able to provide asymmetric cam control, i.e. one intake cam load was fixed and another cam was adjustable for different valve timing and/or lift therefore allowed the LIVC operation. It claimed the LIVC approach reduced pumping loss at part load and gained 15g/kWh decrease in BSFC, which also provided 3.2% improvement of fuel consumption at high load region through knock mitigation even at a slightly increased CR. The asymmetric intake cam control could increase charge motion and shift the dominant mode from tumble to swirl, however the impacts of this effect was not investigated in the study.

(10) Daimler AG

Vent et al. (2012) presented the technologies used in a Mercedes-Benz newly developed 2.0l TGDI engine [136]. Through its Camtronic CPS device, an EIVC cam profile with reduced valve lift was employed to reduce fuel consumption at light load conditions. The issue of slow combustion caused by the low valve lift had been pointed out as well, which was improved by the multiple injection strategy thanks to the flexibility of the piezo DI system.

Rau et al. (2014) discussed kinds of variabilities for gasoline engine operation and their future potentials for reducing CO_2 emission [137]. The favourable technical package included variable valve trains for EIVC/LIVC dethrottling strategy and internal EGR adjustment, continuous CR control, variable turbocharging system and advanced ignition

system. It was believed the CO_2 of gasoline engines could be shifted close to that of diesel engines with these technologies.

(11) IAV

Gottschalk et al. of IAV (2013) designed and performed an experimental study on the potential of the Miller cycle to control engine knock [138]. It was concluded that, Miller cycle was a promising method to suppress knock under steady operation, but instantaneous anti-knock intervention would be constrained by dynamic limits of the induction control devices.

Riess and Benz et al. (2013) investigated the potential of using intake valve variabilities for in-cylinder turbulence generation while realising dethrottling through EIVC / LIVC strategies [139], [140]. The UniAir system from INA Schaeffler was mounted in the cylinder head of a four-valve single cylinder research engine, which allowed the comparison of engine operation under EIVC, LIVC and the reference IVC timing at BDC. Numerical modelling was also carried out to provide detailed analysis of in-cylinder flow field. The results showed LIVC had more or less the same turbulence level and heat release characteristics as the reference IVC timing, while EIVC timing exhibited significantly reduction of turbulence kinetic energy (TKE) leading to much slower burn and heat release. Then an asynchronous intake valve actuation strategy was tested for mitigating charge motion and TKE losses resulting from EIVC and promising effectiveness was proven. Combustion chamber masking could provide further improvement.

Scheidt et al. of Schaeffler and Kratzsch et al. of IAV (2014) carried out experimental study on the potential of optimised ‘Miller/Atkinson’ strategy for reducing CO_2 emission from a highly downsized gasoline engine [141]. A 1.4l I-4 TGDI engine was used as the baseline engine for testing, which was aimed at a maximum BMEP of 29bar for replacing a 1.8l turbocharged engine. It was found that EIVC and LIVC approaches yielded different potential in different engine map regions due to the distinct dependence on in-cylinder turbulence level. Therefore, a combination of both strategies was considered as the solution for the best possible fuel consumption. Test results in the paper showed this concept could reduce vehicle fuel consumption by up to 15.3% under

NEDC mode when a cam shifting system was used to enable the combination of one EIVC and two LIVC profiles.

Sens et al. (2016) discussed the synergy between VCR and EIVC Miller cycle for improving gasoline engine fuel economy [142]. It was concluded that a geometric CR more than 20 is necessary for fully using the potential of dethrottling operation through combined Miller cycle and residual gas, while a low geometric CR between 12 and 14 is favourable for a full load level like 24bar BMEP. Thus a fully variable intake closure in combination with a fully variable geometric CR is required for optimising the fuel consumption of gasoline engines. Sens et al. also pointed out the stroke-bore ratio must be carefully selected when applying this combined approach [143]. Ferrey et al. of MCE-5 Development (2014) stand for this technical combination after analysing the potential of coupling their VCR technology with the Variable Valve Actuation (VVA) [61].

(12) Hyundai Motor

Birckett et al. (2014) introduced the development of Hyundai-Kia mechanically supercharged 2.4l gasoline DI engine [144]. Miller cycle operation through a LIVC cam profile was applied on this engine. Multiple benefits of Miller cycle were reported, including the reduced pumping loss, higher compression ratio of 12.0 and the synergy with cooled EGR, all contributing to the final fuel efficiency improvement.

Ha et al. (2016) reported the development of a Continuously Variable Valve Duration (CVVD) engine in Hyundai Motor Group [145]. The CVVD mechanism can change the valve duration from 180 to 320dCA while maintaining the same valve lift. It was combined with a CVVT (Continuously Variable Valve Timing) device in order to fully optimise the four valve timings (IVO, IVC, EVO, and EVC) at different engine operating conditions. Enabled by this flexibility, the CVVD engine was report to replicate ‘Atkinson’ cycle (LIVC) at part loads and gain fuel consumption improvement by 4 to 5% in average among other benefits.

(13) Ricardo

Osborne and Pendlebury et al. (2015, 16, 17) reported the progress of Magma concept engine development in Ricardo, which is a Miller cycle engine with high CR and also

high degree of downsizing [146]–[149]. The Magma engine has selected a high stroke-bore-ratio, a high CR of 13:1 and 25bar as the maximum BMEP target, aiming to combine the fuel economy advantages of turbocharged downsized DI engine and high CR NA engine. EIVC Miller cycle was employed for ECR control and knock mitigation. Intake tumble motion was increased for combustion speed and stability at EIVC extremes. The combination of a mechanical supercharger in the low-pressure position and a fixed-geometry turbocharger in the high-pressure position was established for supplying the demanded high pressure ratios and sufficient airflow without building excessive exhaust back pressure. Single cylinder engine testing, 1-D simulation and drive cycle analysis have been used to assess this concept, which showed fuel consumption benefits between 1.8 and 9.4% achievable at part load key points and of 12.5% and 16.4% for WLTC and FTP-75 cycles respectively when a larger baseline engine was replaced.

(14) Academic studies

Söderberg and Johansson (1997) investigated the impacts of unthrottling operation via EIVC or LIVC on the in-cylinder flow, combustion and efficiency [150]. A five cylinder gasoline engine was modified to a single cylinder engine for related experimental studies to be performed. In additional to symmetric EIVC/LIVC timing of both intake valves, another three LIVC strategies with asymmetric timings of left and right intake valves were also compared. It was concluded both the EIVC and LIVC methods reduced pumping loss greatly compared to the conventional throttled case. Asymmetrical intake valve events increased turbulence intensity but caused lower gross indicated efficiency, which might result from increase in heat losses as explained.

Wu et al. (2003) carried out a performance analysis of a supercharged Miller cycle Otto engine by using an air standard cycle based computation modelling tool [151]. It claimed that the Miller cycle has no inherent potential for better efficiency than the Otto cycle because of its reduced compression stroke, but can decrease the risk of knocking thence improve the operation of a boosted engine. The report indicated the necessity of increasing geometric CR when applying Miller cycle technology.

Ribeiro et al. (2006) developed a model to calculate the fuel consumption of Miller cycle engine and Otto cycle engine when matching with a 5 speed Manual Transmission (MT)

or a Constant Variable Transmission (CVT) under NEDC cycle [152]. It was observed that Miller engine using CVT was the most efficient and Otto engine using MT was the least efficient, with 25% difference presented. Then direct comparison of Otto cycle, Miller cycle and Diesel cycle was performed by the same team (2007) through both numerical modelling and single cylinder engine demonstrating [153]. It reported Miller cycle with VVT and VCR was the most efficient approach and reduced the fuel consumption by 20% at low speeds and low loads compared to Otto cycle operation.

Stansfield et al. (2007) carried out experimental studies on the impact of unthrottled/EIVC operation on gasoline engine flow field, mixing and combustion processes by using both optical and thermodynamic single cylinder engines [154]. The research examined different EIVC operational variations, including early closing both inlet valves symmetrically and early closing each inlet valve individually. Since the DISI combustion chamber of the research engine had the longitudinal arrangement of spark plug and injector in the centre, there would be differences between using the inlet valve near injector and operating the one close to spark plug. These EIVC approaches were compared to the standard inlet valve profiles at 2000rpm and 2.7bar net IMEP condition. All of them exhibited a significant reduction in ISFC. EIVC operation through the inlet valve near injector had markedly lower ISFC than operating another inlet valve near the spark plug, signifying its positive impact on air/fuel mixing which corresponded to the in-cylinder flow field imaging obtained on the optical engine. More tests were conducted at four speed/load test points later and reported by Patel and Stansfield et al. (2008, 2010) [155], [156]. The advantages of single valve EIVC operation for improving fuel economy and engine raw emissions were further validated.

Miklanek et al. (2012) investigated an approach for improving the indicated efficiency of LIVC / EIVC operation at part load by mixture heating [157]. The in-cylinder charge temperature at the beginning of combustion could be heavily reduced by Miller cycle especially with EIVC method, which could lead to a slower combustion than standard Otto cycle at part load and hence deteriorated indicated efficiency. The proposal was to heat up the mixture in the intake manifold for enhancing the in-cylinder charge temperature. 1-D numerical simulation was carried out to assess the effectiveness. It claimed that further fuel economy improvement has been achieved through the combination of Miller cycle operation and the mixture heating. It was also mentioned the

mixture heating should be implemented through waste heat recovery for overall system efficiency.

Li et al. (2014) assessed the effects of EGR, LIVC, high CR and their combinations on the fuel economy of a 1.6l PFI engine based on experimental studies carried out at 1~10bar BMEP and 2000rpm [158]. The results showed fuel consumption improvement achieved by LIVC plus increased CR was higher than that by using EGR only. Combining the three technologies could reduce BSFC further until increase of EGR rate was limited by the combustion cyclical variation.

Martins et al. (2015) discussed the potential benefits and challenges while applying Miller cycle for full-load operation on an ethanol fuelled engine after conducting a detailed 1-D simulation at 1800rpm and 20bar BMEP [159]. It reported EIVC had higher efficiency than LIVC in this case however an intake pressure higher than 5bar would be required for the very early IVC timing resulting challenge to boosting system. However solutions for overcoming this challenge have not been discussed. The combination of Miller cycle and ethanol fuel allowed geometric CR to increase to 16:1. High EGR rate could provide addition beneficial for knock mitigation and make a 46.5% gross indicated efficiency achievable.

Schenk and Dekraker (2017) evaluated the potential fuel economy improvements through implementing cooled EGR and cylinder deactivation (CDA) technologies on an 'Atkinson' cycle engine as part of greenhouse gas emissions rulemaking performed by US Environmental Protection Agency [160]. A 2.0l four-cylinder engine with 75 degrees of intake cam phase authority and a 14:1 geometric CR was selected as the baseline engine. Cooled EGR and CDA were tested on this LIVC ('Atkinson') capable engine to determine their impacts on CO_2 emissions under two-cycle (FTP and HwFET) running. Vehicle CO_2 was finally analysed by cycle simulation on a full vehicle model (ALPHA). It predicted that cooled EGR could improve two-cycle CO_2 of a future vehicle by 7.6%. Implementation of cooled EGR and CDA on the 'Atkinson' engine could reduce the vehicle two-cycle CO_2 by 9.5%.

(15) Key points

The literatures review shows the Miller cycle technology has been studied and applied on gasoline engines. The key features can be summarised as the followings:

- Miller cycle is able to reduce pumping loss for part load operation through dethrottling;
- Miller cycle is able to decrease charge temperature due to reduced ECR and results in anti-knocking capability for high load operation, which could benefit turbocharged/supercharged downsized engine by increasing the geometric CR;
- The decreased charge temperature might deteriorate the benefits at part load;
- There is no universal conclusion on which of LIVC and EIVC is more superior. It depends on the integration and optimisation of each system. Engines with CPS or VVL valvetrains favour the EIVC method, meanwhile engines with VCT mechanisms typically use LIVC for realising Miller cycle operation, although some of these cases were named as 'Atkinson' cycle.
- It is still quite challenging to apply Miller cycle on a highly downsized gasoline engine when a high peak BMEP is required, mainly due to the demand of very high boost pressure ratio. As a result, these engines have to limit the peak torque target or switch to conventional Otto cycle operation at full load, in which case the geometric CR should be limited if no other technologies implemented for knocking mitigation.
- Miller cycle could be combined with other technologies for providing more fuel economy benefits. EGR has already been utilised on a few products. VCR could be a very promising technology for Miller cycle engines if issues of current VCR systems like friction penalty, NVH, robustness and industrial process compliance and modularity could be solved.

2.6 Summary

This chapter briefly described the development status of passenger car engines. Technical upgrades of the engines have been greatly driven by legislations for achieving the strict emission and fuel consumption/CO_2 standards in the last two decades. Gasoline engine downsizing is already established as a proven technology to reduce automotive fleet CO_2 emissions. However the CR and downsizing degree are constrained by the knocking and LSPI issues due to high thermal load in this kind of engines, which limit the potential of

this concept for improving fuel economy. Miller cycle is a widely applied technology for reducing part load pumping loss and improving high load operation especially for downsized gasoline engines. However, there is a lack of detailed and systematic analysis of the individual process and factors contributing to the overall effect observed with the application of Miller cycle. Both EIVC and LIVC have been used by different automotive manufacturers and their relative merits have not been investigated at extended engine operating conditions. By setting up a single cylinder DI engine and conducting well controlled experiments on such an engine, the current study will lead to much better understanding of the underlying processes and their interactions involved and hence guide the further development of high efficiency gasoline engines.

Chapter Three

Experimental Setup and Methodology

Chapter 3 Experimental Setup and Methodology

3.1 Introduction

The aim of this project is to investigate a technical approach based on Miller cycle operation for improving fuel economy of a highly boosted gasoline DI engine. This chapter describes the research methodology and experimental setup and test facilities used to obtain all measurements and data. Intake and exhaust cam phasers and three different intake cam profiles are utilised for Miller cycle operating. Two pistons with different geometry compression ratio (CR) are employed to extend the range of effective CR. Engine tests were carried out on a fully instrumented single cylinder engine testbed with a flexible Engine Control Unit (ECU).

3.2 Research Design and Methodology

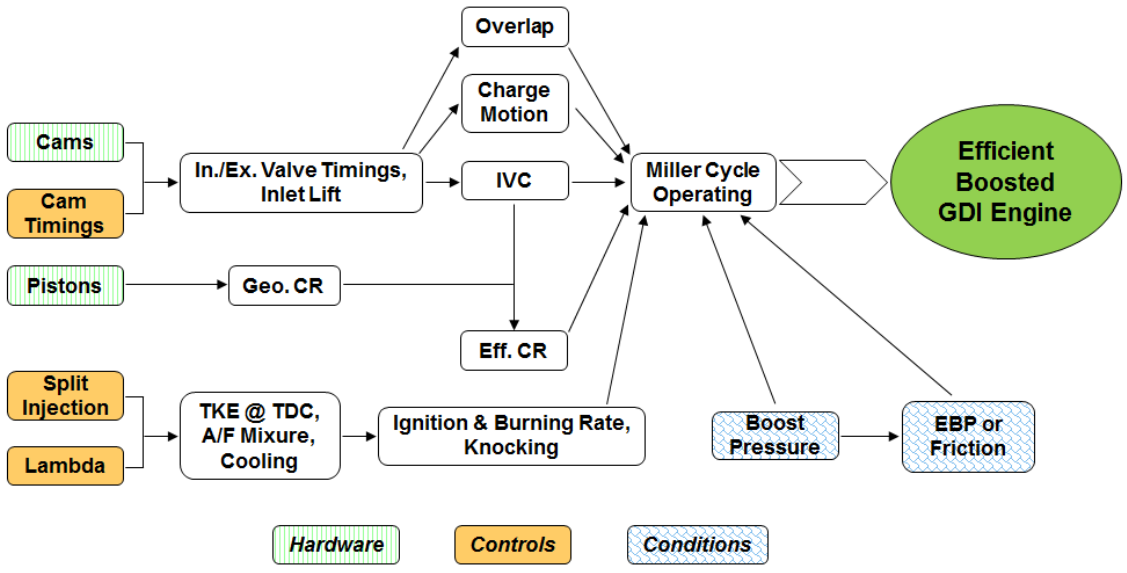

Figure 3.1 Schematic of Engine Hardware and Controls Employed in the Research

The research aim is to improve the fuel conversion efficiency of a highly boosted downsized gasoline DI engine by optimising the Miller cycle operation. Figure 3.1 shows key engine components, controlling variables and conditions which are used to investigate the best hardware configuration and strategy for achieving the optimal fuel

consumption through Miller cycle. Two intake cam profiles have been tested to realize Miller cycle and compared with the standard camshaft. One cam features a long opening duration and standard valve lift for Late Intake Valve Closing (LIVC) and another cam has a short opening duration and low valve lift for Early Intake Valve Closing (EIVC). Two independent cam phasers on intake and exhaust sides are used to adjust the cam timings for the Miller cycle operation. Details of these cam profiles and range of cam timing adjustment are given in Figure 3.3.

One piston with a standard geometric CR of 9.3:1 and the other with an increased geometry CR of 12.8:1 are utilised and described as the Low Compression Ratio (LCR) and High Compression Ratio (HCR) pistons respectively in the thesis. The high CR piston increases the compression ratio by reducing piston recesses without re-optimising its crown geometry as shown in Figure 3.2, which may have negative effects on engine operation and efficiency.

Figure 3.2 LCR Piston (left) and HCR Piston (right)

By means of a flexible ECU, different injection strategies are investigated to understand their impacts on in-cylinder charge motion, air/fuel mixture formation and consequent influence on engine fuel economy. An external boost rig is used to provide adjustable pressurized air charge in dried condition for the single cylinder engine to run up to 4000rpm and 25.6 bar NIMEP. An exhaust back pressure (EBP) control valve is installed in the exhaust system to simulate different EBP conditions considering the real application of a turbocharger system in a multi-cylinder engine. The calculated work

consumption or friction caused by a supercharger device is used to evaluate the benefits of Miller cycle operation.

3.2.1 Details of Cam Profiles, Valve Timings and Effective Compression Ratios

Table 3.1 Exhaust and Intake Cam Specifications and Phasing

Cam	Opening Duration (TOR) [dCA]	Minimum Overlap Phasing [dCA ATDCNF]			Maximum Overlap Phasing [dCA ATDCNF]		
		MOP	IVO/EVO (0.5mm lift)	IVC/EVC (0.5mm lift)	MOP	IVO/EVO (0.5mm lift)	IVC/EVC (0.5mm lift)
EIVC Intake	152	75	16	134	35	-24	94
Standard Intake	240	120	13	227	80	-27	187
LIVC Intake	292	144	16	272	104	-24	232
Exhaust	278	-140	-262	-17	-100	-222	23

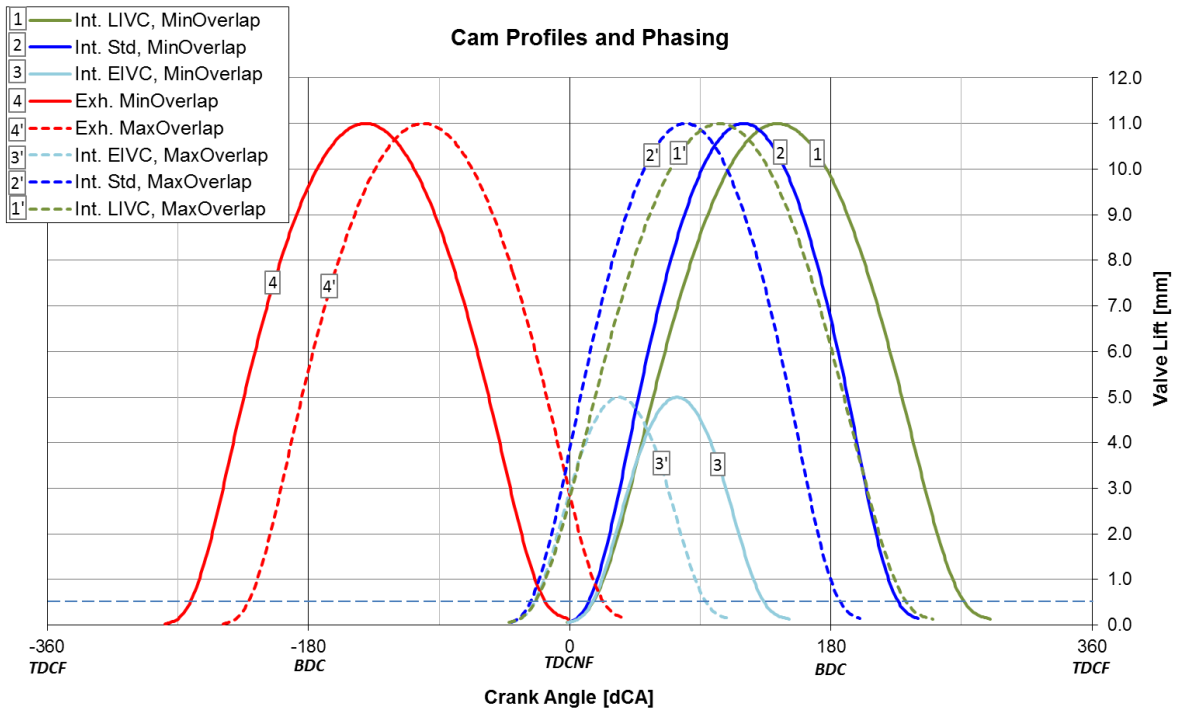

Figure 3.3 Exhaust and Intake Cam Profiles and Phasing

Table 3.1 and Figure 3.3 present the design details and phasing of the exhaust cam and three intake cams used in the experimental study. Cams are locked at the minimum overlap positions at the parked status. Cam phasers on both exhaust and intake side provide 40dCA of cam timing adjustment. With the EIVC and LIVC cams, the IVC

timing could be changed from 94dCA ATDCNF to 272dCA ATDCNF or from 86dCA before BDC to 92dCA after BDC.

Effective compression ratio is reduced with the advanced or retarded IVC timings provided by EIVC or LIVC cam profiles and also the intake cam phaser. In order to measure the effect of valve timings on the Miller cycle operation, the parameter of Miller Cycle Ratio (MCR) is introduced and defined,

$$\mathrm{MCR} = \frac{\text{Geometric CR} - \text{Effective CR}}{\text{Geometric CR}} \qquad \textbf{3-1}$$

Figure 3.4 depicts the changes of IVC timing, relative position of IVC to BDC, effective CR, MCR and valve overlap with varied intake cam timing (IMOP) for the six hardware combinations. When intake cam timings are retarded with the standard cam and LIVC cam, the valve overlap between the intake and exhaust valves opening periods is reduced and IVC timings are moved away from BDC, resulting in a decrease in the effective CR and increased MCR. For the EIVC cam, the situation is reversed. The lower effective CR and higher MCR are achieved by advancing IVC before BDC, which is accompanied by a larger valve overlap period. MCR changes in the range of 0~10%, 10~35%, 13~40% for the standard cam, EIVC cam and LIVC cam respectively. Combined with two pistons with high and low geometry CR, the effective CR is varied from 5.7 to 13 during the experiments.

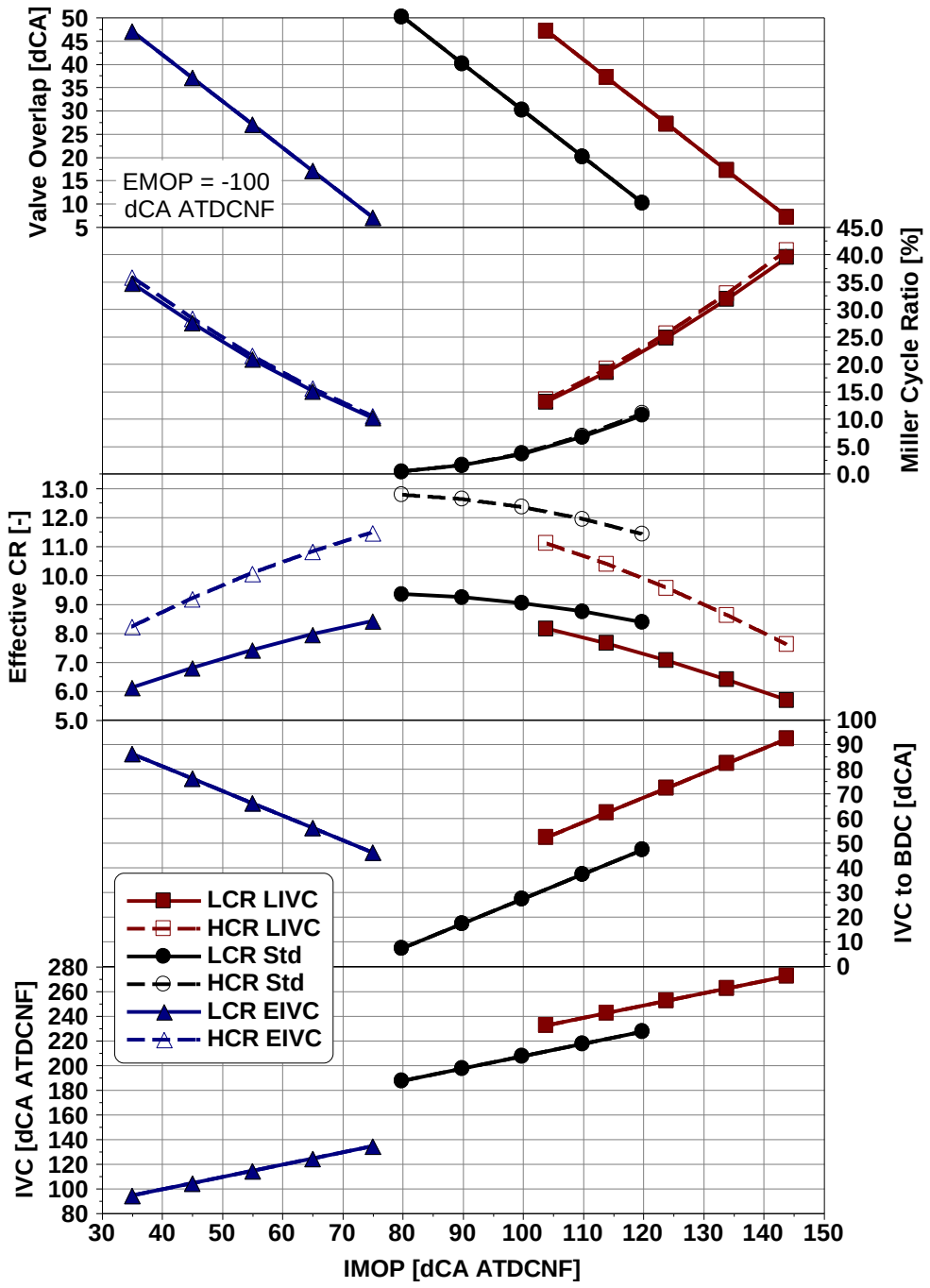

Figure 3.4 IVC, IVC to BDC, Effective CR, MCR and Valve Overlap vs IMOP

3.2.2 Steady State Operation Points for Engine Testing

As shown in Figure 3.5, ten steady state operation points are selected to carry out engine tests with all hardware configurations. These ten points cover four regions which have important impact on the base engine fuel economy: (1) 800rpm and 2.0bar NIMEP which are the minimum engine speed and load that the single cylinder engine could run stably.

It is used to assess the fuel saving strategy for idle like very low load operation condition; (2) Low load area around 5bar NIMEP; (3) Mid load region around 9bar NIMEP; (4) Low speed and high to full load region, which is the most challenging operation region for highly downsized gasoline engine and will have an increased influence on vehicle fuel consumption or CO_2 emission under WLTP and RDE cycle test.

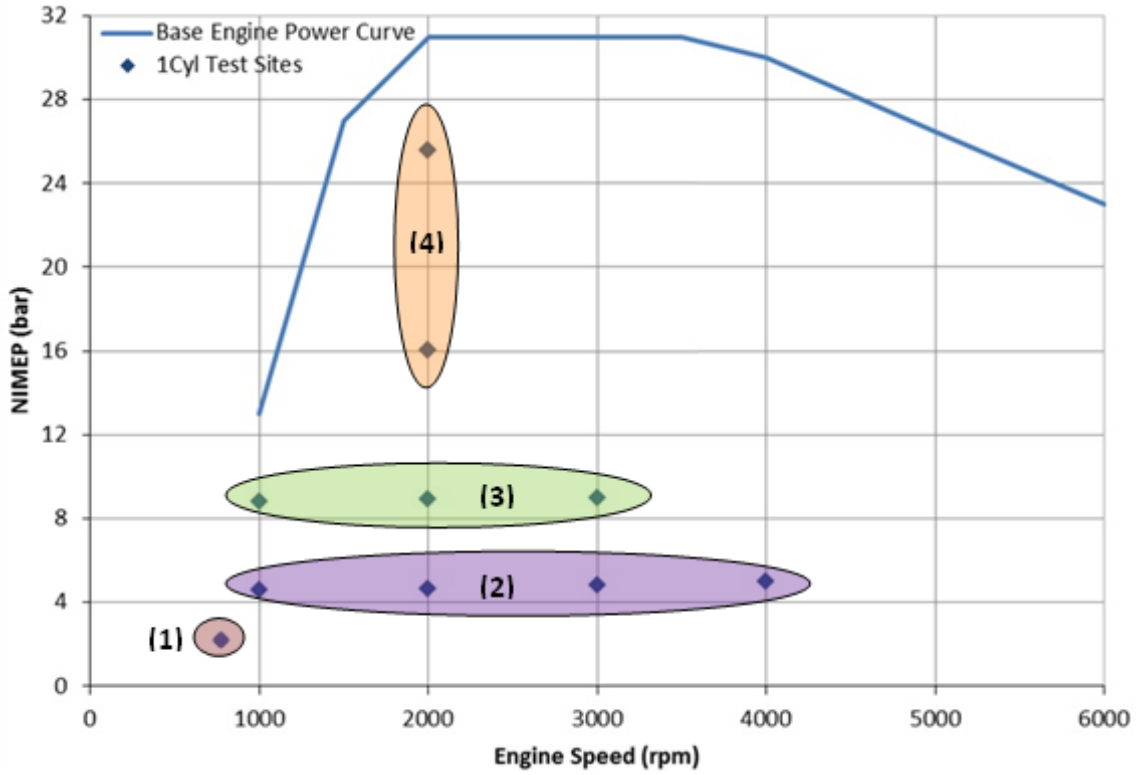

Figure 3.5 Single Cylinder Engine Test Points and Engine Operation Area

3.3 Single Cylinder Engine Testbed

Figure 3.6 shows the schematic of the complete single cylinder engine testbed employed for the experimental study. It comprise a single cylinder engine, the engine testbed, conditioning and supply systems including an external boosting rig, a data acquisition system with measurement devices integrated, and the engine control system. A transient electrical motor dynamometer is fitted in the testbed to load the engine, measure its torque output and maintain the engine speed during experiment.

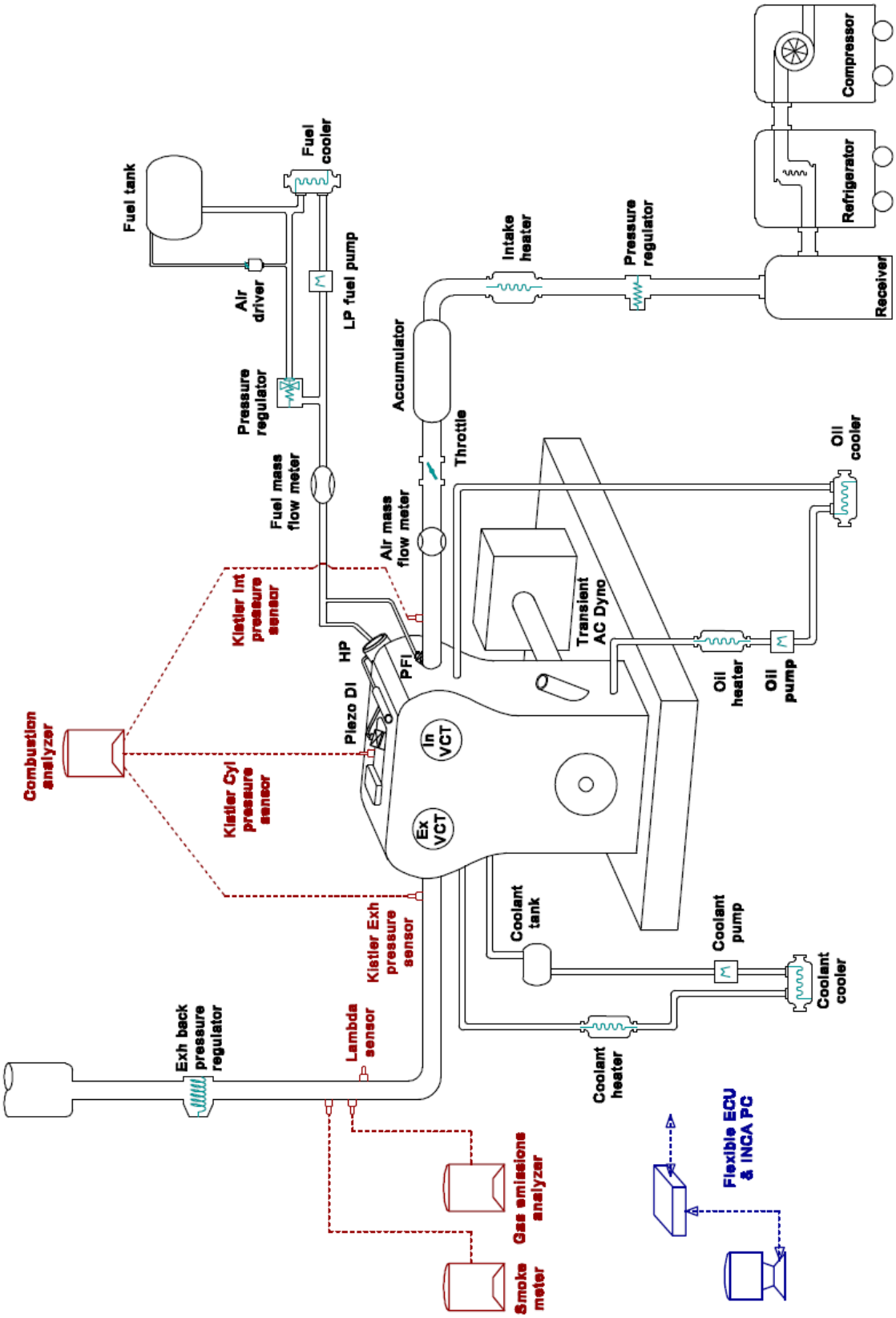

Figure 3.6 Schematic of Single Cylinder Engine Testbed Setup

3.3.1 Single Cylinder Engine

All experiments are performed on a single cylinder gasoline DI engine. The engine comprises a high speed single cylinder crankcase, a standard cylinder head from the MAHLE three cylinder 1.2l downsizing demonstrator engine [161][162] and a bespoke cylinder block designed to mate the cylinder head to the crankcase. The cylinder head is designed to accommodate a centrally mounted piezo DI injector next to the spark plug. It also has the port fuel injection (PFI) system which provides the capability for dual fuel injection study. Two hydraulic variable cam phasers are fitted on both the intake and exhaust sides to provide 40dCA cam timing adjustments. Detailed technical specifications of the test engine are given in Table 3.2. The single cylinder engine fitted on the test bed is shown in Figure 3.7.

Table 3.2 Technical Specifications of the Test Engine

Displaced Volume	400 cm^3
Stroke	73.9 mm
Bore	83.0 mm
Connecting Rod Length	123 mm
Compression Ratio	9.3:1 (LCR); 12.8:1 (HCR)
Number of Valves	4
Maximum Peak Cylinder Pressure	140bar
Parked Intake Cam Timing (MOP)	Three cam profiles: • EIVC cam: 75 dCA ATDCNF; • Standard cam: 120 dCA ATDCNF; • LIVC cam: 144 dCA ATDCNF
Parked Exhaust Cam Timing (MOP)	-140 dCA ATDCNF
Fuel Injection System	Central DI injection: • Outwardly opening hollow-cone spray piezo injector; • 200bar maximum injection pressure PFI injection at 5bar pressure

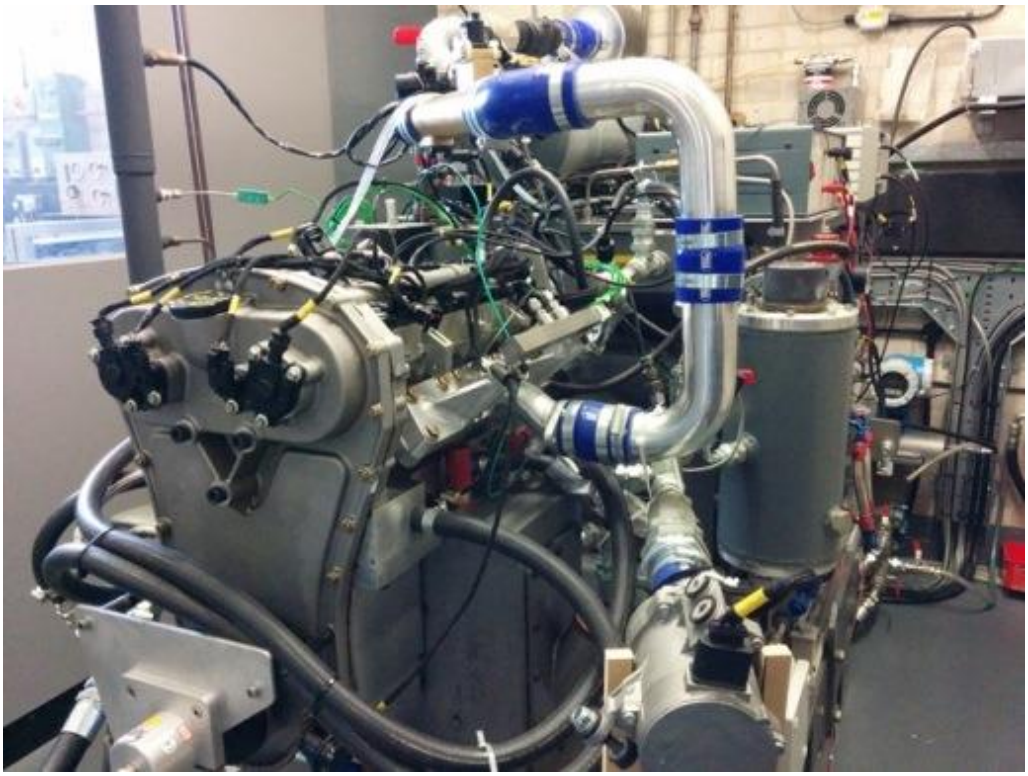

Figure 3.7 Single Cylinder Gasoline DI Engine on Testbed

3.3.2 Oil System

Function of the oil system is to supply the engine with oil at desired pressure and also maintain the oil temperature. The system is composed of the oil sump, oil filter, oil heater, oil pump and a heat exchanger.

The single cylinder engine crankcase features a wet sump lubrication system, which stores the standard Mobil1 0W-40 oil used for all test work. An externally located single speed 3-phase electric oil pump circulates the oil in the system at a nominal flow rate of 9.1 l/min. Two 1kW electric oil heaters are immersed in the oil sump, which is able to pre-heat oil before running and also used to heat up oil to desired temperature at low load. An oil heat exchanger is located upstream of crankcase oil gallery which functions as the oil cooler with the maximum heat rejection rate of 4 kW. It is adjusted by a Spirax Sarco capillary actuator which controls flow rate of raw cooling water through the heat exchanger. The oil temperature is finally controlled by switching on/off the oil heaters and adjusting the cooling capacity of the heat exchanger. The oil is filtered by means of an AC Delco X19 equivalent oil filter mounted next to the oil heat exchanger.

A set of sensors are fitted in the oil circuit to monitor the temperature and pressure. There are three pressure measurements located upstream of crankcase oil gallery where the minimum oil pressure is set to 4.2barA, an analogue pressure gauge for quick reading, a pressure switch for testbed emergency shutdown mechanism and a Druck PTX1400 0-10bar 4.2mA pressure sensor providing oil pressure signal to the low speed data acquisition system. Two Platinum Resistance Thermometers (PRTs) are used to measure the oil temperature into crankcase oil gallery, one for testbed high oil temperature shutdown which is normally set to 100°C and another providing signal to the low speed data acquisition system. The third PRT is located at the outlet of oil sump for temperature acquisition.

3.3.3 Coolant System

The coolant system is established to supply coolant to the engine at desired flowrate and also maintain the coolant temperature. It mainly comprises the coolant tank, coolant pump, ball valves, coolant heater and also the cooler.

The coolant used for all test work is a mixture of 50% de-ionised water and 50% ethylene glycol. A coolant tank is used to store the additional coolant in the circuit and also allows the expansion of coolant when it gets hot. Its location is 120mm higher than the highest point of the engine cylinder head coolant jacket in order to ensure that the cooling jacket is fully submerged in coolant. An external single speed 3-phase electric pump is used to circulate the coolant in the system at a nominal flow rate of 32 l/min. A bypass ball valve installed upstream of engine inlet allows the entire flowrate of coolant into the engine to be varied, which is typically set to 13 l/min to limit the delta coolant temperature between engine outlet and inlet within 6°C. The engine has split cooling circuits for cylinder head and cylinder block, thus two ball valves are fitted at coolant outlets of cylinder head and block respectively to control their coolant flowrate independently.

The coolant temperature is controlled in a similar way to the oil system. A 3kW immersion heater is integrated in the system to heat up the coolant when it is needed, meanwhile a heat exchanger with the maximum heat rejection rate of 53kW in the circuit works as the oil cooler. Engine out coolant temperature is controlled to the setpoint by adjusting the effects of coolant heating and cooling.

A few sensors are fitted in the coolant circuit for coolant flowrate, temperature and pressure measurements. Two Apollo turbine type flow meters are utilised to measure the flowrates of coolant supplied to the whole engine and cylinder block. Coolant pressure is monitored by a Druck PTX1400 0-4bar 4.2mA pressure sensor located upstream of engine coolant inlets, where a PRT is also fitted to monitor the coolant temperature into engine. Two PRTs are used to measure coolant temperatures at the outlets of cylinder head and cylinder block. Another PRT monitors the coolant temperature in the tank for testbed emergency shutdown. As part of the engine control system, an automotive type coolant temperature sensor is fitted at the cylinder block outlet side providing the input to ECU.

3.3.4 Fuel System

The fuel conditioning and supply system contains a low pressure loop and a high pressure system. The low pressure system supplies the fuel at desired temperature and pressure, and also fitted with the fuel flow meter.

The fuel used for all test work is standard pump unleaded gasoline with a Research Octane Number (RON) of 95. A stainless steel fuel tank is used to store fuel, which is higher than all other components in the fuel system. An automotive type 12V low pressure pump sucks the fuel from the fuel tank through a heat exchanger (fuel cooler), which controls the fuel supply temperature by adjusting the flowrate of raw cooling water running through it. There is a fuel filter and a mechanical pressure regulator downstream of the pump, which regulates the fuel supply pressure to 5barA. Extra fuel released by the regulator returns to the inlet of fuel cooler. There is a pipe connected to this loop with another top end connected to the entrance of fuel tank at atmospheric pressure. This pipe goes upwards and the top end is higher than all other pipes and parts in the system, which helps to remove any air bubbles in the low pressure fuel circuit.

A PRT and a Druck PTX1400 0-10bar 4.2mA pressure sensor are fitted downstream of the low pressure regulator to monitor the fuel supply temperature and pressure. A Coriolis mass flow meter is located downstream of these sensors for measuring engine fuel consumption. It is manufactured by Endress+Hauser with a DN01 1/24" sizing sensor for accurate measurement of small flow mass as shown in Figure 3.8.

Figure 3.8 Endress+Hauser Coriolis Mass Flow Meter

The fuel is divided into two paths post the fuel mass flow meter. One fuel line connected directly to the PFI injector. Another fuel line is fed into the high pressure gasoline pump which is driven by the engine intake camshaft and supplies fuel into the common rail at a demanded fuel volume. The rail pressure is up to 200bar and controlled by the ECU with a close-loop control function. A high pressure automotive type sensor is fitted on the common rail to provide the input of current rail pressure into ECU. ECU compares the actual rail pressure with the desired rail pressure and then increases or decreases the fuel volume supplied by the high pressure fuel pump into the fuel rail. The highly pressured fuel in the common rail is then fed into the piezo DI injector through a short stainless steel pipe.

3.3.5 Exhaust System

An austenitic stainless steel pipe is the main part of the testbed exhaust system, which is able to withstand exhaust gas temperatures of up to 980°C and pressures up to 4bar. The exhaust pipe has no sudden/ step changes in pipe diameter in order to keep exhaust flow as smooth as possible and avoid exhaust pressure interfering. There is an automotive type muffler fitted at the exit of the exhaust system. A big muffler is selected to minimise the back pressure. A butterfly valve is installed before the muffler to control the exhaust back pressure. It is actuated by a servo motor and can be remotely adjusted on the testbed computer.

A K-type thermocouple is fitted in the exhaust port to measure the exhaust port temperature since the more accurate PRT cannot withstand the high exhaust temperature. A Druck PTX1400 0-10bar low speed pressure sensor located downstream of exhaust port monitors the mean exhaust pressure. In order to analyse the gas exchange process, a Kistler 4005B type piezoresistive absolute pressure sensor with a water cooling adapter is installed 100mm downstream of exhaust ports for transient exhaust pressure recording, its specification as shown in Figure 3.9. Two automotive type Universal Exhaust Gas Oxygen (UEGO) lambda sensors are fitted on the exhaust pipe. The first one is connected to ECU for closed-loop control of lambda while the second one is used to double check the lambda reading. A few more sampling ports are placed on the exhaust pipe for gaseous emissions and smoke number measurements using a Signal Ambitech Model 443 Chemiluminescent NO/NOx Analyser, a Signal Rotork Model 523 FID HC Analyser, a Horiba MEXA-554JE for measuring the CO, CO_2 and O_2 concentration, and AVL 415SE Smoke Meter for getting the smoke number.

Kistler 4005BA10FA0

Range	0 - 10 bar abs
Pressure range	0 - 10 bar abs
Temperature range	-20 - 125 degC (1100deg C w/cooling adapter)
Linearity	± 0.2%
Size	M5 (M10 w/cooling adapter)
Construction	316 Stainless Steel
Warm up	30 mins
Output	0 - 10V

Figure 3.9 Kistler 4005BA10FA0 Piezoresistive Absolute Pressure Sensor

3.3.6 Intake System

The main part of the intake system is an external boost rig which is set up to provide sufficient pressurised air for the single cylinder engine running. It consists of a Compair HV22RS AERD hydrovane compressor which is driven by a 22kW electric motor, a refrigerant dryer unit, a five micron oil filter and a 272 litres receiver.

The refrigerant dryer is connected to the outlet of compressor to provide air at a consistent humidity for all test work. It dries the air to a humidity level of less than 3% according to the manufacture instruction and cools the air down to approximate 3°C.

The compressor delivers a nominal flow rate of 3.53m^3/min effective at 6 bar absolute pressure and it delivers air at a minimum pressure of 6bar. There is a 272 litres receiver downstream of the refrigerator which stores the dried air and also keeps air supply pressure stable. The rig controller automatically switches on/off the compressor to keep the air pressure in the receiver between 6.5 to 7.0barA. The air pressure is then regulated down to the required pressures for engine running by means of a Parker Hannifin EPDN4 closed-loop controlled pressure regulator located downstream of the receiver.

A 3kW Secomak 632 intake air heater is utilised downstream of the pressure regulator to elevate air temperature to a desired value that is more representative for the charge temperature after the inter-cooler in boosted gasoline engines. The next component in the system is an accumulator which is a 40l stainless steel cylindrical pressure vessel. A K-type thermocouple monitors the air temperature in the accumulator and provides feedback to an Eurotherm PID control unit which controls the intake air heater.

The large volume of the air accumulator allows it to function as a damper to minimise the air pressure fluctuation upstream of the next component, which is a Bosch DV-E5 40mm automotive type electronic throttle controlled by the ECU. A Bosch automotive type boost pressure and temperature sensor is located between the air accumulator and the throttle body, which provides the pressure input for the ECU to adjust the Parker pressure regulator to set desired boost pressure before the throttle body.

The throttle body is the second stage of air pressure regulator in the system, which sets the intake port pressure for engine to achieve the target load. To mitigate the pressure

wave after the throttle body, a large and long pipe is used between it and engine intake ports. On this part of pipework, there is a Bosch automotive type air mass flow meter used for the ECU to measure the air mass flow, and a manifold pressure and temperature sensor for the ECU to get the air temperature and pressure post throttle.

Finally a PRT is fitted in the intake port to measure the air temperature just before intake valves. Another Kistler 4005B piezoresistive absolute pressure sensor is installed here to acquire the transient intake port pressure for the combustion analyser.

3.4 Engine Management System

An advanced Engine Management System (EMS) is engaged to control the engine and some testbed actuators for engine running and testing. The system is composed of a flexible ECU platform, sensors, actuators, the wiring harness and a computer for operating INCA software.

The core part is the flexible ECU platform developed by MAHLE Powertrain. The ECU hardware has sufficient I/O and processing power to drive all kinds of components. Its software includes “standard” function modules for typical modern engine operation and “special” code can be added when additional controls are demanded. Figure 3.10 shows the flexible ECU, which can communicate with the computer through ETAS INCA software.

Figure 3.10 MAHLE Flexible ECU

Only a few I/O channels of the flexible ECU are used for this experimental study, which are listed in the table 3.3.

Table 3.3 ECU Inputs and Outputs Used

Inputs (Sensors)	Outputs (Actuators)
Exhaust cam position	Exhaust cam phaser
Intake cam position	Intake cam phaser
Boost pressure / temp (Pre-throttle)	Boost pressure regulator
Throttle position	Electronic throttle body
Manifold pressure / temp (Post-throttle)	
Air mass flow meter	DI injector
Exhaust lambda	PFI injector
High pressure fuel rail pressure	High pressure fuel pump
Knock sensor	Ignition coil
Crank sensor	
Coolant temp	
Battery Voltage	

3.5 Data Acquisition System

A Data Acquisition (DAQ) system is developed by Brunel University London for the test data acquisition, which includes the DAQ hardware receiving signals from the sensors and devices and the DAQ software processing the signals, conducting combustion analysis and saving processed data.

3.5.1 DAQ Hardware

Figure 3.11 shows the DAQ hardware. All the signal inputs are logged by three data cards: an eDAM-9015 card used for processing PRT inputs; a NI USB-6210 card used for acquiring low speed signals which include thermocouples, low speed pressure transducers and low speed flow meters as described in the previous sections; a NI USB-6353 card used for high speed signals acquisition as listed in Table 3.4.

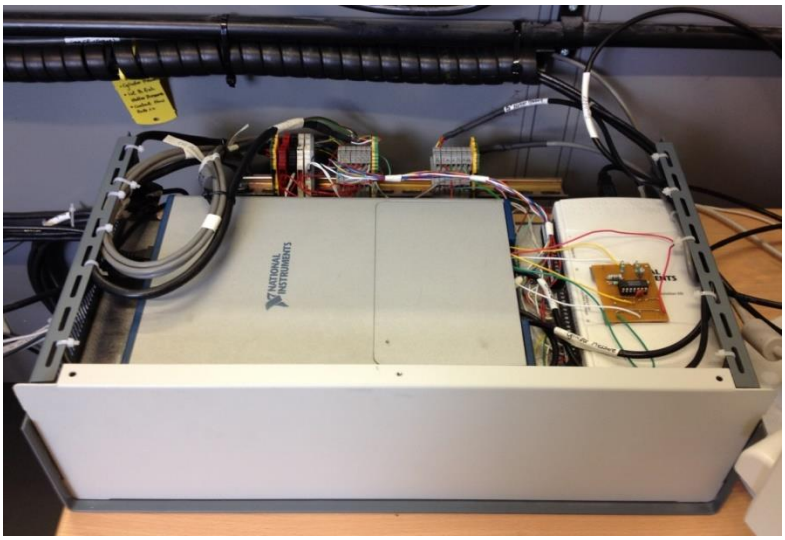

Figure 3.11 DAQ Cards

Table 3.4 High Speed Channels

Measurements	Devices
Exhaust port pressure	Kistler 4005BA10FA0 piezoresistive absolute pressure sensor, with water cooling adapter, plus Kistler type 4618A0 piezoresistive amplifier
Intake port pressure	Kistler 4005BA10FA0 piezoresistive absolute pressure sensor, plus Kistler type 4618A0 piezoresistive amplifier
Cylinder pressure	Kistler 6041B piezoelectric pressure transducer (Figure 3.12), water cooled, plus Kistler type 5011B charge amplifier
Crank angle	Encoder Technology type EB58 optical incremental encoder, fixed to crankshaft, giving crank clock in 0.25 degree resolution
Fuel mass flowrate	Endress+Hauser Promass 83A01 Coriolis mass flowmeter, sensor size DN1 1/24''
Engine brake torque	Dynamometer force cell

Kistler 6041B

Range	0 - 250 bar abs
Pressure range	0 - 250 bar abs
Sensitivity	≈-40 pC/bar
Linearity	± 0.3 %/FSO
Temperature range	-50 - 400 °C
Size	M8
Construction	316 Stainless Steel
Warm up	30 mins
Output	0 - 10V

Figure 3.12 Kistler 6041B Piezoelectric Pressure Transducer

3.5.2 DAQ Software (Combustion Analyser)

Figure 3.13 shows the User Interface (UI) of the DAQ software 'Transient Combustion Analyser' programme which was developed by Dr Yan Zhang in Brunel University London [163]. The programme processes all the signals logged by the three data cards and displays the temperatures, low speed pressures, low speed flowrates and also the fuel mass flow, engine speed and torque, transient pressure traces in intake port, exhaust port and cylinder. In addition, the software performs on-line calculation and display of the heat release, combustion characteristics, engine power out and fuel consumption based on the inputs of engine specification. The software is able to save the data of a number of cycles as defined by the user or in continuous recording mode.

The calculations used in the program regarding heat release, combustion characteristics, and fuel consumption are from [10][164].

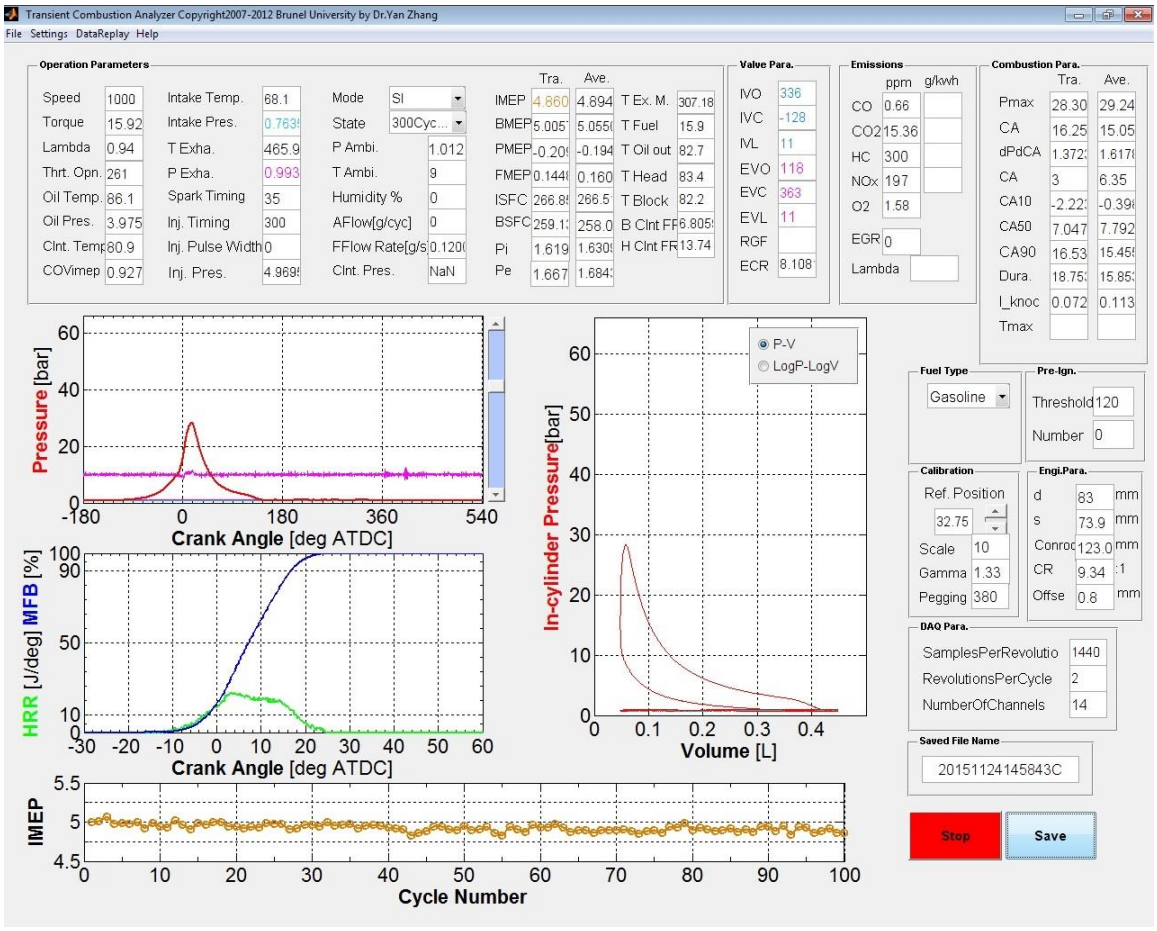

Figure 3.13 Transient Combustion Analyser UI

The Net Indicated Mean Effective Pressure (NIMEP) is calculated by Equation (3-2), which correlates to area A - area B shown in Figure 3.14.

$$\text{NIMEP}=\begin{cases}\int_{-180}^{540}\frac{p}{Vs}\dot{V}(\varphi)d\varphi & (4-stroke)\\ \int_{-180}^{180}\frac{p}{Vs}\dot{V}(\varphi)d\varphi & (2-stroke)\end{cases} \qquad \textbf{3-2}$$

The Gross Indicated Mean Effective Pressure (GIMEP) is given by Equation (3-3), which correlates to area A + area C shown in Figure 3.14.

$$\text{GIMEP}=\int_{-180}^{180}\frac{p}{Vs}\dot{V}(\varphi)d\varphi \qquad \textbf{3-3}$$

Where,

Vs is the engine displacement volume

p is the real-time cylinder pressure

φ is the crank angle, 0 means the firing TDC as shown in Figure 3.13

$\dot{V}(\varphi)$ is the cylinder volume

The Pumping Mean Effective Pressure (PMEP) is defined by Equation (3-4), which correlates to - (area B + area C) shown in Figure 3.14.

PMEP = NIMEP - GIMEP **3-4**

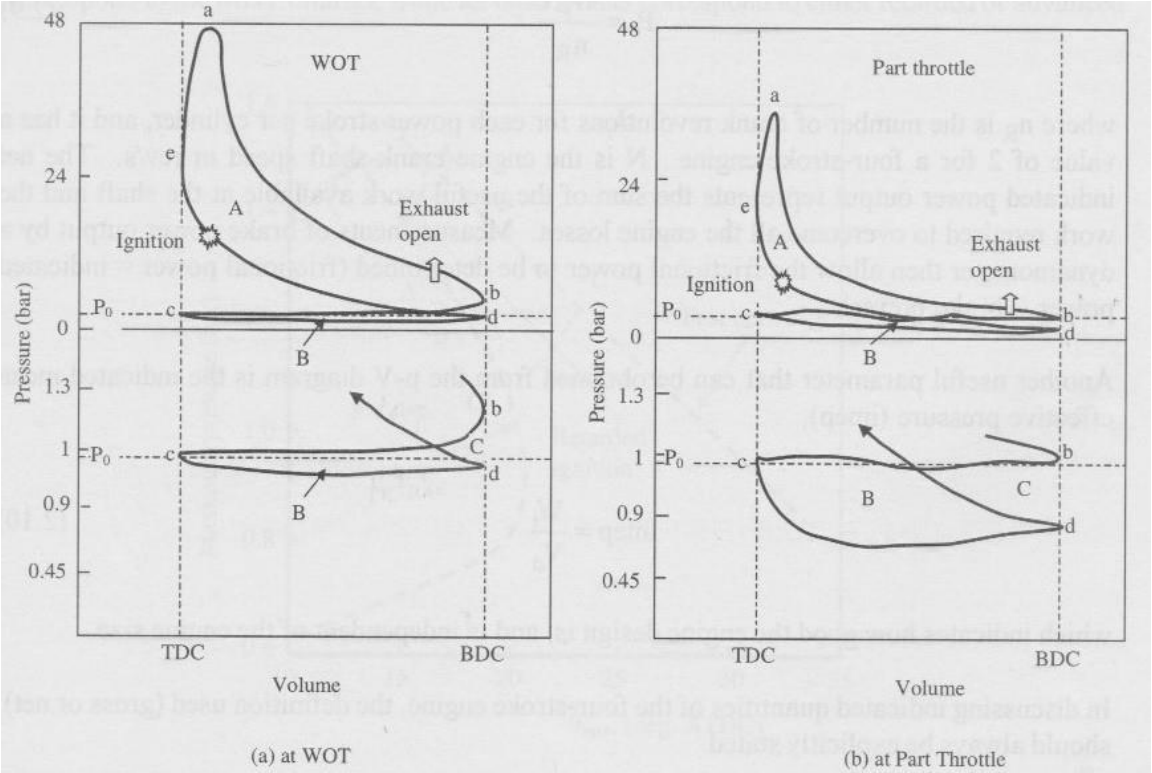

Figure 3.14 p-V Diagrams of a Four-Stroke SI Engine [164]

The Net Indicated Fuel Conversion Efficiency (IEffn), Gross Indicated Fuel Conversion Efficiency (IEffg) and Pumping Indicated Fuel Conversion Efficiency (IEffp) are calculated based on mean effective pressures NIMEP, GIMEP and PMEP and the fuel mass flow consumed by engine, as explained in Figure 3.15. According to Equation (3-4), it is known that IEffn = IEffg + IEffp, which is useful for efficiency breakdown analysis as discussed in the following chapters.

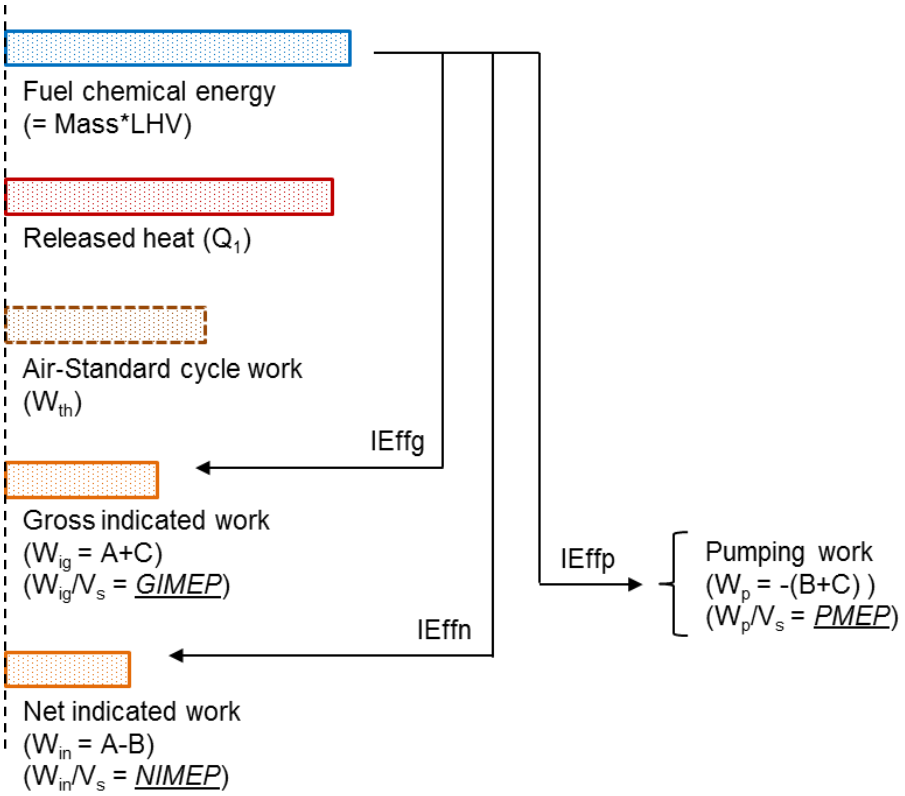

Figure 3.15 Indicated Work and Fuel Conversion Efficiencies

3.5.3 TDC Determination

Correct TDC determination is essential for engine indication process and combustion analysis as small errors in TDC position can cause large errors in the calculations of combustion characteristics. In the experiment a Kistler 2629C capacitive type probe TDC sensor, as shown in Figure 3.16, is used for dynamic determination of engine TDC position providing accuracy within 0.1dCA. However since the resolution of crank encoder is 0.25dCA, the actual accuracy of TDC determination in the system is 0.125dCA.

Figure 3.16 Kistler 2629C TDC Sensor System

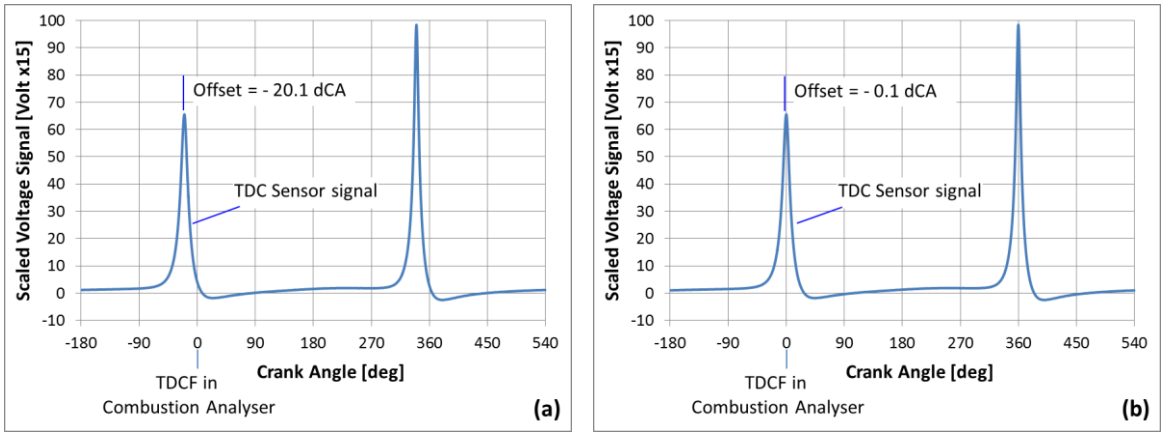

Figure 3.17 TDC Determination for Combustion Analyser TDC Setup

Figure 3.17 shows an example of TDC determination by using the TDC sensor. The peak of sensor signal output means the mechanical piston TDC position. Figure 3.17(a) shows the initial status when there is 20.1dCA offset between piston TDC and zero degree crank angle in the combustion analyser. The offset value of 20dCA is input into combustion analyser. Figure 3.17(b) shows the measurement after the setup. The zero degree crank angle in combustion analyser is set to match piston TDC.

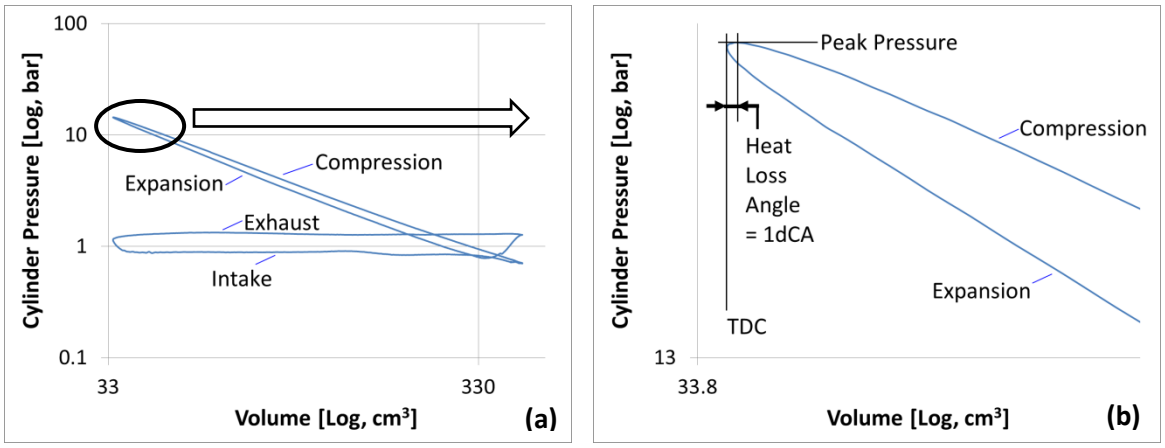

Figure 3.18 Log P-V Diagram from Engine Motoring

Figure 3.18 shows the log P-V diagrams from engine motoring at 1200rpm after combustion analyser TDC is correctly established. As shown in Figure 3.18(b) the peak cylinder pressure occurs slightly before TDC because of heat loss and leakage [164] with a heat loss angle at 1.0dCA in this case.

3.5.4 Pegging

Piezoelectric pressure transducers used for cylinder pressure acquisition respond to pressure differences by outputting a charge referenced to an arbitrary ground. Thus, to quantify absolute pressures, the transducer output must be referenced, or pegged, to a known pressure at some point in the cycle [164]. Randolph summarized nine methods of cylinder pressure pegging [165].

A revised method is used in this study as shown in Figure 3.19. Both the transient intake port pressure and exhaust port pressure, detected by Kistler 4005B piezoresistive absolute pressure sensors, are utilised for cylinder pressure referencing. A variable is given in the combustion analyser software which allows the operator to manually pick up any point on the exhaust port pressure trace for cylinder pressure being matched to. This function moves cylinder pressure upwards or downwards. The variable should finally be set to a suitable value at each testing log to make the cylinder pressure as close as possible to exhaust port pressure during exhaust stroke after EVO and to intake port pressure during intake stroke before IVC. Exhaust port pressure is employed as the

primary reference since intake port pressure can change heavily when engine runs with EIVC or LIVC cam timings.

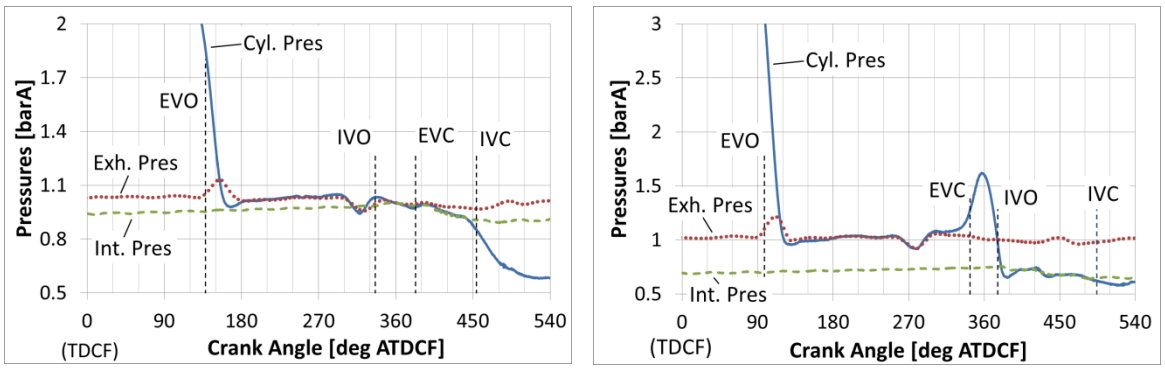

Figure 3.19 Cylinder Pressure Pegging (two examples)

3.6 Test Operation and Data Quality

The engine operation and boundary conditions applied in the experimental study are given in Table 3.5.

Table 3.5 Test Operation and Boundary Conditions

Objective	Description
Engine Speed	Controlled by dynamometer
Engine Load (NIMEP)	Set by adjusting boost pressure and throttle opening
Intake / Exhaust Cam Timing (MOP)	Controlled by ECU : altered for cam timing sweep tests; fixed to optimised settings during other tests
Exhaust Lambda	Controlled by ECU : set to 1.0 except lambda sweep
Rail Pressure	Controlled by ECU
Injection Strategy	Controlled by ECU
Spark Timing	Controlled by ECU : optimised at part load; BLD at high load with knocking combustion
Air Humidity	Dried air, humidity < 3%
Boost Air Temperature	40±3 °C (pre-throttle)
Coolant In Temperature	80±3 °C
Oil In Temperature	85±3 °C

LP Fuel Temperature	20±3 °C
Exhaust Back Pressure	Adjusted by a butterfly valve. Full opening means ambient EBP
Combustion Stability Limit	GIMEP SD ≤ 0.25bar at low load (NIMEP ≤ 2bar); or GIMEP COV ≤4% at loads above 2bar NIMEP

Special attention is given to the data quality for delivering consistent and accurate results through the following activities.

3.6.1 Validation of Cam Timings

Precise control of the cam timings is essential for this experimental study since they have strong impact on Miller cycle operation. Pressure traces as shown in Figure 3.19 are also used for checking the cam and valve timing controls. Intake and exhaust valve opening/closure timings are calculated based on cam profile characteristics and the MOP timings which are controlled and measured by ECU. The valve timings are then identified on cylinder, intake and exhaust pressure traces to validate the controls. This is very important especially after each engine rebuild for camshaft swapping.

3.6.2 Validation of Indicate Pressure and Fuel Flow Measurements

Accuracy of fuel consumption and indicate pressure measurements are critical for this study. The Coriolis mass flow meter is carefully selected. The DN01 1/24" sizing sensor covers a maximum flowrate of 20kg/h for the single cylinder test engine. As shown in Figure 3.20, its measurement error is less than 0.1% in the range of 1kg/h to 20kg/h. The error increases when flowrate becomes below 1kg/h, however it is still less than 0.5% when the flowrate is as low as 0.2kg/h. The flow meter was calibrated by the manufacturer before delivery. The calibration was double checked in the university laboratory by using an accurate scale before the flow meter was integrated into the testbed system. The calibration validation data is given in the appendix of the thesis.

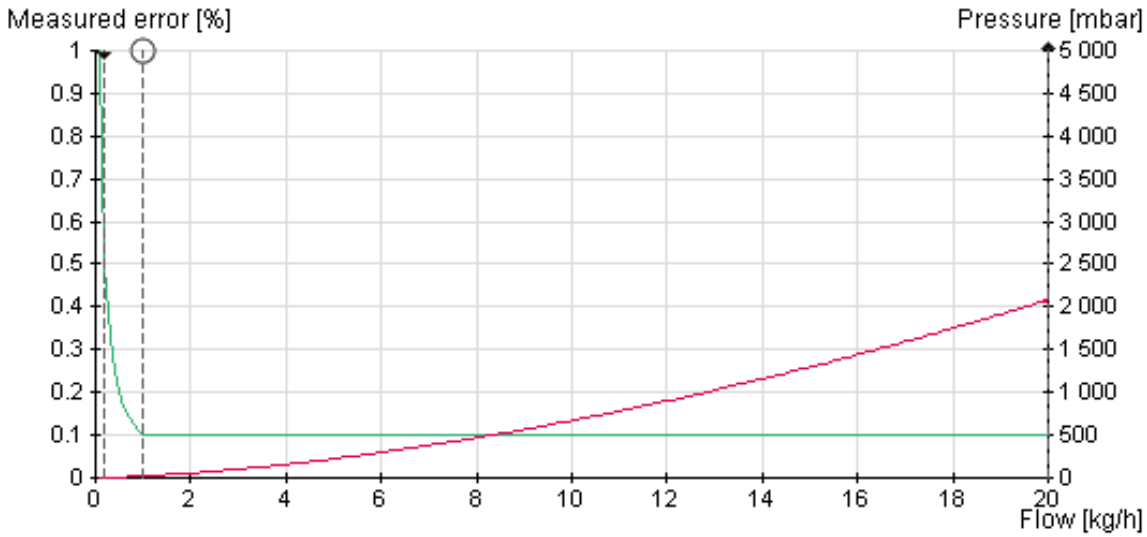

Figure 3.20 Endress+Hauser Promass 83A01 DN01 Measurement Error

In addition to the efforts to deal with TDC setup and pegging as discussed previously, the following actions are taken to minimise the error of indicate pressure detection:

- Kistler transient pressure transducers were calibrated/checked regularly on the dead weight tester;
- Kistler intake / exhaust absolute pressure transducers and their amplifiers were checked and "Zero" adjusted every day according to local barometric pressure reading;
- The Kistler exhaust pressure transducer was cleaned regularly by using an ultrasonic cleaner to avoid carbon accumulation on the detection surface;
- A motoring test was conducted every day at fixed conditions as given in Table 3.6 to check the consistency of peak cylinder pressure (Pmax) and heat loss angle (crank angle of Pmax). The test monitors the status of both engine health and measurement system, especially crank angle encoder and indicate pressure.

Consistency and accuracy of all other measurements were also monitored. All emission analysers were calibrated every day by using high standard pure air as zero gas and specific span gas supplied by BOC.

3.6.3 Daily Checks

Three daily check logs were taken every day before starting formal testing:

- Zero Log: taken after daily calibration activities completed to check the baseline measurement of all channels
- Daily Motoring Log: taken after engine warmed up to desired temperatures for monitoring the indicate measurement
- Daily Running Log: taken when engine runs at fixed operating condition to check the consistency of whole test system and engine health.

Conditions for Daily Motoring Log and Daily Running Log are given in Table 3.6. Figure 3.21 shows an example of the tracks of Daily Motoring Logs.

Table 3.6 Test Conditions for Daily Checks

Objective	Daily Motoring	Daily Running
Engine Speed	1200 rpm	2000 rpm
Engine Load	Throttle fully open (barometric intake pressure)	NIMEP = 4.6 bar
Intake / Exhaust Cam Timing (MOP)	Minimum valve overlap	Minimum valve overlap
Exhaust Lambda		1.0
Rail Pressure		92 bar
Injection Strategy		Single injection, SOI = 320 dCA BTDCF
Spark Timing		CA50 = 8 dCA ATDCF
Air Humidity	Dried air, humidity < 3%	Dried air, humidity < 3%
Boost Air Temperature	40±3 °C (pre-throttle)	40±3 °C (pre-throttle)
Coolant In Temperature	80±3 °C	80±3 °C
Oil In Temperature	85±3 °C	85±3 °C
LP Fuel Temperature		20±3 °C
Exhaust Back Pressure		Ambient EBP

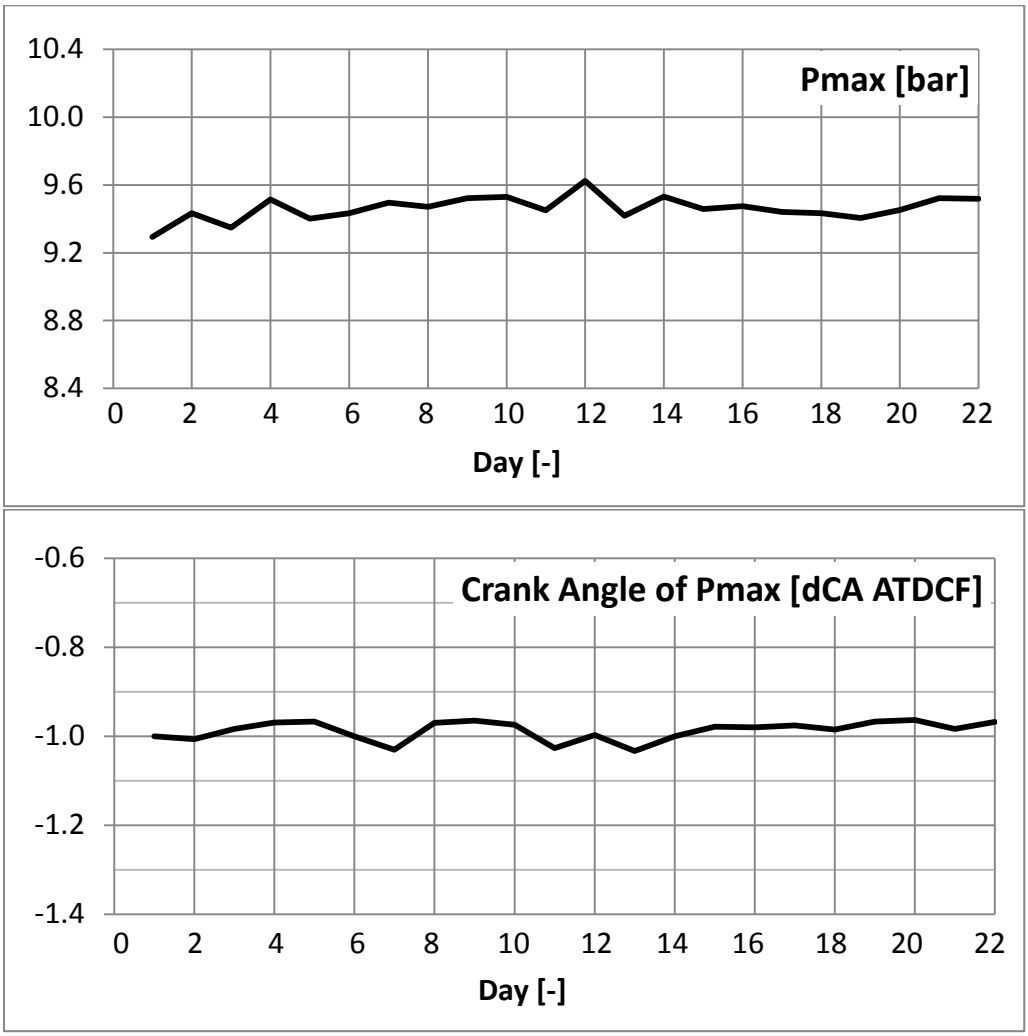

Figure 3.21 Track of Daily Motoring Logs (an example)

3.7 Summary

This chapter presented the details of the single cylinder engine testbed and all the facilities used for all the experimental tests, including the single cylinder gasoline engine with DI and PFI dual fuel injection systems and intake / exhaust cam phasers, fluids supply and conditioning systems, intake and exhaust system. The research methodology is presented and discussed. Operation principle of key devices and calculations used in the combustion analyser were also explained. Special efforts taken to ensure data quality was presented.

Chapter Four

Synergy between Boosting and Valve Timings with Miller Cycle Operation

Chapter 4 Synergy between Boosting and Valve Timings with Miller Cycle Operation

4.1 Introduction

Miller cycle is typically achieved in an engine with reduced effective Compression Ratio (CR) through either Early Intake Valve Closing (EIVC) or Late Intake Valve Closing (LIVC). Most Miller cycle engines apply boosting technologies to maintain the power performance. As described in Chapter 3, three intake camshafts for standard, EIVC and LIVC cam profiles were designed and tested. Twin independent Variable Cam Timing (VCT) phasers were used to provide further valve timing variations for this research, as shown in Figure 3.3. An external boost rig was used to provide adjustable pressurized air charge, allowing conditions of up to 4000rpm and 25.6 bar NIMEP to be studied. This chapter presents the experimental results obtained in the single cylinder engine at ambient exhaust back pressure condition and discusses synergies between valve timings and boost at a compression ratio 9.3:1, which is described as the Low Compression Ratio (LCR) in the thesis. Miller cycle operations at a higher compression ratio and high exhaust back pressure will be discussed in Chapter 5 and Chapter 7.

4.2 Overview of Optimised Valve Timings and Fuel Consumption Improvement

As explained in Chapter 3, ten steady state operation points were selected to carry out tests with all three camshafts. Firstly, intake and exhaust cam timings were changed to optimize fuel consumption at each operation point for each camshaft. The Net Indicated Specific Fuel Consumption (ISFCn) is used to assess fuel consumption of the single cylinder test engine. All tests were carried out at the same boundary conditions as described in Chapter 3, including a combustion stability limit of 0.25bar Standard Deviation of GIMEP (GIMEP SD) at low load or 4% Coefficient of Variation of GIMEP (GIMEP COV) when engine load is above 2.0bar NIMEP. Optimized ISFCn results of standard cam, EIVC cam and LIVC cam were compared and analysed to understand the effect of valve timings and Miller cycle operation on the fuel consumption of the engine at different speeds and loads.

Figure 4.1 shows the optimized cam timings for each cam profile at the low CR setup. The red lines indicated the middle of intake cam timing adjustment range. Cam timing is determined by the valve Maximum Opening Point (MOP) in the engine control system. The three diagrams on the left are the optimised exhaust cam timings when testing with each intake cam profile. The MOP of the exhaust valves was varied in a range from 140dCA to 100dCA BTDCNF via the exhaust cam phaser. Exhaust cam timings at the optimum ISFCn for all three cams throughout the whole minimaps are almost the same, i.e. at the most retarded timing 100dCA BTDCNF, because of the higher effective expansion ratio of the retarded Exhaust Valve Opening (EVO) and hence better fuel economy.

The three diagrams on the right in Figure 4.1 are the optimised intake cam timings for each intake cam. The intake cam phaser allows 40dCA of maximum cam timing adjustment, as illustrated in Figure 3.3. The intake MOP is from 120dCA to 80dCA ATDCNF for standard cam, from 75dCA to 35dCA ATDCNF for EIVC cam and from 144dCA to 104dCA ATDCNF for the LIVC cam. As a result, there is a large range of variation in Intake Valve Closing (IVC) timings among the three intake cams. It directly affects the effective CR in Miller cycle operation among the three intake cam profiles. The effective CR is defined by the ratio of cylinder volume at IVC to the clearance volume at TDC. In addition, the Miller Cycle Ratio (MCR) was introduced in Chapter 3 to measure the effect of IVC timings on the Miller cycle as defined by Equation (3-1).

As shown in Figure 4.1, different intake cam timing strategies are required among the three intake cams for the optimum ISFCn. The main cause is optimised IVC timings depend greatly on the cam profile design and vary with the engine speed and load, especially with the EIVC and LIVC cam profiles which have been designed to achieve a largely reduced effective CR for Miller cycle operation.

In addition, the valve overlap period is changed when the Exhaust Valve Closing (EVC) and Intake Valve Opening (IVO) timings are varied. As mentioned above, the optimised exhaust MOP timing is the most retarded position almost for all three cams at all test points. Thus the valve overlap is mainly decided by the IVO timing. When the intake cam timing is altered by the cam phaser, the IVO timing and valve overlap are adjusted, while the IVC timing and consequently the effective CR are changed simultaneously.

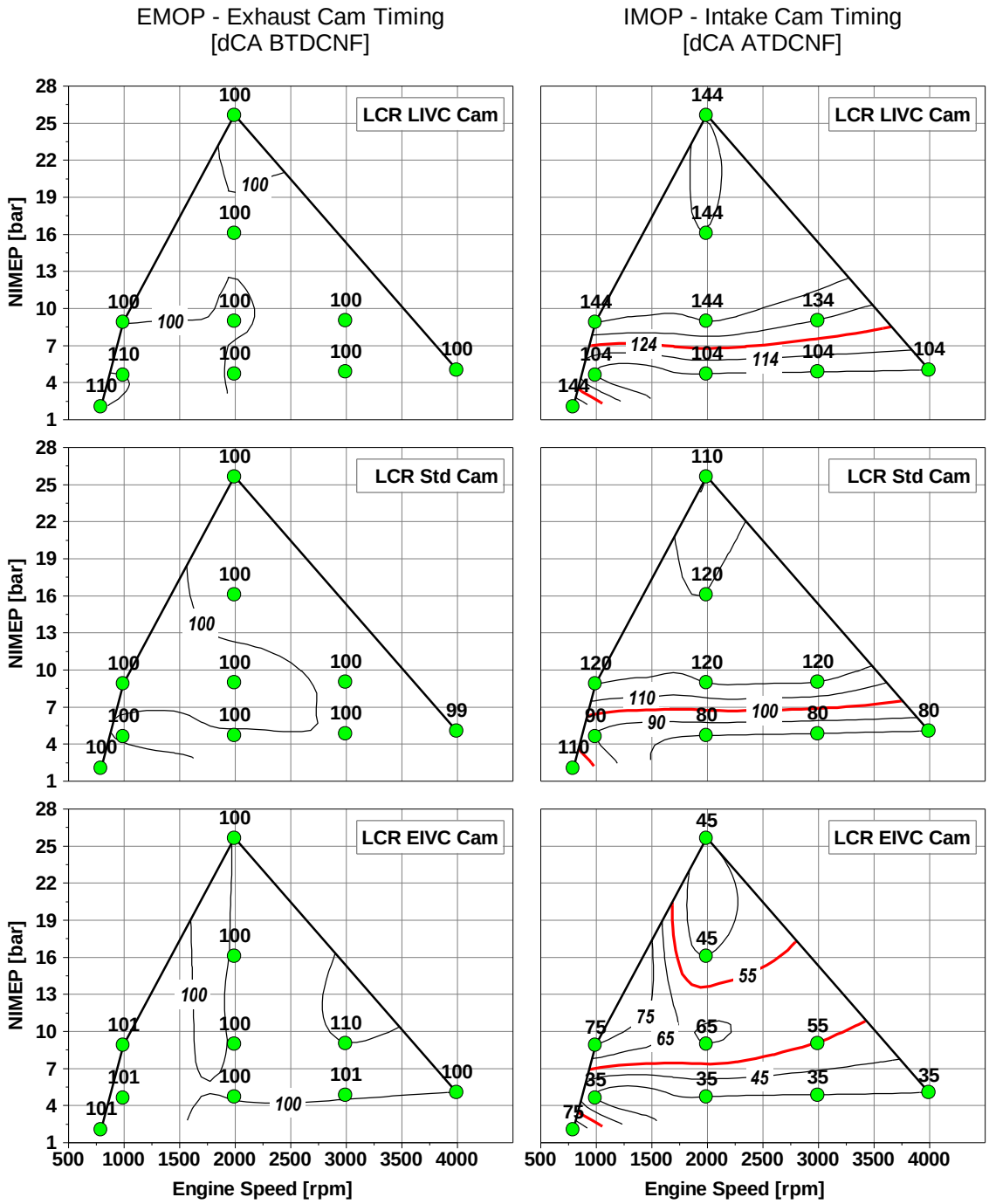

Figure 4.1 Optimised Cam Timings at Low CR

For standard and LIVC cam profiles, retarded cam timing moves the IVC timing away from Bottom Dead Center (BDC), resulting in a reduced effective CR and thus increased Miller cycle ratio. For EIVC cam, the situation is reversed. The lower effective CR and higher Miller cycle ratio are achieved by advancing IVC before BDC.

Therefore, when intake and exhaust cam timings were swept and optimised, their impact on the engine performance were caused by the change in the valve overlap and Miller

cycle ratio, which are dominated by intake valve timings as discussed above. Figure 4.2 shows the Miller cycle ratio and valve overlap associated with the optimised cam timings. The dotted lines in the left three diagrams are scavenging pressures, which is the difference between intake port pressure and exhaust port pressure in each test. When both the scavenging pressure and valve overlap were positive, some of the intake air was used to scavenge the in-cylinder residual gas to minimise the residual gas concentration.

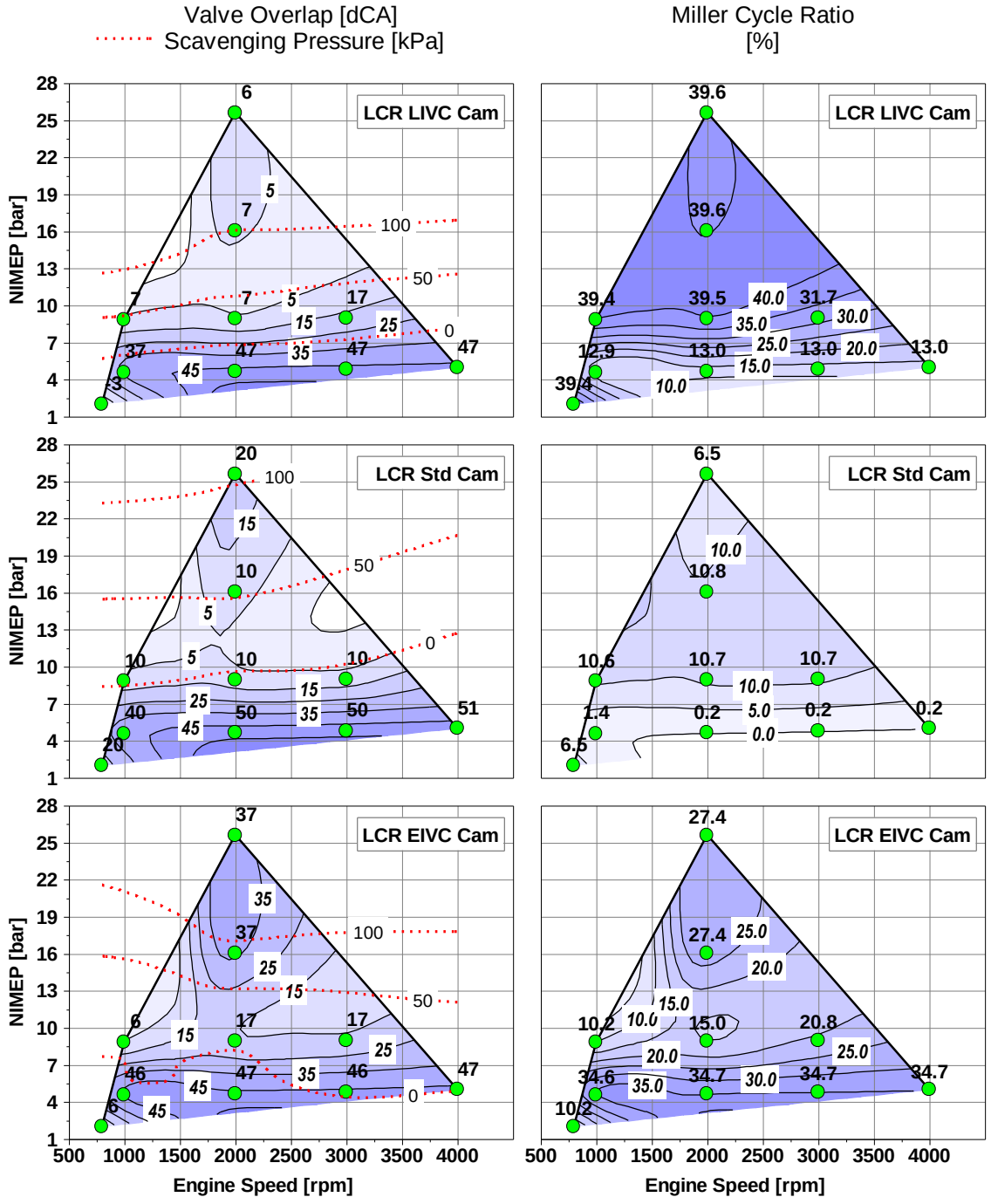

Figure 4.2 Valve Overlap, Scavenging Pressure and Miller Cycle Ratio at Optimised Cam Timings

For all three intake cam designs, a small overlap is required for optimum ISFCn at 800rpm 2.0bar NIMEP. Maximum valve overlap is used to get the best fuel consumption at 5.0bar NIMEP at different engine speeds. As the load is increased to 9.0bar NIMEP, less valve overlap periods are needed to get the minimum fuel consumption. Another common feature of the results obtained with the three intake cams is the high Miller cycle ratio (MCR) at higher load operations for optimising fuel consumption. In the cases of the standard and long LIVC cam designs, retarding the IVC away from BDC results in higher MCR but less valve overlap. For the shorter EIVC cam, retarding the IVC towards BDC leads to both lower MCR and shorter valve overlap period and vice versa.

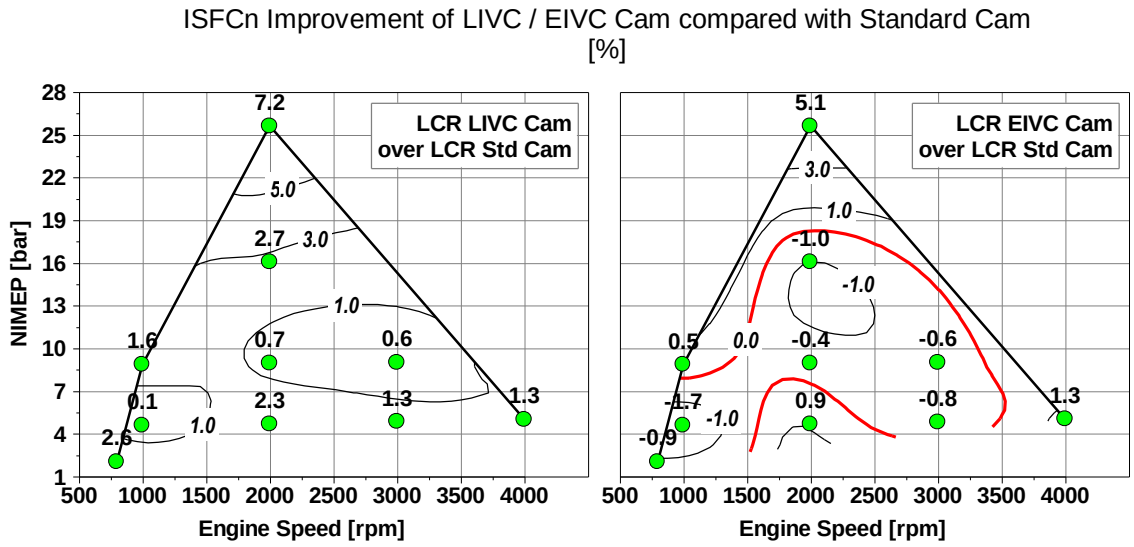

Figure 4.3 ISFCn Improvement of LIVC / EIVC Cam compared to Standard Cam at Low CR

Figure 4.3 shows the percentage improvement in ISFCn obtained by using LIVC and EIVC cams over the standard cam. Both LIVC and EIVC cams improve fuel consumption significantly at the full load point. The LIVC cam improves ISFCn by 7.2% at 2000rpm 25.6bar NIMEP, while the EIVC cam achieves 5.1% reduction of ISFCn at the same point compared with standard cam profile. The LIVC cam also leads to improvement in fuel consumption at low to mid load area while the EIVC cam has the worst fuel economy at this area.

In order to understand the contributions to the fuel consumption improvement, a breakdown of indicated efficiencies is presented in Figure 4.4. The Net Indicated Fuel Conversion Efficiency (IEffn), Gross Indicated Fuel Conversion Efficiency (IEffg) and

Pumping Indicated Fuel Conversion Efficiency (IEffp) are calculated based on mean effective pressures (NIMEP, GIMEP and PMEP) and fuel mass flowrate consumed by engine, which were explained in Chapter 3.

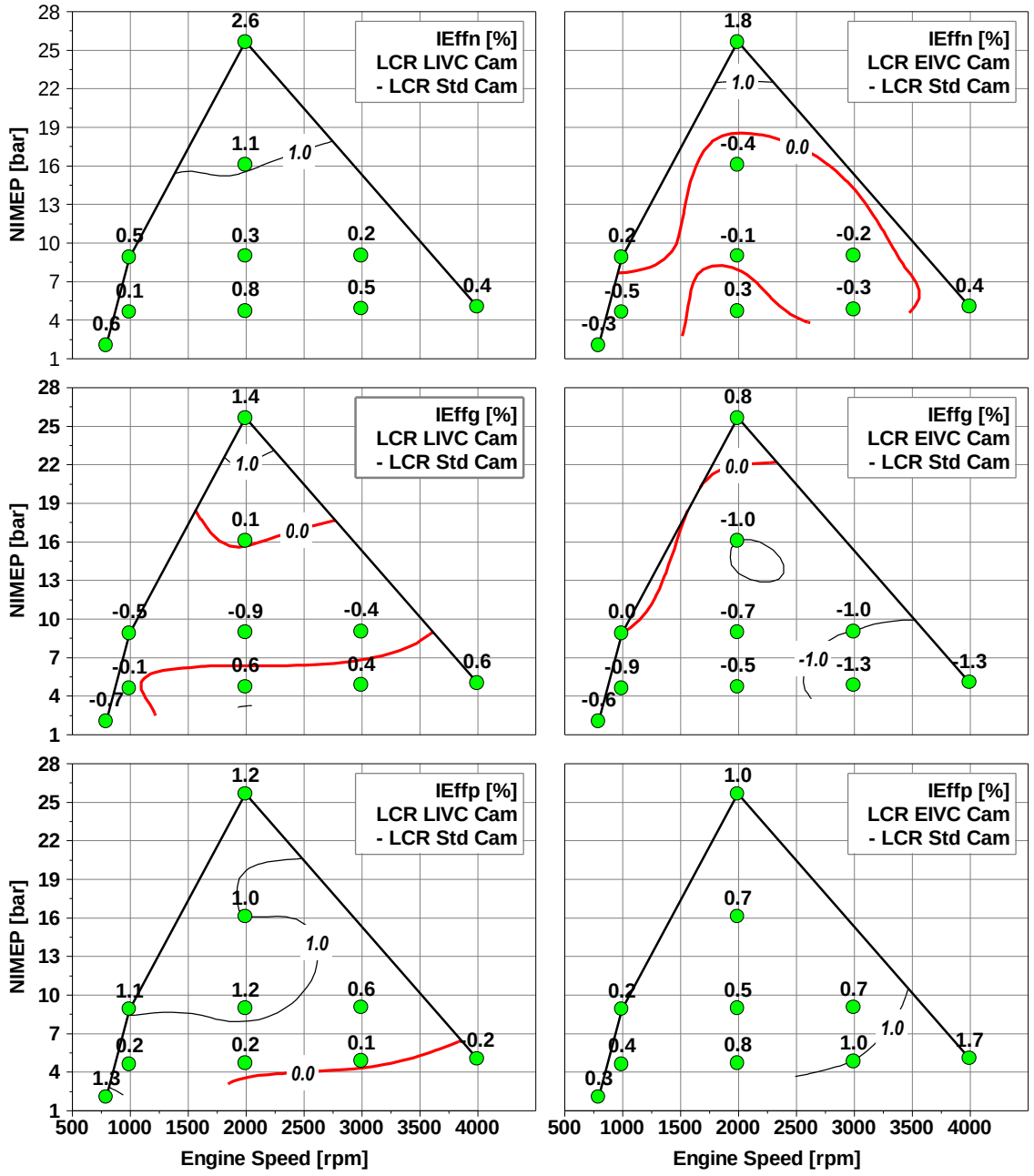

Figure 4.4 Differences between Indicated Efficiencies of LIVC / EIVC Cam and these of Standard Cam at Low CR

Net indicated efficiency minimaps have the same trends as ISFCn minimaps as shown in Figure 4.4. In most part-load region, LIVC and EIVC cams have worse gross indicated efficiencies than the standard cam because of the reduced effective CR. Both of them achieve around 1% higher IEffg compared to standard cam at 2000rpm 25.6bar NIMEP.

Both cams gain higher pumping indicated efficiencies than the standard cam throughout the whole minimaps, due to less pumping loss at low load and more positive pumping work at high load. In the following sections, test results will be analysed and discussed in details to understand the fundamentals of these contributions.

4.3 Impact of Exhaust Valve Timing

As shown in Figure 4.1, late exhaust cam timing is applied for optimum ISFCn at the whole operation minimaps with all three intake cams. Figure 4.5 shows all cam envelope test data acquired at ten operation points with three intake cams. When the exhaust cam timing (EMOP) retarded from 140dCA to 100dCA BTDCNF, the gross indicated efficiency (IEffg) increases as the overall trend.

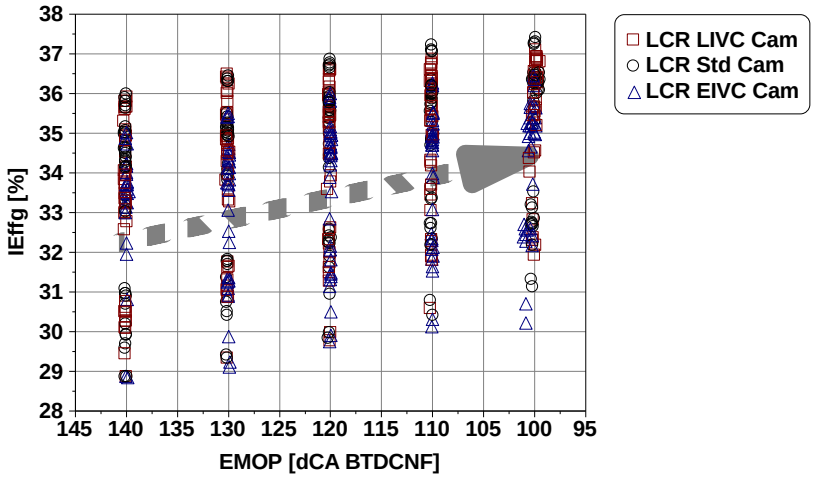

Figure 4.5 Cam Envelope Logs at Ten Test Points with Three Intake Cams

Figure 4.6 shows the exhaust cam timing adjustment and related cylinder pressure trace at 2000rpm 4.6bar NIMEP. As found in practice, 0.5mm valve lift is the best point to represent the valve opening and closing points on this engine. When EMOP is changed from the earliest to the latest timing over the range of 40 degree crank angles, the exhaust valve opening (EVO) is retarded from 80dCA to 40dCA before BDC. It leads to significant reduction of exhaust blowdown loss and increase in the expansion work, which is the main contribution to the improved IEffg as shown in Figure 4.5. On the single cylinder engine, the exhaust cam timing is adjusted by the cam phaser. It means the EVC and valve overlap will change simultaneously when EVO is adjusted. Since the EVC timing and valve overlap have big impact on engine operation and performance, it

is difficult to analyse the exact and single effect of EVO timing. However the impact of EVO timing on IEffg and expansion work discussed here will be important for later discussions.

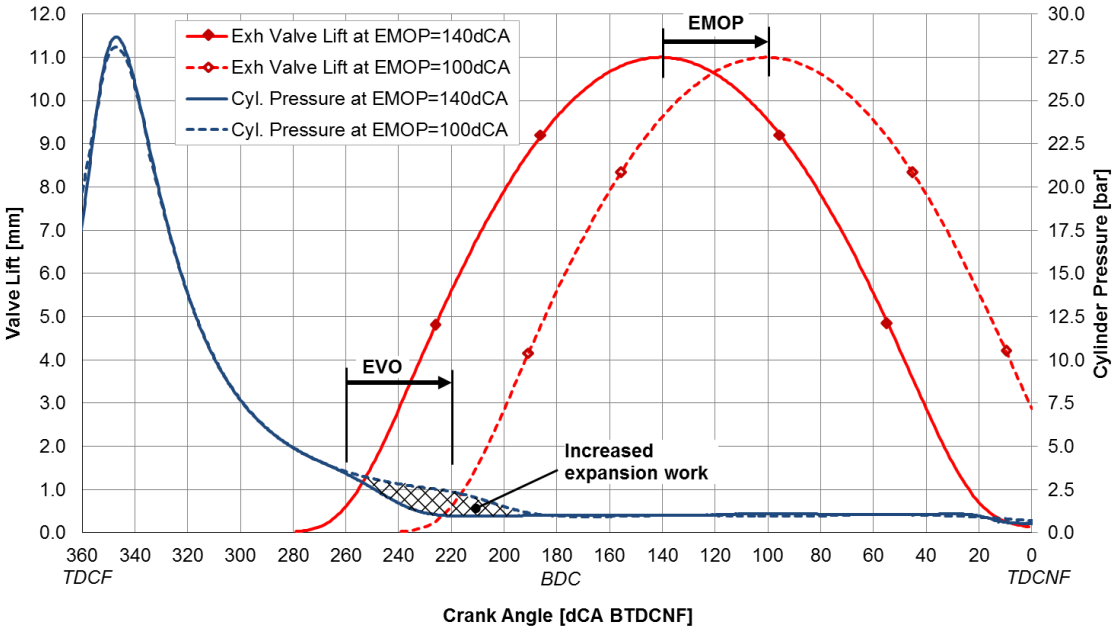

Figure 4.6 Exhaust Cam Timing Sweep and Related Cylinder Pressure Curve at 2000rpm 4.6bar

4.4 Impact of Valve Timings at Idle Operation

The operation at 800rpm and 2.0bar NIMEP is the minimum engine speed and load that the single cylinder engine could run and referred as the idle operation point in this study. As shown in Figure 4.1 and 4.2, the intake cam timing is retarded for less valve overlap at this point with all three cams. Figure 4.7 shows the results of cam envelope test carried out at the idle operation with all three intake cams. When valve overlap is increased above 10dCA, the ignition delay from spark timing to CA10 gets longer. Combustion stability becomes worse than the threshold and the percentage of cycles with misfire increases rapidly. Consequently both HC and CO emissions increase but NOx and exhaust temperature drops. As there is a large depression in the intake port during the idle operation, lots of burned gas will be sucked into intake manifold during the valve overlap period and flow back into the cylinder during the intake stroke, resulting in very high Residual Gas Fraction (RGF). This is the reason for deteriorated combustion and emission with a larger overlap at the idle operation.

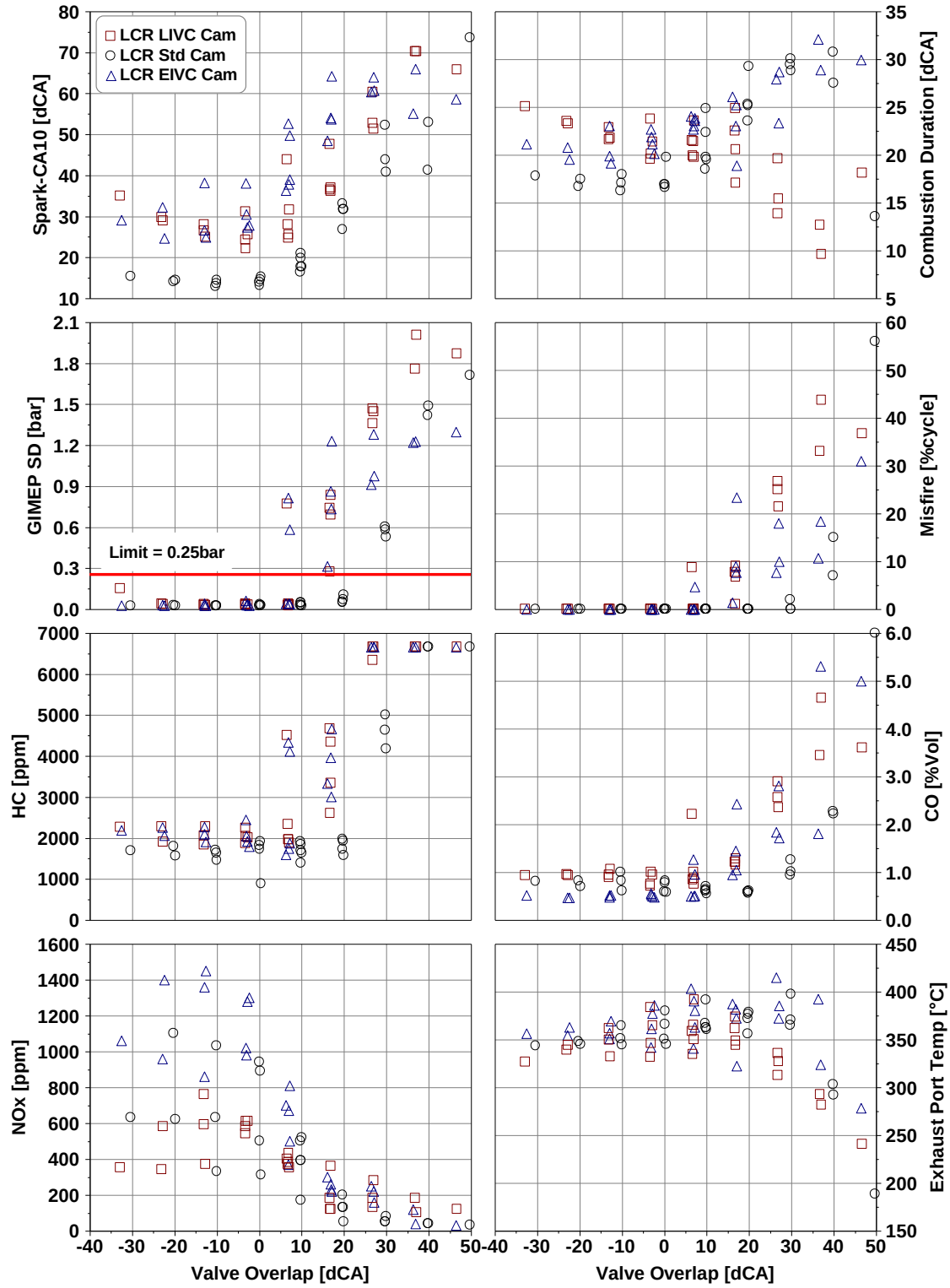

Figure 4.7 Cam Envelope Logs at 800rpm 2.0bar NIMEP with Three Intake Cams

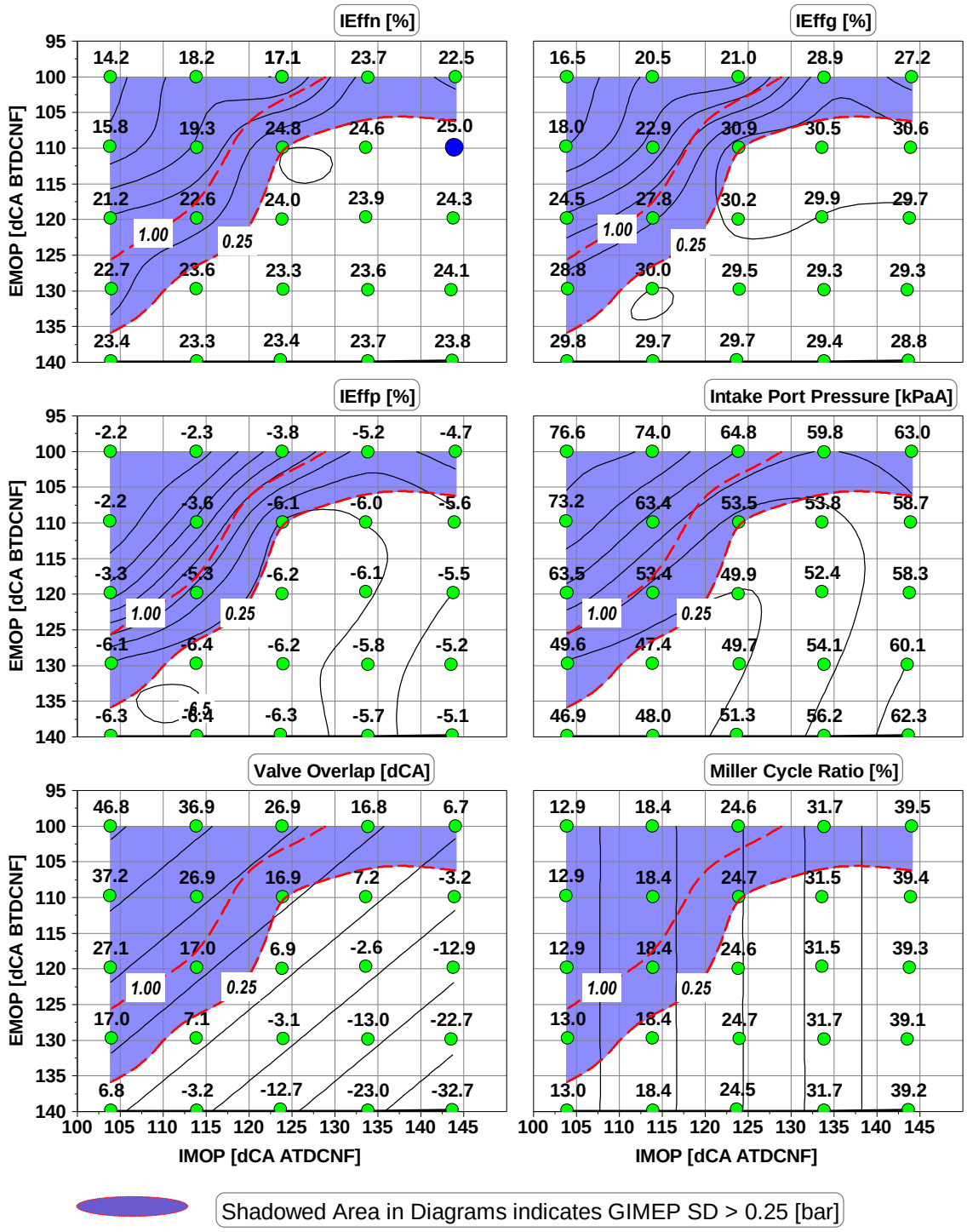

Figure 4.8 Cam Envelope Results at 800rpm 2.0bar NIMEP with LCR LIVC Cam

Figure 4.8 shows the cam envelope test results at idle operation with LCR and LIVC cam configuration. When IMOP is 144dCA ATDCNF and EMOP is 110dCA BTDCNF, the engine operates at the optimized Net Indicated Efficiency (IEffn) of 25%. The shadow area in diagrams shows that GIMEP SD is over the limit of 0.25bar, which occurs when the engine runs with positive valve overlap and becomes worse as the valve overlap

increases. Only the test results with GIMEP SD below 0.25bar are compared. As discussed previously, retarded exhaust valve timing is better for Gross Indicated Efficiency (IEffg). As shown in the IEffg contour, when EMOP is 110dCA BTDCNF, there are two points within the GIMEP SD limit. Their IEffg values are of the highest at 30.5%. When IMOP is retarded from 134dCA to 144dCA ATDCNF, the engine runs at increased Miller cycle ratio from 31.5% to 39.4%. Intake port pressure increases from 53.8kPa to 58.7kPa, consequently the Pumping Indicated Efficiency (IEffp) is improved from -6.0% to -5.6%. The combined effect of similar IEffg and improved IEffp contributes to the optimum IEffn at the selected cam timing setting.

Similar cam envelope optimisation results for EIVC cam is presented in Figure 4.9. In the white area within the GIMEP SD limit, IEffg is highest at 30.7% when IMOP is 75dCA ATDCNF and EMOP is 100dCA BTDCNF, which are the selected optimum cam timings. Miller cycle ratio and intake port pressure are reduced when IMOP is retarded for less valve overlap. This is different from the LIVC cam as explained in Chapter 3. The point with optimum cam timings doesn't have the best IEffp, however IEffg is the dominant contribution to final fuel consumption for EIVC cam at idle.

Figure 4.10 shows the cam envelope data with standard intake cam profile. The combination of optimum cam timing of 110dCA ATDCNF for IMOP and 100dCA BTDCNF for EMOP has the highest IEffg 31.3% because of later EMOP and EVO timing. It also has higher IEffp than the test point with the same EMOP but 120dCA ATDCF for IMOP. There are some visible differences between the standard cam and the other two Miller cycle cam profiles. Firstly the shadowed area with GIMEP SD above 0.25bar limit is smaller than those of EIVC and LIVC cam. Both Miller cycle cams can reduce the large scale flow motion during the intake process and lead to weaker turbulence than the standard cam. The stronger turbulence can benefit the ignition and flame propagation with standard cam, resulting in better combustion stability. This is proved by the diagrams of spark to CA10 duration and combustion duration in Figure 4.7. For all results in the range of valve overlap less than 10dCA, the standard cam has shorter ignition delays than the other two cams by about 10dCA and also faster burn rate.

The results also show that both residual gas fraction (RGF) and Miller cycle ratio (MCR) have an impact on the intake port pressure and IEffp. When the engine runs with a higher MCR, the intake pressure needs to be increased. When the valve overlap is large, both RGF and intake pressure becomes higher, resulting in low pumping loss. For the LIVC

and EIVC cams, the Miller cycle operation can have stronger influence than the valve overlap or RGF. For the standard cam, Miller cycle effect is significantly smaller. When IMOP is retarded from 110dCA to 120dCA ATDCNF at the same EMOP of 100dCA BTDCNF, MCR increases by 4% to 10.6% but valve overlap is reduced by 10dCA. As a result intake port pressure drops and IEffp becomes worse.

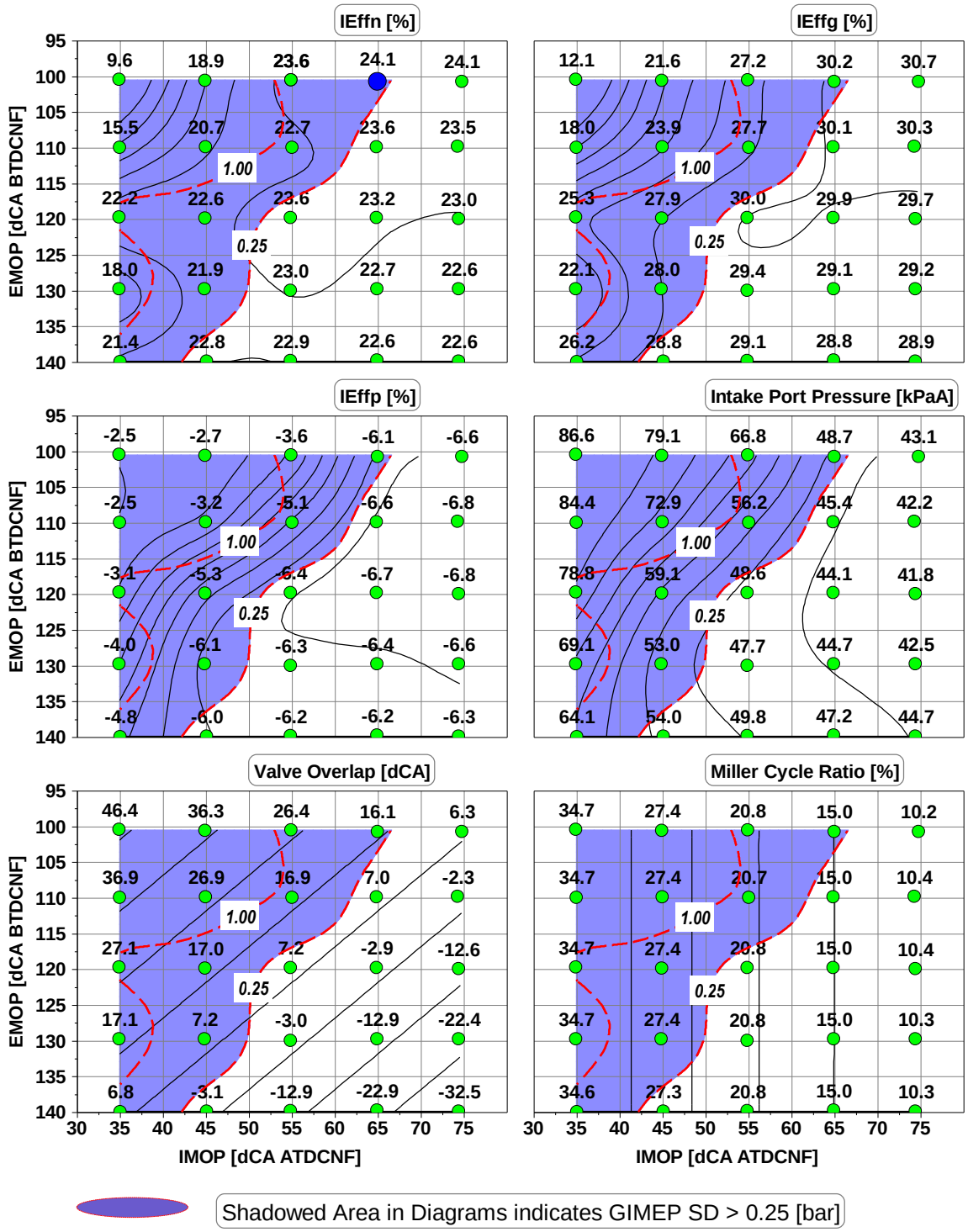

Figure 4.9 Cam Envelope Results at 800rpm 2.0bar NIMEP with LCR EIVC Cam

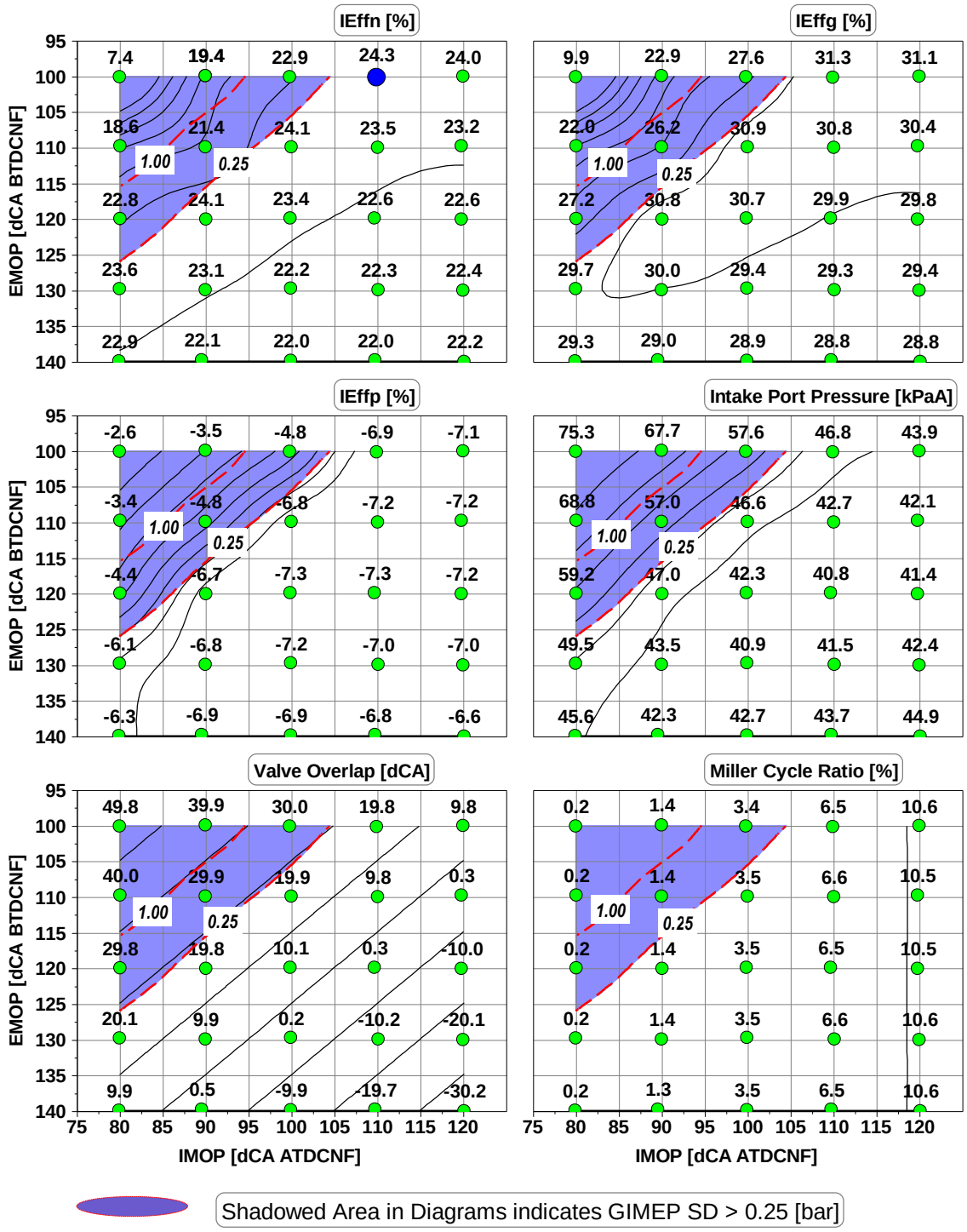

Figure 4.10 Cam Envelope Results at 800rpm 2.0bar NIMEP with LCR Standard Cam

As shown in Figure 4.3, LIVC cam improved ISFCn by 2.6% while EIVC cam made it worse by 0.9% compared with standard cam at this very low load point. This is further discussed in Figure 4.11 by comparing the optimised results among the three intake cams. As mentioned previously, when the intake cam timing is retarded for less valve overlap,

LIVC and standard cams increase Miller cycle ratio while EIVC reduces MCR. In the optimised results, LIVC cam has highest the MCR of 40%. Its effective CR is only 5.5, thus IEffg of LIVC cam is the lowest among the three cams. EIVC has slightly higher MCR than the standard cam, and consequently its effective CR is lower by 0.5. However the combustion duration for EIVC cam is also longer than standard cam because of the known weak in-cylinder turbulence with a reduced valve lift. Finally EIVC achieves a lower IEffg than standard cam by 0.6%.

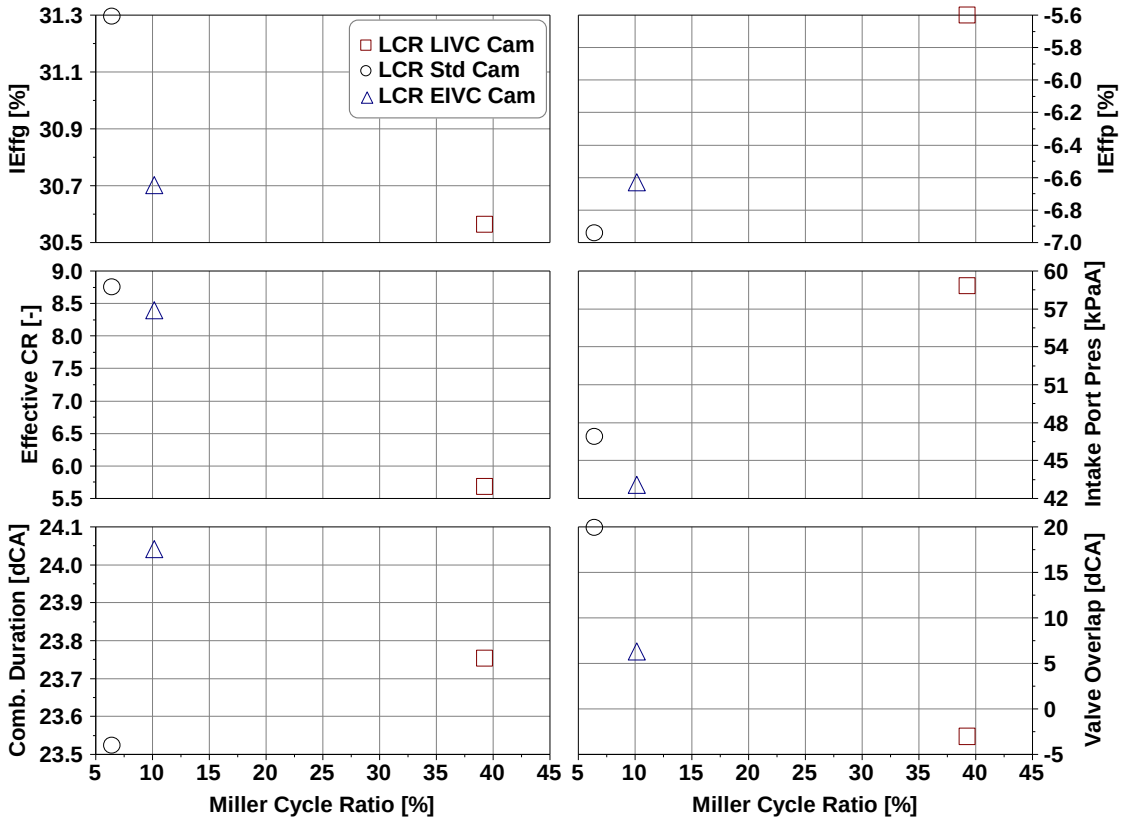

Figure 4.11 Comparison of the Optimised Results of Three Intake Cams at 800rpm 2.0bar NIMEP

LIVC cam runs at the highest MCR thus it needs more than 10kPa higher intake pressure than the standard cam and EIVC cam, which improves IEffp by 1.3% and IEffn by 0.6% respectively compared to the standard cam, as shown in Figure 4.4. The EIVC cam has about 4% higher MCR and reduces the valve overlap by 15dCA than the standard cam. As a result, the EIVC cam achieves 0.3% higher IEffp than the standard cam.

Figure 4.12 shows the P-V diagrams of the three intake cams at this operation point. With the LIVC cam, intake valves close significantly later after BDC. At the beginning of compression stroke, the upward movement of piston expels charge from cylinder into intake system before intake valves closed rather than compresses the charge and increases cylinder pressure. The reduced effective intake stroke increases the intake pressure and decreases the area of low pressure pumping loop, which is the main benefit provided by Miller cycle operating at low load condition. The effective CR is also reduced since the starting point of compression stroke is retarded. However this deteriorates engine thermodynamic efficiency at low load as discussed previously.

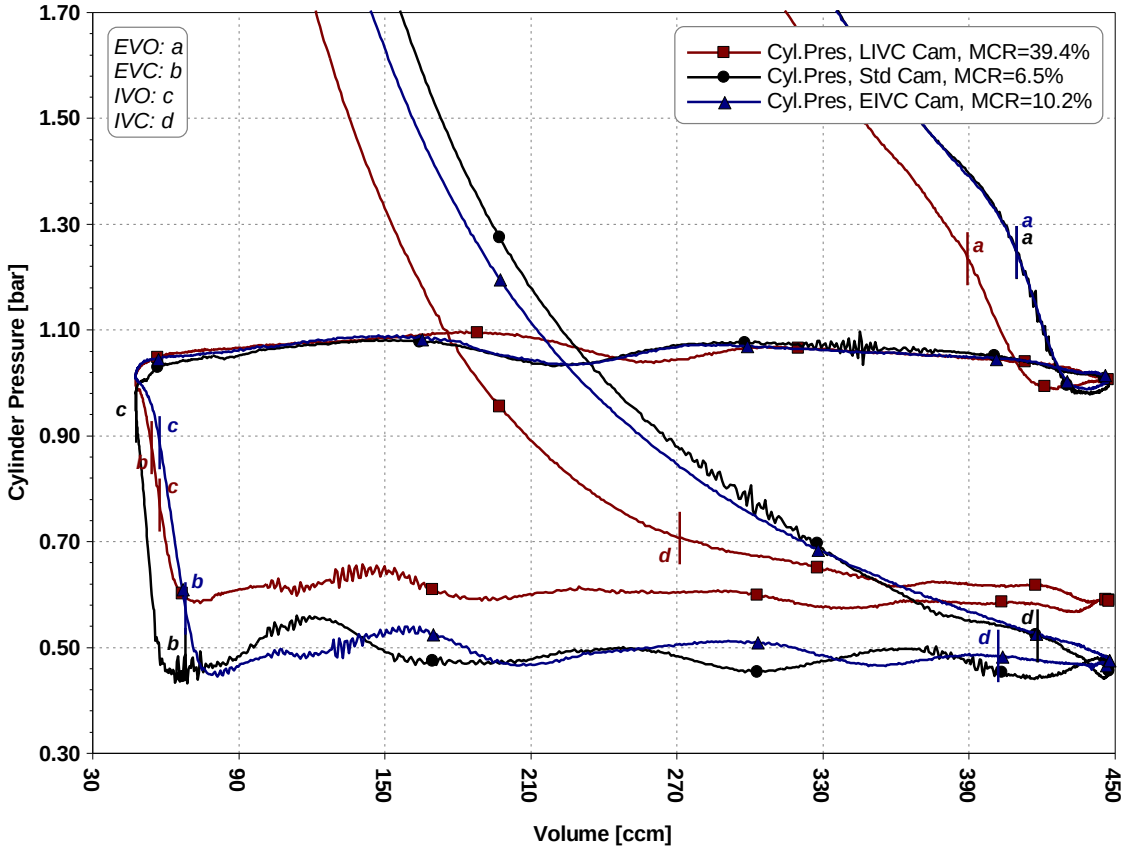

Figure 4.12 P-V Diagrams of Three Intake Cams at 800rpm 2.0bar NIMEP with Optimised Cam Timings

4.5 Impact of Valve Timings at Low Load Operation

This section will discuss low load operations at around 5bar NIMEP. As shown in Figure 4.1 and 4.2, intake cam timing was advanced for larger valve overlap at low load condition with all three cams. Figure 4.13 and 4.14 show the cam envelope results at

2000rpm 4.6bar NIMEP with low compression ratio piston and LIVC cam hardware. As shown in Figure 4.13, the highest IEffn is achieved by the most retarded exhaust cam timing and most advanced intake cam timing. When the intake cam timing is advanced, the intake pressure and IEffp decreases, and Miller cycle ratio is reduced from 39.7% to 13.0%. The engine achieves its best IEffn at the maximum overlap point as dominated by the IEffg trend.

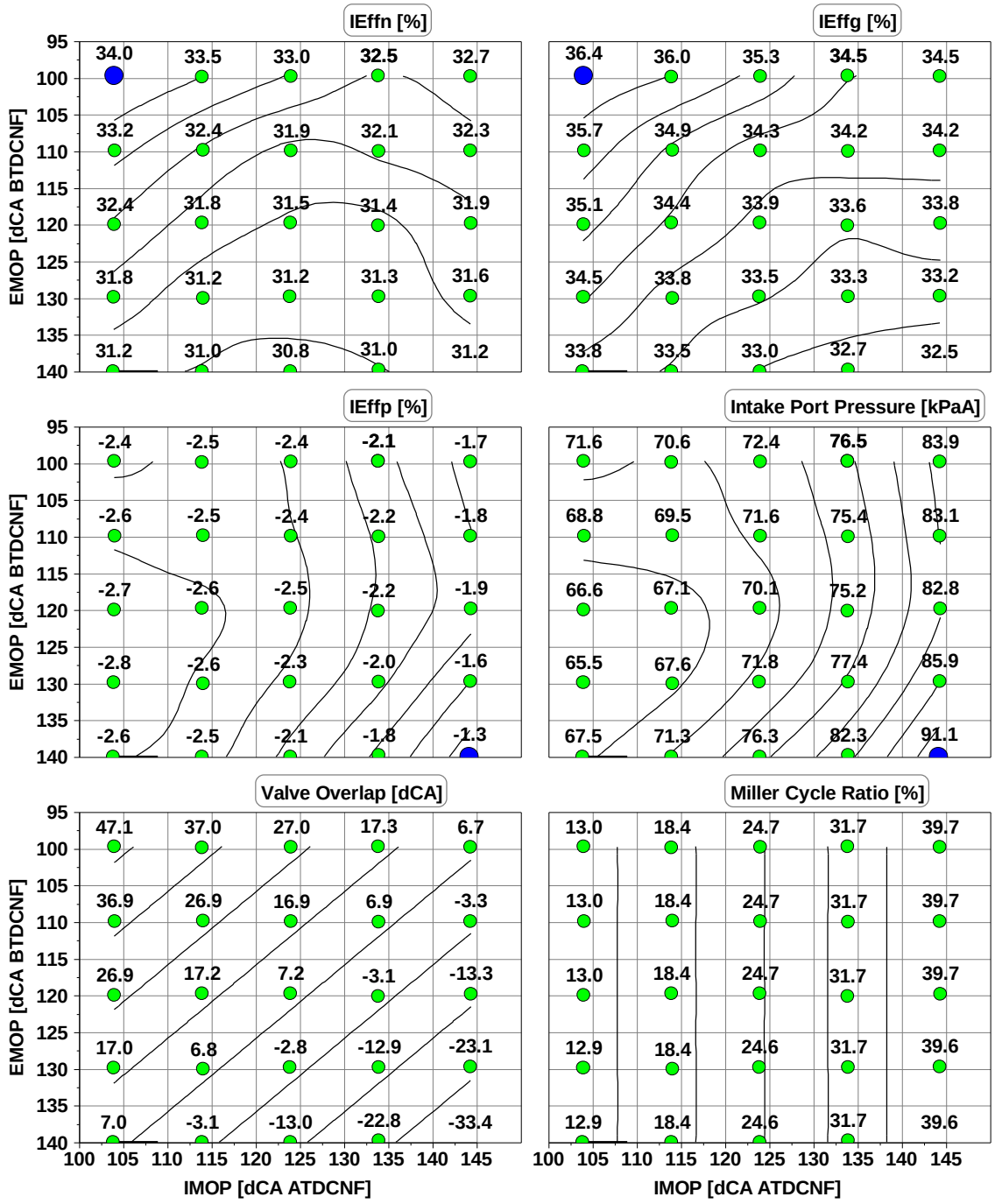

Figure 4.13 Cam Envelope Results at 2000rpm 4.6bar NIMEP with LCR LIVC Cam

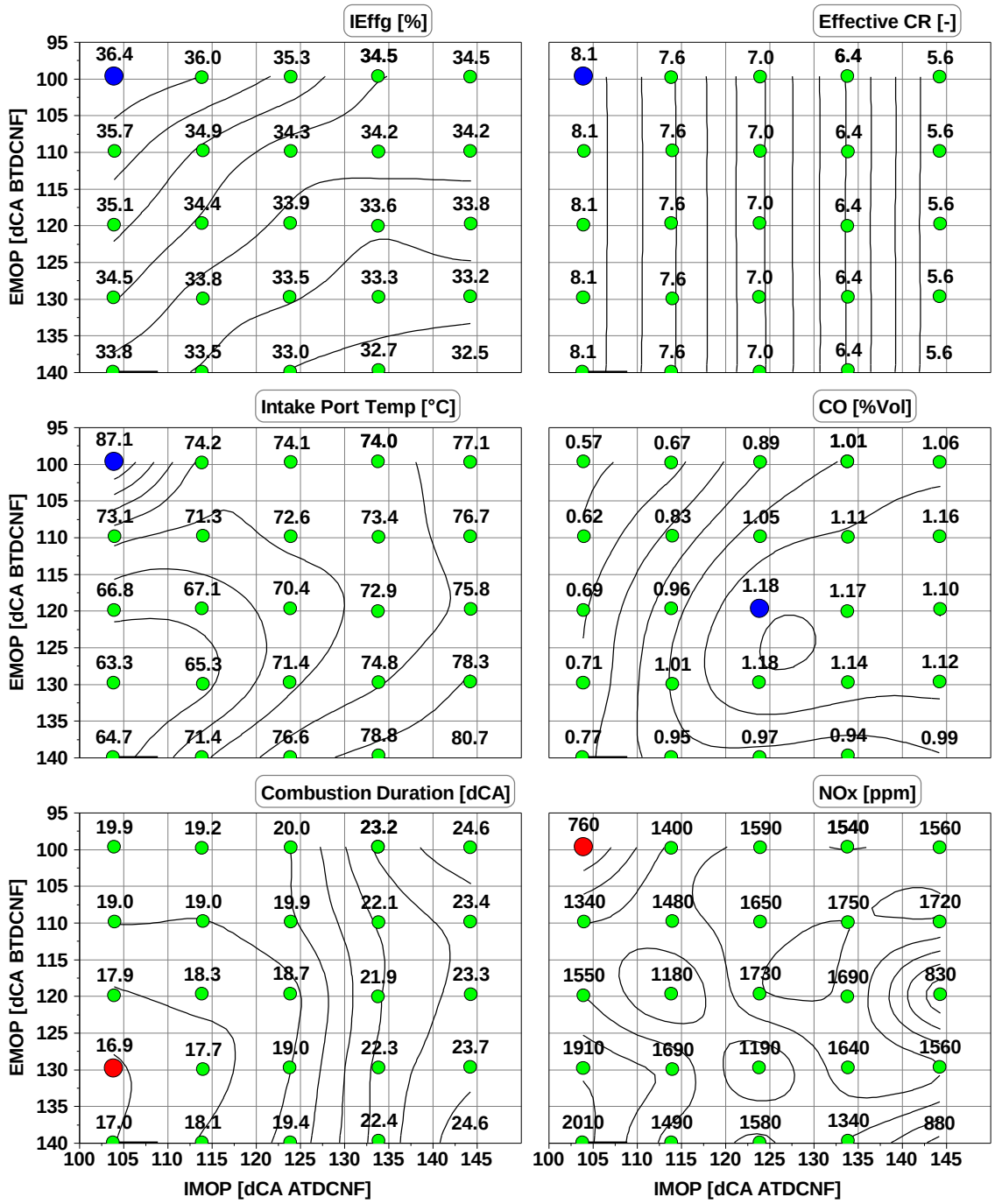

Figure 4.14 Contributions to IEffg at 2000rpm 4.6bar NIMEP with LCR LIVC Cam

Figure 4.14 shows the main contributions to the IEffg results. Effective CR increases when the intake cam timing is advanced. It is the main cause of better IEffg in this direction. At the maximum valve overlap condition, intake port temperature rises up to the maximum because of the back flow from cylinder into the intake manifold during the big valve overlap period near TDC. The back flow also leads to the increased residual

gas fraction (RGF) and hence very low NOx emission. It is observed that CO emission becomes lower when the valve overlap increases. Exhaust lambda is maintained at 1.0 all the time. The higher intake temperature and in-cylinder charge temperature resulted from hot residual gas could benefit the fuel evaporation and mixture formation. Improved mixture quality reduces CO emission and consequently increase combustion efficiency and contributes to the improved IEffg. Combustion duration becomes shortened when the effective CR increases. It becomes slightly longer in the direction when valve overlap increases at IMOP of 104dCA ATDCNF due to increased residual gas fraction, however the relatively faster burn is also contributory to the final IEffg trend.

Figure 4.15 and 4.16 show the cam envelope results at 2000rpm 4.6bar NIMEP with the low compression ratio piston and EIVC cam hardware. As shown in Figure 4.15, the cam timings for the highest IEffn are the most retarded exhaust cam timing and most advanced intake cam timing. It is dominated by the IEffg, which has the similar trend as IEffn. Miller cycle ratio increases from 10% to 34.7%, when the intake cam timing is advanced with EIVC cam. Intake pressure is enhanced and IEffp is improved in the direction.

At the maximum valve overlap with LIVC, there is back flow into intake manifold. It causes higher intake temperature, increased RGF, higher intake pressure and low NOx emission. The situation for the EIVC cam is changed. As shown in Figure 4.16, there are quite flat contour maps of intake port temperature and NOx emission, although intake port temperature is still the highest and NOx concentration is relatively low at large valve overlap condition.

When the intake valve timing is advanced for a bigger valve overlap, Miller cycle ratio increases and causes higher intake port pressure. It could reduce the back flow of cylinder gas into intake port during the valve overlap period. However, the RGF might still increase with lengthened valve overlap through gas in exhaust port being sucked into cylinder at the beginning of intake stroke before exhaust valves closed. As a result, lower CO and HC emissions and hence higher combustion efficiency are achieved at large valve overlap setting. Effective CR decreases while MCR increases. The lower compression ratio reduces combustion temperature then decrease heat transfer and dissociation of combustion products, which contributes to higher IEffg.

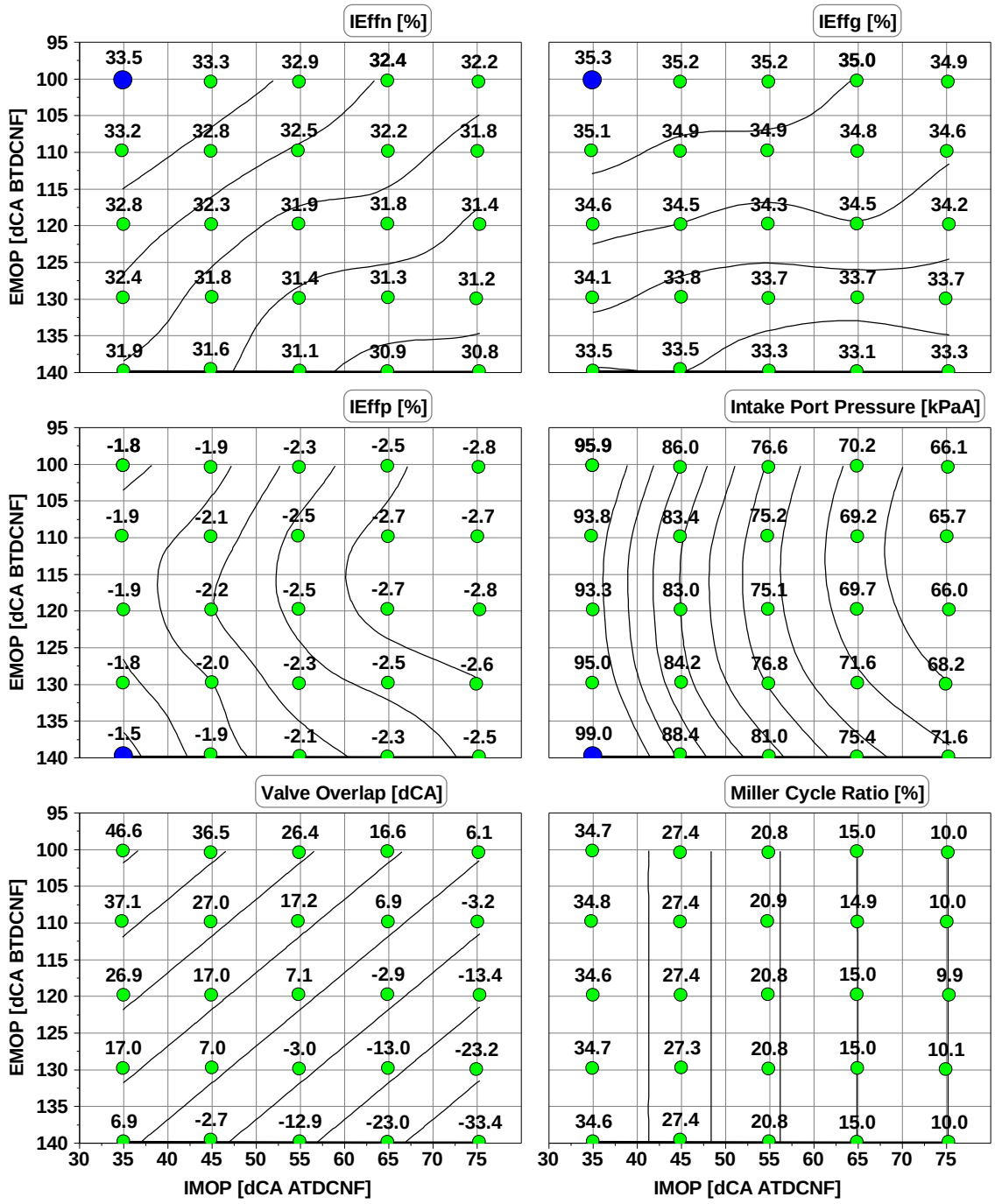

Figure 4.15 Cam Envelope Results at 2000rpm 4.6bar NIMEP with LCR EIVC Cam

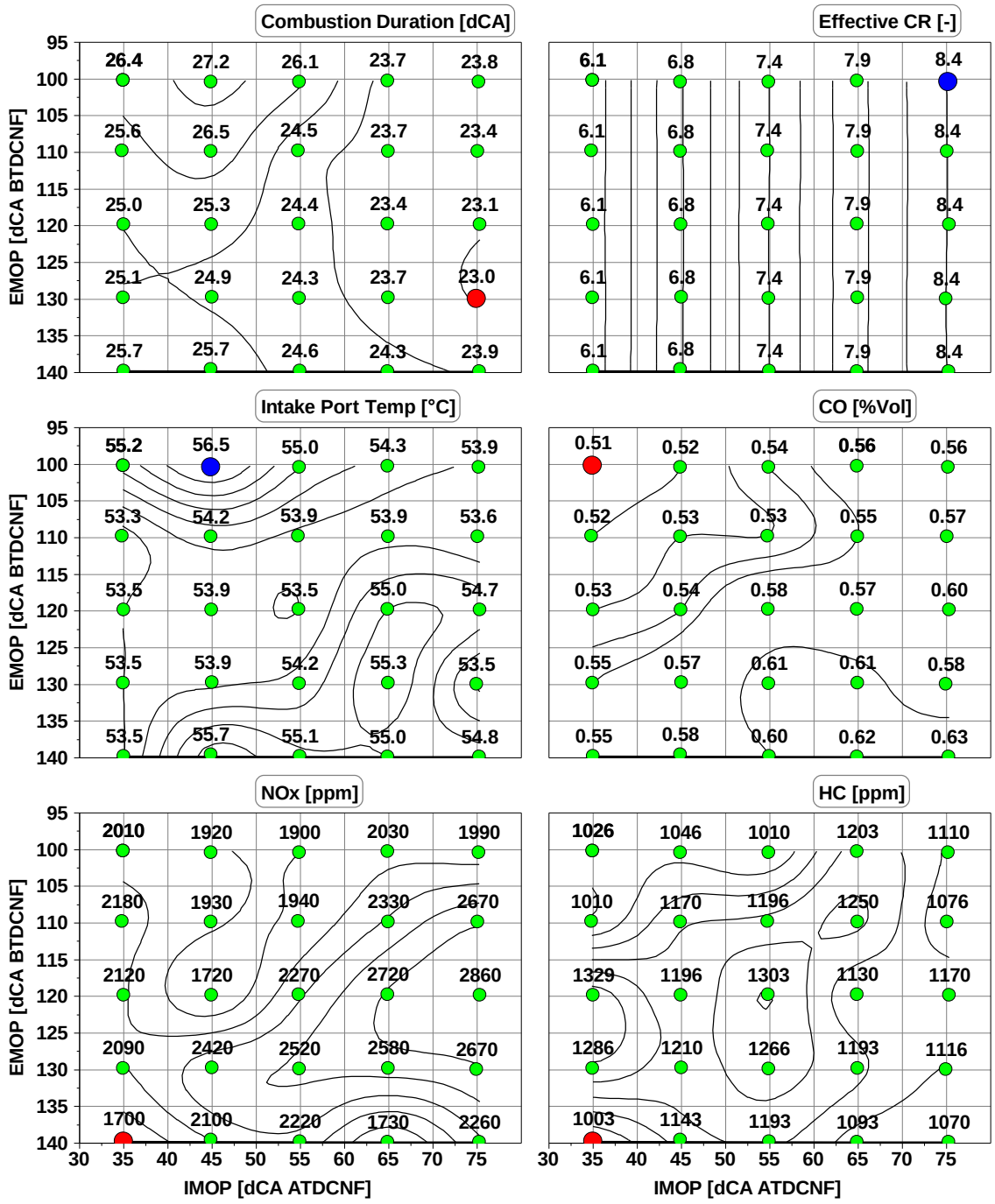

Figure 4.16 Contributions to IEffg at 2000rpm 4.6bar NIMEP with LCR EIVC Cam

Figure 4.17 and 4.18 show the cam envelope results at 2000rpm 4.6bar NIMEP with low compression ratio and standard cam hardware. Generally the standard cam produces similar trends of main results to those of the LIVC cam, since both of them have lower Miller cycle ratios when the intake cam timing is advanced to produce a greater valve overlap. However the Miller cycle ratio only changes in a small range from 0.2% to 10.7%

with the standard cam. As a result, the increased overlap and high internal EGR are the main cause for the higher intake port pressure which leads to high IEffp in the large valve overlap region. High intake temperature at this condition benefits the fuel spray evaporation and mixing with air. It helps to produce low CO and HC and improves the combustion efficiency. Higher effective CRs are also linked to higher IEffg. Higher RGF reduces the NOx emission and extends the combustion duration.

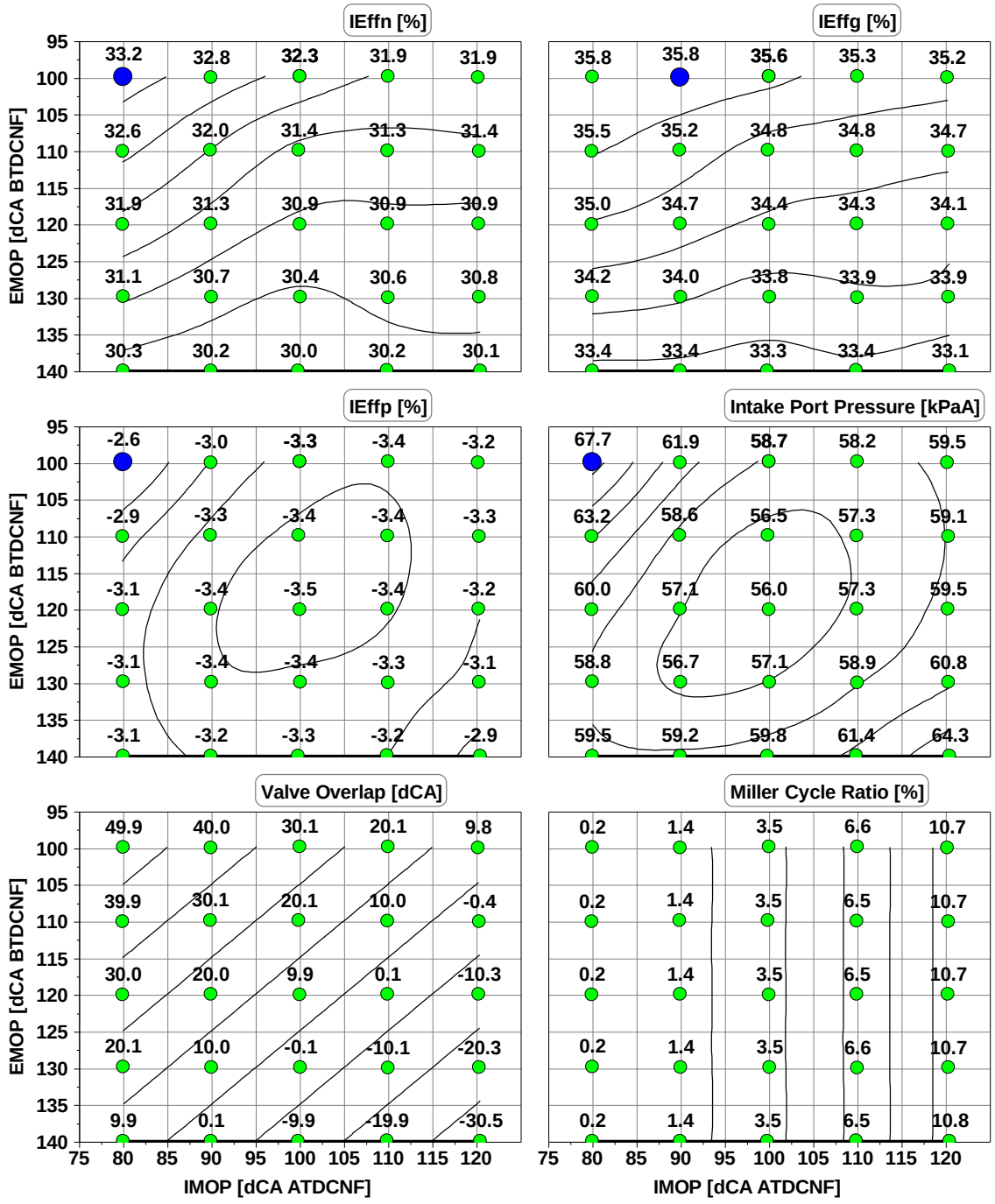

Figure 4.17 Cam Envelope Results at 2000rpm 4.6bar NIMEP with LCR Standard Cam

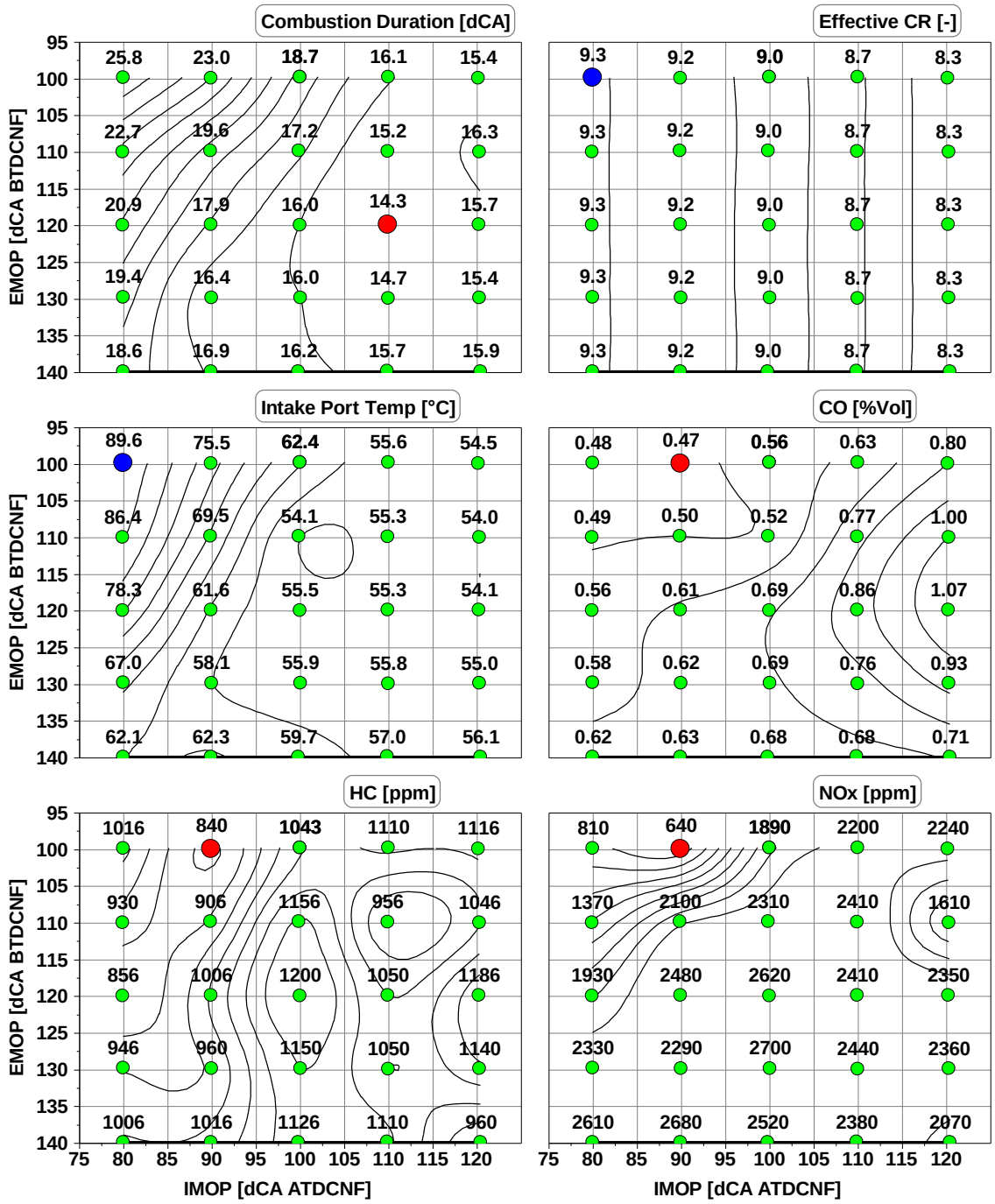

Figure 4.18 Contributions to IEffg at 2000rpm 4.6bar NIMEP with LCR Standard Cam

Figure 4.19 shows the P-V diagrams of all three intake cams at 2000rpm 4.6bar NIMEP with optimised cam timings for each cam. Intake valves are closed quite far before BDC with the EIVC cam, generating visible Miller cycle effect. The advanced IVC timing reduces the effective intake stroke to only 65% of the geometric intake stroke, thus the engine must utilise much higher intake pressure than the other two cam profiles, resulted

in significant reduction of pumping loss. It is also observed the cylinder pressure drops significantly after intake valves closed since piston continues moving downward. The pressure drop is compensated at the beginning period of compression stroke. The cylinder pressure when piston moves upwards back to the same position is only around 0.1bar higher than the cylinder pressure at IVC timing. As a result, the effective compression stroke is also shortened hence the effective CR becomes small.

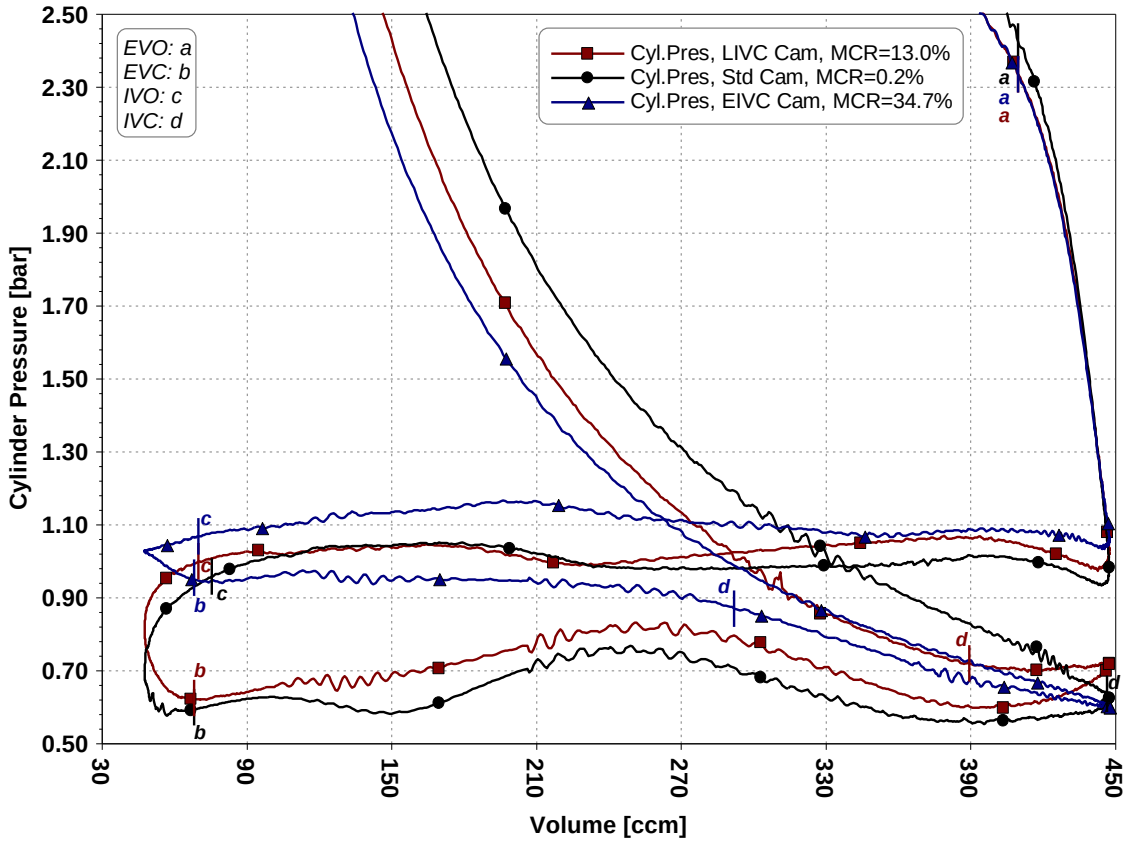

Figure 4.19 P-V Diagrams of Three Intake Cams at 2000rpm 4.6bar NIMEP with Optimised Cam Timings

Figure 4.20 shows the cylinder pressures, intake pressures and exhaust pressures around gas exchange TDC with optimised cam timings of all three intake cams at 2000rpm 4.6bar NIMEP. At this load, the intake port pressure is well below ambient so that even at the end of exhaust stroke the in-cylinder pressure is still higher than the intake port pressure, which leads to significant back flow of burned gas into the intake port after intake valves opened, as indicated by the rise in the intake pressure, as shown in Figure 4.20. When piston moves downwards, this part of burnt gas will be sucked into cylinder

together with fresh air, consequently the in-cylinder residual gas fraction will increase. Because higher intake pressure is used with the EIVC cam, the back flow effect is weaker than the other two cams.

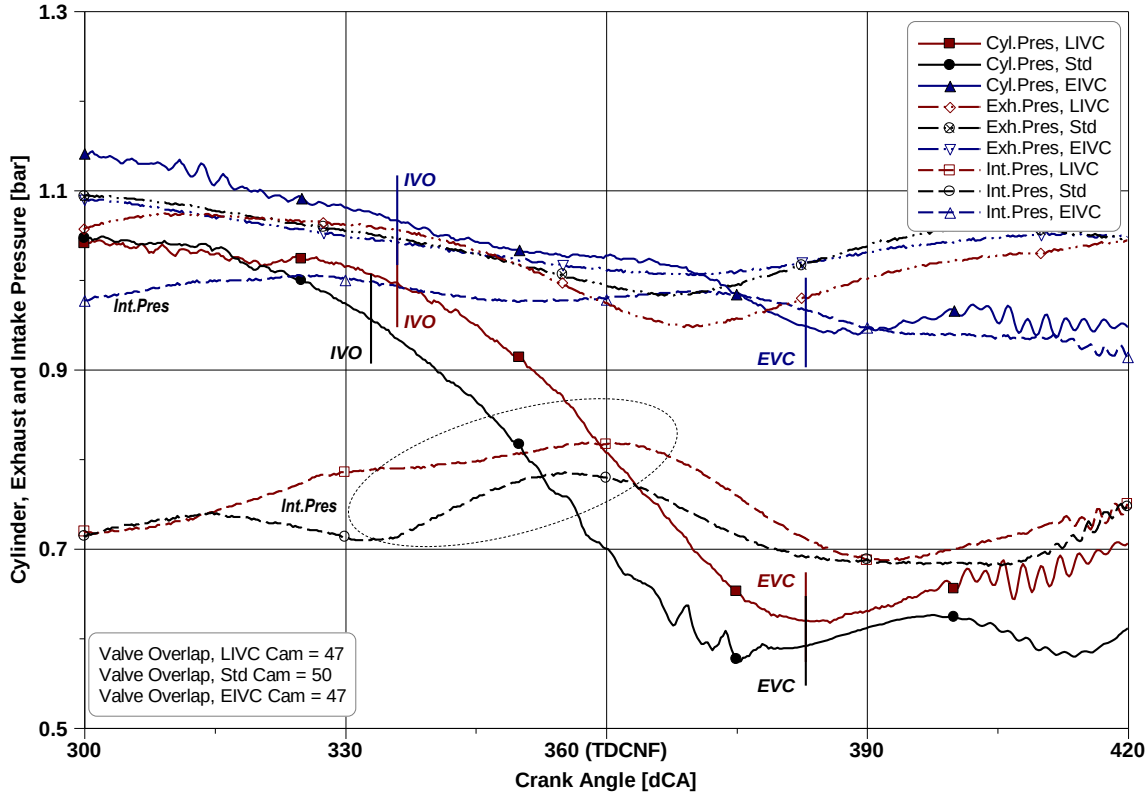

Figure 4.20 Gas Exchange Process of Three Intake Cams at 2000rpm 4.6bar NIMEP with Optimised Cam Timings

Figure 4.21 shows the main optimised results from cam envelope tests of all three intake cams at low load and speed range from 1000rpm to 4000rpm. As shown in Figure 4.4, LIVC cam has the highest IEffn among the three cams at the low load area. EIVC cam has higher IEffn than standard cam at 2000rpm and 4000rpm. All three cams are operated with large valve overlaps. The EIVC cam applies the highest Miller cycle ratio and thus the lowest effective CR. The smaller valve lift of EIVC also causes much slower combustion. These lead to the worst IEffg with the EIVC cam among the three. However, the EIVC cam utilises much higher intake pressure due to Miller cycle operation and results in less pumping loss, which compensates for the partial loss of IEffg.

At low load operations, large valve overlap is shown to be more dominant than Miller cycle effect on improving engine fuel conversion efficiency, because of the lower

pumping loss and improved charge preparation and combustion efficiency due to increased charge temperature by the back flow and residual gas. Miller cycle operates with higher intake pressure and reduces pumping loss. However when Miller cycle ratio becomes too high the effective CR becomes quite low and the engine thermodynamic efficiency deteriorates.

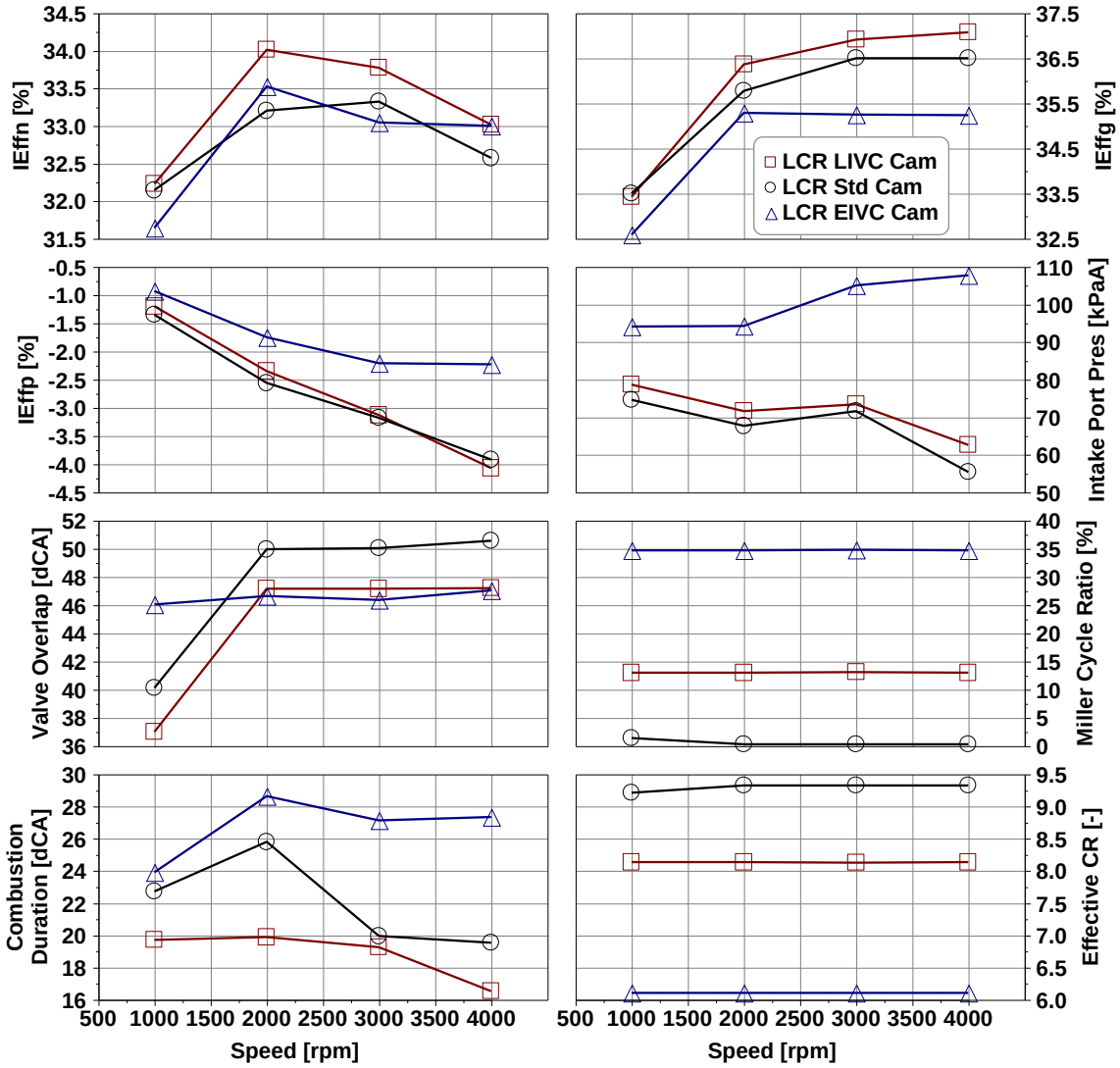

Figure 4.21 Comparison of the Optimised Results of Three Intake Cams at Low Load

4.6 Impact of Valve Timings at Mid Load Operation

This section will discuss mid load results when engine operates at around 9bar NIMEP. As shown in Figure 4.1 and 4.2, intake cam timing was generally retarded for small valve

overlap at mid load condition with all three cams. Figure 4.22 and 4.23 show the cam envelope results at 2000rpm 8.9bar NIMEP with the low compression ratio and LIVC cam hardware. As shown in Figure 4.22, the cam timings for highest IEffn are most retarded exhaust and intake cam timing. It is a combined result based on IEffg and IEffp trend.

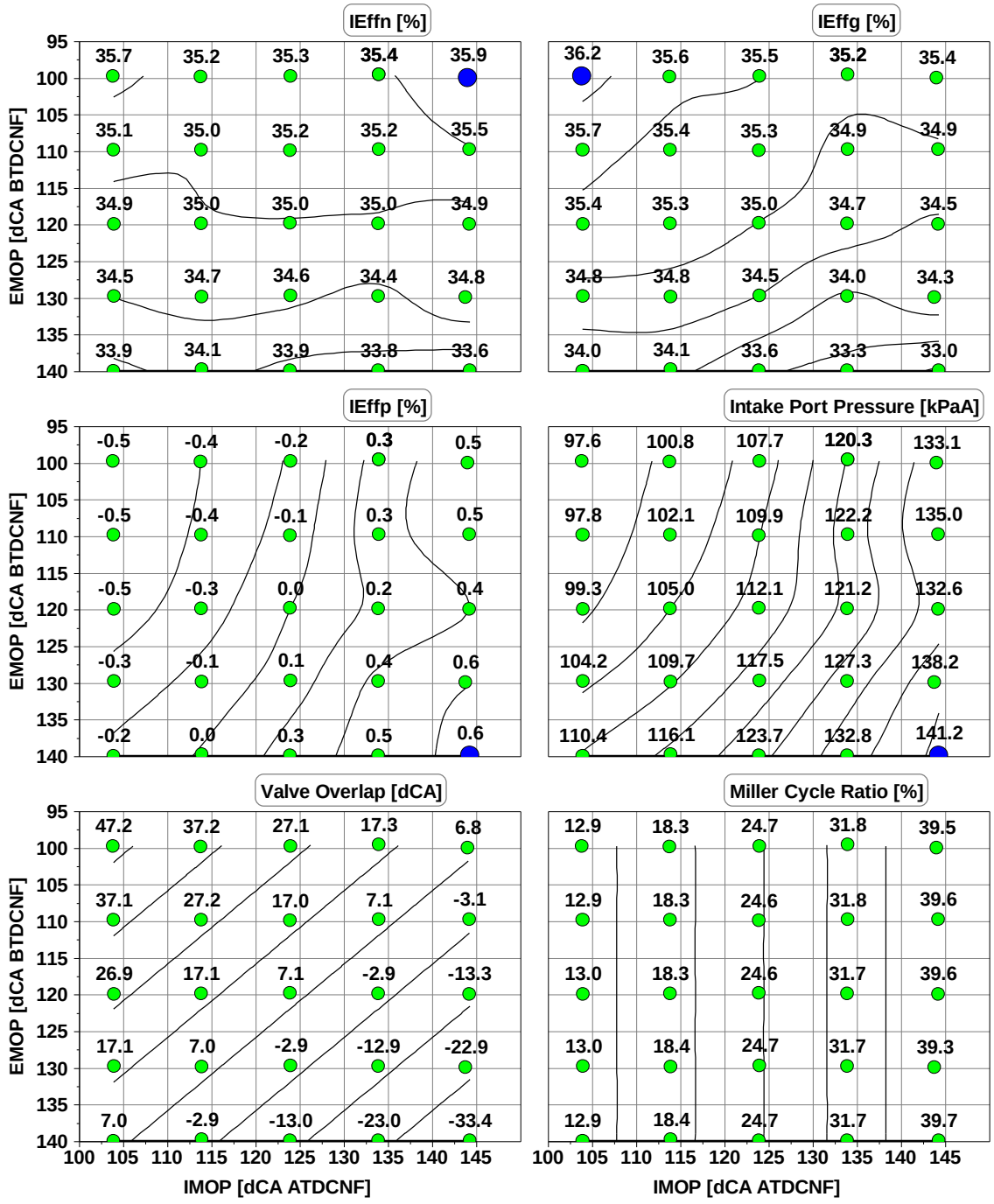

Figure 4.22 Cam Envelope Results at 2000rpm 8.9bar NIMEP with LCR LIVC Cam

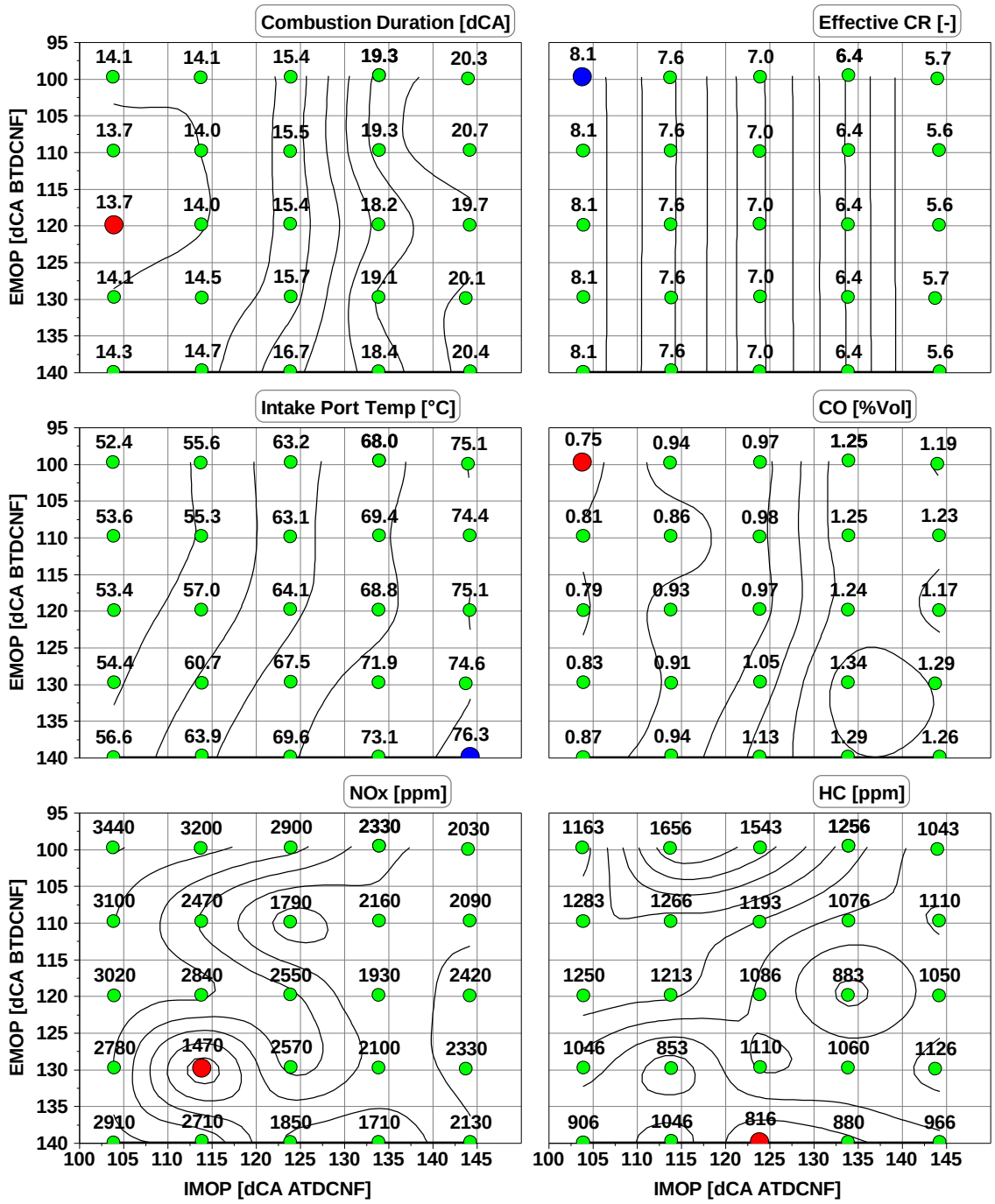

Figure 4.23 Contributions to IEffg at 2000rpm 8.9bar NIMEP with LCR LIVC Cam

When the EMOP timing is 100dCA BTDCNF and the IMOP timing is retarded from 104 to 144dCA ATDCNF, the Miller cycle ratio increases and effective CR decreases. As intake port pressure increases from 97.6kPa to 133.1kPa, the LIVC cam leads to positive scavenging during the valve overlap period. Since the exhaust lambda is set to 1.0 for all the tests, scavenging effect results in slightly fuel rich mixture in cylinder, which causes

increase in CO emission at this condition as shown in Figure 4.23. Combustion duration becomes longer when ECR reduces. Finally IEffg reduces but IEffp increases slightly when IMOP is retarded. Intake port temperature goes up at retarded IMOP timing due to late IVC and in-cylinder gas expelled into the intake system at the beginning of compression stroke.

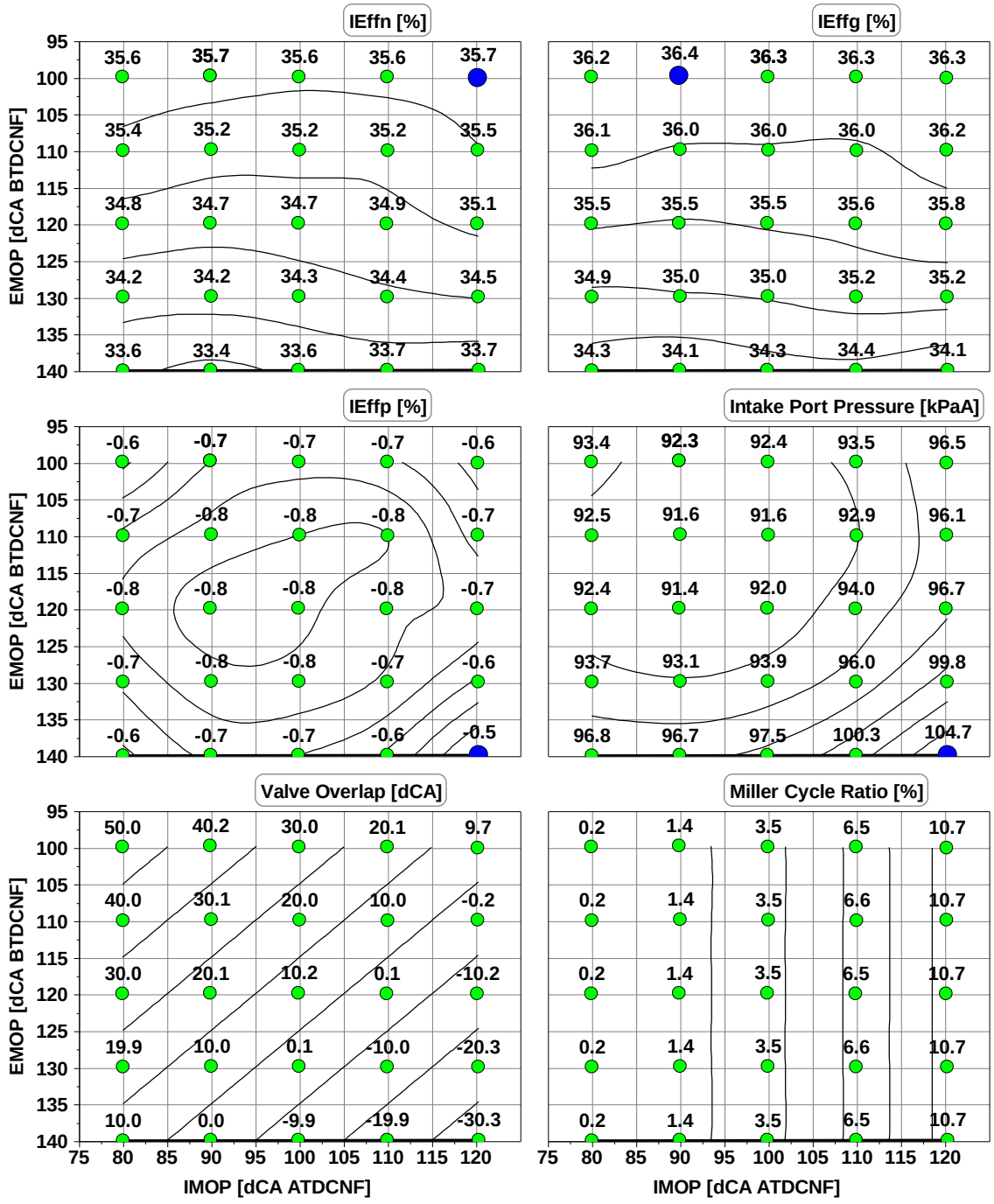

Figure 4.24 Cam Envelope Results at 2000rpm 8.9bar NIMEP with LCR Standard Cam

Figure 4.24 and 4.25 show the cam envelope results at 2000rpm 8.9bar NIMEP with the low compression ratio piston and standard cam hardware. Its highest IEffn also occurs at the most retarded EMOP and IMOP timings. However at 100dCA BTDCNF EMOP timing, IEffg, IEffp and IEffn are hardly affected by the IMOP timing.

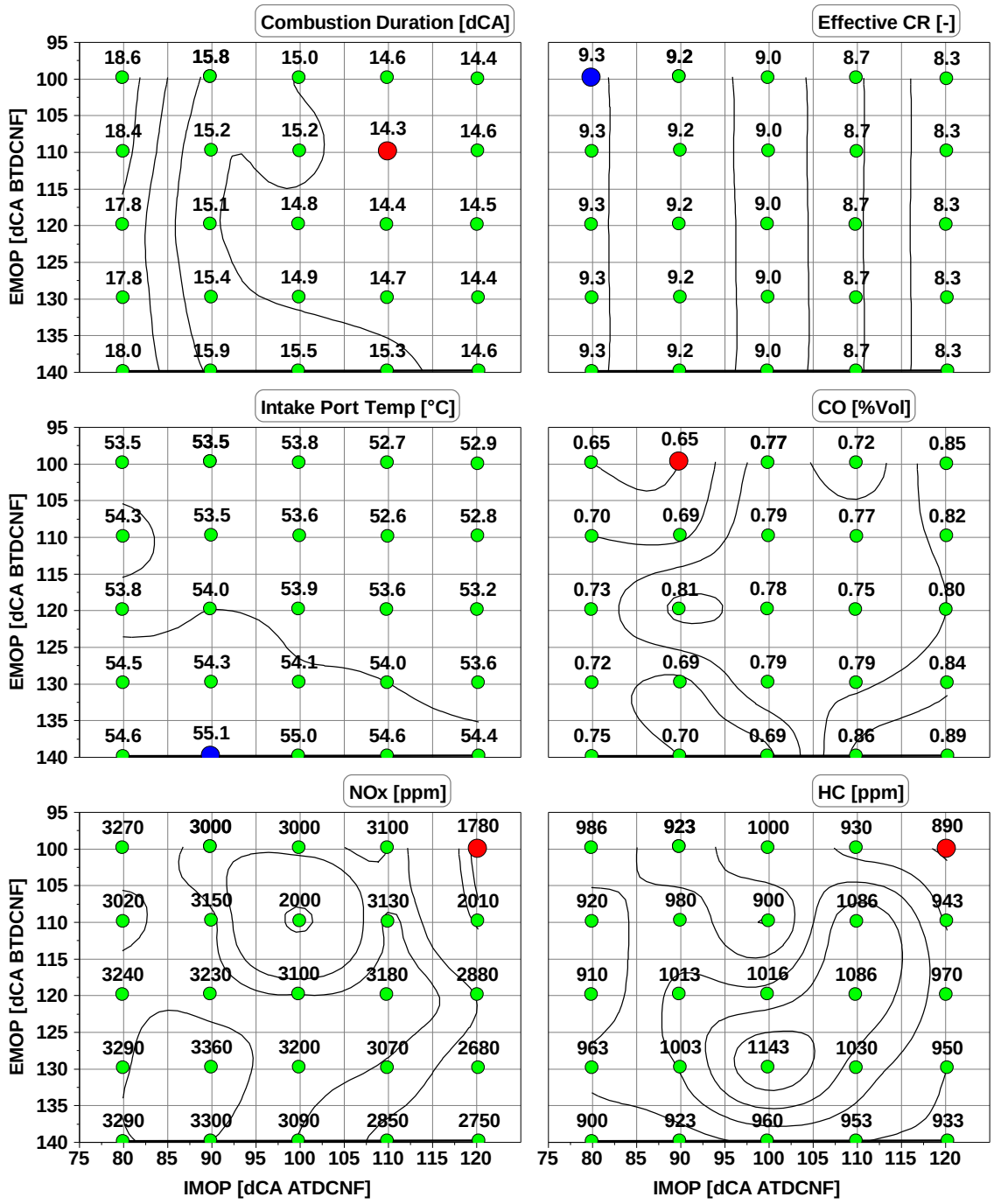

Figure 4.25 Contributions to IEffg at 2000rpm 8.9bar NIMEP with LCR Standard Cam

The standard cam only allows MCR to be changed within around 10%. When IMOP is retarded to 120dCA ATDCNF for maximum MCR 10.7%, intake port pressure goes up to 96.5kPa. It is still lower than average exhaust port pressure but close enough to generate slight scavenging effect. CO increases from 0.65% to 0.85%, which indicates slightly enriched in-cylinder air fuel mixture. NOx emission drops at this IMOP timing, which could also result from the enrichment. The slightly fuel rich mixture makes combustion fast and the combustion duration shortens from 18.6dCA to 14.4dCA. Finally the shortened combustion duration and reduced HC emission compensate the effect of lower effective CR and increased CO emission, resulting in quite flat IEffg trends along with IMOP timing change. IEffg mainly increases with later EVO as discussed previously.

Figure 4.26 and 4.27 show the cam envelope results at 2000rpm 8.9bar NIMEP with low compression ratio and EIVC cam hardware. As shown in Figure 4.26, the EIVC cam achieves the best IEffn at the point of 65dCA ATDCNF IMOP timing and most retarded EMOP timing of 100dCA BTDCNF. It is dominated by the IEffg trends, which increases from 30.6% to 35.7% when IMOP is retarded by 40dCA. In the meantime, Miller cycle ratio changes from the maximum to minimum, and the intake port pressure reduces by 30kPa. IEffp gets worse by 0.5% but it has less impact than the IEffg trend.

The EIVC cam generates the maximum Miller cycle ratio and maximum valve overlap at the same point, when the IMOP timing is advanced to 35dCA ATDCNF with 100dCA BTDCNF EMOP timing. Since the exhaust pipe is connected to atmosphere, there is about 30kPa scavenging pressure and 47dCA valve overlap at this point. It generates strong scavenging effect at this point. To maintain the exhaust lambda at 1.0, in-cylinder mixture has to be greatly enriched. This results in very high CO and HC emission but low NOx emissions at large valve overlap area. The combustion duration becomes shorter as the valve overlap increases because of the better scavenging of residual gas and fast flame speed of the fuel rich mixture. As shown in Figure 4.27, both CO and HC decreases when IMOP is retarded to employ less valve overlap and low MCR and intake port pressure. It results in better combustion efficiency. Effective CR becomes higher as well and is beneficial to a high thermodynamic efficiency. Finally EIVC cam achieves highest IEffg at most retarded IMOP and EMOP timings.

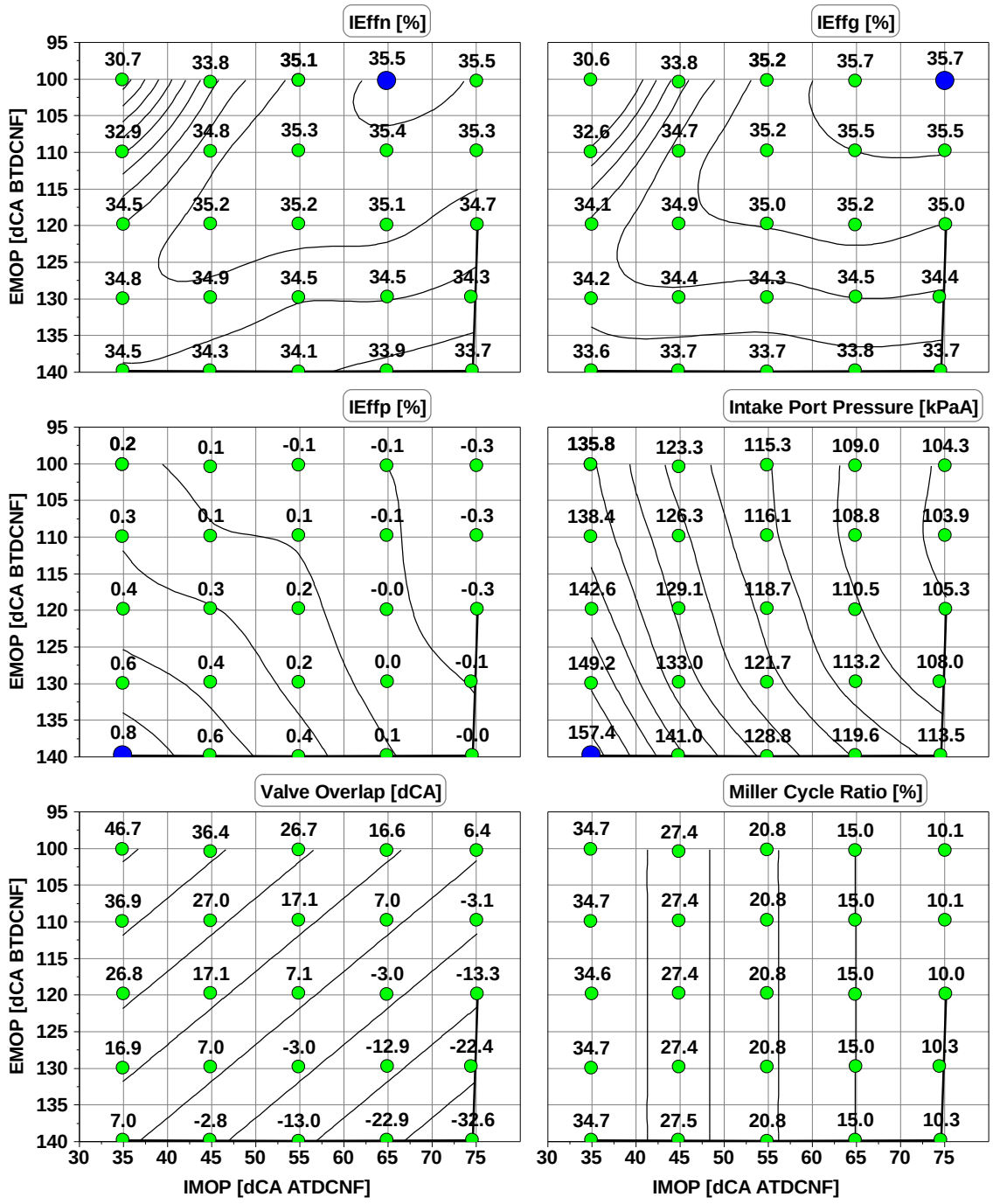

Figure 4.26 Cam Envelope Results at 2000rpm 8.9bar NIMEP with LCR EIVC Cam

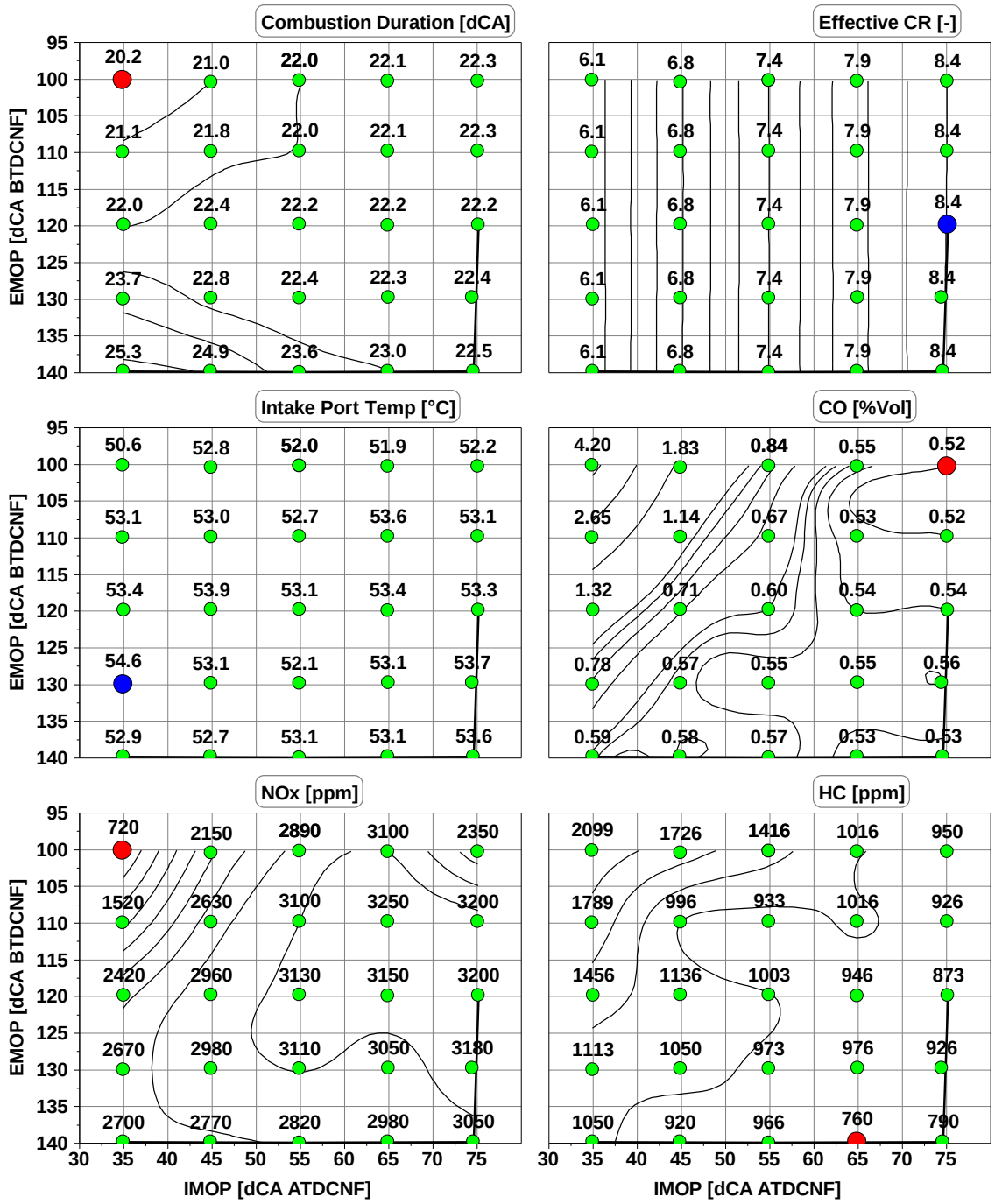

Figure 4.27 Contributions to IEffg at 2000rpm 8.9bar NIMEP with LCR EIVC Cam

Figure 4.28 shows the corresponding in-cylinder pressure, intake pressure and exhaust pressure traces around gas exchange TDC when intake and exhaust valves are at the maximum overlap condition. As discussed previously, EIVC cam has the maximum Miller cycle ratio hence highest intake pressure at this condition. At the time of intake valves opening, intake port pressure is much higher than the in-cylinder pressure and

exhaust port pressure. Fresh air rushes into the cylinder causing the in-cylinder pressure rise rapidly. Then a rise appears on the exhaust pressure trace. It is the result of fresh air scavenged into the exhaust port, so called air short-circuiting. LIVC cam and standard cam have the minimum Miller cycle ratio at this condition, which are 12.9% and 0.2% respectively. Intake port pressure of LIVC cam is close to exhaust port pressure at IVO timing, while standard cam has intake port pressure lower than exhaust port pressure. There is no visible scavenging behaviour for these two cams.

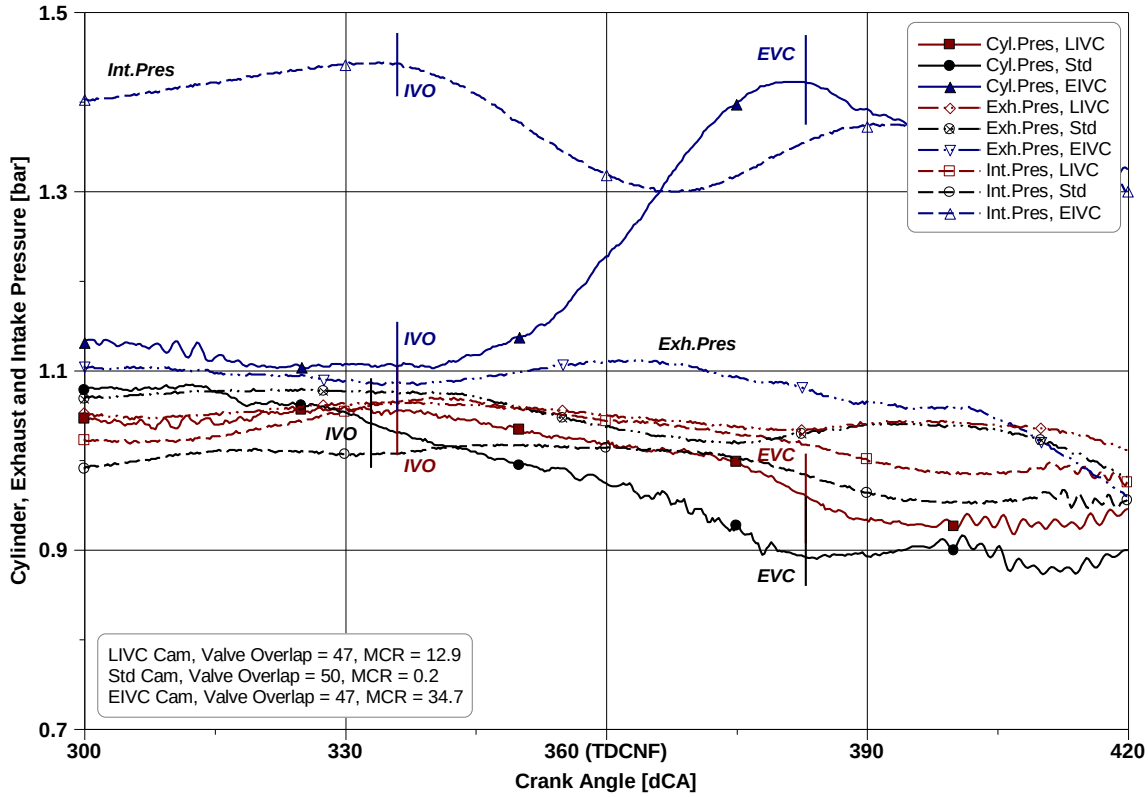

Figure 4.28 Gas Exchange Process of Three Intake Cams at 2000rpm 8.9bar NIMEP with Maximum Valve Overlap

Figure 4.29 shows cylinder pressure, intake pressure and exhaust pressure traces around gas exchange TDC when intake and exhaust valve timings are optimised. At this condition, LIVC cam applies high MCR thus high intake pressure. The scavenging behaviour is not obvious due to a small valve overlap of 7dCA. However some scavenging must occur considering the large pressure difference between the intake ports and exhaust ports. Cylinder pressure drops after TDC since intake valves open later after TDC. It rises rapidly after IVO due to considerably higher pressure in the intake ports

and reaches above 1.0bar at about 30dCA after TDC. EIVC cam applies 15% MCR and its intake port pressure is also higher than the exhaust pressure.

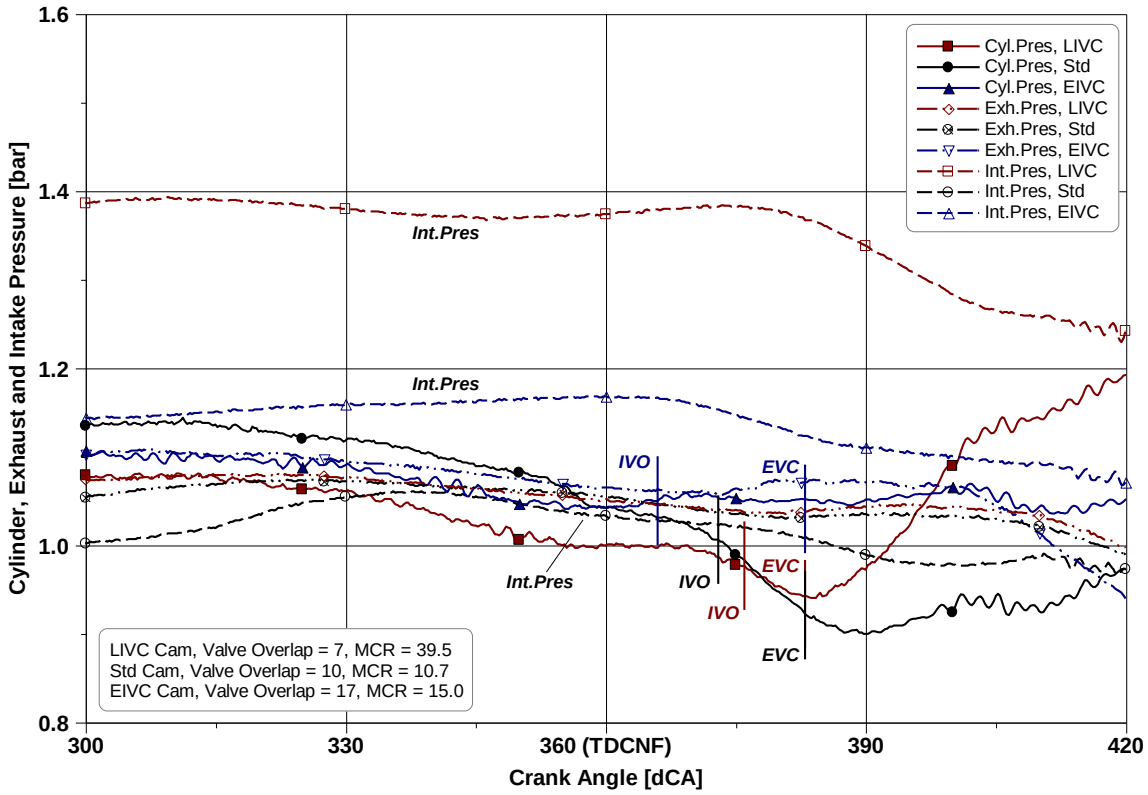

Figure 4.29 Gas Exchange Process of Three Intake Cams at 2000rpm 8.9bar NIMEP with Optimised Cam Timings

Figure 4.30 shows the P-V diagrams of all three intake cams at 2000rpm 8.9bar NIMEP with optimised cam timings for each cam. In the case of LIVC cam, the Intake valves are closed well after BDC generating visible Miller cycle effect. Its in-cylinder pressure rises rapidly in the intake stroke and stays above exhaust pressure during most of the exhaust stroke, producing positive pumping work. EIVC cam still has some pumping loss since Miller cycle ratio is only 15%. The area of its low pressure loop is noticeably smaller than that of the standard cam, reducing the pumping loss and improving the IEffp from -0.6% to -0.1%, as presented in Figure 4.31.

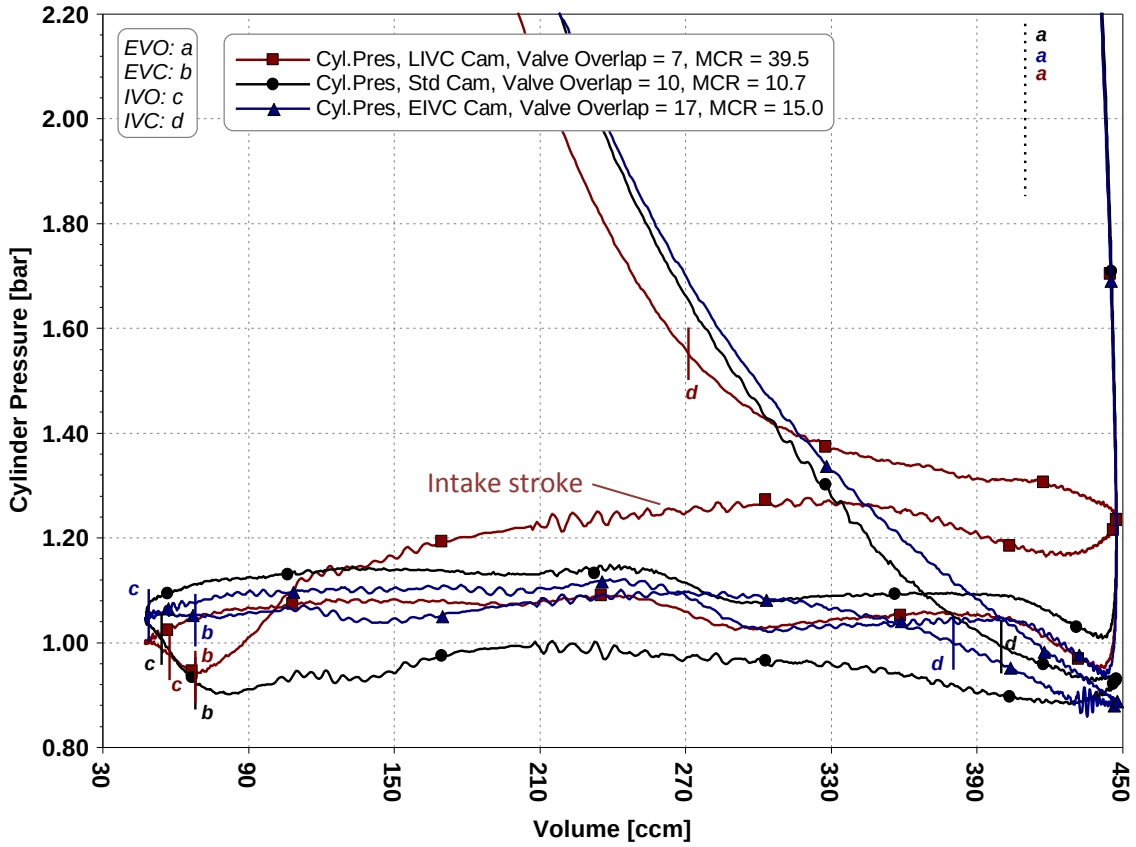

Figure 4.30 P-V Diagrams of Three Intake Cams at 2000rpm 8.9bar NIMEP with Optimised Cam Timings

Figure 4.31 shows the main optimised results from cam envelope tests of all three intake cams at mid load and speed range from 1000rpm to 3000rpm. LIVC cam has higher IEffn than standard cam and EIVC cam at all speeds. Its IEffg is worst among the three cams at 1000rpm and 2000rpm and is lower than standard cam at 3000rpm. The strategy to apply LIVC cam for optimum fuel consumption is Miller cycle operation for more positive pumping work or less pumping loss, i.e. best IEffp. Thus as shown in Figure 4.31, LIVC cam applies highest Miller cycle ratio and intake pressure or scavenging pressure at all speeds. One penalty for this strategy is reduced effective CR and its contribution to the deteriorated IEffg. The fuel consumption, CO and HC emission are higher, due to the presence of in-cylinder fuel rich mixture to keep the exhaust lambda at 1.0 when positive scavenging takes place during the positive overlap period. At 1000rpm and 2000rpm, CO emission of LIVC cam is above 1.1%, indicating quite rich in-cylinder mixture. When engine runs Miller cycle operation with LIVC cam, intake port temperature is higher because of gas expelled from cylinder.

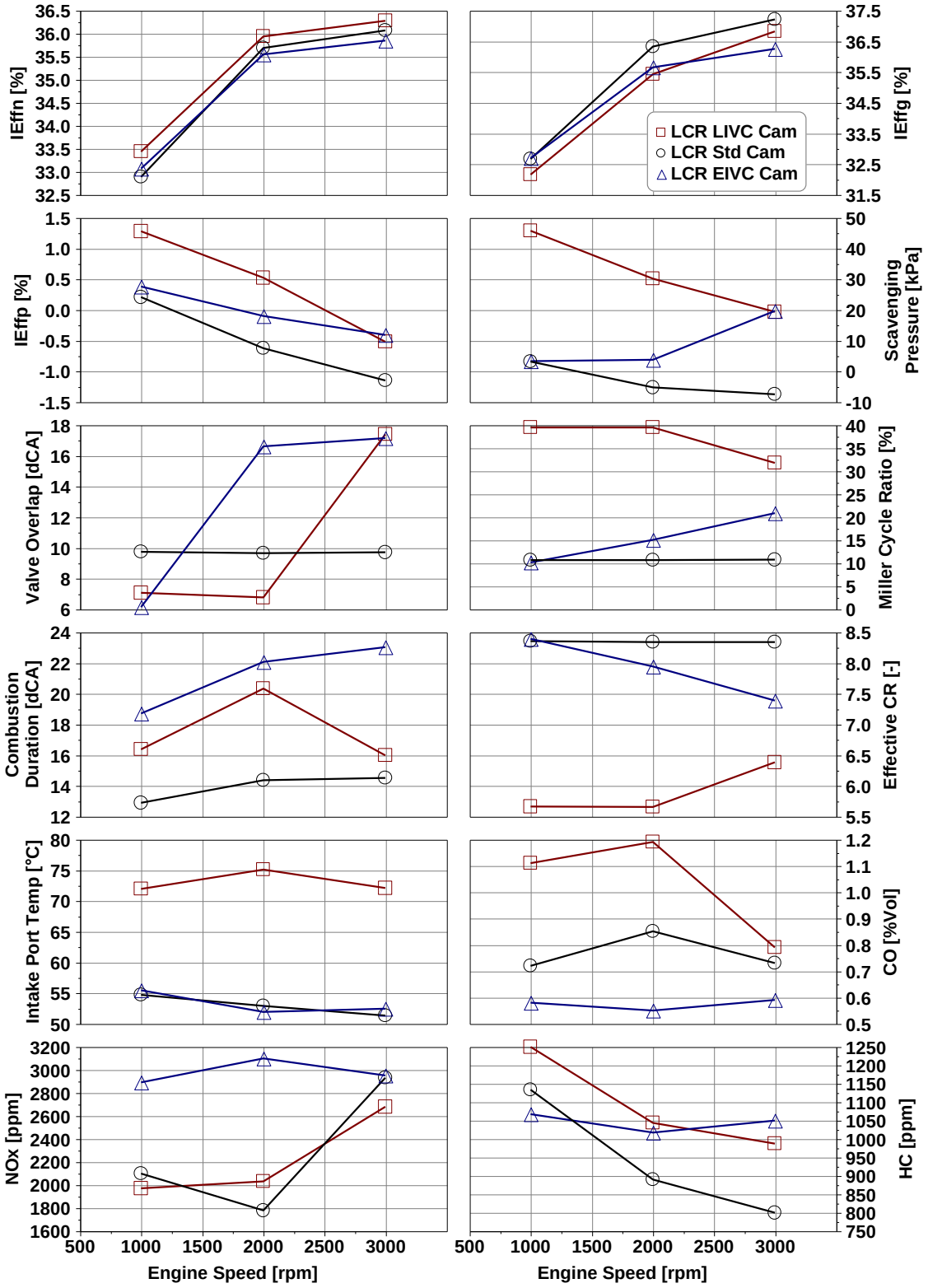

Figure 4.31 Comparisons of the Optimised Results of Three Intake Cams at Mid Load

EIVC cam achieves higher IEffn than standard cam at 1000rpm but lower IEffn at 2000rpm and 3000rpm. This difference is dominated by IEffg. EIVC cam and standard cam have equal IEffg at 1000rpm but IEffg of EIVC cam is lower than the standard cam at other speeds. Optimised intake cam timing for EIVC cam is retarded at mid load, thus Miller cycle ratio is not very high, but it is still higher than standard cam at 2000rpm and 3000rpm. As a result its effective CR is lower than the standard cam at these two speeds. It is one of the reasons for the IEffg difference between the two cams. Another cause is that combustion duration of EIVC cam is much longer than that of the standard cam, which is about 9dCA at 3000rpm because of the weaker tumble flow of the reduced valve lift and duration. As discussed previously based on Figure 4.26 and 4.27, the strategy of EIVC for improving fuel conversion efficiency at mid load is to retard intake valve timing. It is to get more advantage of increased IEffg than the disadvantage of reduced benefit from IEffp. One reason is to reduce Miller cycle effect for high effective CR. Another mechanism is Miller cycle operation and consequent high intake pressure plus a large valve overlap result in strong scavenging behaviour. It cause in-cylinder enrichment and deteriorate combustion efficiency. At mid load conditions, knocking is still not an issue. Scavenging is not beneficial by reducing knocking tendency and advancing combustion. Therefore, EIVC cam cannot gain benefit from scavenging effect. Since EIVC cam runs at weak Miller cycle operation, the benefit gained on IEffp is not big enough to compensate the loss of IEffg compared to standard cam. Finally EIVC cam doesn't improve engine fuel conversion efficiency at this load area.

4.7 Impact of Valve Timings at High Load Operation

The experimental study was also carried out at 2000rpm 16.0bar and 25.6bar NIMEP. As shown in Figure 4.1 and 4.2, all three cams apply intake valve timing for achieving high Miller cycle ratio at high load. Figure 4.32 and 4.33 show the cam envelope results at 2000rpm 16.0bar NIMEP with low compression ratio and LIVC cam hardware. LIVC cam achieves the highest IEffn at the most retarded EMOP timing 100dCA BTDCNF and most retarded IMOP timing 144dCA ATDCNF, when IEffg is highest. The engine also has to operate at over 200kPaA intake pressure to achieve the target load at the retarded IMOP timing, due to high Miller cycle ratio with LIVC cam. It produces increased positive pumping work, i.e. high IEffp. However the change of IEffn follows the same trend as IEffg.

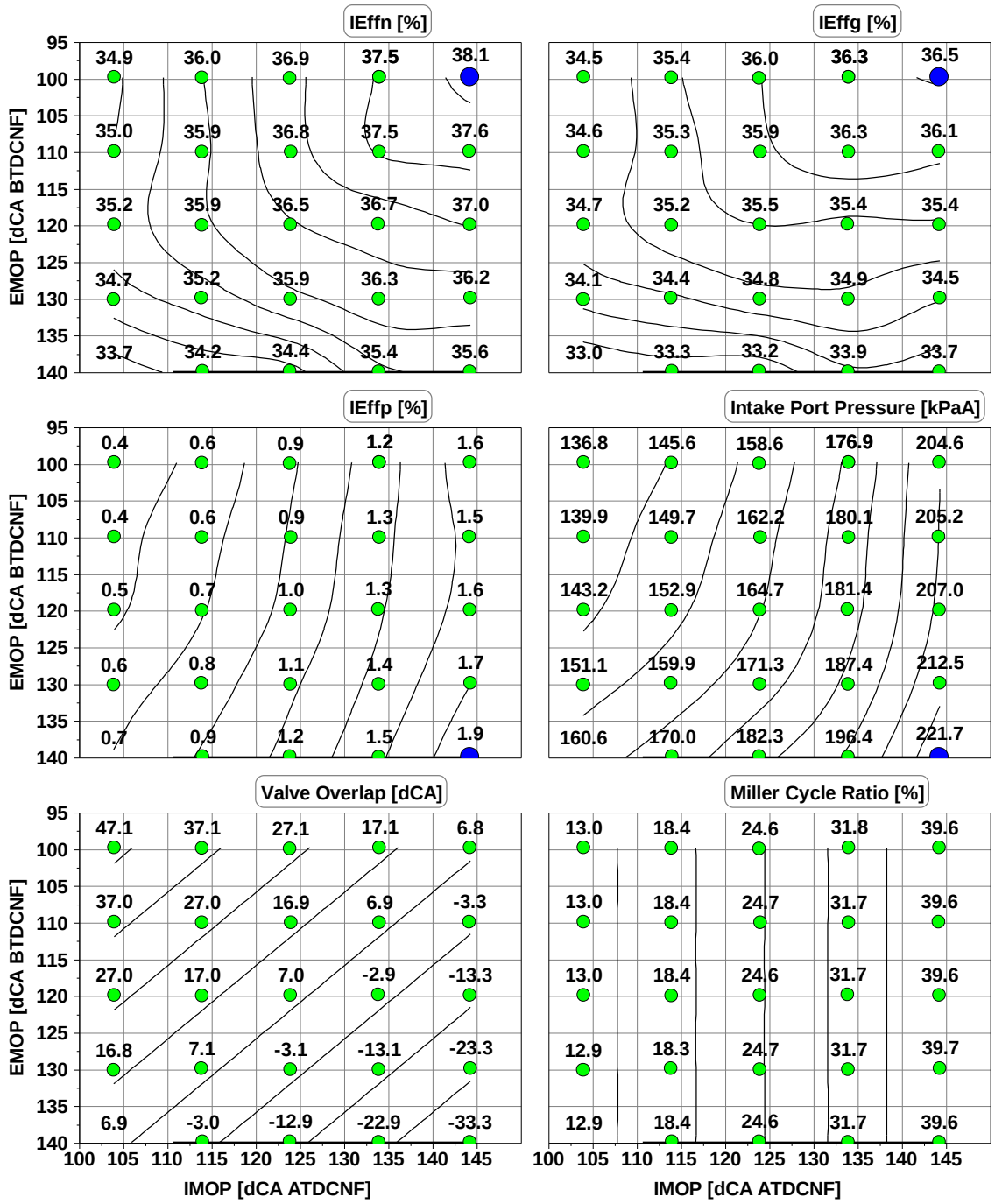

Figure 4.32 Cam Envelope Results at 2000rpm 16.0bar NIMEP with LCR LIVC Cam

Figure 4.33 shows the variations of IEffg with different parameters. When Miller cycle ratio increases, the effective CR decreases from 8.1 to 5.6. Combustion duration becomes longer by 2dCA and CO emission increases as well. However the spark timing is advanced by 5dCA without knocking combustion, which results in about 4dCA advance of CA50 timing. This is the reason for high fuel conversion efficiency at high Miller

cycle ratio condition, which reduces effective CR consequently reduces the knocking tendency.

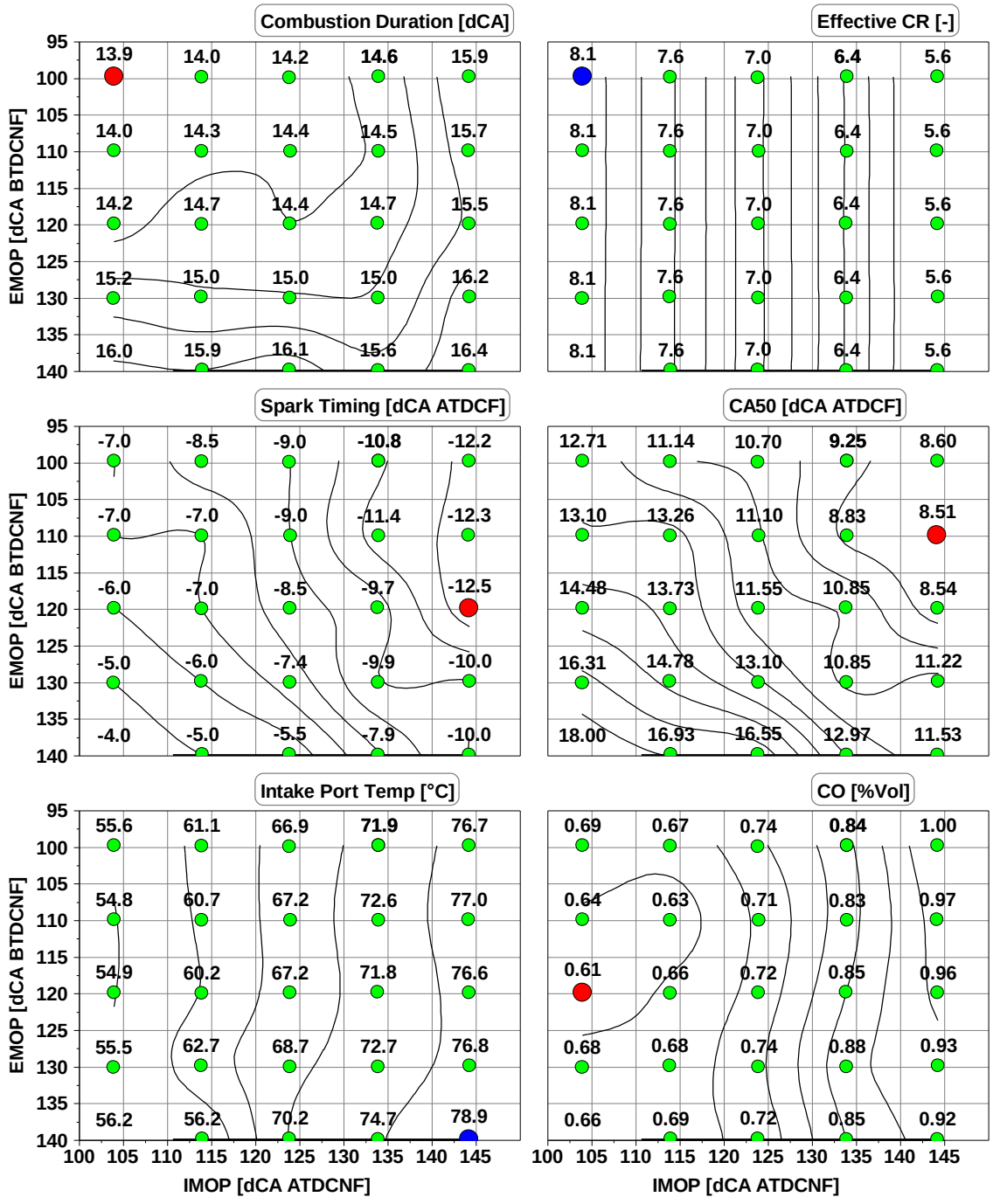

Figure 4.33 Contributions to IEffg at 2000rpm 16.0bar NIMEP with LCR LIVC Cam

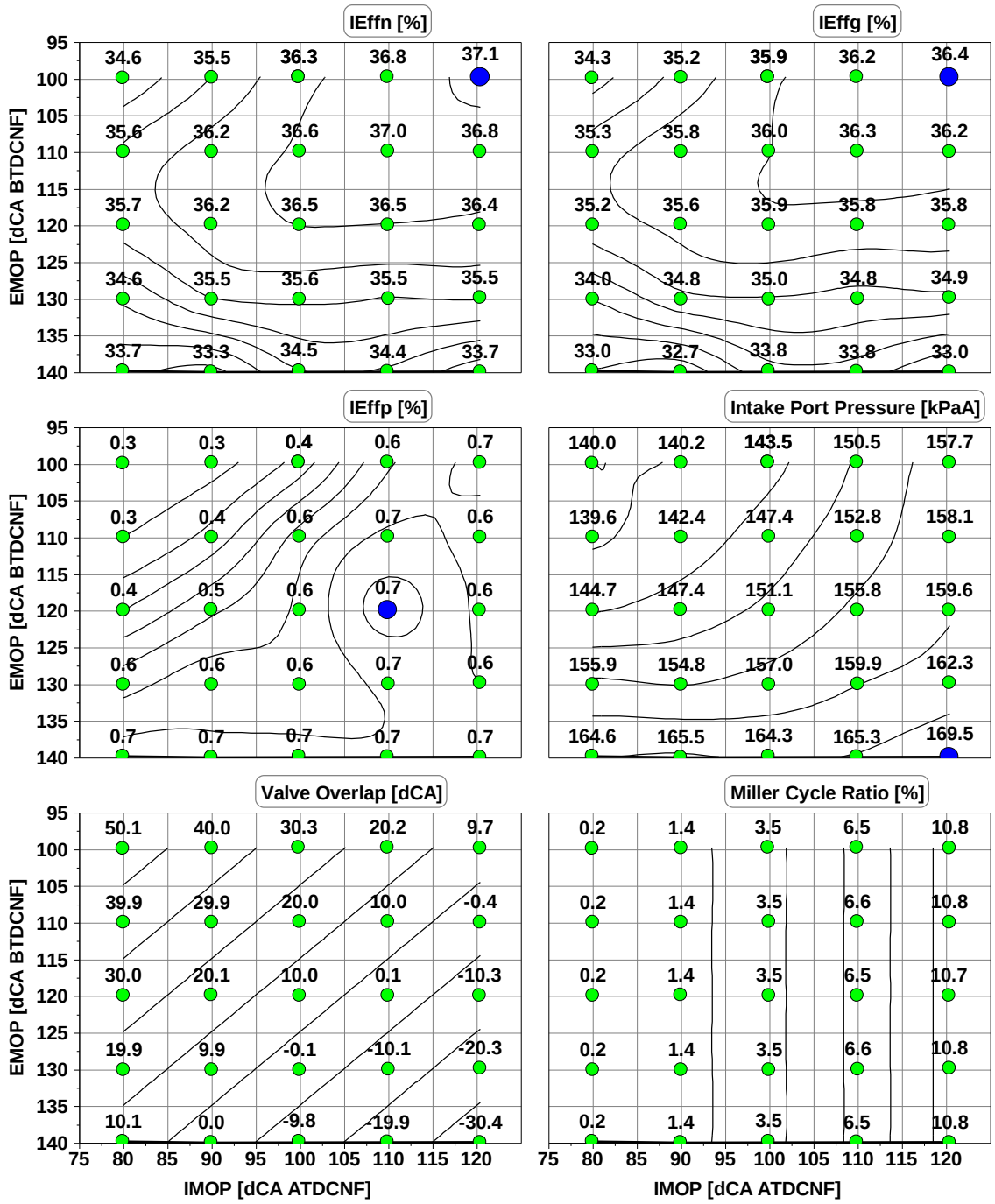

Figure 4.34 Cam Envelope Results at 2000rpm 16.0bar NIMEP with LCR Standard Cam

Figure 4.34 shows the cam envelope results at 2000rpm 16.0bar NIMEP with low compression ratio and standard cam hardware. Since both standard cam and LIVC cam achieve high Miller cycle ratio by retarding intake cam timing after BDC, IEffg and IEffn contour maps of standard cam are quite similar with those of LIVC cam. The highest IEffg occurs when EMOP and IMOP timings are at the latest position, with which the

highest IEffn is obtained. IEffp is also high at retarded intake cam timing and thus contributes to the best IEffn, though IEffp improvement is small since change of Miller cycle ratio is small with standard cam. Another visible difference from LIVC cam is that the intake pressure is more dominated by the amount of the valve overlap rather than the Miller cycle operation. At low speed high load operations with a standard cam profile, scavenging effect will reduce residual gas fraction thus improves the volumetric efficiency. As shown in figure 4.35, scavenging is still present at maximum overlap region even the scavenging pressure is relatively low.

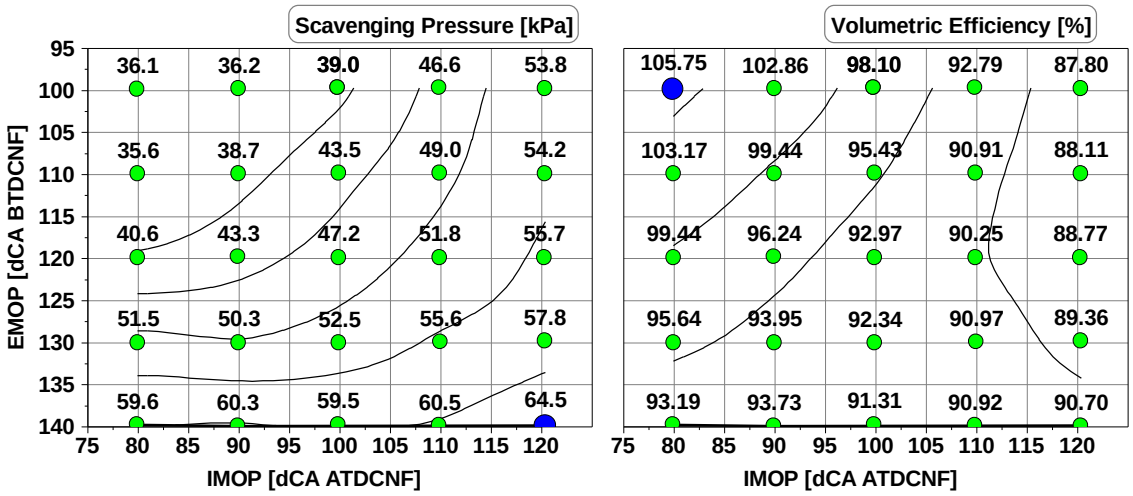

Figure 4.35 Scavenging Pressure and Volumetric Efficiency Changes along Cam Timing Envelope at 2000rpm 16.0bar NIMEP with LCR Standard Cam

Figure 4.36 and 4.37 show the cam envelope results at 2000rpm 16.0bar NIMEP with low compression ratio and EIVC cam hardware. IEffn and IEffg follow almost the same trend along cam envelope. They achieve the optimum value at 100dCA BTDCNF EMOP timing and advanced IMOP timing at 45dCA ATDCNF. Intake port pressure increases while Miller cycle ratio increases along advanced IMOP timing. At the advanced IMOP timing of 35dCA ATDCNF, intake port pressure is lower at 100dCA BTDCNF EMOP timing than 140dCA. EIVC cam still achieves relatively high IEffp at 100dCA BTDCNF EMOP and 45dCA ATDCNF, which also contributes to the final optimum IEffn result.

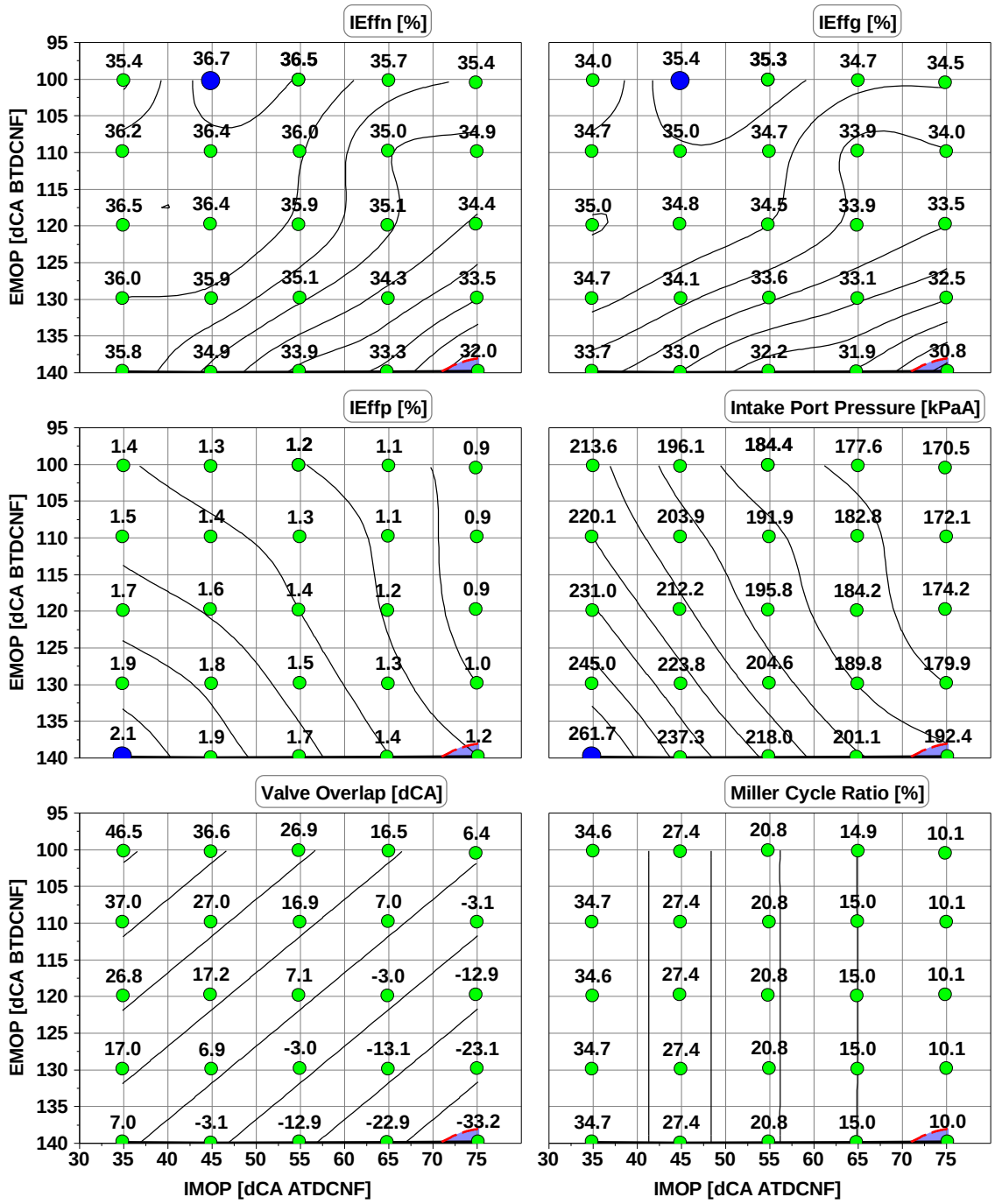

Figure 4.36 Cam Envelope Results at 2000rpm 16.0bar NIMEP with LCR EIVC Cam

Figure 4.37 shows the analysis of the IEffg trend. When effective CR is lowered by 2.3, the knock limited spark timing is advanced by more than 10dCA and leads to over 10dCA advance of CA50. This is the key contribution to high IEffg at advanced IMOP timing. It is also observed that combustion duration is shortest in the large overlap region. When advanced cam timing and high Miller cycle ratio are used with the EIVC cam, the

large valve overlap period coupled with the positive pressure difference creates strong scavenging and minimises the knocking combustion through reduced residual gas concentration and end-gas temperature, though it leads to richer than stoichiometric mixture and high CO and HC emissions.

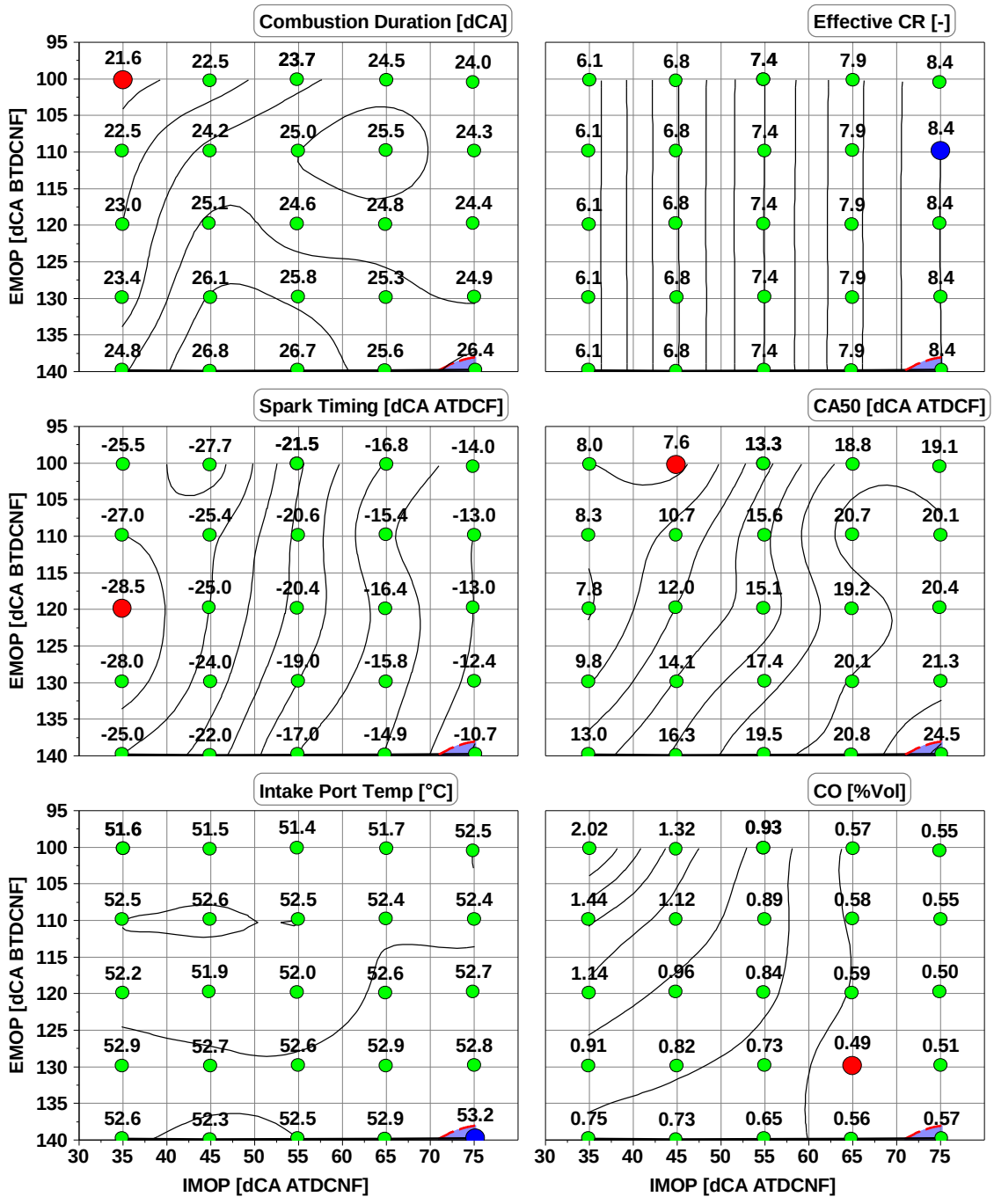

Figure 4.37 Contributions to IEffg at 2000rpm 16.0bar NIMEP with LCR EIVC Cam

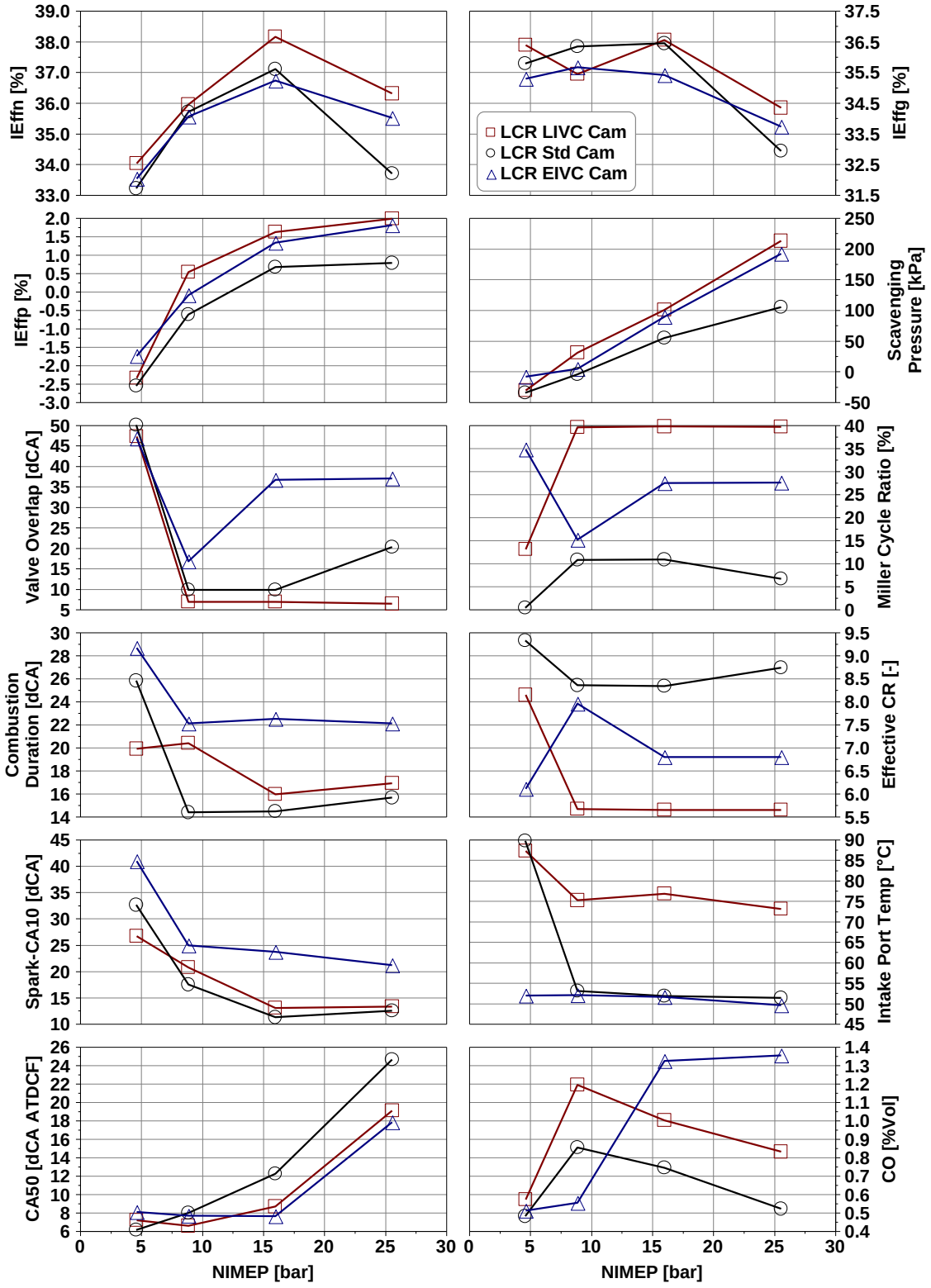

Figure 4.38 Comparison of the Optimised Results of Three Intake Cams at 2000rpm

Figure 4.38 compares the optimised results of three intake cams at 2000rpm while engine load NIMEP increases from 4.6bar up to 25.6bar. LIVC cam has the highest IEffn among

the three cams in the whole load range. The two Miller cycle cams have better IEffn than the standard cam at low load 4.6bar as discussed in the previous section. They also improve engine fuel conversion efficiency at high load operation because of Miller cycle operation. Miller cycle reduces effective CR and consequently decreases in-cylinder charge temperature at the end of compression stroke, resulting in reduced knocking tendency. This helps to advance spark timing and CA50 timing, which is restricted by detonation borderline at high load running for a gasoline engine. Miller cycle operation also produces more positive pumping work when high intake pressure has to be employed to reach the target load. The disadvantage of LIVC for Miller cycle running is the increased temperature in intake system especially at high load condition. It may raise the concern about heat rejection from intake system and also intake component protection.

EIVC cam combines the Miller cycle operation and scavenging effect. It advances CA50 more than LIVC cam as presented in Figure 4.38. The disadvantage of scavenging is enriched in-cylinder lambda, which leads to increase of CO emission. Another disadvantage of EIVC cam is the slow combustion. The duration from spark timing to CA10 and combustion duration of EIVC cam are both longer than other two cams at all load conditions. It is because of weak in-cylinder air charge motion and reduced turbulence at the end of compression stroke caused by its small valve lift and short valve opening period.

Miller cycle operation itself can lead to slow combustion as well. The reduced effective CR decreases in-cylinder gas temperature at end of compression, resulting in a longer ignition delay as indicated by sparking timing to CA10 duration and also lengthened combustion duration. For LIVC cam, when Miller cycle ratio increases and effective CR reduces from 8.9bar NIMEP, its ignition delay and combustion duration becomes longer than standard cam. This also explains why the combustion speed of the EIVC cam is particularly slower at 2000rpm 4.6bar, where all three cams apply most advanced intake cam timings for large valve overlap. EIVC cam has the highest MCR thus quite lower ECR than other two cams. The negative effect of Miller cycle operating is stronger at low load due to low engine temperature level. The lengthened combustion duration deteriorated the efficiency of LIVC and EIVC cams at low load points, but was compensated for by the advanced combustion timing at high load situations.

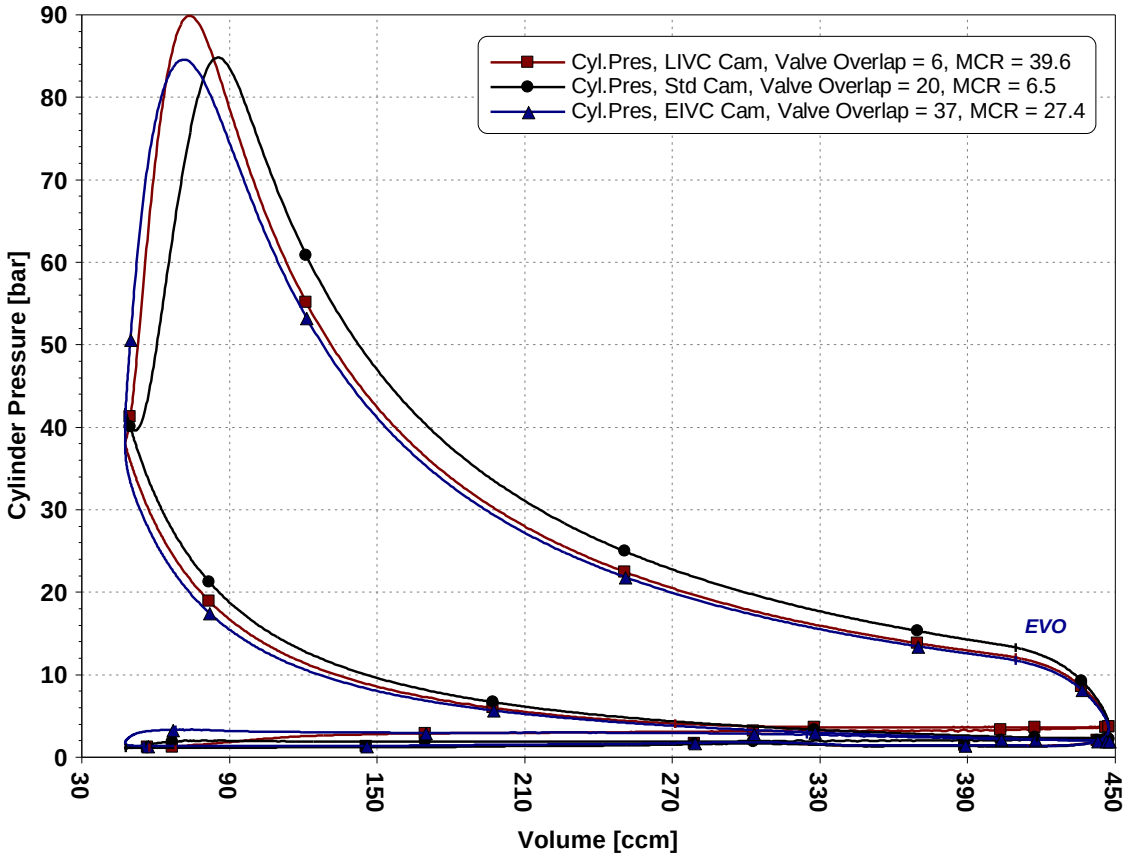

Figure 4.39 Entire P-V Diagrams of Three Intake Cams at 2000rpm 25.6bar NIMEP with Optimised Cam Timings

Figure 4.39 and 4.40 show the P-V diagrams at 2000rpm 25.6bar NIMEP with optimised cam timings. The timing for in-cylinder pressure reaches its maximum point is noticeably advanced by EIVC and LIVC cams compared with situation with the standard cam. Peak cylinder pressure of LIVC is higher than these of EIVC and standard cam. It is because of its advanced CA50 timing and relatively normal combustion rate.

In Figure 4.40, it is the enlarged low pressure loop in P-V diagram showing gas exchange process. For LIVC cam, cylinder pressure stays quite flat at the beginning of compression stroke until intake valves are closed at about 270ccm cylinder volume. Effective compression starts from this point. For EIVC cam, cylinder pressure drops after intake valves closure at around 325ccm cylinder volume in the intake stroke. When piston moves upwards after BDC, cylinder pressure increases slowly and almost just compensates the pressure drop caused by earlier IVC. Both are the representative feature of Miller cycle operation and make the compression stroke shortened. Thus the mean

cylinder pressure level during compression with LIVC or EIVC is lower than that of standard cam, which is also contributory to the improved fuel conversion efficiency.

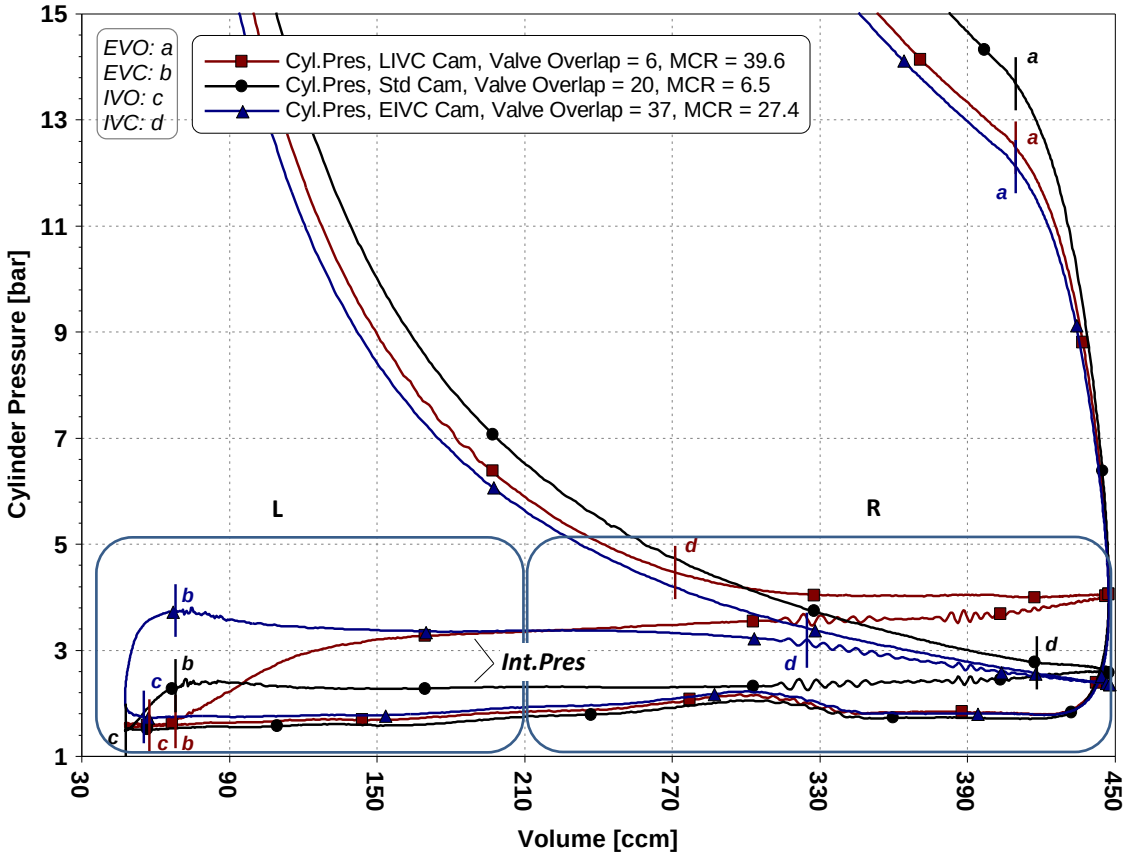

Figure 4.40 Low Pressure Loop in P-V Diagrams of Three Intake Cams at 2000rpm 25.6bar NIMEP with Optimised Cam Timings

R box in the P-V diagrams is to highlight gas exchange process close to BDC. The area between intake pressure curve and exhaust pressure curve of LIVC cam is bigger than that of the EIVC cam, when intake and exhaust pressure conditions are similar. It suggests that LIVC cam can generate more pumping work than EIVC cam.

Figure 4.41 shows the gas exchange process around TDC. Intake cam timing is advanced to achieve earlier IVC timing for Miller cycle operation with EIVC cam, and meanwhile IVO timing is also advanced. Intake valves are opened before TDC with EIVC cam, which is much earlier than those of standard cam and LIVC cam. EIVC cam has 37dCA valve overlap while the Miller cycle ratio is also high at 27.4%. Since intake pressure is much higher than cylinder pressure and exhaust pressure at IVO timing, cylinder pressure is enhanced rapidly after IVO. Exhaust pressure also increases again after IVO

due to the scavenging effect. It is also shown in the P-V diagram as highlighted in box L. In this region, EIVC cam generates more pumping work than LIVC cam.

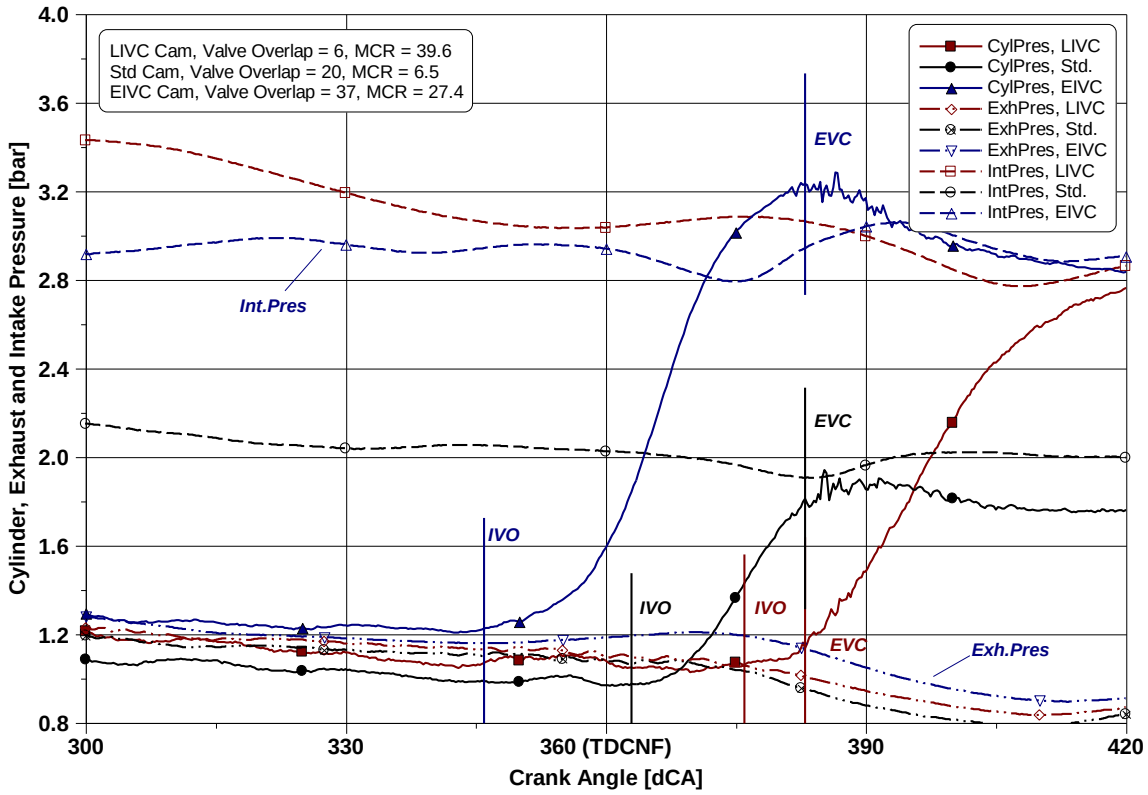

Figure 4.41 Gas Exchange Process of Three Intake Cams at 2000rpm 25.6bar NIMEP with Optimised Cam Timings

4.8 Summary

This chapter has presented the experimental results obtained with three cam designs in a single cylinder GDI engine at a low compression ratio of 9.3. The impact of exhaust back pressure and friction loss connected to boosting supply in real engine were not considered in this chapter. The engine was operated at exhaust lambda one through closed loop control. Based on the test results, the impact of Miller cycle operation on engine fuel conversion efficiency was discussed. Difference between two approaches of EIVC or LIVC for realising Miller cycle have been compared as well. The relative effects were analysed of the valve overlap and Miller cycle operation through variable valve timings and boost pressure.

Both LIVC and EIVC cams were found to benefit the engine efficiency by reducing pumping work at part load and suppressing knocking at high load. LIVC cam is able to improve engine fuel economy at all tested points by up to 2.6% higher IEffn than standard cam, while EIVC cam is particularly effective at highest load. The impact of the two cams on the engine performance and emissions can be divided into 4 regions as shown in Figure 3.5.

(1) At the lowest load (idle) operation, the optimum performance is achieved with small valve overlap. Large overlap leads to high residual gas fraction, which can cause long ignition delay, slow combustion, unstable combustion even misfire and high HC, CO emissions. The LIVC cam design enables small valve overlap operation with later IVC timing and high Miler cycle ratio, thus resulting in much less pumping loss and consequently better IEffn than the standard cam and EIVC cam.

(2) In the low load region 2, higher engine fuel conversion efficiency is obtained with a large valve overlap, which enables the back flow of burned gas from cylinder to intake ports. This will increase intake air temperature and in cylinder charge temperature for better mixture formation and faster combustion. Increased internal EGR is also contributory to reduced pumping loss, which has great impact on engine fuel economy at part load for gasoline engines. The advanced intake valve timing of EIVC cam improves the IEffp through both higher Miller cycle ratio and the longer valve overlap period.

(3) At mid load area around 9.0bar NIMEP, generally the intake valve timings are retarded for optimum ISFCn. However, the underlying processes are different between LIVC cam and EIVC cam. ISFCn is improved by higher IEffg and IEffp. In the case of LIVC cam retarded intake cam timing leads to a high Miller cycle ratio and it has greater impact on improving IEffp but less impact on IEffg. In contrast, IEffg is more affected by the intake valve timings of EIVC cam. As the intake valve timing is retarded, the effective compression ratio is increased and the fuel enrichment reduced with less scavenging taking place during shortened overlap period.

(4) When operating at the higher load conditions in region 4 where the spark timing is knock limited, optimum intake valve timings are found at the lower effective CR so that the spark timing can be advanced to optimise the combustion phasing

without incurring knocking combustion. In particular, EIVC cam provides both the advantage of Miller cycle operation and scavenging effect through advanced intake valve timings and is shown most effective in improving the performance and efficiency of the highly downsized direct injection gasoline engine at higher load operations.

Finally, it is noted that the ignition and combustion process were compromised by the EIVC and LIVC cams at most operating conditions because of reduced turbulence at the end of compression. In order to achieve maximum benefits from the Miller cycle operation, Intake ports and combustion chamber design should be optimised for higher tumble flows for faster combustion.

Chapter Five

Synergy between High Compression Ratio and Miller Cycle Operation

Chapter 5 Synergy between High Compression Ratio and Miller Cycle Operation

5.1 Introduction

In Chapter 4, the experimental study on Miller cycle operations with LIVC and EIVC cams at a low compression ratio was discussed. Miller cycle has the potential to improve engine fuel conversion efficiency by reducing the pumping loss at part load and suppressing knocking combustion at high load. However it was found that the reduced effective CR could limit the benefit gained by Miller cycle, especially at low load where spark timing is not restricted by detonation. To explore the full potential of Miller cycle for improving engine efficiency, a further study was carried out at an increased compression ratio of 12.8:1, which is described as the High Compression Ratio (HCR) in the thesis. The same engine setups and procedures as described in Chapter 4 were adopted. This chapter will discuss the results and findings.

5.2 Overview of Optimised Valve Timings

Three configurations were tested on the single cylinder engine installed with a high compression ratio piston, including the standard exhaust camshaft with the standard intake camshaft, the long duration LIVC intake cam, or the short duration EIVC intake cam. For each camshaft combination, cam envelope tests were carried out at ten steady operation points as shown in Figure 4.42. Optimised cam timing strategies were identified for the best ISFCn for the three intake camshafts at the higher compression ratio. The engine performance and emission results were then compared between the standard and high compression ratio operations.

Figure 5.1 shows the optimised exhaust cam timings of both the standard and higher compression ratio operations. The optimised exhaust cam timings for all three intake camshafts are the most retarded EVO with the minimum exhaust blowdown loss as discussed in Chapter 4. As shown in Figure 5.2, the optimised intake cam timings for each intake cam profile are also very similar between the two compression ratios. These results suggest the compression ratio has a negligible impact on the optimised valve

timing strategy. Details of valve timing optimisation were discussed in Chapter 4. This chapter will focus on the impact of increased compression ratio on engine fuel efficiency and emissions during Miller cycle operation.

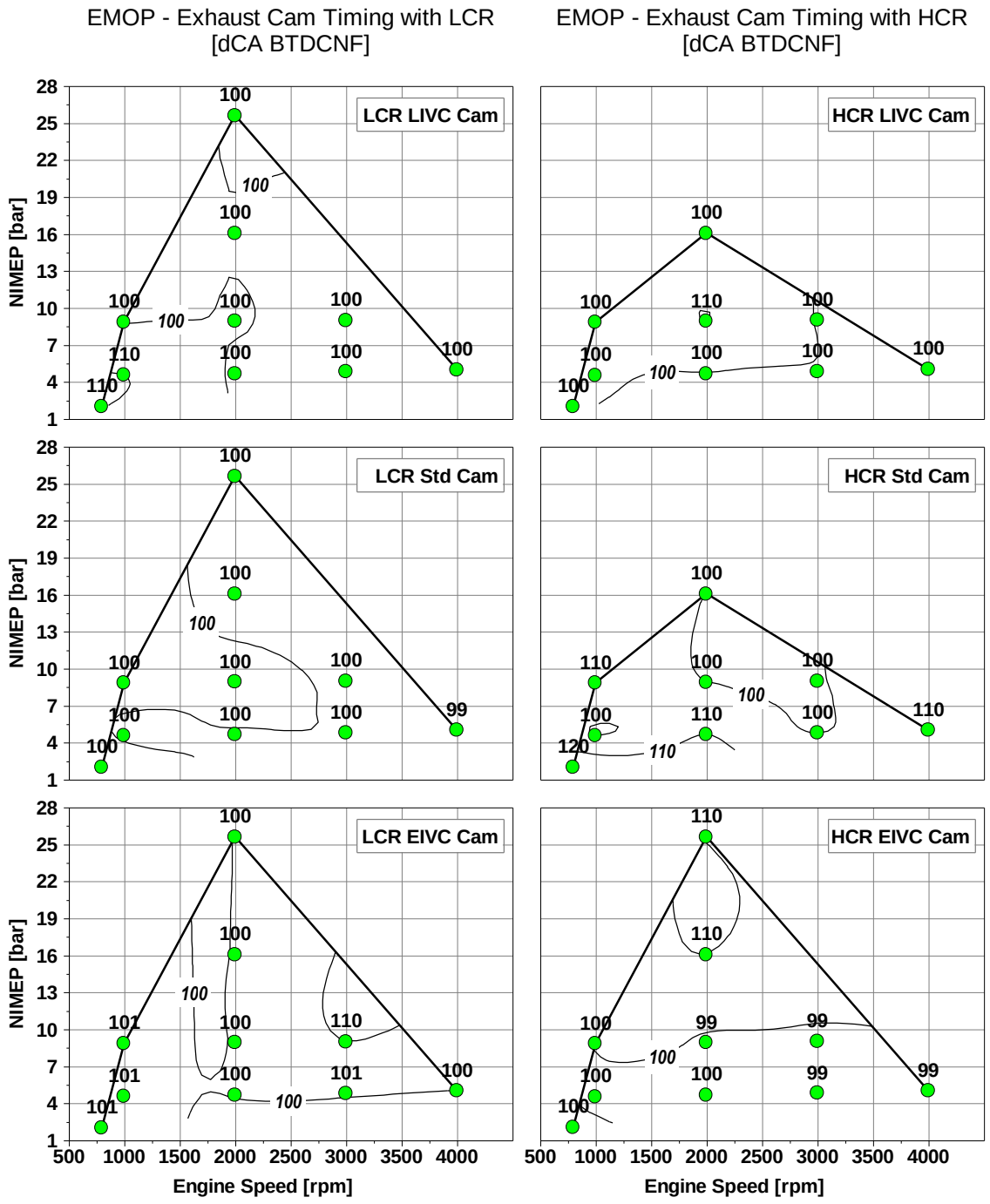

Figure 5.1 Optimised Exhaust Cam Timings at Low CR vs at High CR

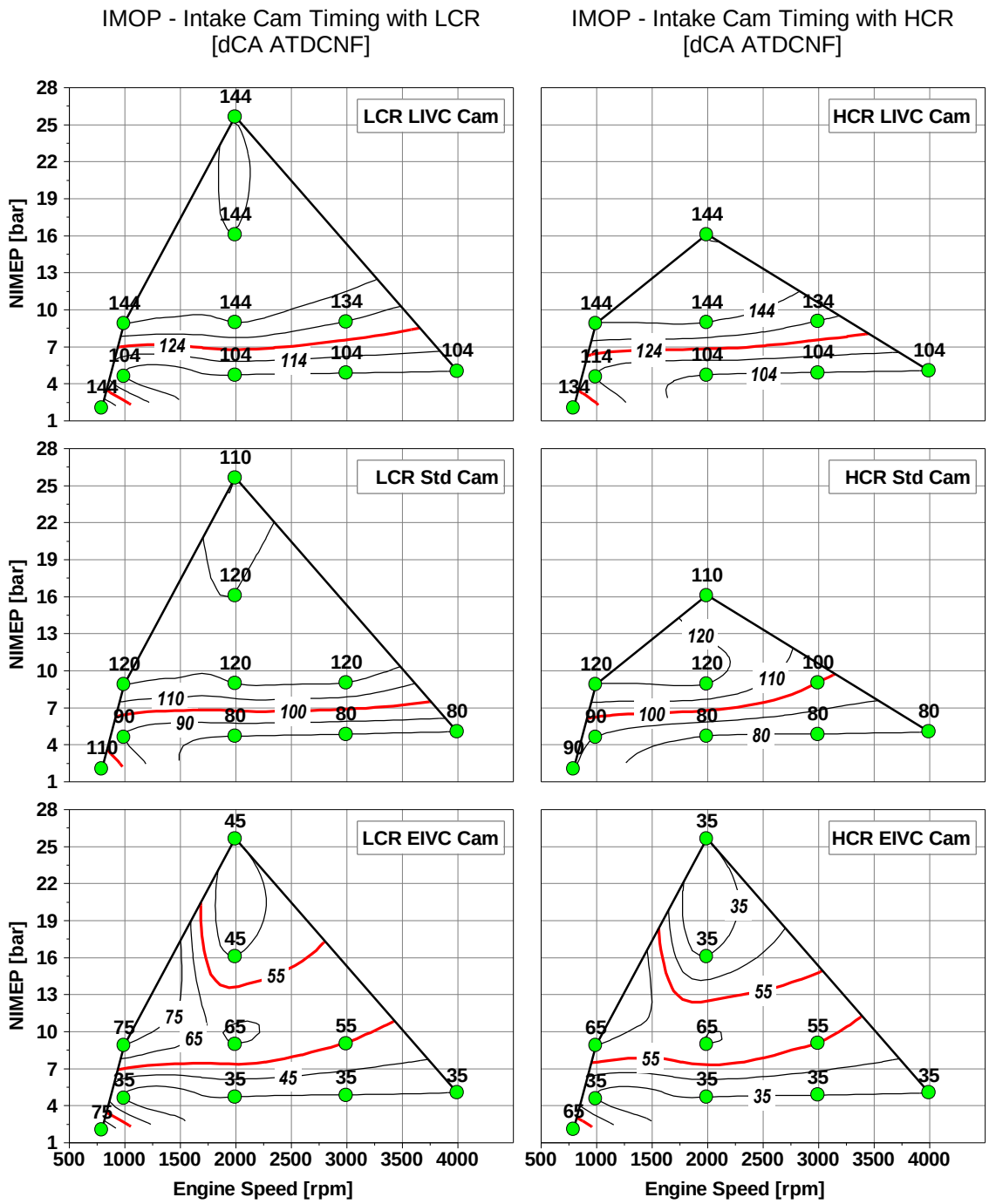

Figure 5.2 Optimised Intake Cam Timings at Low CR vs at High CR

Low Speed Pre-Ignition (LSPI) or Super-knock occurred when the engine was operated at 2000rpm 25.6bar NIMEP with HCR LIVC cam and HCR standard cam, which resulted in randomly excessive high peak cylinder pressure over 200 bar. The tests were not continued to avoid damage of the single cylinder research engine, hence no data was obtained at such conditions. A small range of cam envelope testing could be carried out at this point with the EIVC cam and high CR, as shown in Figure 5.3. As discussed in

Chapter 4, the EIVC cam applies high ratio of Miller cycle operation and scavenging effect simultaneously during the longer valve overlap period. Together with a lower effective CR by the earlier IVC, the in-cylinder charge thermal load is further reduced due to decreased residual gas fraction by the increased scavenging process. These two factors allow the EIVC cam to supress the knocking and pre-ignition combustion at low speed high load operation. However the combustion stability gets worse than the guideline of 4% COV of GIMEP quickly if the cam timings are shifted away from the optimum point, because the combustion timing CA50 has to be retarded quite late and combustion duration becomes long.

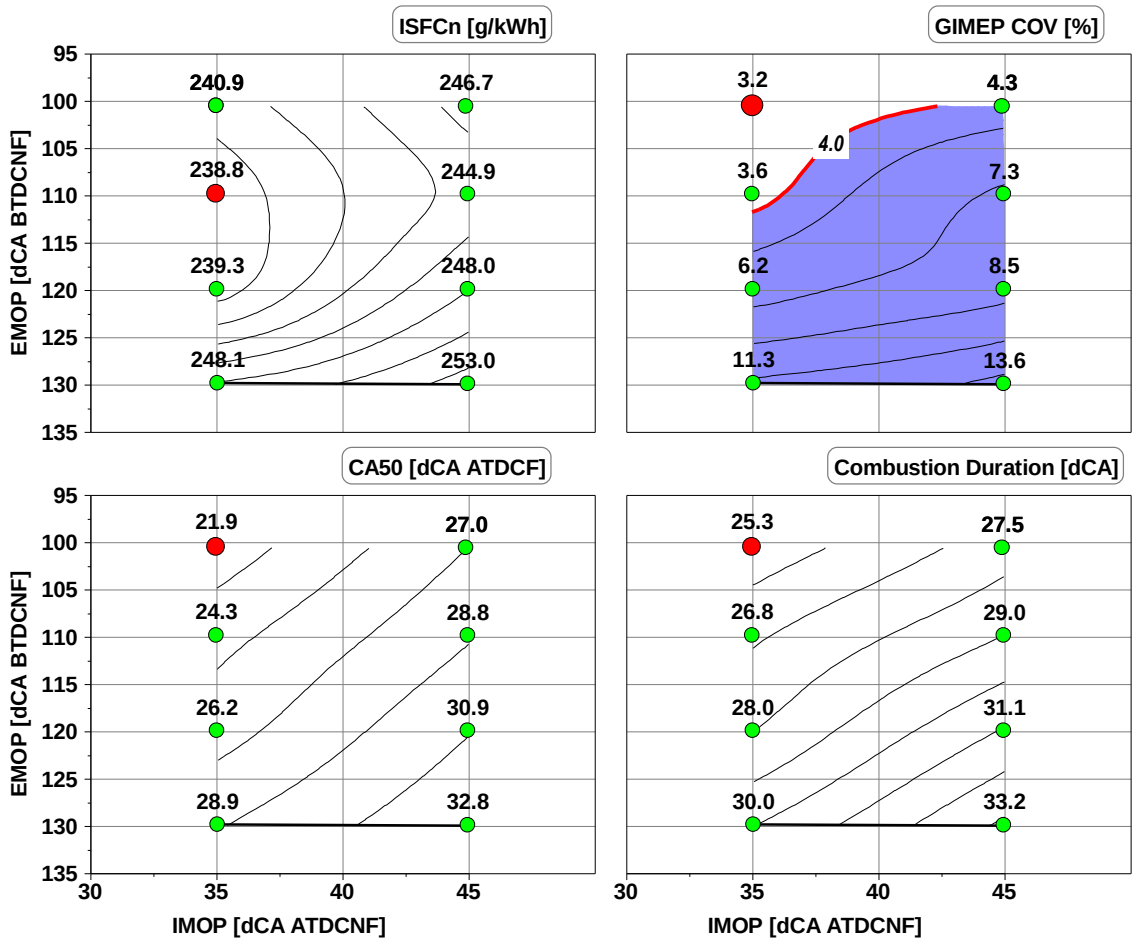

Figure 5.3 Cam Envelope Results at 2000rpm 25.6bar NIMEP with HCR EIVC Cam

5.3 Impact of High Compression Ratio with Standard Intake Cam

Figure 5.4 shows the differences of indicated efficiencies between HCR and LCR while running with the standard intake cam, based on the optimised ISFCn results of these two hardware setups. High CR increases IEffg at low to mid load points hence improves IEffn in this area of operation. However both IEffg and IEffn get much worse with HCR than with LCR at high load region, where knocking combustion is the main limit to gasoline engine efficiency. As mentioned earlier, the highest NIMEP achievable by HCR and standard cam hardware is limited by low speed pre-ignition and mega-knock with a peak cylinder pressure over 200bar.

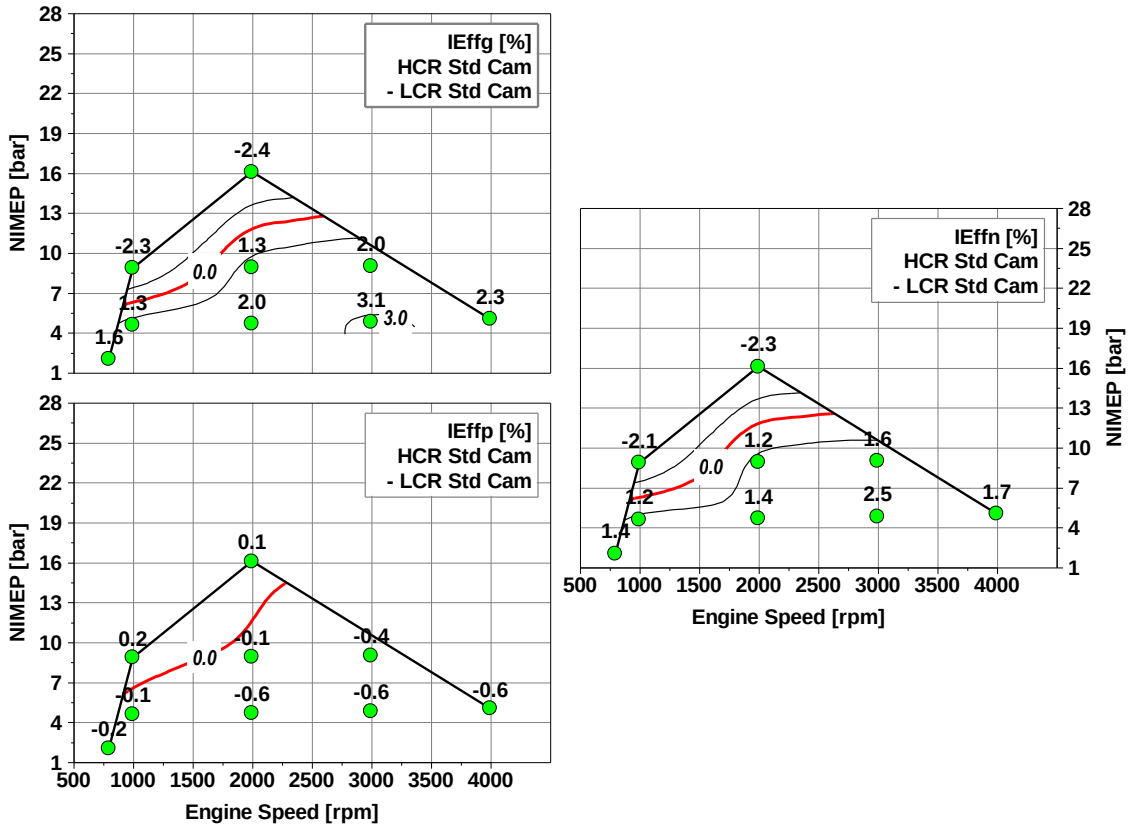

Figure 5.4 Differences of Indicated Efficiencies between HCR and LCR with Standard Cam

Figure 5.5 shows the intake port pressure employed by the two hardware configurations for achieving the target load. At low load area, HCR engine operation has higher overall fuel conversion efficiency, thus it uses less fuel and also air for the defined NIMEP. As a result, intake port pressures at these points are lower with HCR than with LCR, hence LCR experiences less pumping loss and higher IEffp. At low speed and high load points

when IEffn gets worse with HCR, engine needs more fuel and air, which results in higher intake port pressure and higher IEffp. However the difference in IEffg between two CR conditions is the main cause to the change in IEffn.

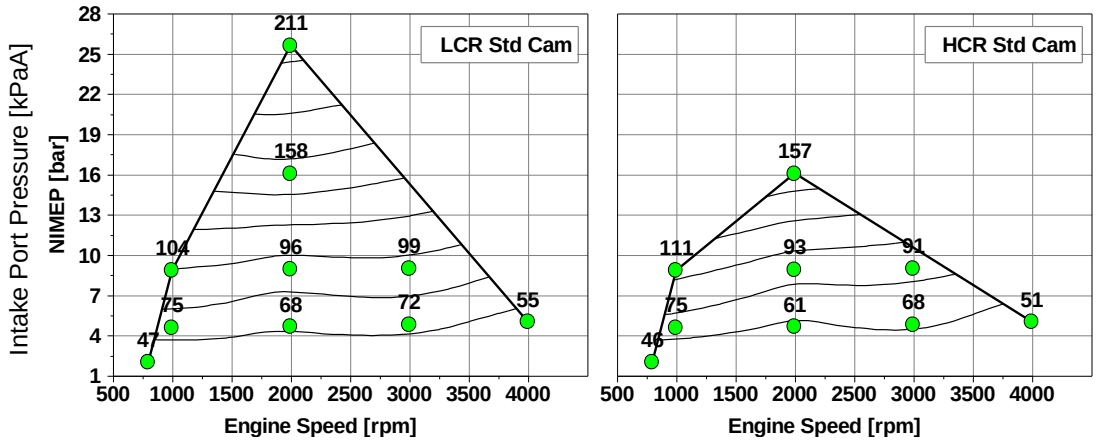

Figure 5.5 Comparison of Intake Pressure between HCR and LCR with Standard Cam

Figure 5.6 compares the spark timing, combustion duration and timing between LCR and HCR at different engine speeds and load conditions when valve timings were optimised for the lowest ISFCn with standard cam. The spark timing is set to optimise CA50 around 8dCA ATDCF for the best engine efficiency at part load where it is not limited by knocking, as indicated by the shadowed area in the contour map. In this area, spark timings between LCR and HCR are very close. Both IEffg and IEffn become higher with increased CR.

At mid load around 9bar NIMEP, engine is still able to run at optimum spark timing for CA50 around 8dCA ATDCF at low CR setup. However spark timing and CA50 have to be retarded at high CR due to knocking combustion. Spark timing is retarded by 11dCA and 8dCA respectively at 2000rpm 8.9bar and 3000rpm 9.0bar at HCR. As a result the combustion duration becomes longer. The higher CR increases the in-cylinder charge temperature hence the ignition delay from spark timing to CA10 is shortened. HCR still achieves better IEffg and consequently higher IEffn than LCR at these two points since CA50 timing is still not too late.

At low speed high load area, spark timing has to be retarded by more than 10dCA to avoid knocking combustion with the HCR piston, resulting in longer combustion

duration and very late CA50 timing close to 30dCA ATDCF. As a result, both IEffg and IEffn of HCR become much worse than those of LCR.

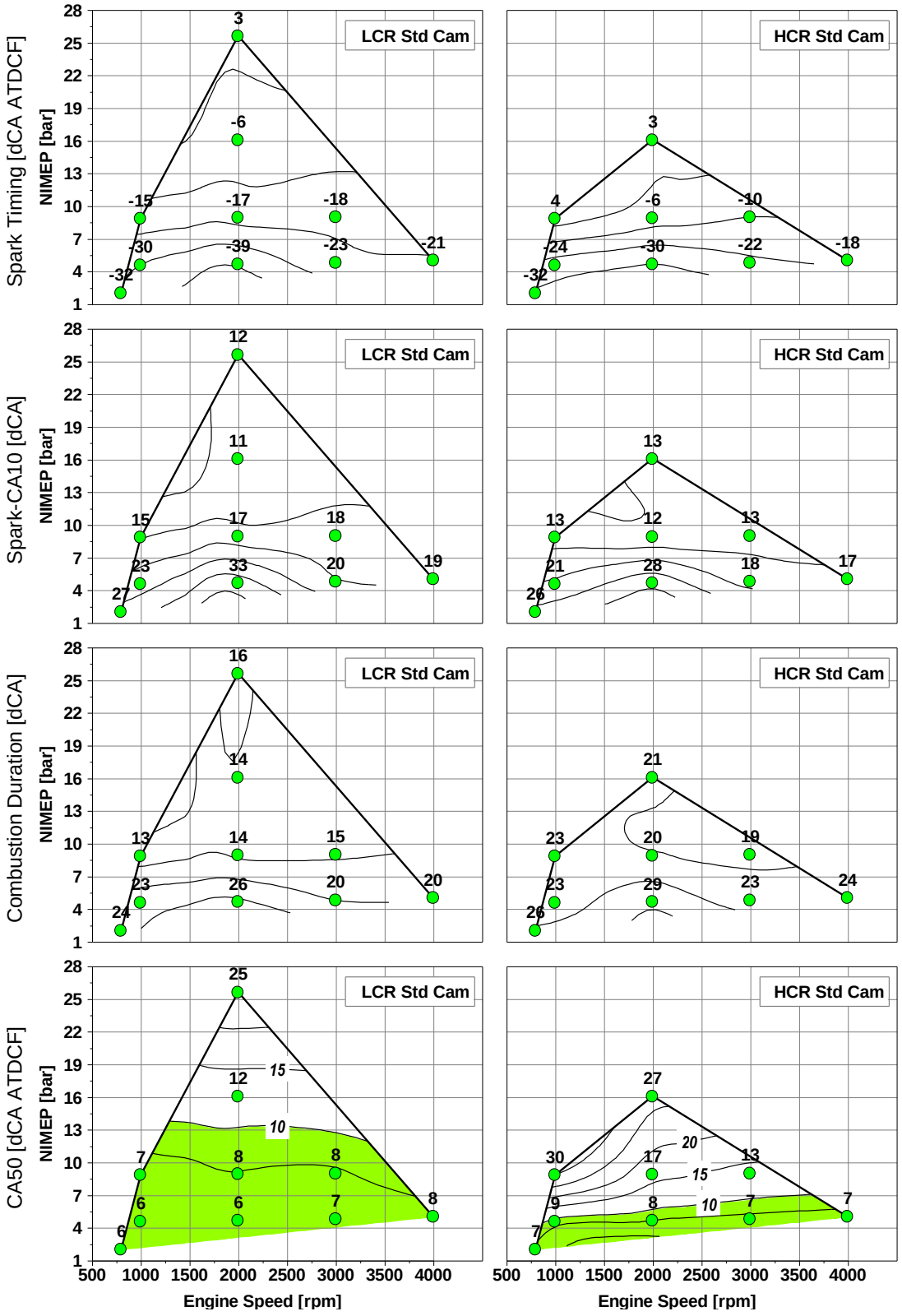

Figure 5.6 Comparisons of Spark Timing, Combustion Duration and Timing between HCR and LCR with Standard Cam

5.4 Impact of High Compression Ratio with LIVC Intake Cam

Figure 5.7 shows the differences of indicated efficiencies between high CR and low CR operations while the ISFCn was optimised with the LIVC intake cam. Higher CR improves IEffg by up to 3.5% and consequently better IEffn than LCR at almost all test points, except the high load operation of 16.0bar at 2000rpm where its gross and net indicated fuel conversion efficiencies are lower than those of LCR when spark timing is limited by the knocking combustion. The highest load of NIMEP 25.6bar could not be achieved by the HCR and LIVC setup due to the occurrence of pre-ignition and mega-knock.

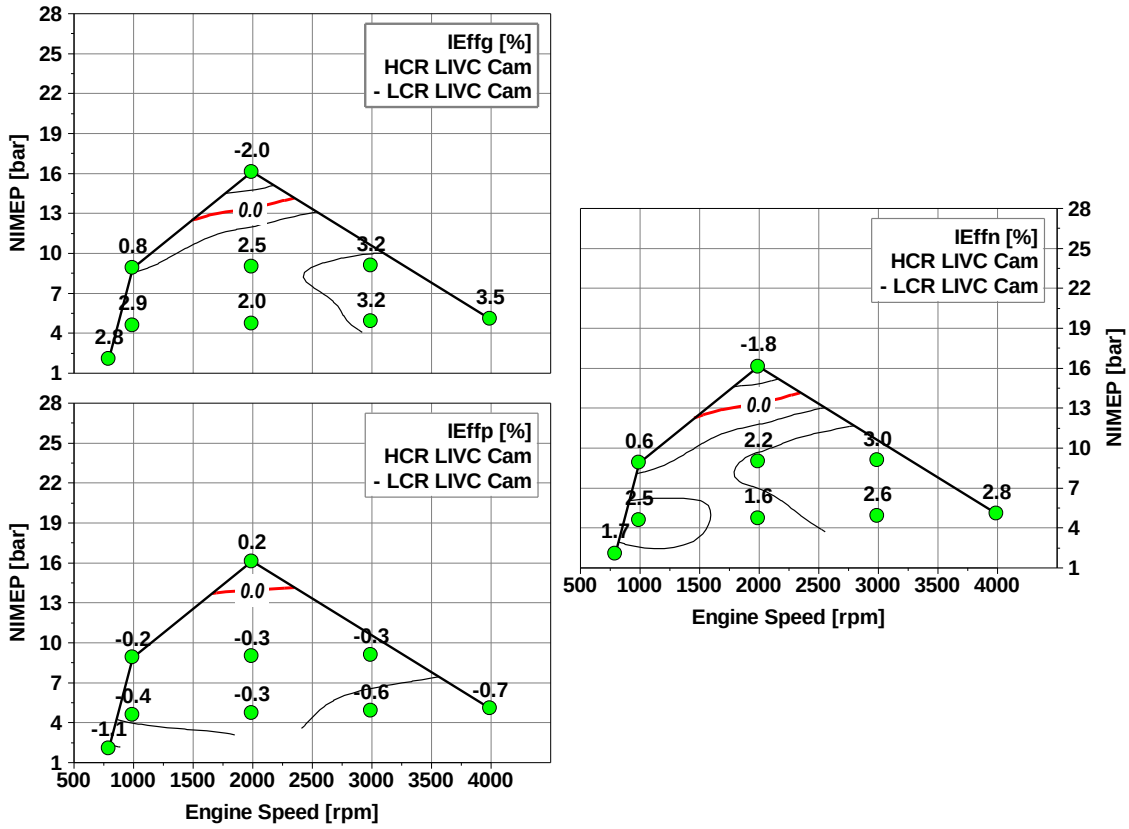

Figure 5.7 Differences of Indicated Efficiencies between HCR and LCR with LIVC Cam

Figure 5.8 shows the intake port pressure used for HCR LIVC and LCR LIVC hardware configurations to run at each test points. In the area where HCR has higher gross and net fuel conversion efficiencies, less fuel and air and hence lower intake port pressures are required. Although this makes HCR hardware suffer from more pumping loss, i.e. lower IEffp than that of LCR, increased IEffg by higher CR is the dominant factor to improve engine fuel economy.

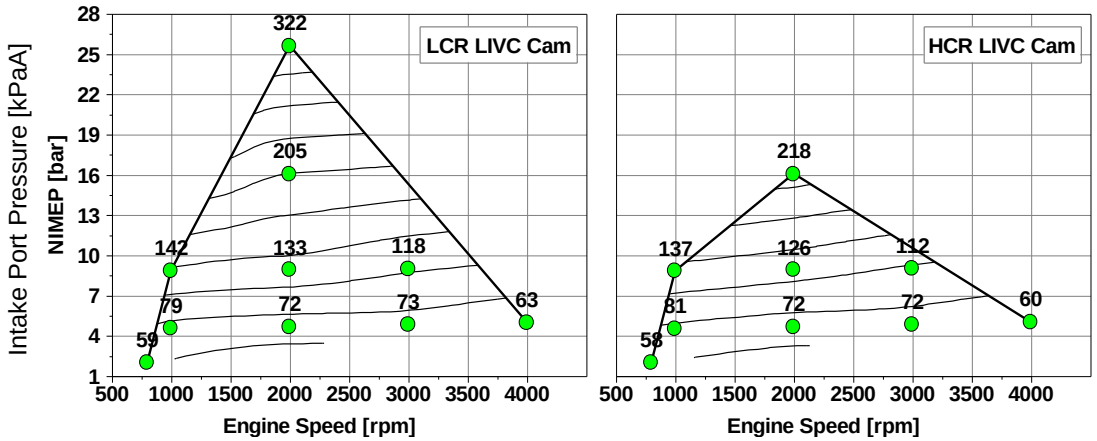

Figure 5.8 Comparison of Intake Pressure between HCR and LCR with LIVC Cam

The optimised spark timing, combustion duration and timing of LCR LIVC cam and HCR LIVC cam are presented and compared in Figure 5.9. The shadowed area in the contour map of CA50 shows that the spark timing is optimised to place CA50 around 8 dCA ATDC for the best engine efficiency. In these areas, high CR improves engine thermodynamic efficiency hence it increases the gross and net indicated fuel conversion efficiencies.

Figure 5.9 also shows that LIVC cam extends the shadowed area compared with the results of standard cam as shown in Figure 5.6. At mid load region around 9bar NIMEP and high load area, optimised valve timing strategy for LIVC cam is to retard IVC timing for Miller cycle operation as discussed in Chapter 4. The LIVC cam allows the high CR operation to have more advanced CA50 timing than the standard cam without knocking combustion. For example, at 1000rpm 8.8bar CA50 is 15 and 30 dCA ATDCF respectively for the LIVC cam and the standard cam, which allows the higher thermal efficiency to be achieved by increased expansion process without being compromised by the knocking combustion.

In the mid-load area, combustion duration is extended due to retarded spark timing at HCR. However ignition delay becomes shorter at HCR because of high charge temperature at the end of compression stroke, which compensates the disadvantage of longer combustion duration and is beneficial for earlier CA50. At 2000rpm 16.0bar NIMEP, the spark timing is retarded by 10dCA, combustion duration is lengthened by 7dCA and consequently the CA50 timing is retarded by 15dCA at HCR. As a result HCR has worse efficiency than LCR at this point.

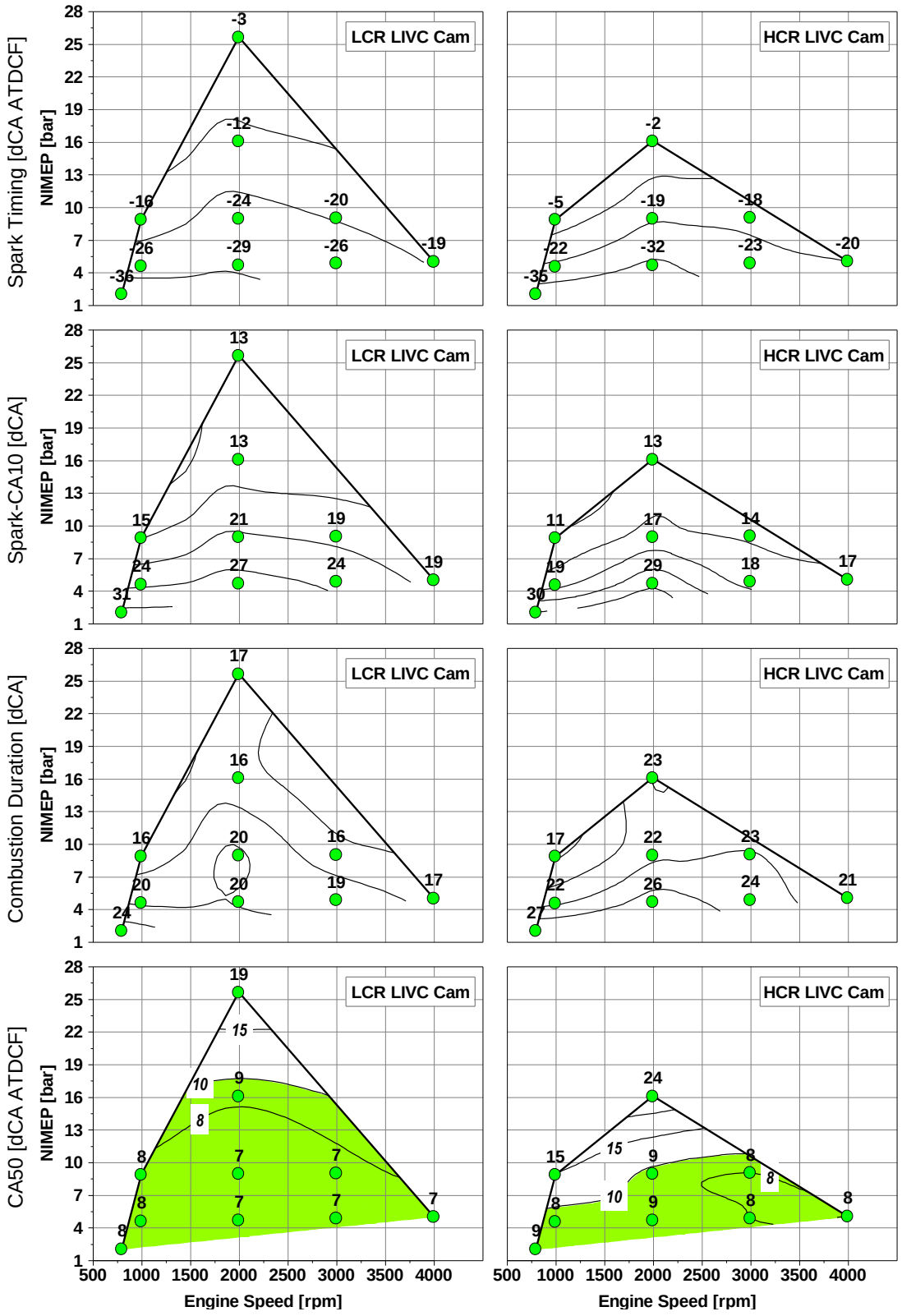

Figure 5.9 Comparisons of Spark Timing, Combustion Duration and Timing between HCR and LCR with LIVC Cam

5.5 Impact of High Compression Ratio with EIVC Intake Cam

Figure 5.10 shows the differences of indicated efficiencies between HCR and LCR with the EIVC intake cam which timings are optimised for maximum net indicated efficiency. High CR increases IEffg and subsequent IEffn in the whole operation map except the highest load point of 25.6bar NIMEP at 2000rpm. The improvement is up to 4.7% on IEffg and up to 3.6% for IEffn, which shows strong synergy between high CR and Miller cycle operation with EIVC cam.

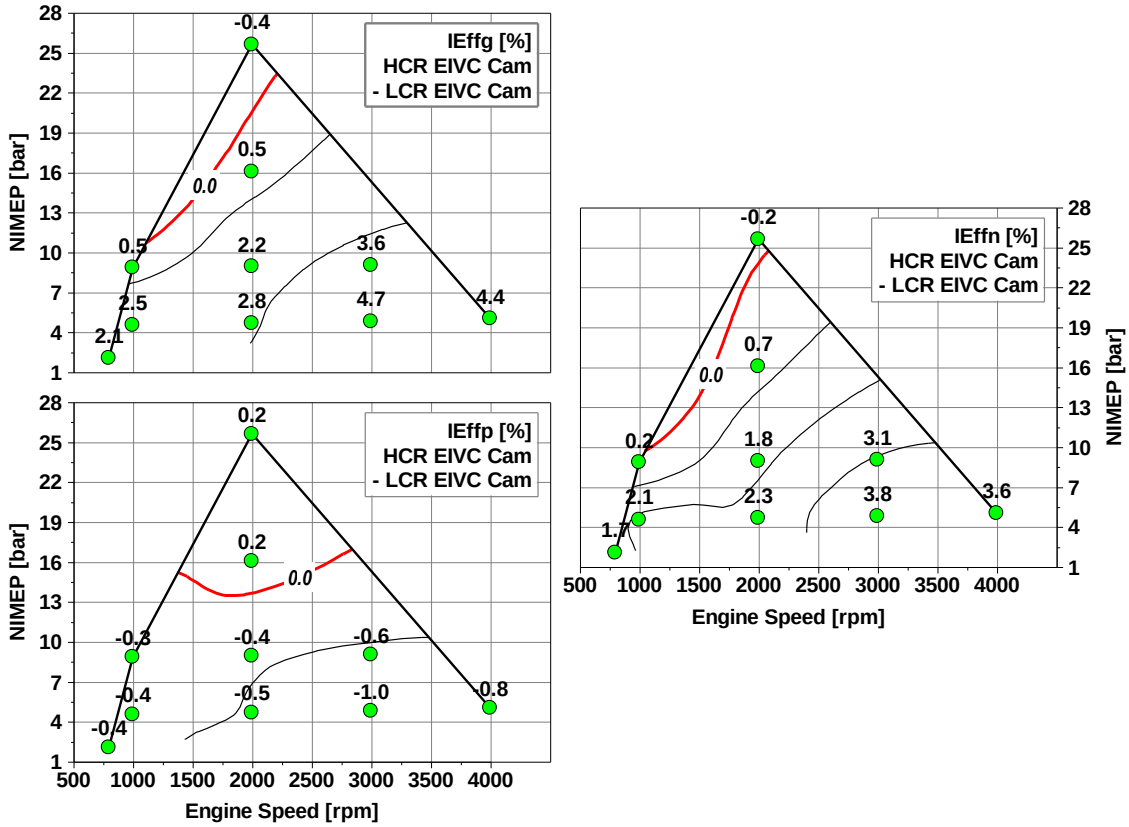

Figure 5.10 Differences of Indicated Efficiencies between HCR and LCR with EIVC Cam

Figure 5.11 shows the intake port pressure employed by the HCR EIVC and LCR EIVC hardware configurations to achieve target NIMEP at each test points. HCR setup needs lower intake pressure than LCR at part load hence produces more pumping loss shown in Figure 5.10. As shown in Figure 5.2, IMOP timings of EIVC cam are advanced slightly for HCR at low speed high load region, which applies a higher Miller Cycle Ratio (MCR) to reduce knocking tendency but needs higher intake pressure. As a result, HCR EIVC gets more positive pumping work than LCR EIVC status at high load points shown in Figure 5.10.

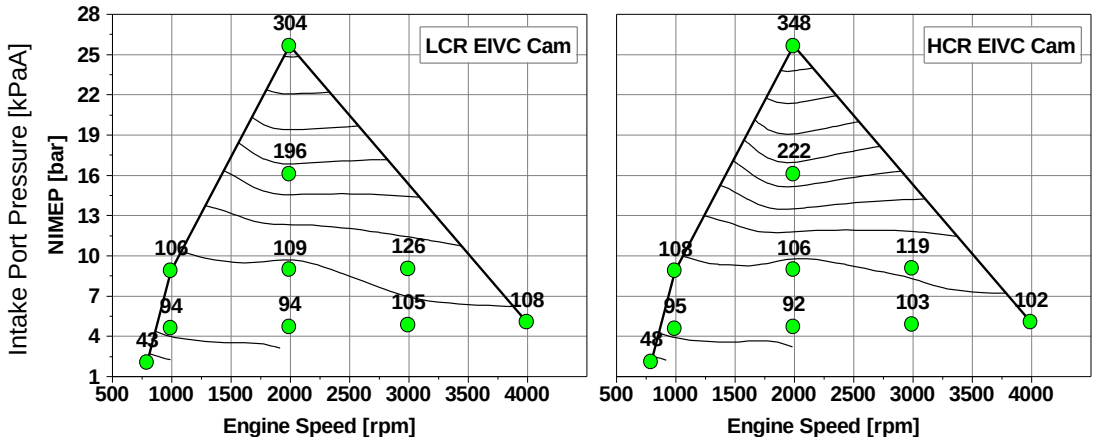

Figure 5.11 Comparison of Intake Pressure between HCR and LCR with EIVC Cam

Figure 5.12 compares the optimised spark timing, combustion duration and timing between LCR and HCR when tested with the EIVC cam. Spark timing is adjusted to optimise CA50 around 8dCA ATDCF at low load region with HCR EIVC, where the increased CR achieves the biggest improvement in IEffg.

As discussed in Chapter 4, retarded IVC timing of the shorter EIVC cam is used in the mid load area to improve IEffg by increasing effective CR. Although the EIVC cam doesn't advance CA50 timing as much as the LIVC cam does, it still enables earlier CA50 timing than the standard cam at HCR. As a result, HCR is still able to gain some fuel economy benefits compared with LCR EIVC cam in this region.

HCR EIVC cam combination applies the most advanced intake valve timings at high load points for maximum Miller cycle ratio and also strong scavenging effect as discussed previously. The synergy between these two technologies provides the engine with excellent capability to suppressing knocking combustion. The engine with such a combination can run at the highest load of 25.6bar NIMEP without occurrence of mega-knock during engine testing, while the engine cannot be run at this load with other two intake cams at HCR because of mega-knock. When all tested at HCR, EIVC cam achieves 18dCA ATDCF CA50 timing at 2000rpm 16.0bar, while LIVC cam can only reach 24dCA and standard cam has to retard to 27dCA. The advanced combustion timing with EIVC cam at high load provides several benefits, such as higher fuel conversion efficiency, reduced risk of low speed pre-ignition and better combustion stability.

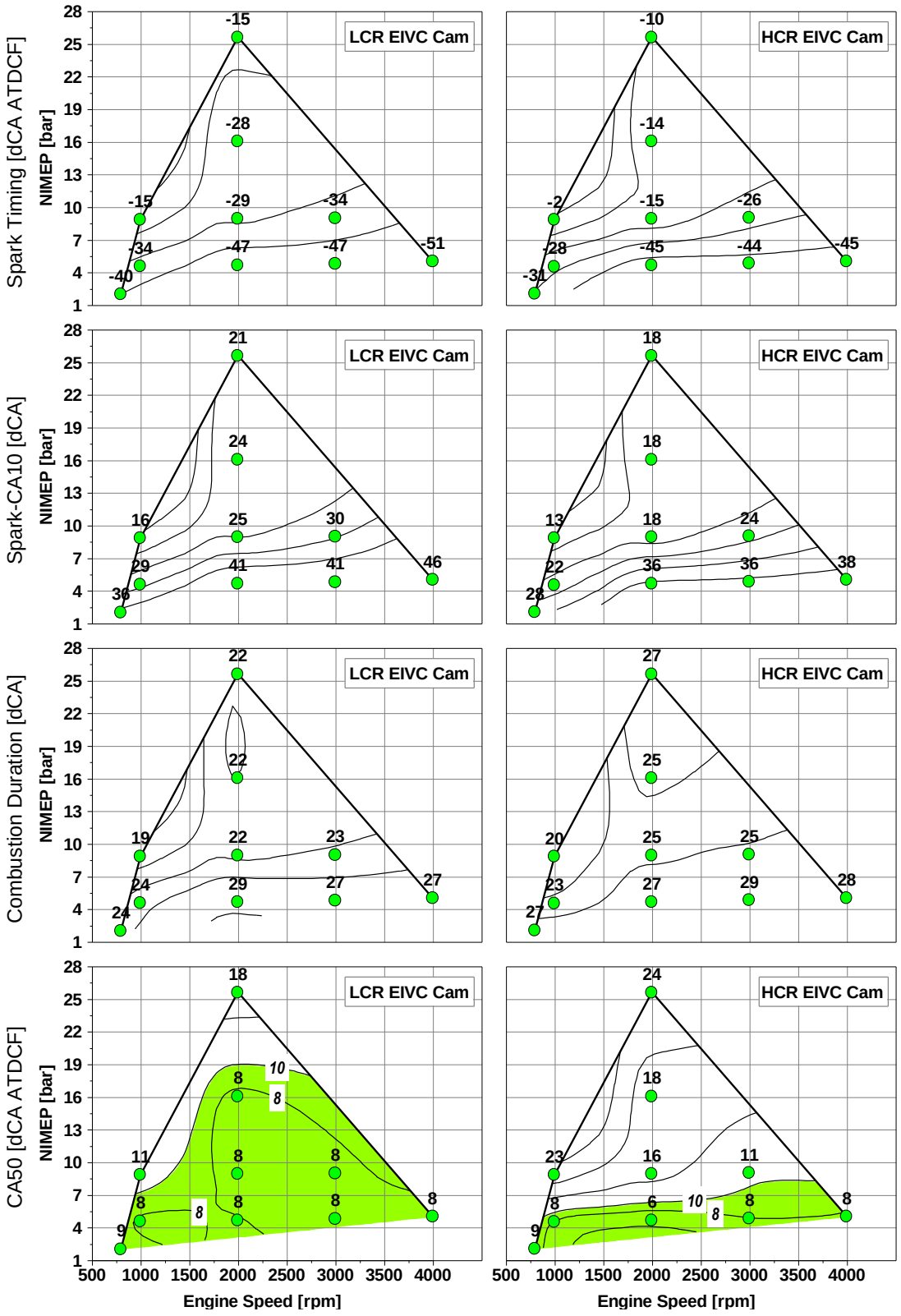

Figure 5.12 Comparisons of Spark Timing, Combustion Duration and Timing between HCR and LCR with EIVC Cam

5.6 Comparison among Three Intake Cams at High Compression Ratio

Figure 5.13 shows the differences of IEffn, IEffg and IEffp between LIVC or EIVC cam and standard cam with the high CR piston. Figure 4.4 presented in previous Chapter 4 did a similar analysis at low CR condition. Comparison of the two figures can reveal the synergy between Miller cycle and high CR operations for improving engine fuel conversion efficiency.

As shown in Figure 4.4, both Miller cycle cams gained worse IEffg than the standard intake cam at most test points. It is because that the effective CR becomes too low during Miller cycle operation when the geometric CR is low at 9.3:1. The smaller effective CR reduces the thermodynamic efficiency. Knocking combustion is only present at high load conditions when the standard CR of 9.3 is used. Thus Miller cycle operation can only improve the IEffg at very high load conditions by reducing knocking tendency and advancing the combustion timing. When the geometry CR is increased from 9.3 to 12.8, the engine starts to have knocking issue at mid load region. Hence the benefits of Miller cycle operation extend to greater engine operating conditions. Both LIVC cam and EIVC cam have higher Miller cycle ratio (MCR) than the standard cam. The reduced effective CR can decrease in-cylinder charge temperature which may be too high for standard cam at high geometry CR condition. As a result, both LIVC cam and EIVC cam achieve higher IEffg than the standard cam almost in the whole engine testing map when running with high CR piston, which is shown in Figure 5.13.

Figure 4.4 also shows that with the standard compression ratio of 9.3 the shorter EIVC cam only gained better IEffn than standard cam at high load, but its net efficiencies were always lower than LIVC cam. However as shown in Figure 5.13, when used with the high CR piston the EIVC cam achieves the highest IEffn among the three cams at high load and most part load test points, because of the optimised combustion timing and maximum scavenging. At 2000rpm 16.0bar NIMEP, the EIVC cam improves IEffn by 2.7% than the standard cam and 1.2% more than the LIVC cam.

All three cams employ a large valve overlap period for low load optimisation. In addition the EIVC cam applies higher MCR simultaneously and hence it has the highest IEffp

among the three cams. Furthermore the EIVC cam gets the best net indicated efficiency among the three cams at low load around 5bar NIMEP from 2000rpm to 4000rpm.

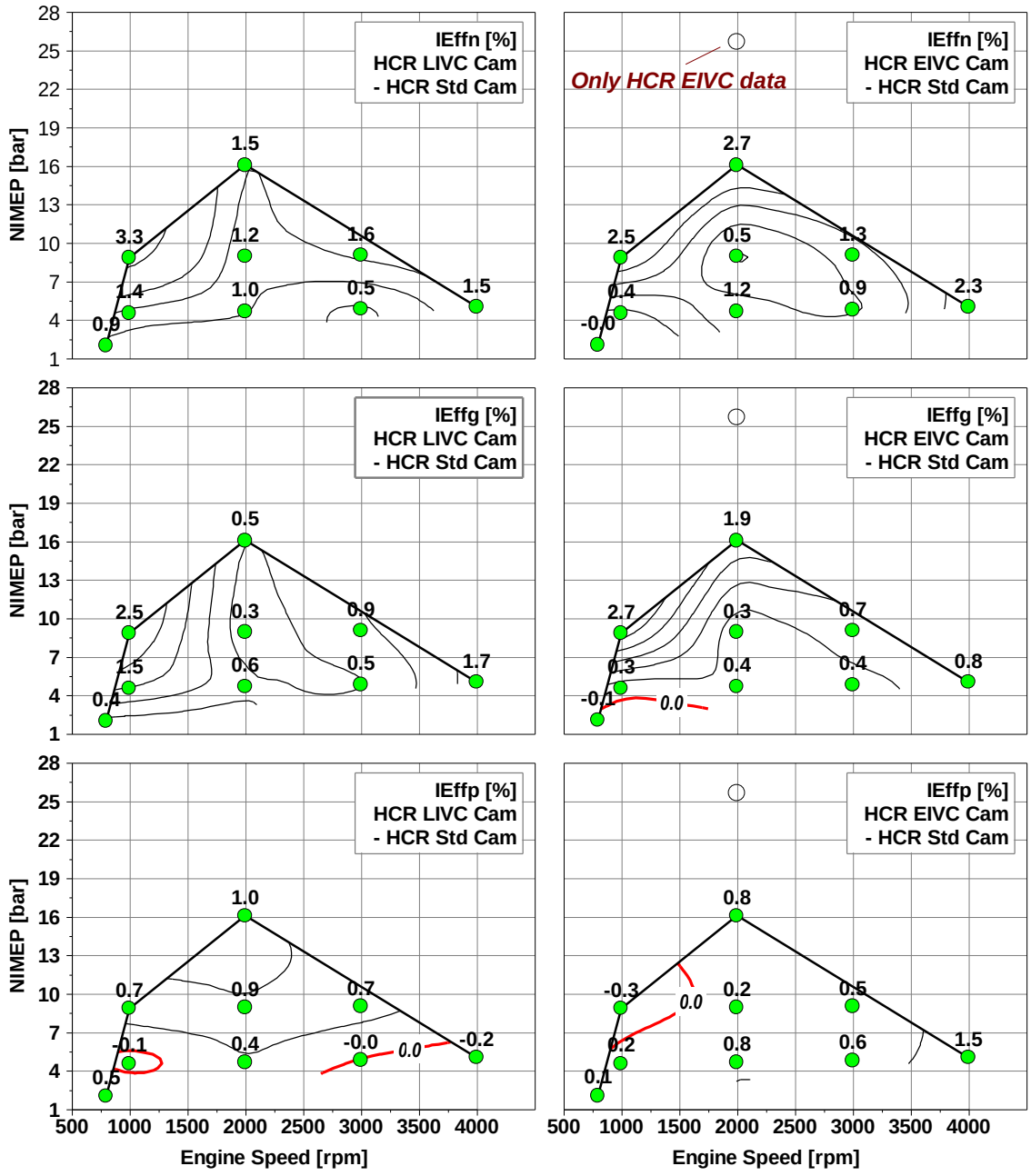

Figure 5.13 Differences between Indicated Efficiencies of LIVC / EIVC Cam and these of Standard Cam at High CR

5.7 Fuel Economy Improvement by combining Miller Cycle and High Compression Ratio

Figure 5.14 shows the improvement on engine net indicated fuel consumption achieved by Miller cycle operation and high CR while compared with the baseline, i.e. standard intake cam and low CR configuration. The EIVC cam with a high CR piston reduces engine fuel consumption at all test points and achieves the maximum benefits at low load and high load regions.

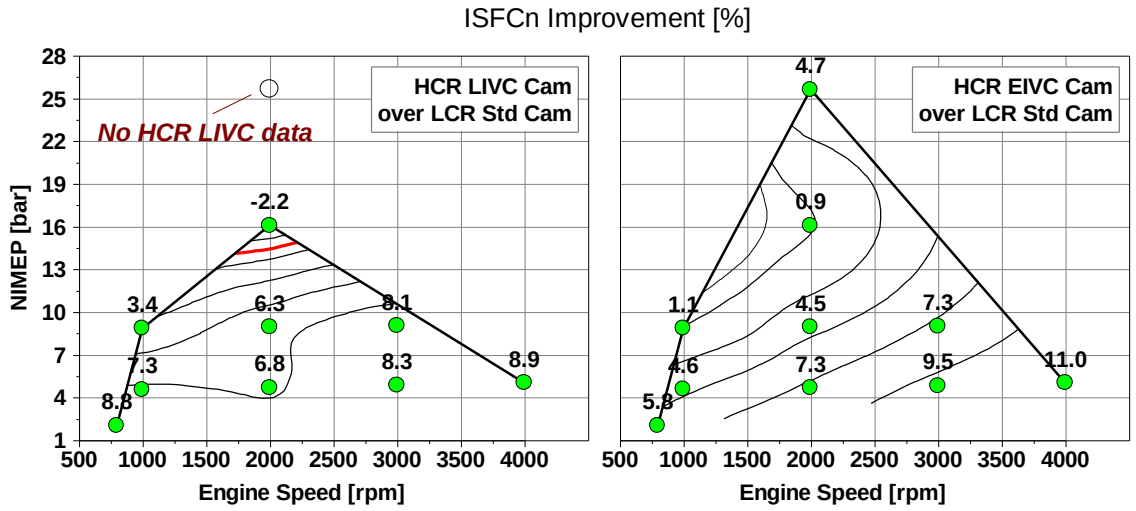

Figure 5.14 ISFCn Improvement of LIVC / EIVC Cam with HCR compared to Standard Cam with LCR (baseline)

As discussed in Chapter 2, pumping loss is the main cause for low fuel conversion efficiency on gasoline engines at low load area, which gets worse when engine speed goes higher. The pumping loss at low load condition is significantly reduced by the EIVC cam due to a larger valve overlap for more internal EGR and reduced throttling with Miller cycle operation. As a result, the combination of the EIVC cam and high CR piston improves ISFCn by up to 11% at this region.

When engine load becomes high, fuel conversion efficiency of gasoline engines is mainly deteriorated by the retarded combustion timing due to knocking combustion, which will become severer when higher CR is applied. The EIVC cam provides the synergy between Miller cycle operation for reduced effective CR and scavenging effect for decreased residual gas fraction, which are both helpful to reduce knocking tendency

and risk of pre-ignition and mega-knock at high load running. Thus EIVC cam extends the operation load at high CR setup, and it reduces the ISFCn by 4.7% at 2000rpm 25.6bar NIMEP compared with baseline engine. To be noted the baseline engine design was fully optimised including the geometry of low CR piston. However the high CR piston used in this study increases compression ratio by reducing piston recesses without re-optimising its geometry. It should make negative effect on the tumble generation and preservation especially when utilised with EIVC cam. Thus the potential benefit on fuel conversion efficiency to be achieved by the combination of EIVC cam profile and high CR can be even more than the level depicted in Figure 5.14.

In some mid-load conditions, the LIVC cam and high CR enable more ISFCn reduction to be achieved because of the lowest pumping work and slightly more advanced spark timing. For example, at 9bar NIMEP the LIVC cam improves ISFCn by 2.3% at 1000rpm, 1.8% at 2000rpm and 0.8% at 3000rpm more than the EIVC and higher CR setup.

At higher load condition above 16.0bar NIMEP, the LIVC cam still achieves lower fuel consumption than the standard cam when both cams tested with the high CR piston, as presented in Figure 5.13, because of the reduced charge temperature from the Miller cycle operation and hence slightly more advance of combustion process than the standard cam. However LIVC cam and HCR combination has worse ISFCn than the baseline standard cam and low CR piston setup at the high load point, where knocking combustion becomes extremely challenging.

Combination of the LIVC cam and EIVC cam with high CR can maximise the engine fuel consumption reduction, considering each of them is more beneficial for fuel conversion efficiency at a particular area. Figure 5.15 shows the maximised system benefits achieved by Miller cycle operation with LIVC and EIVC cam switching and high CR while compared to the baseline hardware configuration at ambient exhaust back pressure condition.

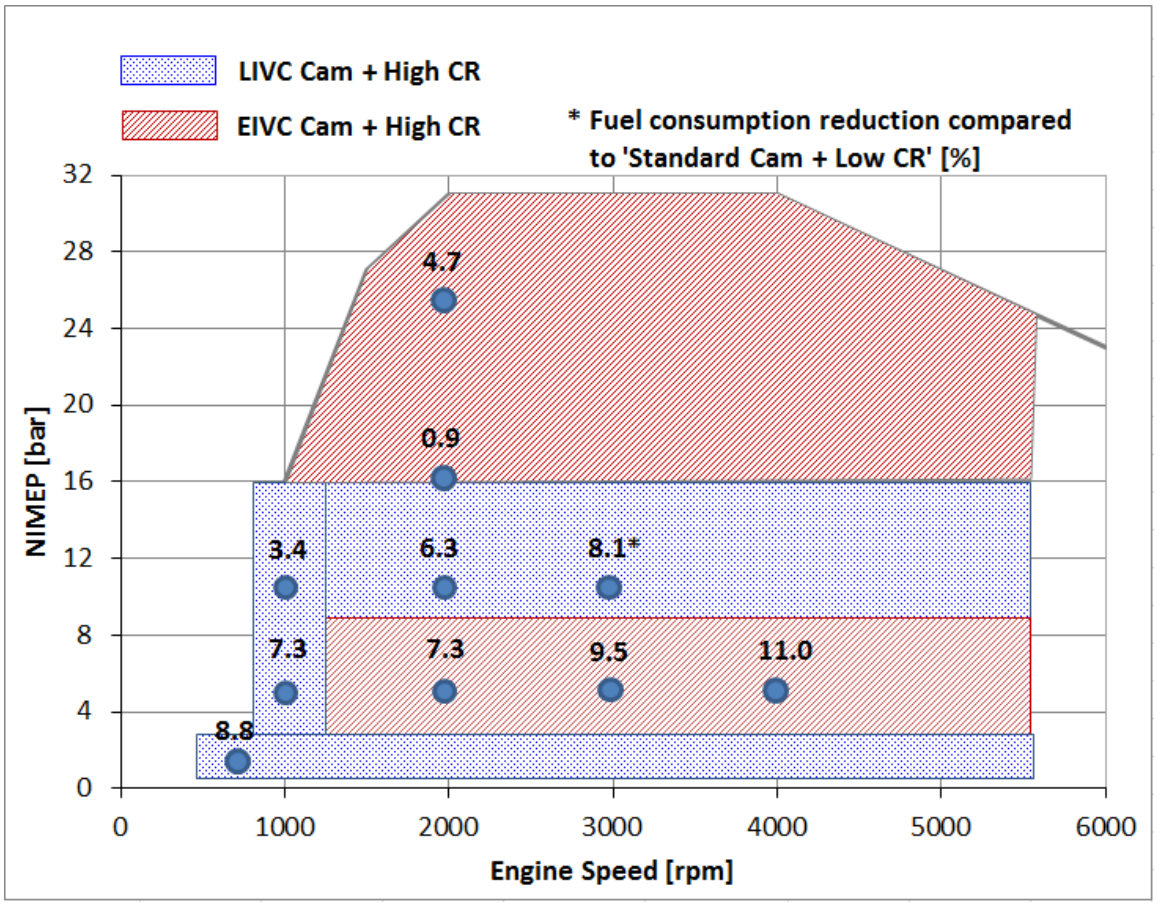

Figure 5.15 ISFCn Improvement of LIVC-EIVC Cam Switching with HCR compared to Standard Cam with LCR (baseline)

5.8 Summary

This chapter has presented the experimental results obtained with three cam designs in a single cylinder GDI engine at a high compression ratio of 12.8:1. Other boundary conditions for engine testing are the same as used for studies discussed in Chapter 4. Based on the test results, the benefits of combined Miller cycle operation with high geometry CR for improving engine fuel conversion efficiency are presented and discussed.

It is found that the increased CR hardly has impact on the optimisation strategy for valve timings of all three cams. Both LIVC and EIVC cams reduce the pumping loss at part load or increasing positive pumping work at high load through Miller cycle operation despite of compression ratio condition.

The advantage of Miller cycle operation for improving engine fuel economy is further enhanced by high geometric CR, which decreases the loss of thermodynamic efficiency caused by reduced effective CR due to early or retarded IVC timings of the short EIVC and long LIVC cams. Miller cycle operation reduces knocking tendency and advancing CA50 timing. As a result both LIVC and EIVC cams are able to achieve higher gross indicated fuel conversion efficiency (IEffg) than the standard cam at high CR condition in a large operating region.

Finally, it is noted that there is greater synergy in combining the EIVC cam with the high CR to achieve high Miller cycle ratio and large valve overlap period for maximum improvement in the overall engine efficiency. Larger valve overlap generates more internal EGR at low load and reduces pumping loss together with reduced intake duration by the shorter EIVC cam. At higher load, the large overlap enables more complete scavenging effect to reduce in-cylinder residual gas fraction and the lower effective compression ratio of Miller cycle reduces the charge temperature at the end of compression. As a result, advanced combustion timing can be used for better engine efficiency and combustion stability without the occurrence of knocking and low speed pre-ignition. These advantages enable the EIVC cam to gain the highest improvement on fuel economy at both low load and high load areas with a high compression ratio piston, which makes the EIVC cam very beneficial to highly downsized gasoline DI engines.

Chapter Six

Injection Optimisation for Miller Cycle Operation

Chapter 6 Injection Optimisation for Miller Cycle Operation

6.1 Introduction

As discussed in Chapter 4, Miller cycle operation might compromise the ignition and combustion process particularly with EIVC cam because of the reduced turbulence at the end of compression. Thus intake ports and combustion chamber design are desired to be optimised for higher tumble flows for faster combustion in order to achieve maximum benefits from the Miller cycle operation on a product engine. However optimisation of intake ports and combustion chamber designs is not covered in this research project. Alternatively the split injection strategy was investigated as a possible means to speeding up the combustion process. This chapter will presents the experimental results of split injection study conducted with both EIVC and LIVC cams and two different CRs. Lambda sweep tests were also carried out at low speed high load region where scavenging was applied. During these testing, the optimised intake and exhaust cam timings presented in Chapter 4 and 5 were employed. Other boundary conditions remained the same as before, as shown in Table 3.5.

6.2 Impact of Split Injection on Engine Fuel Consumption at Low Load

Figure 6.1 shows the results of split injection test at 2000rpm 4.6bar NIMEP with LCR LIVC cam hardware. Injection timing of the first main injection was fixed at pre-optimised timing of 320dCA BTDCF. At this test point, the second late injection duration was set to the ECU minimum injection pulse width of 0.2ms, which accounted for 40% of the total fuel injection mass. The end of injection (EOI) of the second injection was adjusted in the testing.

The split injection results in higher ISFCn than single injection at this test point. The optimal ISFCn of split injection is achieved when EOI of the second injection is 60dCA BTDCF. CA50 timings are optimised at around 8dCA ATDCF for all test logs. There is hardly any change in the combustion duration. When EOI of the second injection is later than 60dCA, the ignition delay between the spark timing and CA10 timing becomes shorter, which would indicate a more favourable air/fuel mixture is formed around the

spark plug at the time of spark ignition. It is also observed the HC emission is reduced when second injection is retarded. However the CO emission deteriorates greatly at this condition due to decreased time for fuel mixing with air. When EOI of the second injection is earlier than 60dCA, CO emission stays low and close to the CO level of single injection but its HC emission and ignition delay become higher than those of the single injection operation, which results in high ISFCn than that of the single injection.

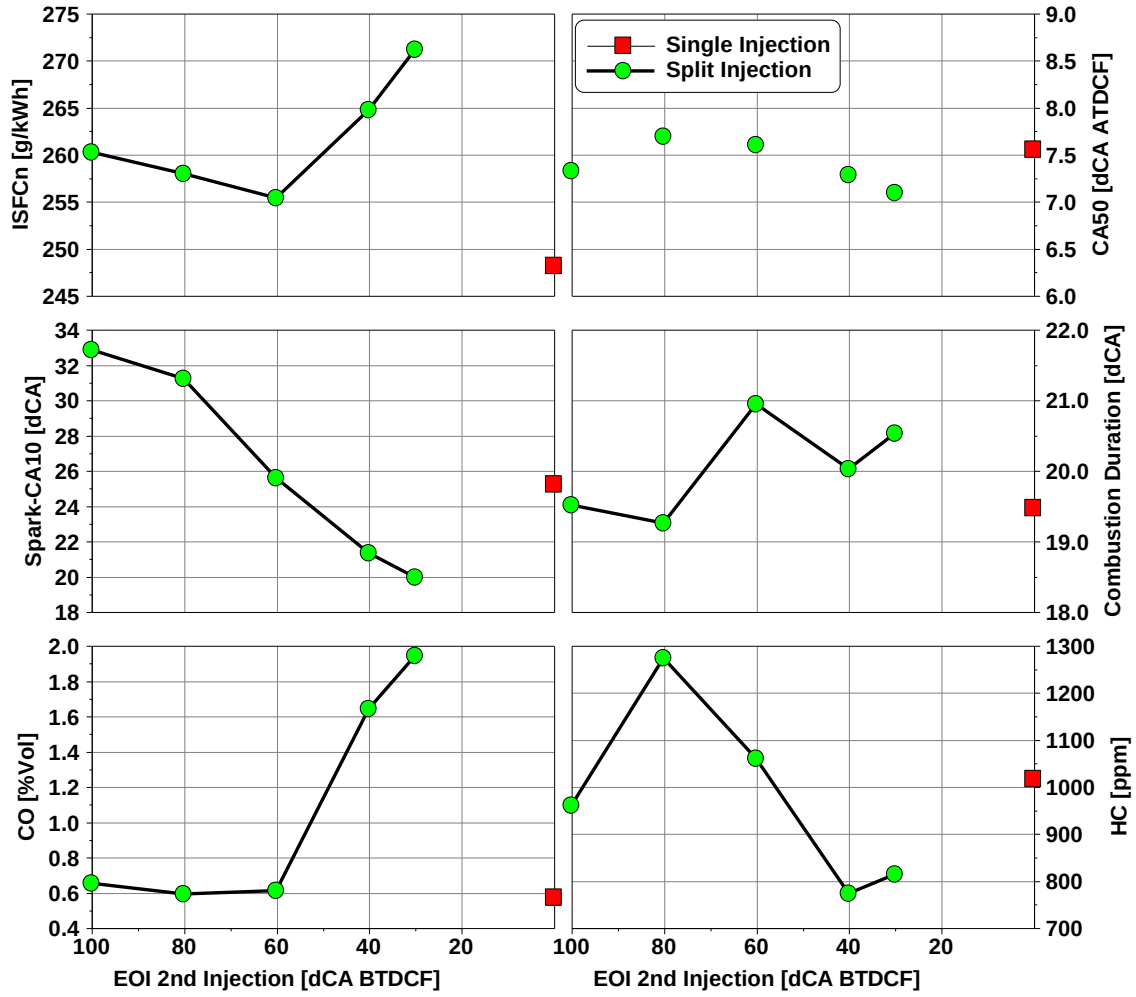

Figure 6.1 Split Injection Test Results with LCR LIVC Cam at 2000rpm 4.6bar NIMEP

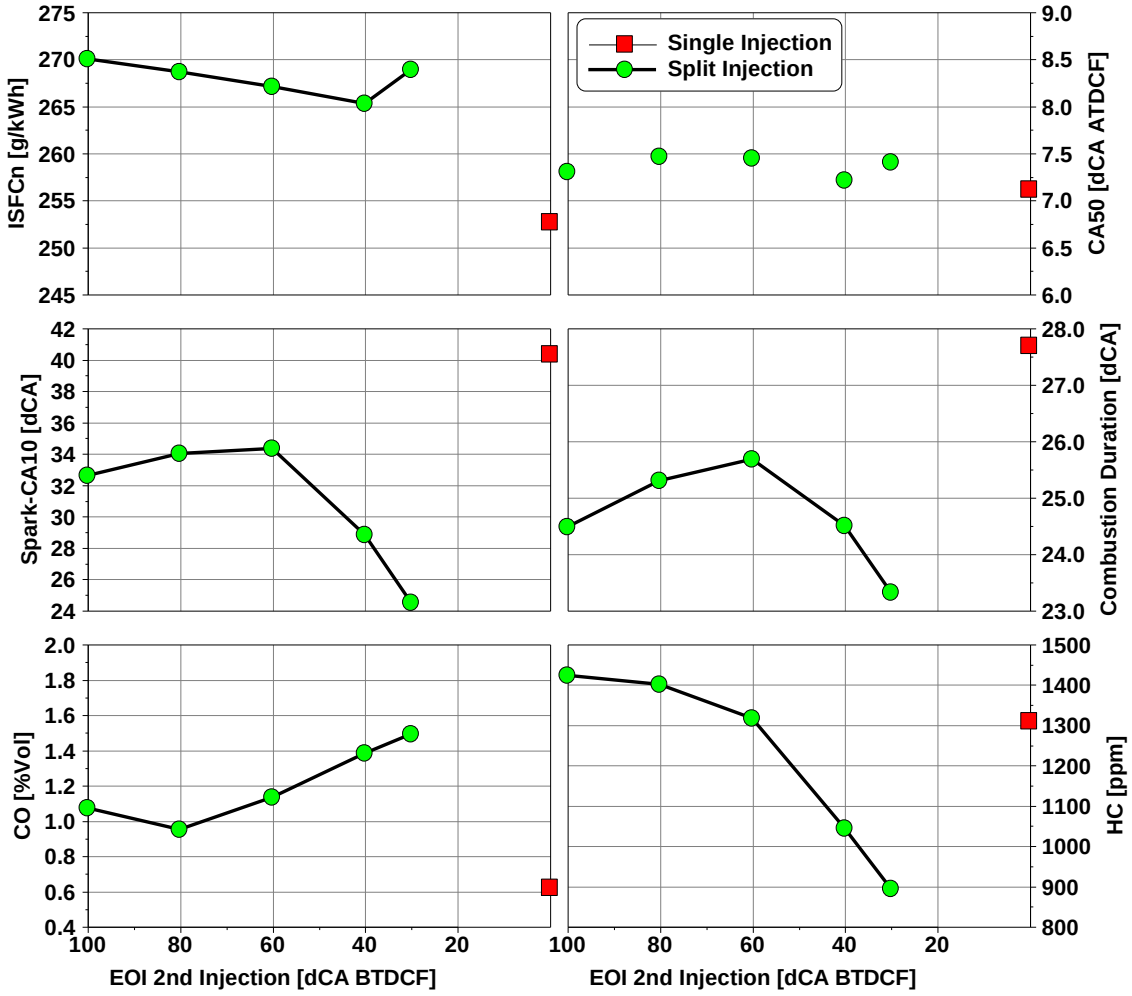

Figure 6.2 Split Injection Test Results with LCR EIVC Cam at 2000rpm 4.6bar NIMEP

Figure 6.2 shows the results of split injection test at 2000rpm 4.6bar NIMEP with LCR EIVC cam setup. Test condition is the same as previous test as presented in Figure 6.1. Injection timing of the first main injection is fixed when the second injection EOI timing is changed. The pulse width of second injection is kept at the minimum limit value of 0.2ms.

When EOI of the second injection is delayed from 100dCA to 30dCA BTDCF, the change in ISFCn is less than that of LIVC cam. However even the optimum ISFCn of split injection is still higher than the ISFCn of single injection by more than 10g/kWh. The split injection leads to greater increase in ISFCn than the LIVC cam. The increase in ISFCn seems to correlate with the higher CO emission. CO is around 0.6 %Vol for single injection with both EIVC cam and LIVC cam, which indicates homogenous mixture

formed in-cylinder. It is always above 1.0 %Vol during the split injection operation with the EIVC cam. As discussed previously, the EIVC cam has a lower maximum valve lift hence weak tumble level generated during the intake process and consequently reduced turbulence at the end of compression, which has great negative impact on the air fuel mixing of the late injected fuel.

Split injection has stronger impact on ignition delay and combustion duration with EIVC cam than with LIVC cam. The ignition delay is shortened by up to 16dCA by split injection and combustion duration is reduced by up to 4dCA compared to those of single injection. The results show that the late second injection has the effect to enhance the ignition process. However this advantage is not transferred to fuel consumption benefits at low load condition when the combustion timing CA50 is at optimal setting for all test conditions. The higher CO emission and hence lower combustion efficiency is more dominant at the low load test point on fuel consumption.

Figure 6.3 shows the split injection test results at 2000rpm 4.6bar NIMEP with HCR EIVC cam hardware. In addition to the split injection with the minimum pulse width for the second injection, another split injection test is also presented in the figure with the second injection increased to 50%. The results are quite similar to the LCR results in Figure 6.2. The split injection with 35% second injection reduces ignition delay and combustion duration but increases CO emission hence makes ISFCn worse than single injection. When the second injection is increased to 50%, CO and HC emissions become further higher hence ISFCn gets even worse. In addition, GIMEP COV and LNV become worse. Therefore, it can be concluded that the single injection is better than the split injections tested at low load area.

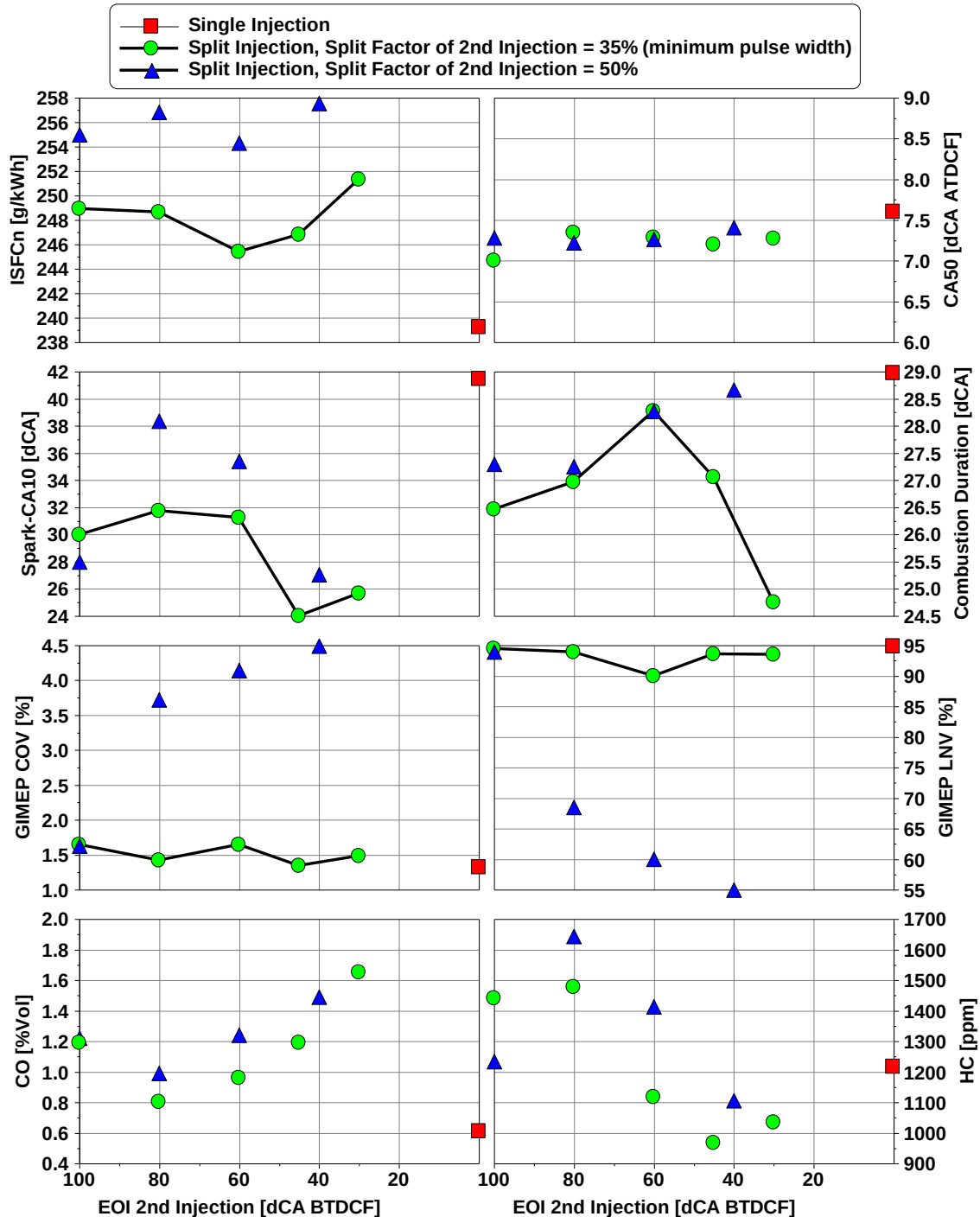

Figure 6.3 Split Injection Test Results with HCR EIVC Cam at 2000rpm 4.6bar NIMEP

6.3 Impact of Split Injection on Engine Fuel Consumption at High Load

Further study was also carried out at 2000rpm 16.0bar NIMEP. Figure 6.4 shows the split injection test results at this point with LCR LIVC cam hardware. EOI of the second

injection is adjusted between 40dCA to 120dCA BTDCF while injection timing of the first injection is fixed to 290dCA BTDCF. The second injection duration was set to the minimum allowed injection pulse width of 0.2ms, which equalled to 13% of the total fuel mass per cycle. As a result, the minimum CO emission of the split injection operation is only 0.1% higher than the CO level of single injection. Both single and split injections can achieve the optimal CA50 timing at around 8dCA ATDCF and they have negligible impact on the ignition delay and combustion duration. Split injection reduces HC emission due to less fuel trapped in the crevices from the first injection and leads to a slight reduction on ISFCn by split injection.

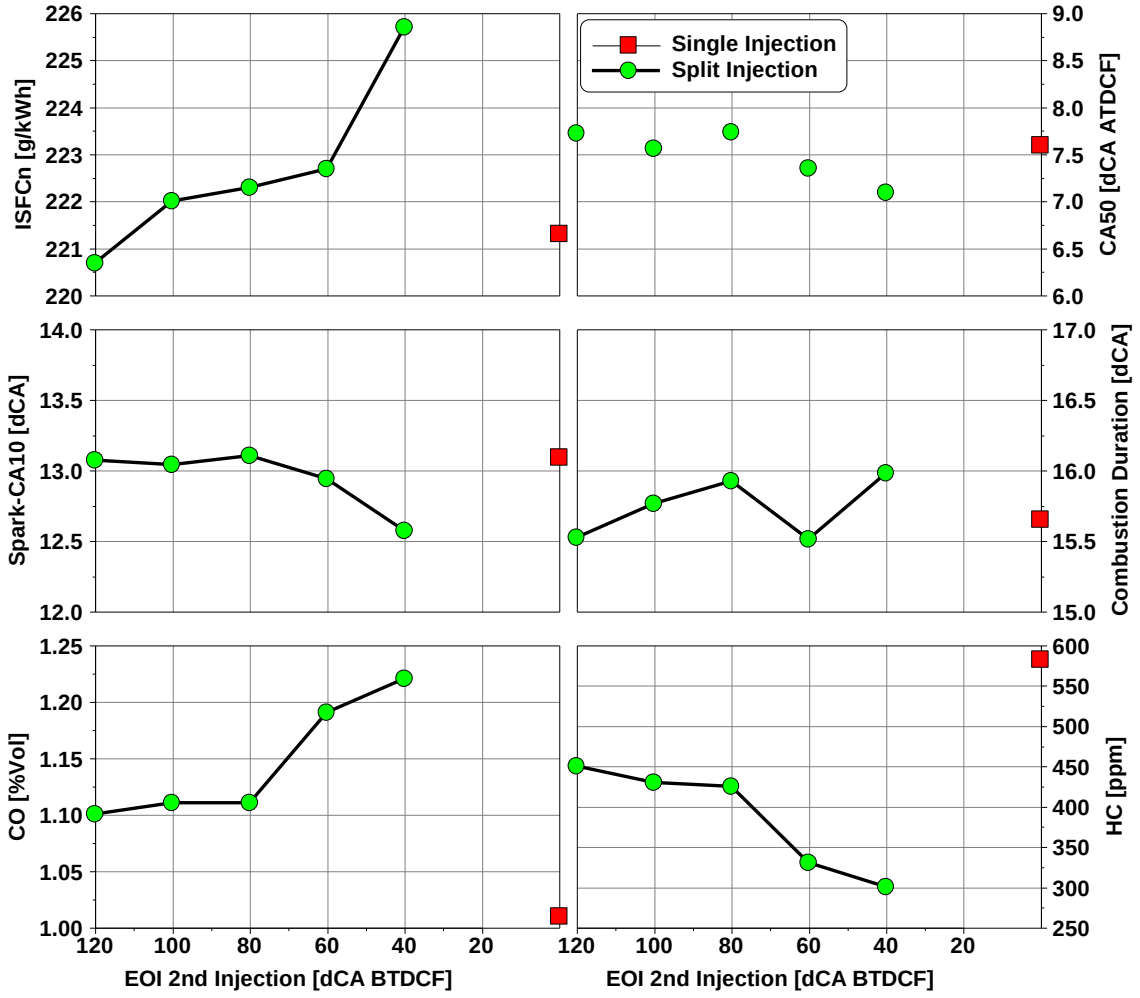

Figure 6.4 Split Injection Test Results with LCR LIVC Cam at 2000rpm 16.0bar NIMEP

Figure 6.5 shows the results of the same test carried out with the LCR EIVC hardware. Split injection shows a clear potential to improve the ISFCn, although the maximum

decrease is still only 1g/kWh. When EOI of the second injection is earlier than 40dCA BTDCF, CO emission of split injection is very close to that of the single injection. When the second injection timing is further retarded, the shortened period for air fuel mixing makes CO emission worse and consequent the deterioration of ISFCn. When used with the EIVC cam, the split injection helps to speed up the ignition process and flame propagation. Split injection decreases the ignition delay by more than 6dCA and shortens the combustion duration by 2dCA compared to single injection. HC reduction is also observed while engine runs with split injection.

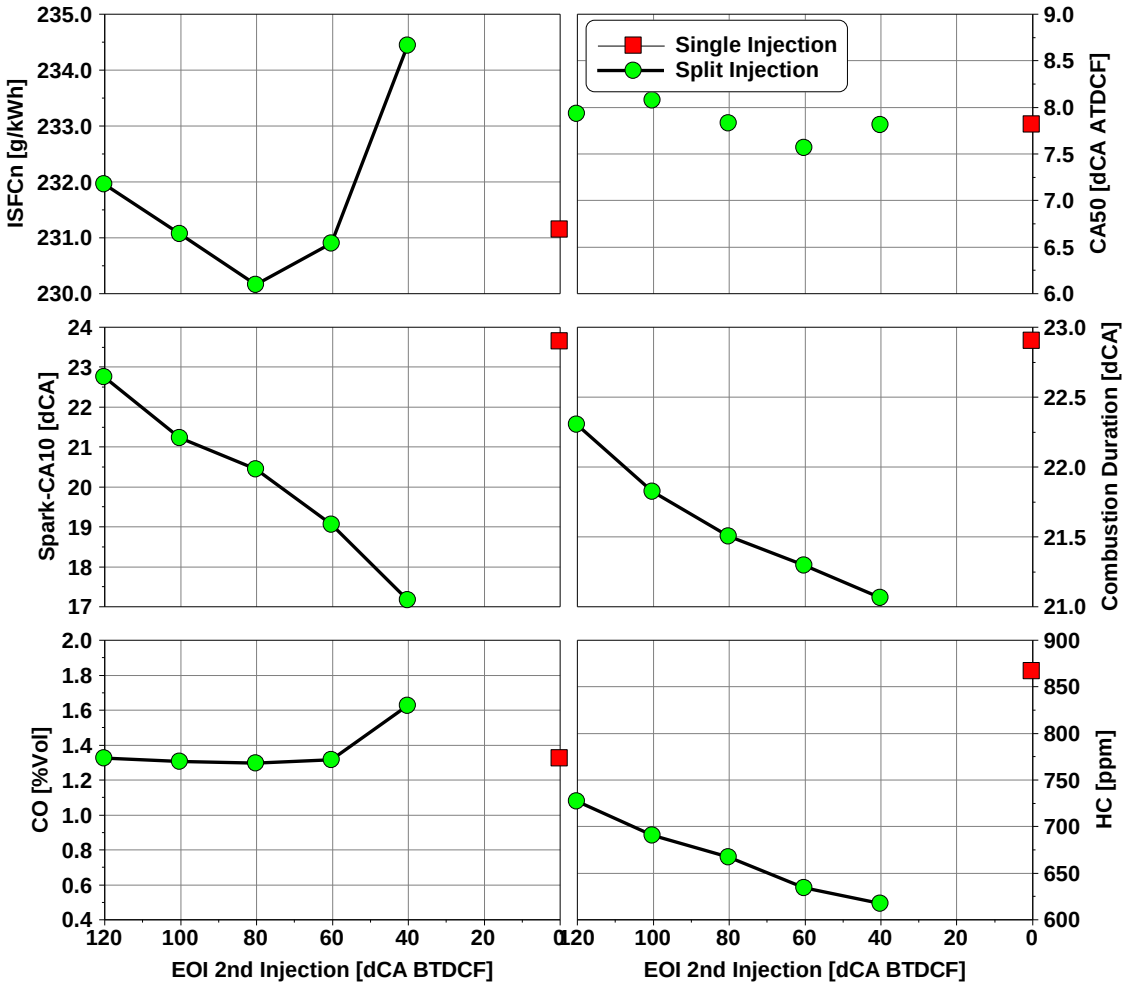

Figure 6.5 Split Injection Test Results with LCR EIVC Cam at 2000rpm 16.0bar NIMEP

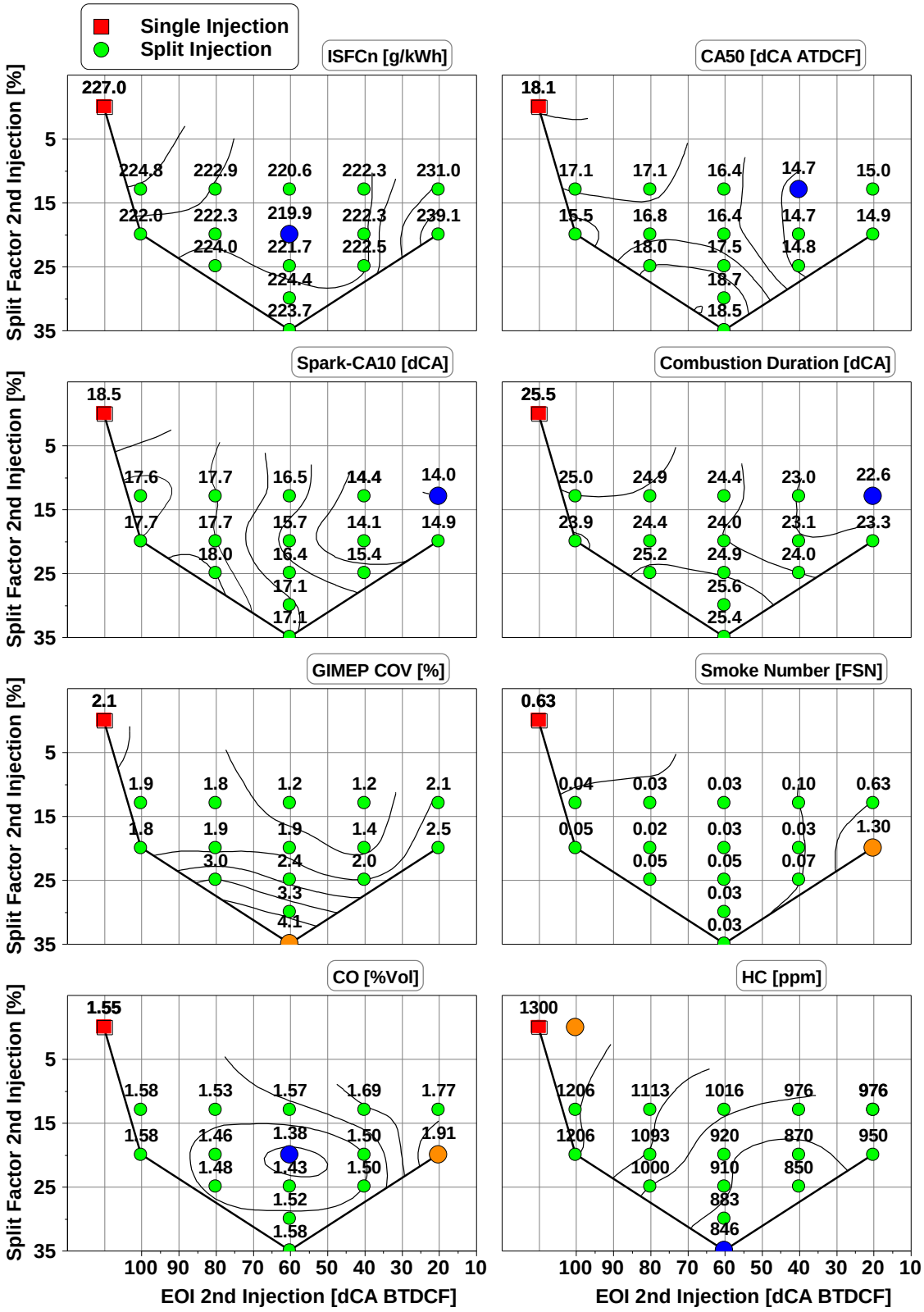

Figure 6.6 Split Injection Test Results with HCR EIVC Cam at 2000rpm 16.0bar NIMEP

Figure 6.6 shows the split injection optimisation at 2000rpm 16.0bar NIMEP on engine with the HCR piston and EIVC cam. Square dots in the contour maps are results of the single injection. Round dots in the maps are split injection results with both EOI and split factor of second injection under optimisation and first injection timing being fixed. Split injection produces significant improvement of ISFCn at high CR setup, i.e. up to 7g/kWh or 3.1% improvement while compared with single injection. The benefit of split injection is more than that achieved with the low CR piston.

Split injection produces the lowest CO emission with 60dCA BTDCF EOI timing and 20% second injection. Split injection also reduces HC and smoke number in a large region, as well shortens the ignition delay and combustion duration. CA50 is limited by knocking combustion when CR is increased with both single and split injection strategies. In the split injection operation, the late second injection is able to improve flame development through the formation of a more ignitable mixture and enhanced turbulence at the end of compression stroke. As a result, split injection is able to reduce the fuel consumption by advancing the knock limited spark timing and CA50 phasing by 2 to 3dCA without knocking combustion. Split injection needs to be optimised since smoke number and CO will get much worse if the second injection is too late or too large to avoid the formation of very fuel rich region.

6.4 Impact of Split Injection on Engine Fuel Consumption at Full Load

Figure 6.7 shows test results obtained at 2000rpm 25.6bar NIMEP with LCR LIVC cam hardware. EOI of the second injection was swept between 130dCA and 50dCA BTDCF. The second injection was set to the minimum and accounted for 10% of the total fuel mass injected. It can be seen that the lowest ISFCn of split injection is equal to that of the single injection. Split injections reduce HC emission but produce higher CO emission. Split injections have little effect on combustion speed and phasing.

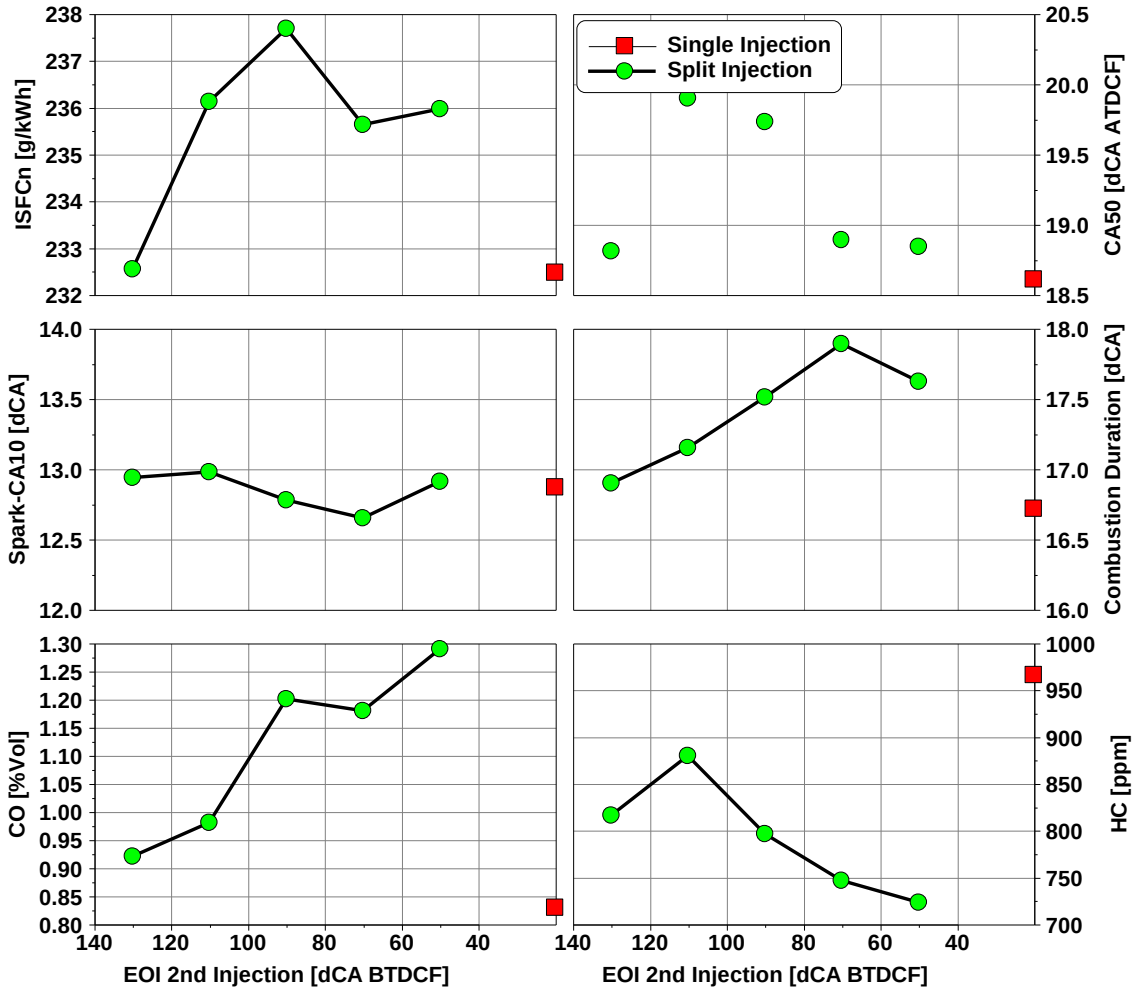

Figure 6.7 Split Injection Test Results with LCR LIVC Cam at 2000rpm 25.6bar NIMEP

Figure 6.8 shows the split injection optimisation results with LCR EIVC cam hardware at 2000rpm full load. The optimal split injection strategy reduces ISFCn by 5.8g/kWh or 2.4% compared with the single injection operation. Split injections speed up the flame development and propagation speed, allowing more advanced CA50 timing without causing knocking combustion. In addition, split injection strategy significantly reduces smoke number and HC emission but increases CO emission compared with the single injection operation.

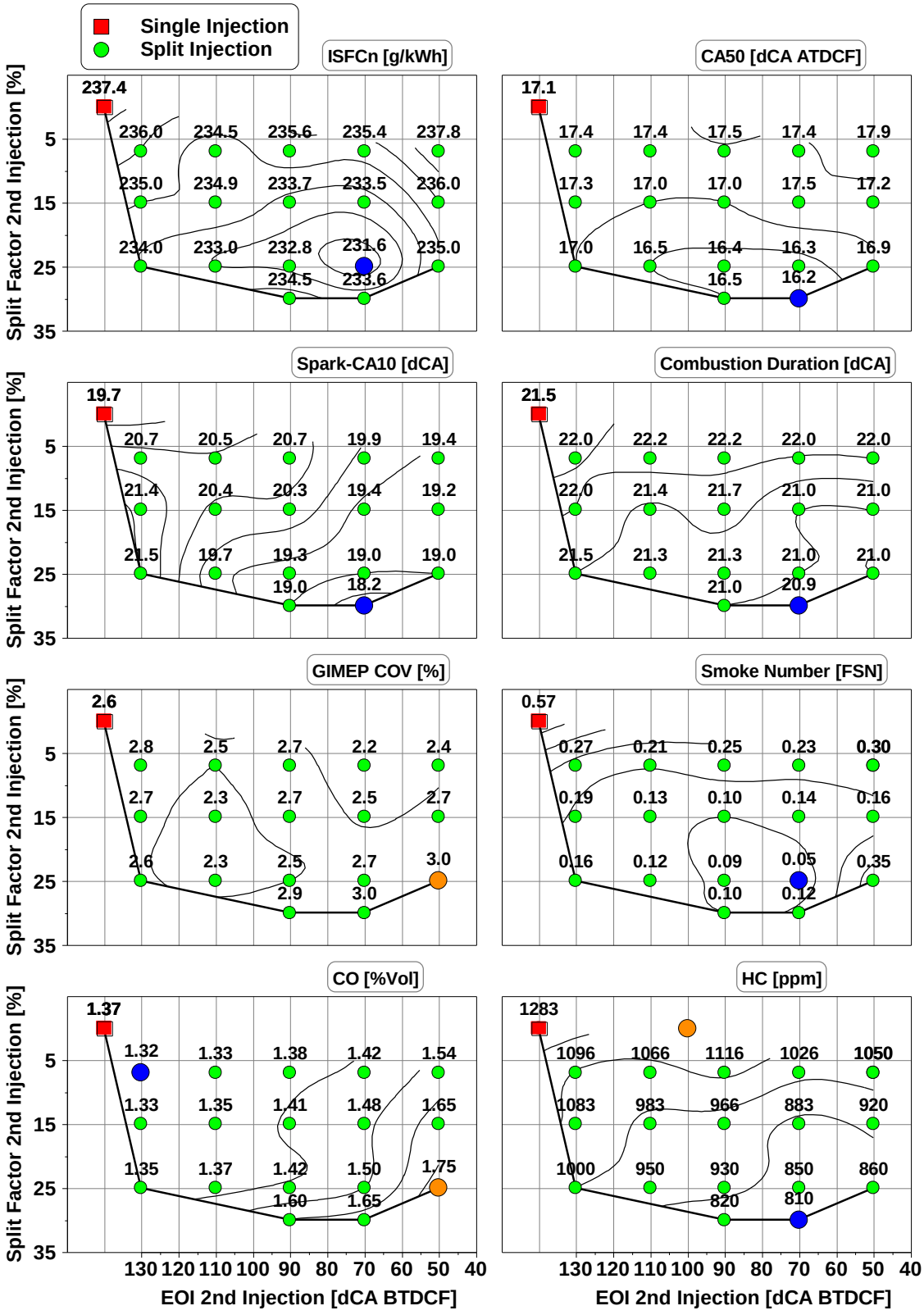

Figure 6.8 Split Injection Test Results with LCR EIVC Cam at 2000rpm 25.6bar NIMEP

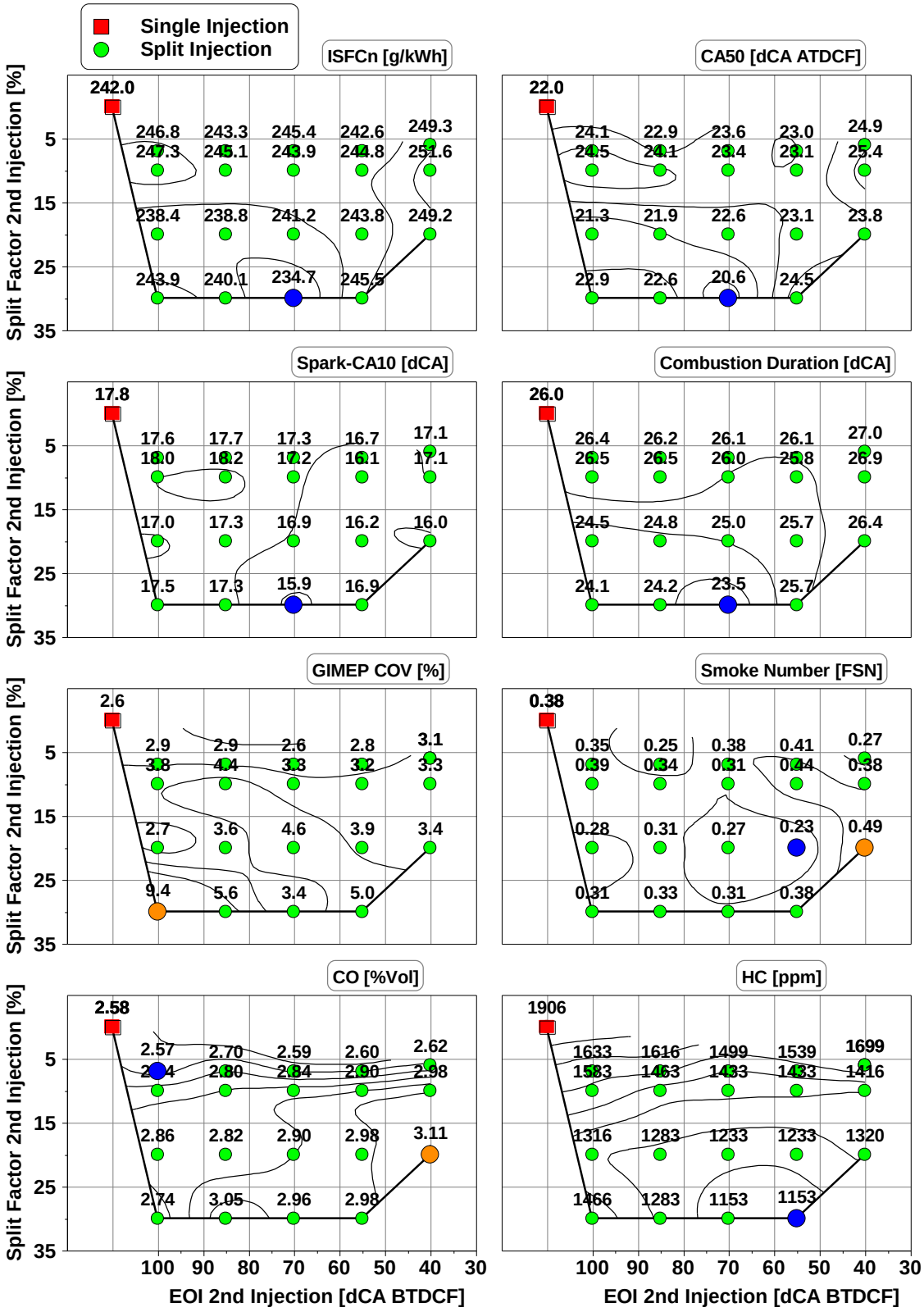

Figure 6.9 Split Injection Test Results with HCR EIVC Cam at 2000rpm 25.6bar NIMEP

Figure 6.9 shows the results at 2000rpm full load when the high CR piston was used. Further reduction in fuel consumption is achieved with the high CR and EIVC setup. ISFCn is reduced from 242g/kWh to 234.7g/kWh or 3% improvement.

At the increased CR, the engine becomes more prone to knocking combustion. The use of split injections has greater impact to advancing CA50 and shortening the flame development angle and combustion duration. The optimised ISFCn of split injections is obtained at a relatively large split factor of second injection, probably due to the improved cooling effect on cylinder charge temperature and formation of slightly richer mixture near the spark plug, which resulted in higher CO emission. However, HC emission is reduced with a larger split injection.

The timing of the second injection also shows strong impacts on engine combustion and emission especially when more fuel is injected during the second injection, since it changes the dynamics of charge cooling and charge stratification formation. More advanced or retarded second injection timing away from the optimum setting results in retarded CA50 timing, increased flame development period and combustion duration, and deteriorated combustion stability. Smoke number increases rapidly when second injection becomes closer to TDC, while improvement of HC is reduced when the second injection occurs too early in the compression stroke.

6.5 Fuel Consumption Reduction through Split Injection

Figure 6.10 summaries the ISFCn improvement achieved by split injection optimisation when compared with single injection strategy at different operating conditions. Split injections lead to higher ISFCn at low load condition but less fuel consumption at higher load at or above 16.0bar NIMEP load area with the EIVC cam. The best ISFC is achieved by split injections at higher CR with the EIVC cam.

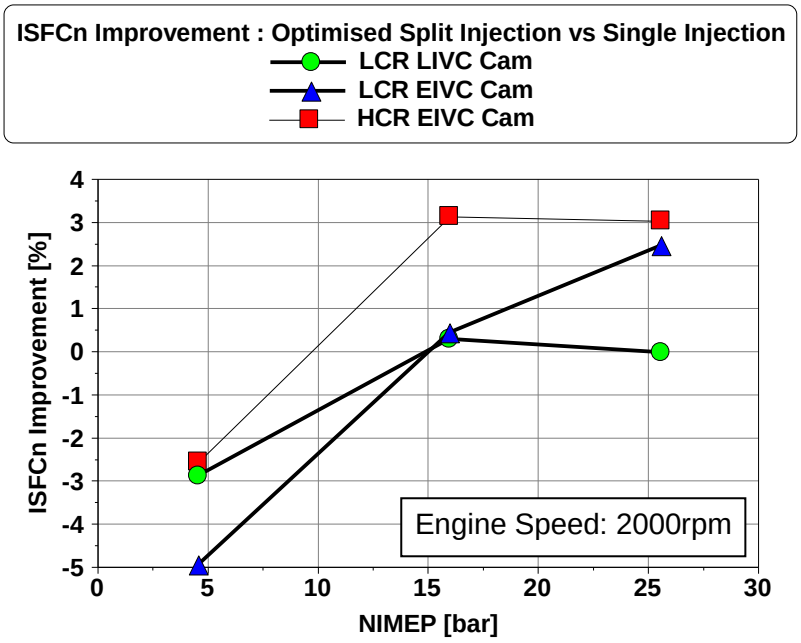

Figure 6.10 ISFCn Improvement Achieved by Split Injection Compared to Single Injection at Different Load and Hardware

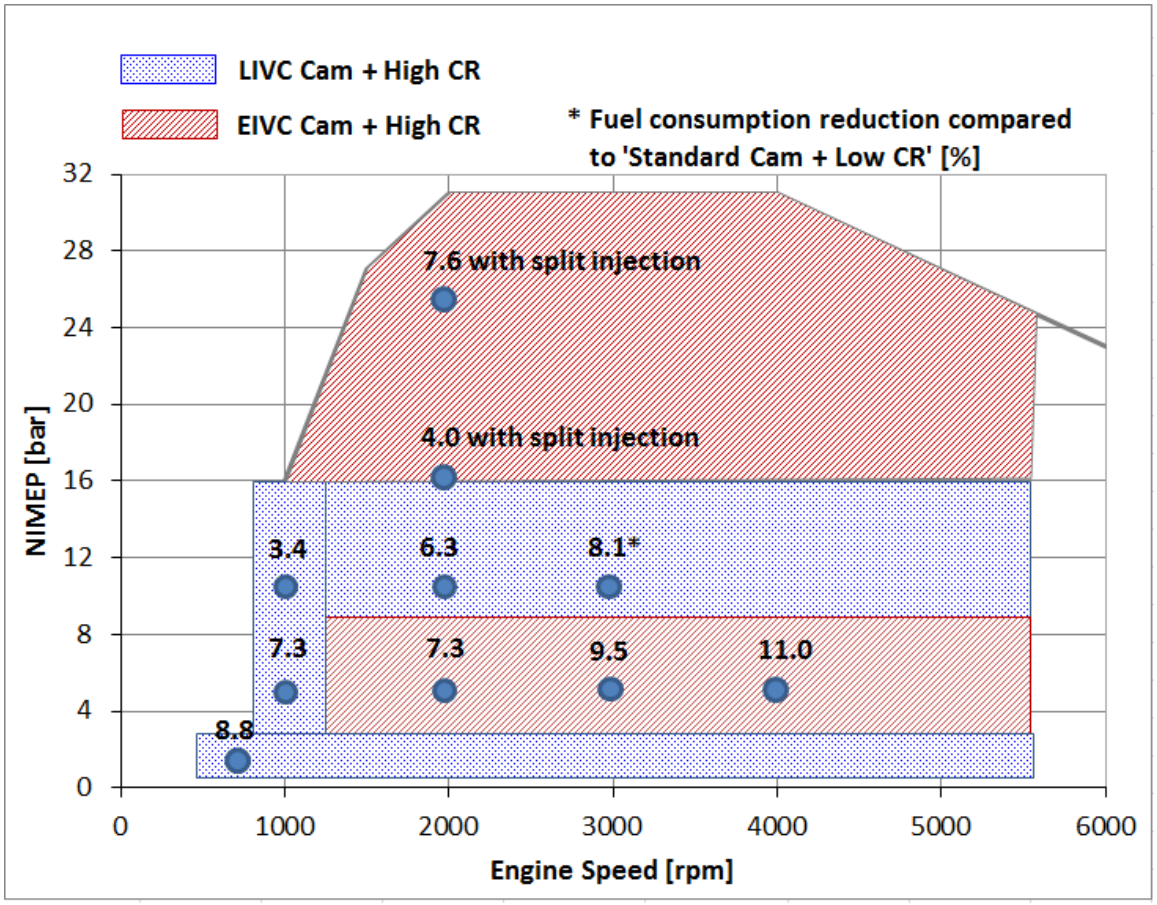

Figure 6.11 ISFCn Improvement of LIVC-EIVC Cam Switching with Split Injection and HCR compared to Standard Cam with LCR (baseline)

Based on Figure 5.15 and results presented in Figure 6.10, Figure 6.11 shows the further evolution of fuel consumption reduction through Miller cycle operation with LIVC-EIVC cam switching and high CR piston, plus split injection strategy applied at low speed high load area. Ambient exhaust back pressure and external boosting were conditions for obtaining these results.

6.6 Lambda Strategy for Low Speed High Load Operation

Figure 6.12 presents an exhaust lambda sweep test carried out at 2000rpm 16.0bar with EIVC cam. As discussed in Chapter 4, EIVC cam utilises both Miller cycle and scavenging at low speed high load region to reduce knocking tendency and improve engine efficiency. However the scavenging can make in-cylinder lambda richer than the exhaust lambda. As shown in Figure 6.12, CO emission is 1.5 %Vol when the exhaust lambda is at 1.0, indicating an enriched in-cylinder mixture which deteriorates the combustion efficiency and increases ISFCn. CO concentration is decreased to 0.79 %Vol and 0.43 %Vol respectively when the exhaust lambda is increased to 1.05 and 1.10. The lean exhaust lambda strategy here is to achieve in-cylinder lambda 1.0 for a low CO level and improve combustion efficiency. Further increase of the exhaust lambda provides little improvement in CO emission and fuel consumption.

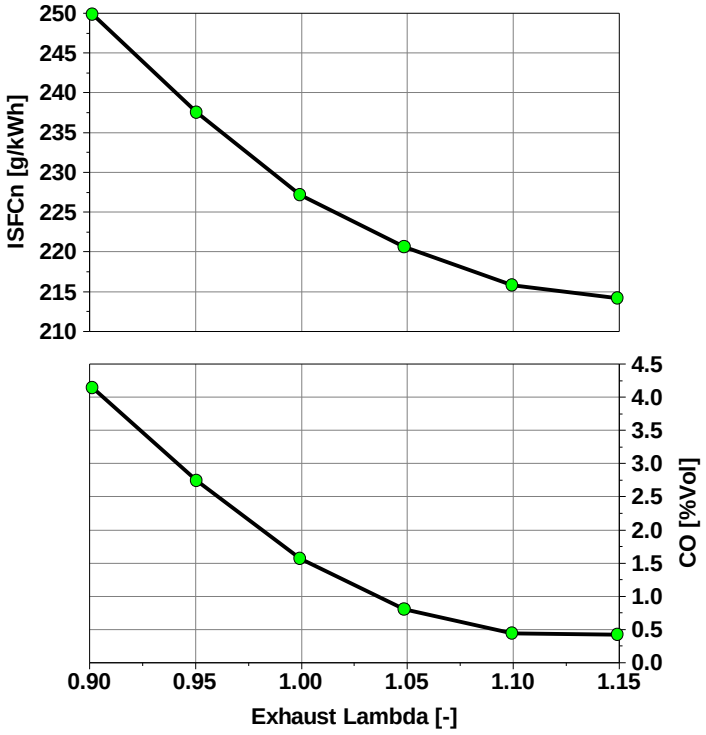

Figure 6.12 Exhaust Lambda Sweep at 2000rpm 16.0bar NIMEP with LCR EIVC Cam

6.7 Summary

This chapter has presented and discussed the experimental results for impact of the split injection strategy on the fuel consumption and emissions of a single cylinder boosted direct injection gasoline engine operating with the LIVC cam and EIVC cam at two compression ratios.

Split injections lead to higher fuel consumption at low load operations, primarily due to the presence of inhomogeneous mixture and hence higher CO emissions generated by the relatively large percentage of fuel injected during the second injection, which is limited by the minimum pulse width of the ECU. Split injections provide little benefits to the ignition and combustion process since the engine can achieve the optimal CA50 timing with the single injection at low load.

Split injections can reduce ISFCn at higher load conditions when the spark timing is knocking limited. The percentage of the second injection can be adjusted to a smaller value. The presence of more ignitable mixture near the spark plug and also the enhanced turbulence at the end of compression stroke favour the flame development and propagation. In addition, the charge cooling effect of fuel injected and evaporated in compression stroke helps to minimise the autoignition of the end gas region, preventing the occurrence of knocking combustion. Therefore, the best ISFCn is achieved by split injection with the high CR piston and EIVC setup.

When the positive scavenging is used with the EIVC cam at high load operation, the best fuel consumption is achieved by running the exhaust lambda at around 1.1 which corresponds to the in-cylinder lambda 1.0. However according to the latest Real Driving Emissions (RDE) test conditions, lean exhaust lambda even at low speed high load region might not be permitted in order to keep the three-way catalyst NOx conversion efficiency high.

Chapter Seven

Impact of Boost Device on Miller Cycle Application

Chapter 7 Impact of Boost Device on Miller Cycle Application

7.1 Introduction

The experimental studies presented in the previous chapters were carried out at ambient exhaust back pressure condition. An external boosting rig was utilised to provide air at demanded pressure for the single cylinder engine to achieve the target load for testing. These simplified setups are helpful for understanding the fundamentals of improvement in engine efficiencies by Miller cycle operation and its combination with high compression ratio or multiple injection strategy. In production engines, a turbocharger is typically used as the boosting device and the exhaust back pressure is increased by the presence of the turbine. If a mechanical supercharger is used, there will be little change of exhaust back pressure but the work consumed to drive the supercharger will become higher along with the increase in boosting pressure. The increased exhaust back pressure with turbocharger or increased driving work with a supercharger can reduce the benefits gained by Miller cycle operation. This chapter will present engine testing results with increased exhaust back pressure and analyse its impact on engine performance. Exhaust back pressure sweep tests were carried out at high load to explore its impact. In addition, power consumption of a mechanical boosting device is calculated and discussed.

7.2 Exhaust Back Pressure Impacts at High Load

As discussed in Chapter 3, a butterfly valve was installed in the exhaust system of the single cylinder engine to control the Exhaust Back Pressure (EBP) which was measured by the exhaust port pressure transducer. It represents the exhaust gauge pressure at the turbine outlet in turbocharged engines or at the exhaust manifold outlet in naturally aspirated engines. During the experiments with different exhaust back pressure settings, optimised cam timings presented in Chapter 4 and 5 were used for each hardware configuration with other engine control parameters and boundary conditions fixed as given in Table 3.5.

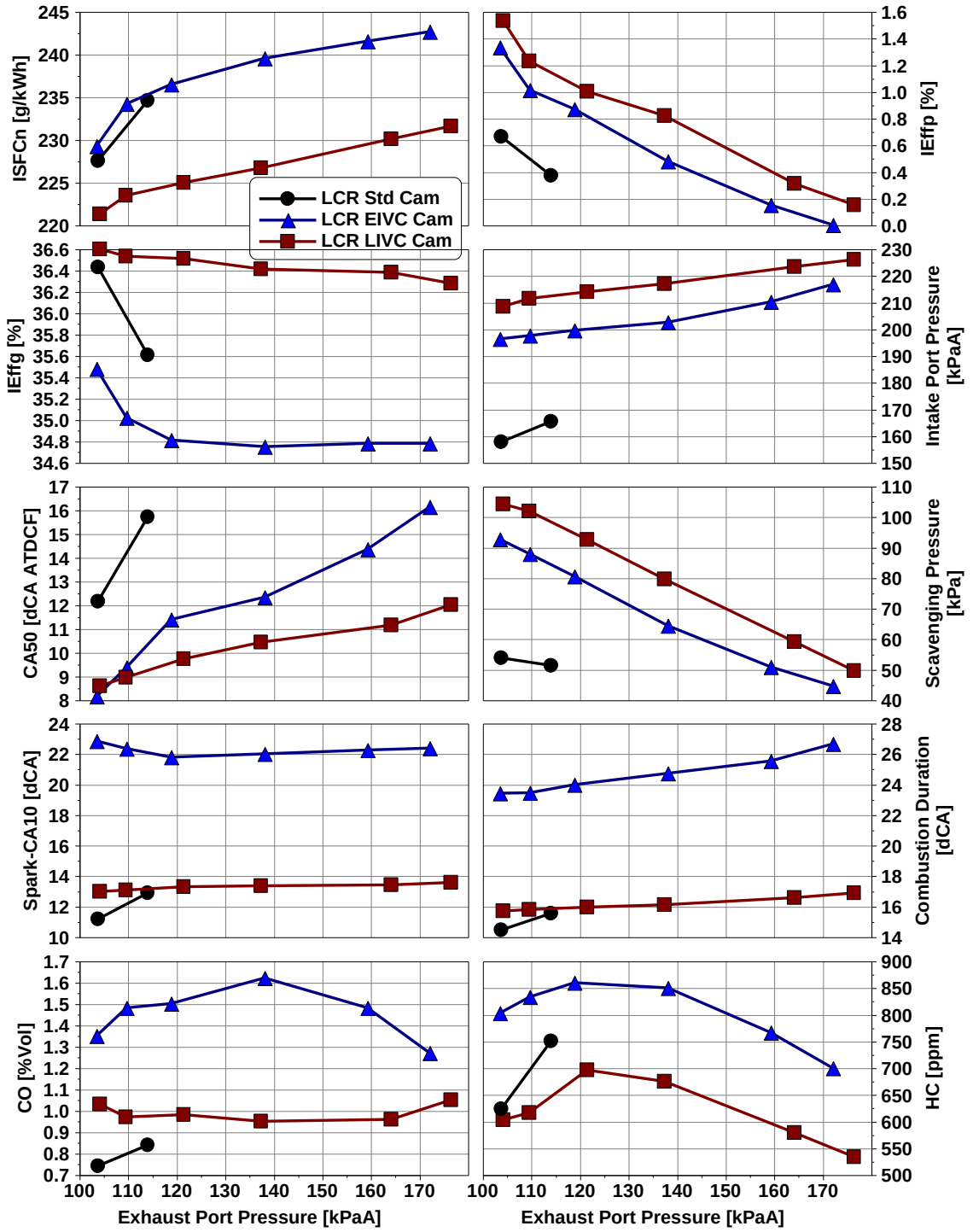

Figure 7.1 EBP Sweep Test Results at 2000rpm 16.0bar NIMEP with LCR and Three Intake Cams

Figure 7.1 shows the test results at 2000rpm 16.0bar NIMEP obtained with the low CR piston and three intake cam profiles. The LIVC cam achieves the lowest ISFCn at this test point at the ambient exhaust back pressure as discussed in Chapter 4. When EBP becomes higher, the ISFCn values of all three cams increase in a similar way. IEffp gets

worse with higher boost pressure because the scavenging pressure, i.e. the difference between the intake port pressure and exhaust port pressure, is decreased.

Increased EBP has little impact on the flame development period. However it increases in-cylinder residual gas fraction hence increased tendency of knocking combustion, as indicated by the retarded CA50. CA50 timings of the EIVC cam and standard cam are retarded more than that of the LIVC cam. Combustion duration of the EIVC cam is lengthened by up to 3dCA but it remains almost constant with the LIVC cam. With the EIVC cam, both CO and HC emissions initially increase due to the higher residual gas fraction with higher EBP, and then decrease because of the retarded combustion timing and more exhaust trapped in the cylinder. With the LIVC cam, HC emission exhibits a similar trend as EIVC but its CO emission changes much less. Thus the IEffg value of the EIVC cam decreases faster than that of the LIVC cam operations. These results demonstrate the EBP has greater impact on the combustion process of EIVC cam operation than that of LIVC cam.

Figure 7.2 compares the results obtained with the EIVC cam at high and low CR pistons and those with the baseline setup of a low CR piston and standard intake cam at the same engine speed and load. The HCR piston and EIVC cam combination produces the lowest ISFCn when the exhaust port pressure is less than 140 kPaA. Its ISFCn becomes higher than that of the LCR EIVC setup when EBP is further increased. For all three combinations, when EBP rises higher intake pressure is demanded to maintain engine load. But the IEffp value decreases because of the lower scavenging pressure. Increased EBP shows little impact on the ignition delay, combustion duration and less increase in CA50 timing of engine combustion with the HCR EIVC setup. However it causes more increase in CO with the HCR EIVC setup than the other two combinations. As a result, IEffg of the HCR EIVC combination deteriorates and becomes lower than that of the LCR EIVC setup when EBP is above 140kpA. This can be resulted from the heavily retarded combustion timing and the increased residual gas fraction during the HCR EIVC operations.

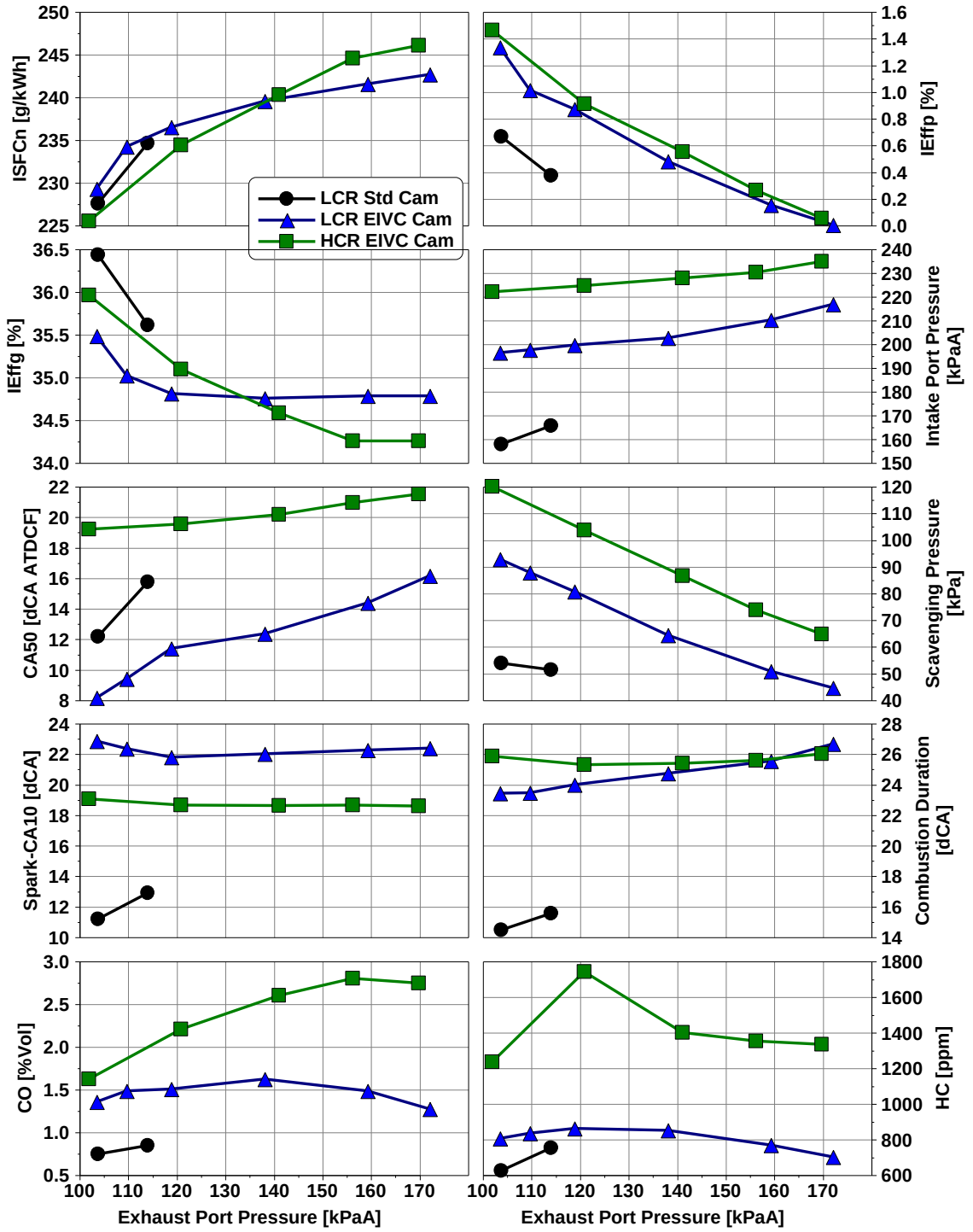

Figure 7.2 EBP Sweep Test Results at 2000rpm 16.0bar NIMEP with Standard and EIVC Cams at Different CRs

7.3 Exhaust Back Pressure Impacts at Full Load

EBP sweep tests were also carried out at the full load of 25.6bar NIMEP at 2000rpm. Figure 7.3 compares the three intake cams with the low CR piston. Exhaust pressure is

increased up to 250kPaA for the LIVC cam when misfiring occurs. In the data processing program, if GIMEP of an engine cycle is negative the cycle is recorded as a misfiring cycle. There are eight misfiring cycles detected out of the one hundred engine cycles. The maximum EBP could be increased to 300kPaA for the EIVC cam which was limited by the capability of the EBP control valve used.

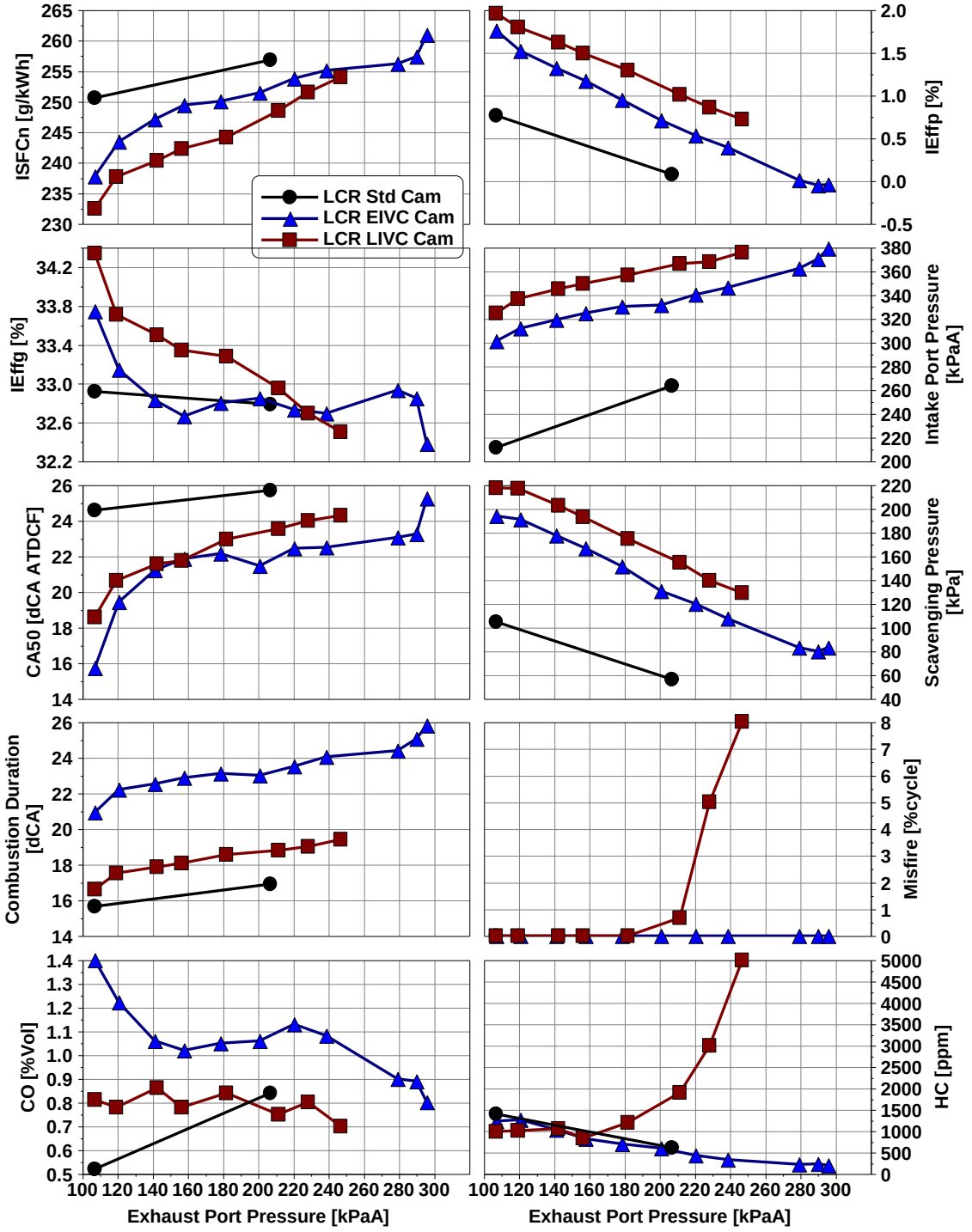

Figure 7.3 EBP Sweep Test Results at 2000rpm 25.6bar NIMEP with LCR and Three Intake Cams

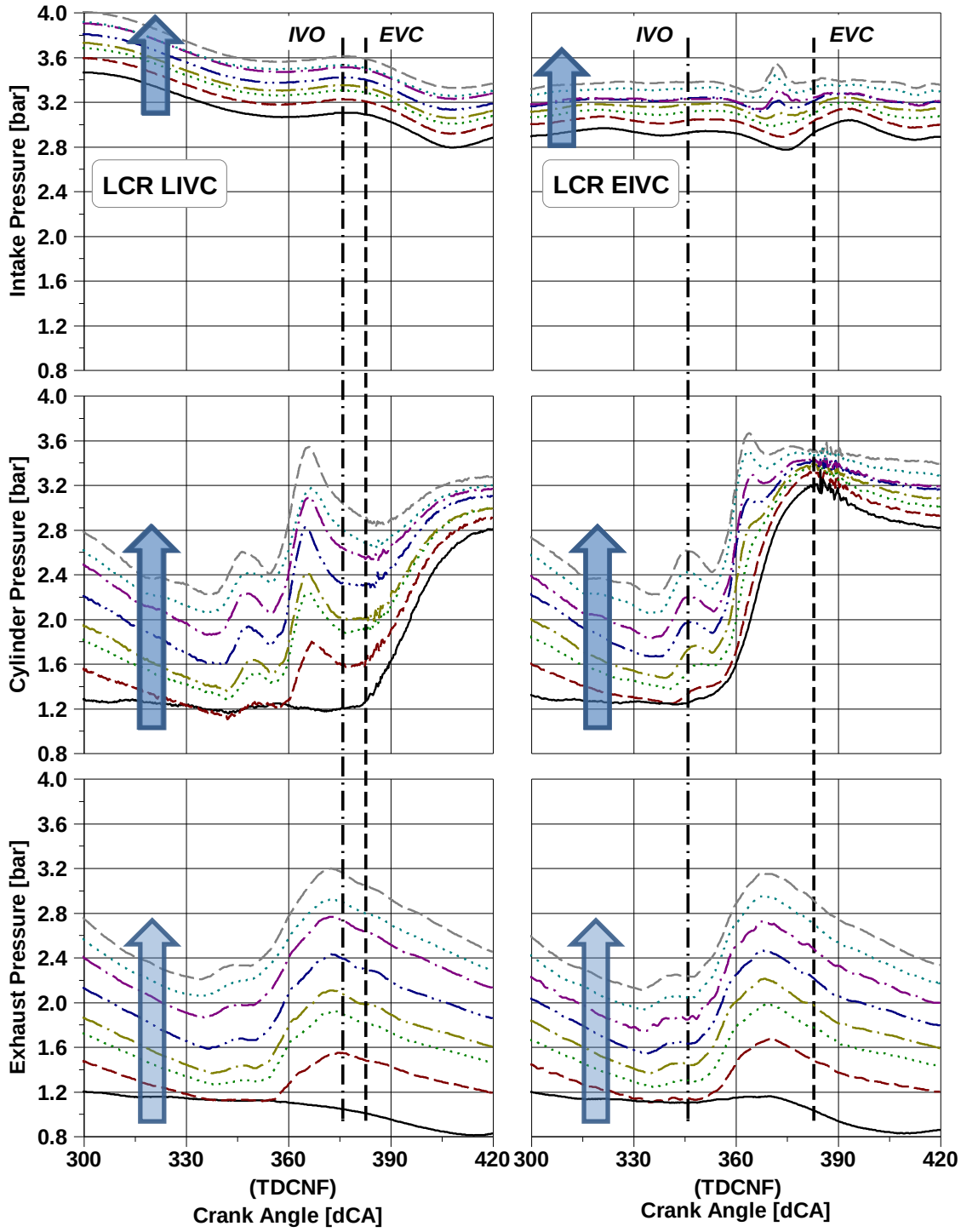

Figure 7.4 EBP Sweep Pressure Traces at 2000rpm 25.6bar NIMEP with LCR and Three Intake Cams (arrows indicating increase of EBP)

The best fuel economy is achieved with the LIVC cam and low CR setup at the exhaust port pressure up to 240kPaA. With the increased EBP, higher intake port pressures is required and the scavenging pressure drops. Increased residual gas fractions caused by

higher EBP make the engine more prone to knocking combustion, combustion timing more retarded and combustion duration longer, resulting in worse IEffg and ISFCn.

CO emission increases from 0.5%Vol to 0.8%Vol as the exhaust port pressure is doubled with the standard cam but little affected with the LIVC cam, while EIVC cam engine produces less CO when EBP rises. The engine starts to have misfiring combustion with LIVC cam when the exhaust port pressure is above 180kPaA, leading to a rapid rise in HC emission. No abnormal combustion is experienced with EIVC cam even when EBP is increased to 300kPaA. As a result, the ISFCn of LCR LIVC cam setup becomes equal to that of the LCR EIVC cam combination at EBP of 240kPaA.

Figure 7.4 depicts the transient traces of intake port pressure, exhaust port pressure and cylinder pressure around gas exchange TDC when the exhaust pressure is increased. As discussed in Chapter 4, the LIVC cam setup employs the retarded IVC and IVO timings for Miller cycle operation at high load area. Its IVO timing is 376dCA while exhaust valves close at 383dCA. The exhaust pressure wave rises at the exhaust port before exhaust valves are closed, leading to the back flow of exhaust gas into the cylinder. This is indicated by the in-cylinder pressure rise at the beginning of the intake stroke when the piston moves downwards and intake valves are still closed. This leads to the increase of residual gas and causes the abnormal combustion with LIVC cam.

The EIVC cam is set to operate with advanced intake valve timings for Miller cycle operation and provide a large valve overlap period for more effective exhaust scavenging. However, the scavenging action becomes less effective with higher exhaust port pressure at a given boost pressure.

Figure 7.5 shows the impact of EBP change on the EIVC operation with the high CR setup. The change of IEffp is similar as other hardware configurations. Engine fuel economy with HCR and EIVC cams decreases rapidly when EBP is above 220kPaA, and the ISFCn of HCR EIVC cam becomes worse than that of the LCR EIVC cam.

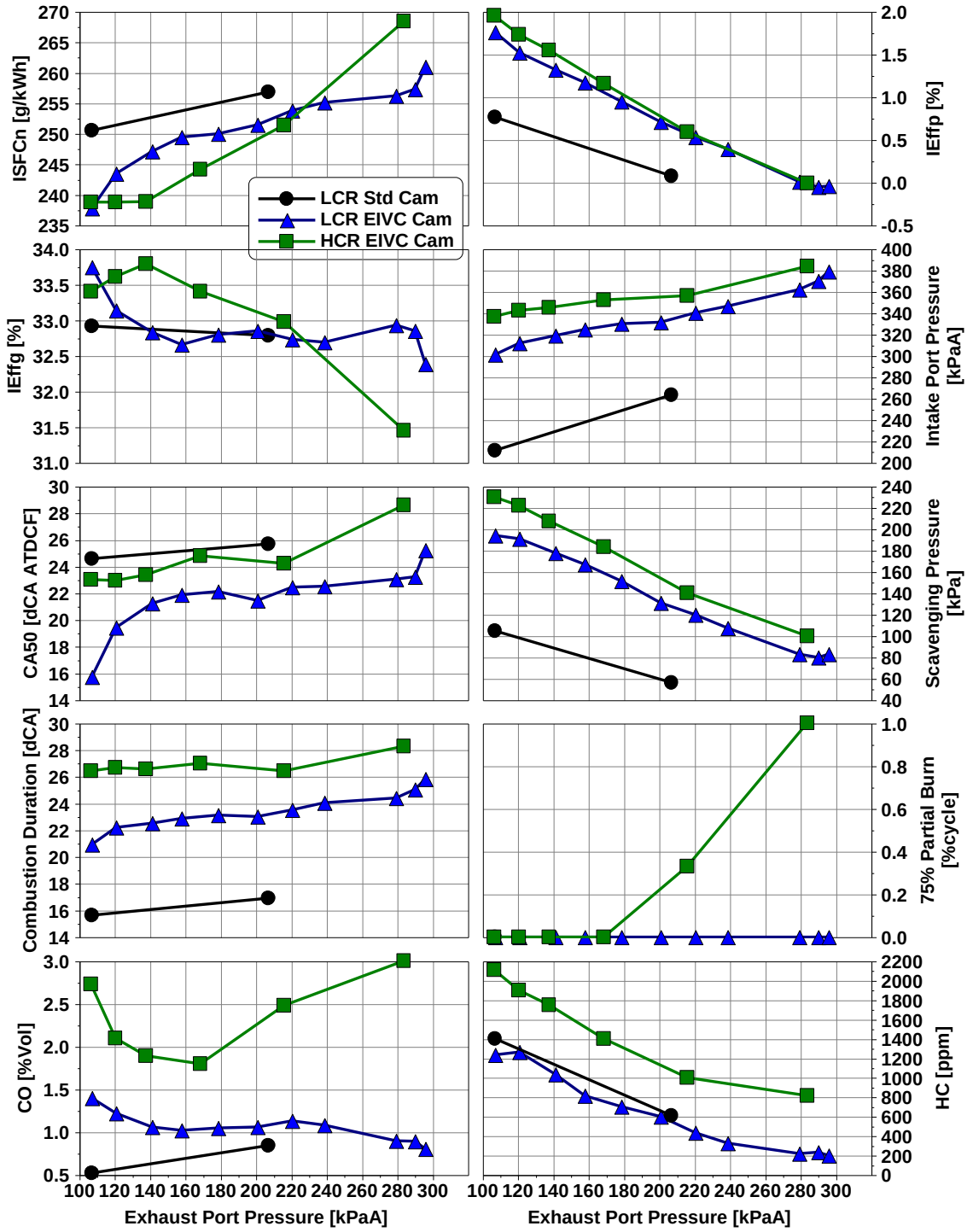

Figure 7.5 EBP Sweep Test Results at 2000rpm 25.6bar NIMEP with Standard and EIVC Cams at Different CRs

7.4 Compare ISFCn of Hardware Options at Equivalent EBP Condition

Exhaust port pressure on a turbocharged gasoline engine is affected by turbine operation and also by turbine out pressure. Turbines out pressure is decided by the technical

specifications of the whole vehicle exhaust system and also changes with exhaust mass flow. Most of turbochargers use a wastegate to adjust boosting pressure. The wastegate needs to close more when higher boosting pressure is demanded, which will enhance turbine inlet pressure, i.e. the exhaust port pressure.

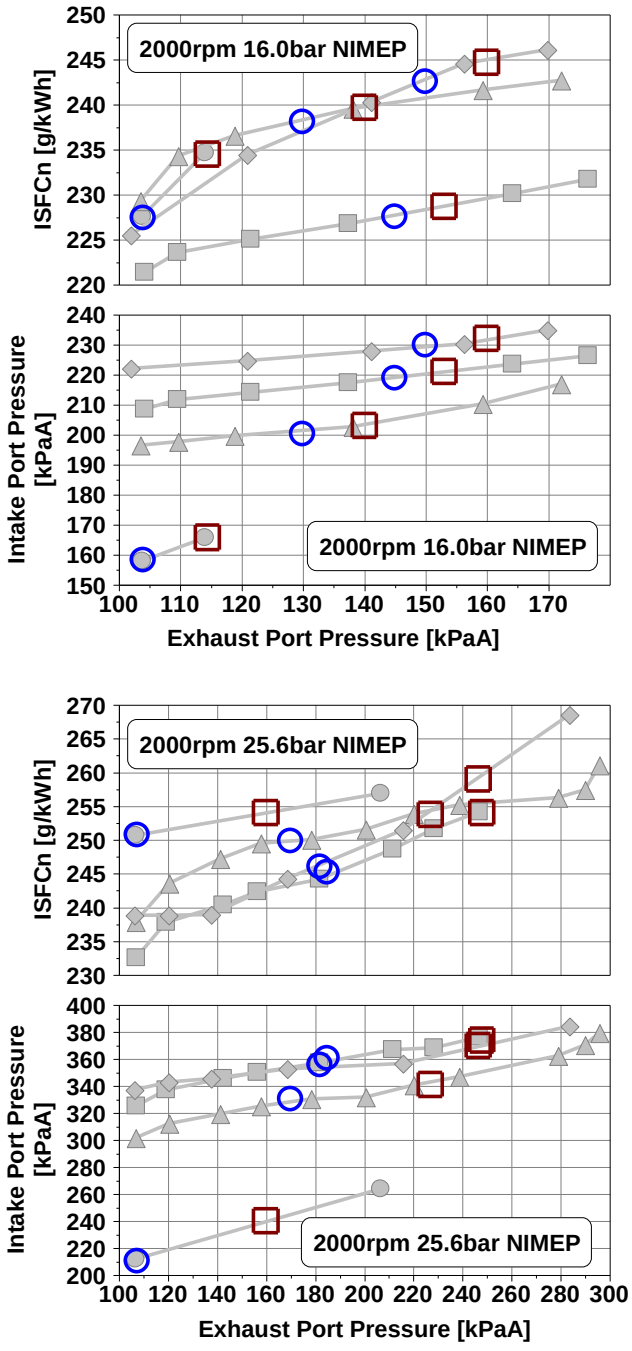

LCR Std Cam
LCR LIVC Cam
LCR EIVC Cam
HCR EIVC Cam

2000rpm 16.0bar NIMEP

Equ. Set 1 ○	LCR Std	LCR LIVC	LCR EIVC	HCR EIVC
Int. Pres	158	220	200	230
Exh. Pres	103	143	130	150
ISFCn	227	227	238	243

Equ. Set 2 □	LCR Std	LCR LIVC	LCR EIVC	HCR EIVC
Int. Pres	165	221	203	232
Exh. Pres	114	153	140	160
ISFCn	235	228	240	245

2000rpm 25.6bar NIMEP

Equ. Set 1 ○	LCR Std	LCR LIVC	LCR EIVC	HCR EIVC
Int. Pres	210	360	330	355
Exh. Pres	108	185	170	182
ISFCn	251	245	250	246

Equ. Set 2 □	LCR Std	LCR LIVC	LCR EIVC	HCR EIVC
Int. Pres	240	374	341	370
Exh. Pres	160	249	227	247
ISFCn	254	254	254	259

Figure 7.6 ISFCn Comparison at Equivalent EBP Conditions

It could be assumed that the exhaust port pressure is proportional to the intake pressure. According to the intake pressures utilised by different hardware configurations to achieve 16.0bar or 25.6bar NIMEP, test logs with equivalent EBP conditions are picked and compared in Figure 7.6. At 2000rpm 16.0bar NIMEP, the LCR LIVC cam setup still achieves the best fuel economy among the four tested hardware combinations at equivalent EBP condition. The LCR EIVC cam configuration produces higher ISFCn than the LCR standard cam, while the HCR EIVC cam setup makes ISFCn even worse. At full load of 25.6bar NIMEP, four hardware options have quite similar ISFCn values at equivalent EBP conditions. To be noted that the potential of EIVC cam and high CR to improve engine fuel efficiency might not be full explored in this study, since intake port and combustion chamber especially the geometry of high CR piston have not been optimised. However the test results have shown the increased EBP has strong negative impact on the fuel economy benefits provided by Miller cycle operation at high load when boosting is provided by turbocharger.

7.5 Impact of Supercharger Work Consumption

This section will discuss engine fuel consumption at high loads if the boosting pressure is provided by a mechanical supercharger which consumes engine power to drive. The compression work consumed by the supercharger is calculated as follow [163],

$$Wc = Air\ flow\ rate * Cp * T1 * \left[\left(\frac{P2}{P1}\right)^{\frac{\gamma-1}{\gamma}} - 1\right] * \left(\frac{1}{\eta c * \eta mechanical}\right) \qquad \textbf{7-1}$$

Where,

For the air, Cp = 1.012 J/(g·K) [10]

$\gamma = 1.4$

Compressor efficiency $\eta_c = 60\%$ [10]

Compressor Mechanical efficiency $\eta_{mechanical} = 90\%$ [10]

T1 Supercharger inlet temperature

P1 Supercharger inlet pressure

P2 Supercharger outlet pressure

Finally, this part of work is converted to additional FMEP to correct for the BSFC. Figure 7.7 and 7.8 compare the corrected BSFC and ISFCn of different hardware configurations.

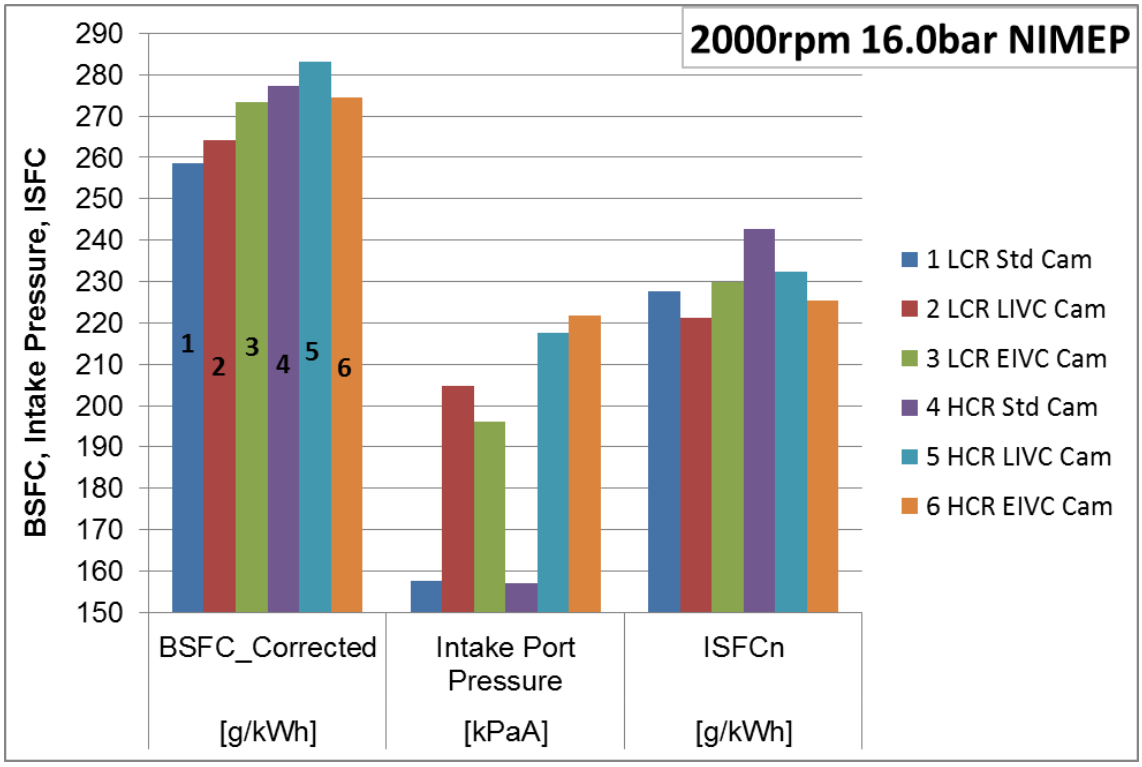

Figure 7.7 ISFCn and Corrected BSFC Comparison at 2000rpm 16.0bar NIMEP

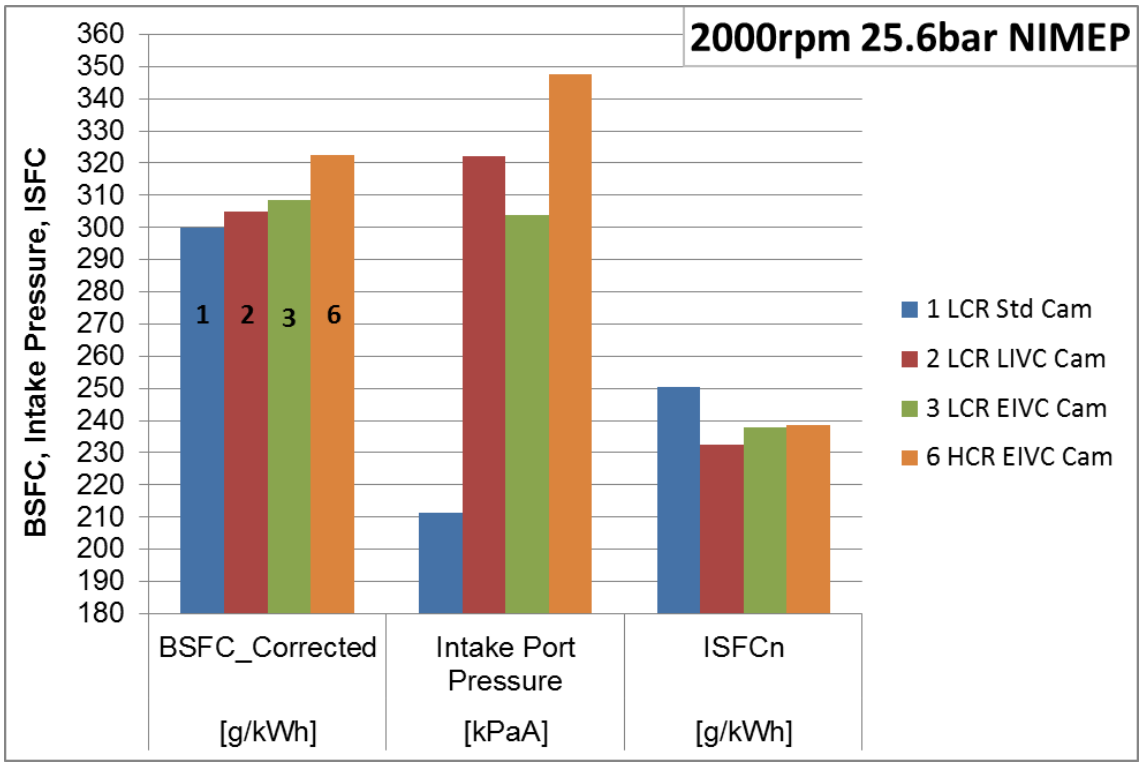

Figure 7.8 ISFCn and Corrected BSFC Comparison at 2000rpm 25.6bar NIMEP

At both high load test points, the trends of corrected BSFC are quite different from the trends of ISFCn. The corrected BSFC of the baseline hardware, i.e. LCR and standard intake cam, is the lowest among all hardware combinations. Miller cycle cams lose fuel economy advantages due to higher intake pressure demand for maintaining engine load. When comparing three intake cam profiles at high CR, the EIVC cam produces the lowest corrected BSFC at 2000rpm 16.0bar NIMEP. Most engines have no variable compression ratio and cam profile switching systems to change the geometry compression ratio and intake cam profile. High CR plus EIVC cam configuration will still be the best option, considering its potential to reduce fuel consumption at part load and the capability to run at full load as high as the LCR standard cam could.

7.6 Systematic Balance for Miller Cycle Application

The geometric CR, Miller cycle ratio (MCR), maximum BMEP and boosting pressure need to be considered together when applying Miller cycle technology to improve the engine fuel consumption, as shown in Figure 7.9. Increased geometric CR is essential for Miller cycle operation to achieve the optimal fuel conversion efficiency. However if geometric CR is too high, great MCR is required at high load to reduce effective CR to avoid knocking combustion. As a result, the engine needs to utilise high boosting pressure to achieve the torque output, which is challenging for the boosting system and can deteriorate the fuel economy benefits at high load as discussed in the previous sections. For a given geometric CR, there is a trade-off between maximum BMEP and fuel economy. The higher maximum BMEP to be achieved, the higher MCR is required for high load operating. Thus maximum BMEP, geometry CR and MCR needs to be carefully balanced and selected.

With higher boosting demand, increased exhaust back pressure of a turbocharger will not only increase fuel consumption, but also lead to abnormal combustion problems like knocking, pre-ignition and misfiring. Mechanical supercharger mainly affects engine total parasitic loss and has less impact on combustion process hence it could be more suitable for a Miller cycle engine.

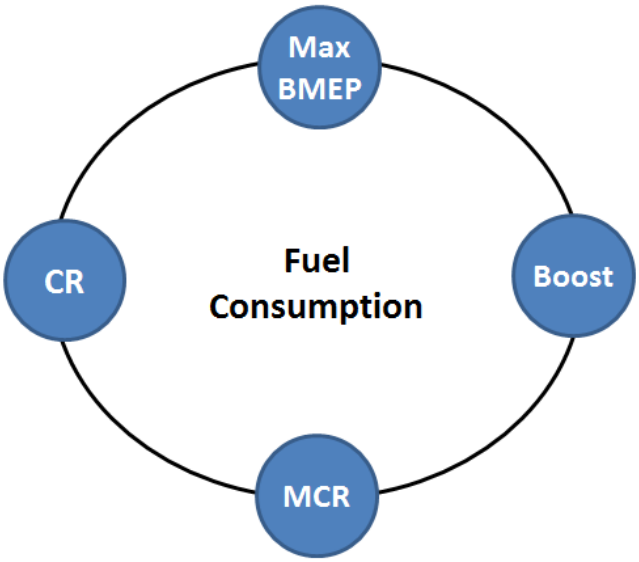

Figure 7.9 Factors Affecting Fuel Consumption of a Miller Cycle Engine

7.7 Fuel Consumption Benefits through Miller Cycle with CPS and VCR

Figure 7.10 illustrates a favourable strategy for a gasoline engine equipped with three-step CPS, two-step VCR and dual VCT variabilities to achieve the optimal fuel conversion efficiency. The engine speed and load for mode switching could vary on each specific engine. The potential improvement of fuel consumption compared to the standard cam and low CR configuration is given here for reference only. An engine with fully optimised designs could gain more benefits. LIVC cam is preferable for the areas which demand a reduced valve overlap period, while EIVC cam is favourable for other part load regions using larger valve overlap for high internal EGR rate. The engine should run at high geometric CR mode for Miller cycle operation at part loads with either LIVC or EIVC cam, and switch to a low or normal CR setting for Otto cycle running at high load area. The Otto cycle operation at normal CR and standard intake cam profile minimises the requirements on boosting system for lowering the whole engine complexity and cost, and it will also benefit the fuel economy at high loads according to the discussion in the previous section. Split injection strategies should be utilised at low speed high load region for knock control and combustion advancing hence improving fuel consumption. However split injection strategy was not tested for comparison with single injection at standard cam and low CR hardware configuration, hence no data is available here to quantify the fuel consumption reduction.

This engine should have great capability to reduce vehicle fuel consumption through downsizing and large region of part load with high efficiency. Some technologies such as water injection, ethanol fuel and cooled EGR can be added to increase CR for Otto cycle operation at high loads, which will maximise the overall fuel conversion efficiency of the gasoline engine for meeting future legislation requirement.

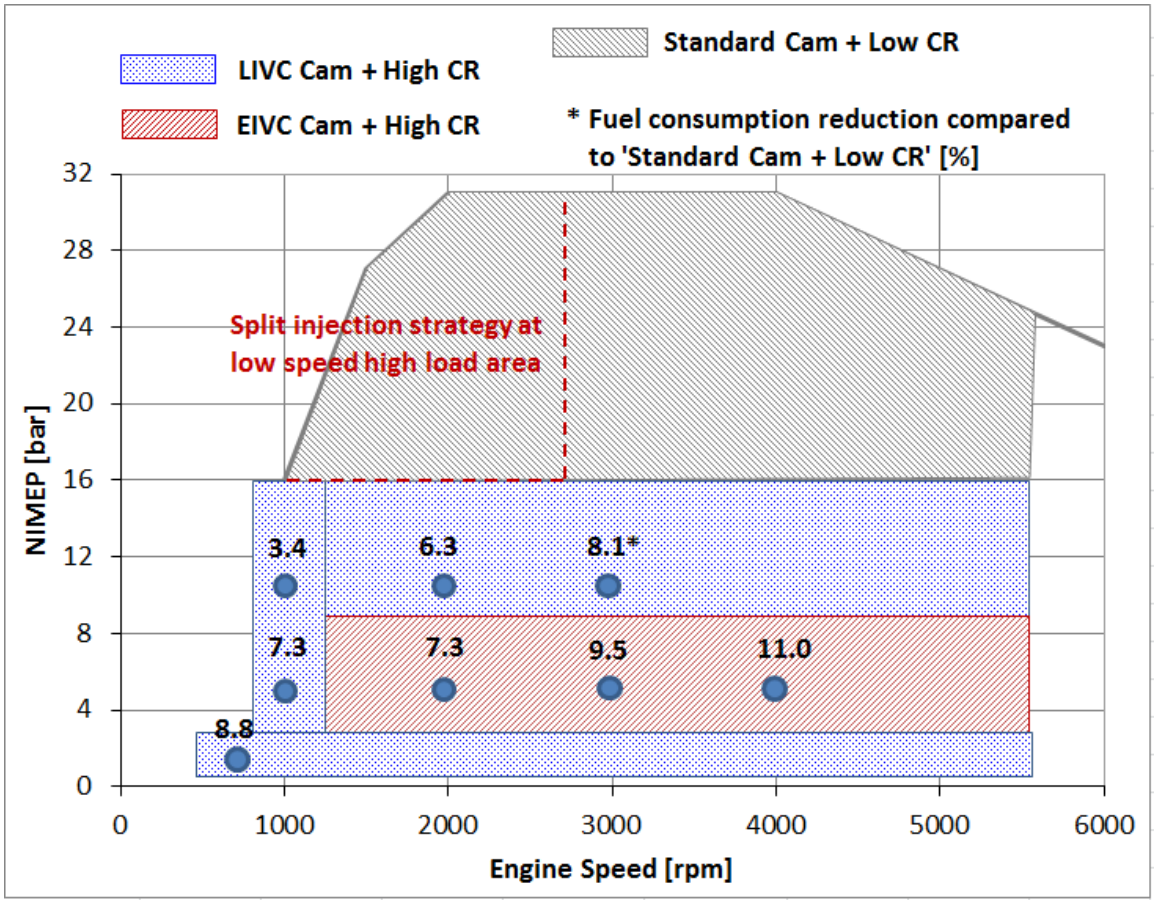

Figure 7.10 Maximise Efficiency of a Gasoline Engine through Miller Cycle Approach Combining CPS and VCR Technologies

7.8 Summary

This chapter has presented the test results of exhaust back pressure sweep and the estimation of work consumed by a supercharger. Fuel consumption of different engine hardware configurations were compared at equivalent EBP conditions or with engine parasitic loss corrected.

Both the increased EBP of a turbocharger and work consumed by a supercharger can significantly reduce the fuel economy benefits provided by Miller cycle operating at high load conditions as higher boosting pressure is needed. Higher EBP also can cause abnormal combustion problems, thus supercharger is considered as a better option for Miller cycle application. The EIVC cam offers the best fuel consumption results when a high CR piston is adopted.

Engine maximum BMEP, geometric CR, Miller cycle ratio and boosting pressure need to be carefully balanced when applying Miller cycle technology for achieving the optimal fuel economy. Cam profiles switching and variable compression ratio technologies for the engine to utilise different combinations of intake cam profile and geometric CR at different engine operation map areas will enable a gasoline engine to achieve the best overall fuel conversion efficiency for meeting the future standard.

Chapter Eight

Conclusions and Recommendation for Future Work

Chapter 8 Conclusions and Recommendation for Future Work

8.1 Conclusions

In this work, extensive engine experiments have been performed to study the Miller cycle operation with different hardware configurations and conditions, including independent intake and exhaust cam timing variations, three intake cam profiles, standard / LCR and HCR pistons, EBP sweep and injection strategy tuning.

Both EIVC and LIVC approaches are effective in reducing engine pumping losses at part load due to shortened effective intake stroke and enhanced intake pressure, which make Miller cycle a simple and effective technology to improve the fuel economy of gasoline engines. In comparison, CR has little impact on the pumping loss. However the shortened intake stroke is the main challenging when applying Miller cycle at full load, where the shifted IVC timings lead to extremely high boosting pressure requirement. As a result, complicated and advanced boosting system is demanded or maximum BMEP has to be reduced resulting in compromised engine performance. Furthermore, very high boosting pressure could cause penalty to even deteriorate the final fuel consumption at high loads since it might be supplied at a cost of increased EBP or friction loss in the boosting system, although it can also generate more positive pumping work.

Miller cycle with either EIVC or LIVC has a reduced effective CR therefore a lowered charge temperature at the end of compression. Thus Miller cycle is effective in mitigating knocking and pre-ignition tendency, which is particularly beneficial for downsized gasoline engines to advance the combustion phasing (CA50) and enable a higher geometric CR to be adopted for better fuel conversion efficiency. However, at part load, the reduced ECR and charge temperature could bring negative impacts. Reduced ECR results in thermodynamic efficiency loss when optimal combustion timing is not limited by knocking combustion. Low charge temperature could contribute to a slow flame propagation and combustion process although it might decrease the heat transfer and losses. Therefore, increasing geometric CR to balance the ECR for part load operation and also to run at a high expansion ratio is essential for Miller cycle to achieve the fuel economy benefits.

When the EIVC strategy is employed, the in-cylinder charge is initially cooled down during expansion to BDC after intake valves closed, hence EIVC could reduce the charge temperature more than LIVC could if other conditions are equal. This can provide EIVC approach with superior capability for suppressing knocking combustion and pre-ignition at high load conditions. On the other hand, it may deteriorate the gross indicated efficiency at part loads due to decreased burning rate and peak pressure.

It becomes known that the ignition and combustion process can be compromised by the EIVC and LIVC cams at some operating conditions because of reduced turbulence at the end of compression. This can be worse for an EIVC cam with short valve open duration and small valve lift, which reduce the level of charge motion generated during induction process. In addition, early closing of intake valves increases the time between tumble generation and combustion hence lengthens the period for charge motion to be dissipated. Thus the intake port, combustion chamber including piston geometry and also the bore-stroke-ratio must be optimised for a Miller cycle engine utilising EIVC cam and high geometric CR in order to achieve a reasonable turbulence level and combustion duration.

Combination of modified cam profiles and VCT mechanisms can produce great synergy for a Miller cycle engine, where IVC timing is typically dominated by the intake cam profile. The VCT device can provide further adjustment of IVC timing for extended Miller cycle management, meanwhile providing the capability for tuning valve overlap period. As demonstrated in the experiments, retarding the LIVC cam timing during idle operation can simultaneously reduce valve overlap for less residual gas and better combustion stability and increase throttle opening for reduced pumping loss. EIVC cam combined with VCT can have larger valve overlap while maintaining high Miller cycle ratio via inlet cam timing advancing, which can generate efficient synergy at part load and also the low speed high load region. At part load, increased hot internal EGR can compensate the charge cooling and enhance charge temperature for better fuel evaporation, fuel/air mixture formation and combustion quality. The improvement in the pumping efficiency is also maximised by higher EGR rate and higher Miller cycle ratio together. At high loads, the large valve overlap enables more complete scavenging effect to reduce in-cylinder residual gas fraction and meanwhile the lower ECR of Miller cycle reduces the charge temperature. As a result, an engine with EIVC cam and very high geometric CR is able to operate at high BMEP and advanced CA50 timing without

occurrence of knocking and low speed pre-ignition. Hence, the fuel saving potential of downsizing concept could be fully realised.

8.2 Strategies for Miller Cycle Application and Potential Benefit

According to the results obtained in this work, EIVC cam combined with high geometric CR is the best configuration for a Miller cycle engine without VCR and CPS devices to change the geometry CR and intake cam profile, considering its potential to reduce fuel consumption at a large region of part loads and the capability to run at full load BMEP as high as the baseline engine, i.e. low CR and standard cam could. The Miller cycle operation might not improve fuel conversion efficiency compared to the baseline at high load area. However, the significantly improved part load efficiency and preserved downsizing level will considerably reduce the fuel consumption of a vehicle equipped with this engine compared to a larger displacement engine. Development of a boosting system to supply sufficient pressure ratio and air flow without excessive increase of exhaust back pressure and parasitic losses is the main challenging for this type of applications.

Alternative applications of Miller cycle are featured by the engine full load operating strategy. One embody is to decrease the maximum BMEP hence degrade the downsizing level, in order to reduce the requirement on the boosting system. Another option is to switch to Otto cycle operation at high load through a 2-step CPS mechanism. In this case, the engine geometric CR has to be compromised if no other countermeasure for suppressing knocking is employed. As a result, the fuel economy benefits of these approaches would be limited.

As illustrated in Figure 7.10, a gasoline engine can maximise the overall fuel conversion efficiency through employing more variabilities including a three-step CPS, a two-step VCR and dual VCT system. The engine shall run at high geometric CR mode for Miller cycle operation at part loads with either LIVC cam or EIVC cam for the best fuel economy. At high load area, Otto cycle operation with standard cam and normal CR configuration will minimise the requirements on boosting system for decreased engine complexity and cost and also reduce the fuel consumption.

8.3 Recommendations for Future Work

The followings are some recommendations for any continuous work to be considered:

(1) Some conditions in current work could be improved. Intake port design and HCR piston geometry need to be optimised for fully exploring the potential of Miller cycle particular the EIVC approach, which might provide some fresh results and conclusion.

(2) The gas exchange process has critical impacts on the performance and efficiencies of a Miller cycle engine. A multi-cylinder engine should have quite different gas exchange characteristics as the single cylinder engine, especially the transient scavenging process and hence the exhaust back pressure. Therefore, the results and findings obtained on the single cylinder engine need to be validated on a targeting multi-cylinder engine.

(3) The boosting system is the key for realising the Miller cycle operation on a highly downsized gasoline engine, and also has considerable impact on the final fuel economy benefits. Development of a boosting system fulfilling the demand and assessment of the system on real engine will be very interesting and productive work.

(4) The Miller cycle based concept presented in Figure 8.1 could be a favourable solution for future highly efficient boosted downsized gasoline DI engines. Develop a prototype engine and carry out numerical and experimental studies could be a meaningful continuum of this research.

References

[1] P. Miller and M. Solomon, “A brief history of Technolgy-Forcing Motor Vehicle Regulations,” *Experientia*, vol. 49, no. 5, pp. 366–368, 2009.

[2] Delphi, “Delphi-worldwide-emissions-standards-passenger-cars-light-duty-2017-2018.pdf.” Delphi, 2017.

[3] Dieselnet, “EU Emission Standards for Passenger Cars,” *www.dieselnet.com*, 2017.

[4] International Organization of Motor Vehicle Manufacturers, “Climate Change and CO2 Brochure.” p. 9, 2008.

[5] SMMT, “New Car CO2 Report 2017 - The 16th Edition.” 2017.

[6] Z. Yang and A. Bandivadekar, “2017 Global update: Light-duty vehicle greenhouse gas and fuel economy standards.” ICCT, 2017.

[7] Fraunhofer Institute for Systems and Innovation Research (ISI), “Technologies and incentives to reduce CO2 emissions from passenger cars.” BSEC, 2010.

[8] Automotive Council Technology Group, “Automotive Council Roadmaps,” *Automotive Council Technology Group*. 2013.

[9] “2016 WardsAuto Survey | DuPont Automotive | DuPont USA,” *WardsAuto*, 2016. [Online]. Available: http://www.dupont.com/industries/automotive/press-release/WardsAuto-survey-2016.html. [Accessed: 16-Aug-2017].

[10] J. B. Heywood, *Internal Combustion Engine Fundementals*, vol. 21. 1988.

[11] C. F. Taylor, *The Internal-combustion Engine in Theory and Practice*. MIT Press, 1985.

[12] R. Stone, *Introduction to Internal Combustion Engines*, 4th ed. SAE International and Macmillan Press, 2012.

[13] H. Zhao, *Advanced Direct Injection Combustion Engine Technologies and Development, Volume 1: Gasoline and Gas Engines*. Woodhead Publishing Limited, 2014.

[14] J. Wang and S. Shuai, *Automotive Engine Fundamentals*. Tsinghua University Press, 2011.

[15] J. Yang, *Combustion System Development of Automotive Gasoline Engines*. China Machine Press, 2009.

[16] Robert Bosch GmbH, *Automotive Handbook*, 9th ed. Wiley, 2014.

[17] F. Weberbauer, M. Rauscher, A. Kulzer, M. Knopf, and M. Bargende, "Generally applicate split of losses for new combustion concepts," *MTZ Worldw.*, vol. 66, no. 2, pp. 17–19, Feb. 2005.

[18] IEA, "INTERNATIONAL COMPARISON OF LIGHT-DUTY VEHICLE FUEL ECONOMY 2005-2015," 2017.

[19] M. B. Ç. and B. Özdalyan, "Gasoline direct injection," in *SIA / CNAM 2012*, 2012, pp. 1–18.

[20] R. Basshuysen, *Gasoline Engine with Direct Injection: Processes, Systems, Development, Potential*. Vieweg+Teubner, 2009.

[21] T. Inoue, S. Matsushita, K. Nakanishi, and H. Okano, "Toyota Lean Combustion System - The Third Generation System," in *SAE Technical Paper*, 1993, p. 930873.

[22] M. Kühn, J. Abthoff, R. Kemmler, and T. Kaiser, "Influence of the Inlet Port and Combustion Chamber Configuration on the Lean-Burn Behaviour of a Spark-Ignition Gasoline Engine," in *SAE Technical Paper*, 1996, p. 960608.

[23] M. Matsuki, K. Nakano, T. Amemiya, Y. Tanabe, D. Shimizu, and I. Ohmura, "Development of a Lean Burn Engine with a Variable Valve Timing Mechanism," in *SAE Technical Paper*, 1996, p. 960583.

[24] F. Zhao, M. C. Lai, and D. L. Harrington, "Automotive spark-ignited direct-injection gasoline engines," *Prog. Energy Combust. Sci.*, vol. 25, no. 5, pp. 437–562, 1999.

[25] R. Krebs, E. Pott, T. P. Kreuzer, U. Göbel, and K.-H. Glück, "Exhaust Gas Aftertreatment of Volkswagen FSI Fuel Stratified Injection Engines," in *SAE Technical Paper*, 2002, pp. 2002-01–0346.

[26] F. Rohr *et al.*, "The Impact of Sulfur Poisoning on NOx-Storage Catalysts in Gasoline Applications," in *SAE Technical Paper*, 2005, pp. 2005-01–1113.

[27] G. Vent, C. Enderle, N. Dr Merdes, F. Kreitmann, and R. Dr Weller, "The new

2.0l turbo engine from the Mercedes-Benz 4-cylinder engine family," in *2nd Aachen Colloquium China 2012*, 2012.

[28] H. Zhao, *HCCI and CAI engines for the automotive industry*, no. 1. Woodhead Publishing Limited, 2007.

[29] A. Fuerhapter, W. F. Piock, and G. K. Fraidl, "CSI - Controlled Auto Ignition - the Best Solution for the Fuel Consumption - Versus Emission Trade-Off?," in *SAE Technical Paper*, 2003, pp. 2003-01–0754.

[30] D. Fritz, "DiesOtto: a diesel-gasoline technology blend," *aei*, Oct-2007.

[31] "Green Car Congress: GMs HCCI Demonstrator Combines a Set of Enabling Technologies and Strategies for Extending Operating Range." [Online]. Available: http://www.greencarcongress.com/2009/05/gm-hcci-20090528.html. [Accessed: 19-Aug-2017].

[32] W. Steiger, U. Stolte, I. Scholz, and S. Schmerbeck, "The CCS Combustion System from Volkswagen," *MTZ worldwide*, p. 4, Mar-2008.

[33] Y. Yamasaki *et al.*, "Development of Dynamic Models for an HCCI Engine with Exhaust Gas Rebreathing System," in *SAE Technical Paper*, 2015, pp. 2015-01–1803.

[34] "Green Car Congress: Mazda announces SKYACTIV-X gasoline Spark Controlled Compression Ignition," 2017. [Online]. Available: http://www.greencarcongress.com/2017/08/20170808-mazda.html. [Accessed: 19-Aug-2017].

[35] "Engine Technology | Mazda Unveils Petrol Engine with Homogeneous Compression Ignition | springerprofessional.de." [Online]. Available: https://www.springerprofessional.de/engine-technology/emissions/mazda-unveils-petrol-engine-with-homogeneous-compression-ignitio/13534078?fulltextView=true&wt_eCircle_oad=279880&wt_eCircle_nwsl=121980&wt_eCircle_u=19229430313&wt_mc=nl.red.automotive.19008. [Accessed: 19-Aug-2017].

[36] A. Königstein, U. D. Grebe, K.-J. Wu, and P.-I. Larsson, "Differentiated analysis of downsizing concepts," *MTZ Worldw.*, vol. 69, no. 6, pp. 4–11, Jun. 2008.

[37] M. Kratzsch and M. Günther, *Knocking in Gasoline Engines*. DCM Druck Center

Meckenheim GmbH, 2013.

[38] “Low Speed Pre-ignition (LSPI), Oxidation and Wear - Lubrizol Additives 360 - Passenger.” [Online]. Available: https://passenger.lubrizoladditives360.com/low-speed-pre-ignition-lspi-oxidation-and-wear/. [Accessed: 19-Aug-2017].

[39] O. Lang, J. Geiger, K. Habermann, and M. Wittler, “Boosting and Direct Injection -Synergies for Future Gasoline Engines,” in *SAE Technical Paper*, 2005, pp. 2005-01–1144.

[40] W. Bandel, G. K. Fraidl, P. E. Kapus, H. Sikinger, and C. N. Cowland, “The Turbocharged GDI Engine: Boosted Synergies for High Fuel Economy Plus Ultra-low Emission,” in *SAE Technical Paper*, 2006, pp. 2006-01–1266.

[41] P. Wolfram, J. German, P. Mock, and U. Tietge, “Deployment of passenger car technology in Europe and the United States,” 2016.

[42] W. Hannibal, “Lecture: Variable Valve Timing Systems on Modern Spark Ignition Engines.” p. 108, 2009.

[43] T. Kim, “Variable Intake Manifold Development trend and technology,” in *2010 Shanghai PIM Conference*, 2010, vol. 2, no. 1, pp. 1–7.

[44] S. Potul, R. Nachnolkar, and S. Bhave, “Analysis Of Change In Intake Manifold Length And Development Of Variable Intake System,” *Int. J. Sci. Technol. Res.*, vol. 3, no. 5, pp. 223–228, 2014.

[45] Y. Moriya, A. Watanabe, H. Uda, H. Kawamura, M. Yoshioka, and M. Adachi, “A Newly Developed Intelligent Variable Valve Timing System - Continuously Controlled Cam Phasing as Applied to a New 3 Liter Inline 6 Engine,” in *SAE Technical Paper*, 1996, p. 960579.

[46] T. G. Leone, E. J. Christenson, and R. A. Stein, “Comparison of Variable Camshaft Timing Strategies at Part Load,” in *SAE Technical Paper*, 1996, p. 960584.

[47] J. H. Tuttle, “Controlling Engine Load by Means of Late Intake-Valve Closing,” in *SAE Technical Paper*, 1980, p. 800794.

[48] J. H. Tuttle, “Controlling Engine Load by Means of Early Intake-Valve Closing,” in *SAE Technical Paper*, 1982, p. 820408.

[49] Y. Urata, H. Umiyama, K. Shimizu, Y. Fujiyoshi, H. Sono, and K. Fukuo, “A Study of Vehicle Equipped with Non-Throttling S.I. Engine with Early Intake Valve Closing Mechanism,” in *SAE Technical Paper*, 1993, p. 930820.

[50] P. Kreuter, P. Heuser, J. Reinicke-Murmann, R. Erz, U. Peter, and O. Böcker, “Variable Valve Actuation - Switchable and Continuously Variable Valve Lifts,” in *SAE Technical Paper*, 2003, pp. 2003-01–0026.

[51] W. Hannibal, R. Flierl, L. Stiegler, and R. Meyer, “Overview of Current Continuously Variable Valve Lift Systems for Four-Stroke Spark-Ignition Engines and the Criteria for their Design Ratings,” in *SAE Technical Paper*, 2004, pp. 2004-01–1263.

[52] H. Hong, G. B. Parvate-Patil, and B. Gordon, “Review and analysis of variable valve timing strategies--eight ways to approach,” *Proc. Inst. Mech. Eng. Part D J. Automob. Eng.*, vol. 218, no. 10, pp. 1179–1200, 2004.

[53] P. Kreuter, P. Heuser, J. Reinicke-Murmann, R. Erz, P. Stein, and U. Peter, “Meta - CVD System An Electro-Mechanical Cylinder and Valve Deactivation System,” in *SAE Technical Paper*, 2001, pp. 2001-01–0240.

[54] A. Falkowski, M. McElwee, and M. Bonne, “Design and Development of the DaimlerChrysler 5.7L HEMI® Engine Multi-Displacement Cylinder Deactivation System,” in *SAE Technical Paper*, 2004, pp. 2004-01–2106.

[55] M. Rebbert, G. Kreusen, and S. Lauer, “A New Cylinder Deactivation by FEV and Mahle,” in *SAE Technical Paper*, 2008, pp. 2008-01–1354.

[56] W. Hentschel *et al.*, “Optical Diagnostics and CFD-Simulations to Support the Combustion Process Development of the Volkswagen FSI® Direct-Injection Gasoline Engine,” in *SAE Technical Paper*, 2001.

[57] R. Szengel, H. Middendorf, E. Pott, and J. Theobald, “The TSI with 90 kW – the expansion of the Volkswagen family of fuel-efficient gasoline engines,” in *Internationales Wiener Motorensymposium 2007*, 2007.

[58] H.-J. Neußer, H. Endres, and M. Breuer, “New Variable Intake and Mixture Formation System for Multi-Valve SI Engines,” in *SAE Technical Paper*, 1994, p. 940449.

[59] M. Roberts, “Benefits and Challenges of Variable Compression Ratio (VCR),” in

SAE Technical Paper, 2003, pp. 2003-01–0398.

[60] V. Rabhi, J. Beroff, and F. Dionnet, "Study of a Gear-Based Variable Compression Ratio Engine," in *SAE Technical Paper*, 2004, pp. 2004-01–2931.

[61] P. Ferrey, Y. Miehe, C. Constensou, and V. Collee, "Potential of a Variable Compression Ratio Gasoline SI Engine with Very High Expansion Ratio and Variable Valve Actuation," *SAE Int. J. Engines*, vol. 7, p. 468–487 (2014–01–1201), 2014.

[62] T. Pohjalainen and M. Larmi, "Novel Crank Mechanism Increasing Engine Efficiency and Reducing CO2 Emissions," in *SAE Technical Paper*, 2015, pp. 2015-01–1259.

[63] "Gomecsys VCR Technology." [Online]. Available: http://www.gomecsys.com/#home/product/gomecsys-vcr-technology/total-fuel-and-co2-reduction-potential%7C%7Ctotal-fuel-and-co2-reduction-potential-description. [Accessed: 23-Aug-2017].

[64] "INFINITI VC-Turbo: The world's first production-ready variable compression ratio engine - Global Newsroom." [Online]. Available: https://newsroom.nissan-global.com/releases/infiniti-vc-t-the-worlds-first-production-ready-variable-compression-ratio-engine. [Accessed: 10-Sep-2016].

[65] J. E. Nicholls, I. A. EI-Messiri, and H. K. Newhali, "Inlet Manifold Water Injection for Control of Nitrogen Oxides — Theory and Experiment," in *SAE Technical Paper*, 1969, p. 690018.

[66] W. D. Weatherford and R. D. Quillian, "Total Cooling of Piston Engines by Direct Water Injection," in *SAE Technical Paper*, 1970, p. 700886.

[67] S. S. Lestz, W. E. Meyer, and C. M. Colony, "Emissions from a Direct-Cylinder Water-Injected Spark-Ignition Engine," in *SAE Technical Paper*, 1972, p. 720113.

[68] J. A. Harrington, "Water Addition to Gasoline-Effect on Combustion, Emissions, Performance, and Knock," in *SAE Technical Paper*, 1982, p. 820314.

[69] "Green Car Congress: BMW shows future drive technologies; 2 Series PHEV prototype, direct water injection in 3-cyl. engine, and fuel cell eDrive." [Online]. Available: http://www.greencarcongress.com/2015/07/20150702-bmw.html. [Accessed: 23-Aug-2017].

[70] “Bosch developing new water-injection system for production engines - SAE International.” [Online]. Available: http://articles.sae.org/14176/. [Accessed: 23-Aug-2017].

[71] Robert Bosch GmbH, “WaterBoost - Water Injection.” 2016.

[72] F. Hoppe, M. Thewes, H. Baumgarten, and J. Dohmen, “Water injection for gasoline engines: Potentials, challenges, and solutions,” *Int. J. Engine Res.*, vol. 17, no. 1, pp. 86–96, 2016.

[73] S. Diana, V. Giglio, B. Iorio, and G. Police, “A Strategy to Improve the Efficiency of Stoichiometric Spark Ignition Engines,” in *SAE Technical Paper*, 1996, p. 961953.

[74] S. Han and W. K. Cheng, “Design and Demonstration of a Spark Ignition Engine Operating in a Stratified-EGR Mode,” in *SAE Technical Paper*, 1998, p. 980122.

[75] B. Grandin, H.-E. Ångström, P. Stålhammar, and E. Olofsson, “Knock Suppression in a Turbocharged SI Engine by Using Cooled EGR,” in *SAE Technical Paper*, 1998, p. 982476.

[76] S. Diana, V. Giglio, B. Iorio, and G. Police, “Evaluation of the Effect of EGR on Engine Knock,” in *SAE Technical Paper*, 1998, p. 982479.

[77] T. Alger, T. Chauvet, and Z. Dimitrova, “Synergies between High EGR Operation and GDI Systems,” *SAE Int. J. Engines*, vol. 1, p. 101–114 (2008–01–0134), 2008.

[78] C. Chadwell, T. Alger, J. Zuehl, and R. Gukelberger, “A Demonstration of Dedicated EGR on a 2.0 L GDI Engine,” *SAE Int. J. Engines*, vol. 7, p. 434–447 (2014–01–1190), 2014.

[79] K. Siokos, R. Koli, R. Prucka, J. Schwanke, and J. Miersch, “Assessment of Cooled Low Pressure EGR in a Turbocharged Direct Injection Gasoline Engine,” *SAE Int. J. Engines*, vol. 8, p. 1535–1543 (2015–01–1253), 2015.

[80] “New 2.5-liter Direct-injection, Inline 4-cylinder Gasoline Engine | TOYOTA Global Newsroom.” [Online]. Available: http://newsroom.toyota.co.jp/en/powertrain/engine/. [Accessed: 08-Jan-2017].

[81] T. Toda, M. Sakai, M. Hakariya, and T. Kato, “The New Inline 4 Cylinder 2.5L Gasoline Engine with Toyota New Global Architecture Concept,” in *38. Internationales Wiener Motorensymposium 2017*, 2017.

[82] R. Miller, “High-Pressure Supercharging System,” USA Patent 2670595, 1954.

[83] R. Miller, “High Expansion, Spark Ignited, Gas Burning, Internal Combustion Engines,” USA Patent 2773490, 1956.

[84] R. Miller, “Supercharged Engine,” USA Patent 2817322, 1957.

[85] J. Atkinson, “Gas Engine,” USA Patent 336505, 1886.

[86] J. Atkinson, “Gas Engine,” USA Patent 367496, 1887.

[87] D. Luria, Y. Taitel, and A. Stotter, “The Otto-Atkinson Engine - A New Concept in Automotive Economy,” in *SAE Technical Paper*, 1982, p. 820352.

[88] E. Schutting, O. Dumböck, T. Kraxner, and H. Eichlseder, “Thermodynamic consideration of the Miller cycle on the basis of simulation and measurements,” in *Internationaler Motorenkongress 2016: Mit Konferenz Nfz-Motorentechnologie*, J. Liebl and C. Beidl, Eds. Wiesbaden: Springer Fachmedien Wiesbaden, 2016, pp. 259–280.

[89] “Honda Worldwide | Technology Picture Book | EXlink.” [Online]. Available: http://world.honda.com/powerproducts-technology/exlink/. [Accessed: 03-Sep-2017].

[90] J. A. C. Kentfield, “A Simple Variable Expansion-Ratio, Spark Ignition, Four-Stroke, Engine,” in *SAE Technical Paper*, 1993, p. 932874.

[91] J. A. C. KENTFIELD, “Extended, and Variable, Stroke Reciprocating Internal Combustion Engines,” in *SAE Technical Paper*, 2002, pp. 2002-01–1941.

[92] P. A. Rosso, J. Beard, and J. R. Blough, “A Variable Displacement Engine with Independently Controllable Stroke Length and Compression Ratio,” in *SAE Technical Paper*, 2006, pp. 2006-01–0741.

[93] A. A. Boretti, J. Scalzo, and H. Masudi, “Alternative Crankshaft Mechanisms and Kinetic Energy Recovery Systems for Improved Fuel Economy of Passenger Cars,” in *SAE Technical Paper*, 2011, pp. 2011-28–0053.

[94] V. Gheorghiu, “Ultra-Downsizing of Internal Combustion Engines,” in *SAE Technical Paper*, 2015, pp. 2015-01–1252.

[95] R. H. Sherman and P. N. Blumberg, “The Influence of Induction and Exhaust Processes on Emissions and Fuel Consumption in the Spark Ignited Engine,” in

SAE Technical Paper, 1977, p. 770880.

[96] S. C. Blakey, R. J. Saunders, T. H. Ma, and A. Chopra, "A Design and Experimental Study of an Otto Atkinson Cycle Engine Using Late Intake Valve Closing," in *SAE Technical Paper*, 1991, p. 910451.

[97] D. L. Boggs, H. S. Hilbert, and M. M. Schechter, "The Otto-Atkinson Cycle Engine-Fuel Economy and Emissions Results and Hardware Design," in *SAE Technical Paper*, 1995, p. 950089.

[98] N. Al-Hasan, J. Beer, J. Ehrhard, T. Lorenz, and L. Stump, "Charging Technologies for CO2 Optimization by Millerization," in *SAE Technical Paper*, 2015, pp. 2015-01–1250.

[99] M. K. Anderson, D. N. Assanis, and Z. S. Filipi, "First and Second Law Analyses of a Naturally-Aspirated, Miller Cycle, SI Engine with Late Intake Valve Closure," *SAE Pap.*, no. 724, p. 980889, 1998.

[100] Y. He, J. Liu, B. Zhu, and D. Sun, "Research on and development of a Miller cycle engine with multi-stage boosting," *Proc. Inst. Mech. Eng. Part D J. Automob. Eng.*, vol. 230, no. 11, pp. 1546–1557, 2016.

[101] T. Li, Y. Gao, J. Wang, and Z. Chen, "The Miller cycle effects on improvement of fuel economy in a highly boosted, high compression ratio, direct-injection gasoline engine: EIVC vs. LIVC," *Energy Convers. Manag.*, 2014.

[102] Y. He, J. Liu, B. Zhu, and D. Sun, "Development of a Miller cycle engine with single-stage boosting and cooled external exhaust gas recirculation," *Proc. Inst. Mech. Eng. Part D J. Automob. Eng.*, vol. 231, no. 6, pp. 766–780, 2017.

[103] S. Hara, Y. Nakajima, and S. Nagumo, "Effects of intake-Valve Closing Timing on Spark-Ignition Engine Combustion," in *SAE Technical Paper*, 1985, p. 850074.

[104] T. Sugiyama, R. Hiyoshi, S. Takemura, and S. Aoyama, "Technology for Improving Engine Performance using Variable Mechanisms," in *SAE Technical Paper*, 2007, pp. 2007-01–1290.

[105] K. Kishi and T. Satou, "The new Nissan high efficient 1.2L 3cyl GDI Supercharged Engine enables 95g/km CO2 emissions and high driving performance," in *33. Internationales Wiener Motorensymposium 2012*, 2012.

[106] E. Aiyoshizawa and K. Hori, "The New Nissan High Efficient 4-Cylinder 1.6L

GDI turbocharged engine with low pressure EGR - Evolution for Lower Fuel Consumption combined with High Output Performance," in *35. Internationales Wiener Motorensymposium 2014*, 2014.

[107] S. Ando, H. Ishii, A. Shikata, and T. Sui, "The New VR30DDTT Engine from Infiniti – Outstanding Power and Response Combined with Environmental Performance," in *25th Aachen Colloquium Automobile and Engine Technology 2016*, 2016.

[108] S. Kono, "Study Of Influences Of Inlet Valve Timings On In-Cylinder Flow, Gas Temperature And Combustion in Spark Ignition Engines," in *SAE Technical Paper*, 1988, p. 885093.

[109] M. Choshi, K. Asanomi, H. Abe, S. Okamoto, and M. Shoji, "Development of V6 Miller cycle engine," *JSAE Rev.*, vol. 15, pp. 195–200, 1994.

[110] T. Goto, K. Hatamura, S. Takizawa, N. Hayama, H. Abe, and H. Kanesaka, "Development of V6 Miller Cycle Gasoline Engine," in *SAE Technical Paper*, 1994, p. 940198.

[111] M. Hitomi, J. Sasaki, K. Hatamura, and Y. Yano, "Mechanism of Improving Fuel Efficiency by Miller Cycle and Its Future Prospect," in *SAE Technical Paper*, 1995, p. 950974.

[112] K. Hatamura, M. Hayakawa, T. Goto, and M. Hitomi, "A study of the improvement effect of Miller-cycle on mean effective pressure limit for high-pressure supercharged gasoline engines," *JSAE Rev.*, vol. 18, no. 2, pp. 101–106, Apr. 1997.

[113] "MAZDA: Mazda Develops New Naturally-Aspirated MZR 1.3L Miller-cycle Engine | News Releases." [Online]. Available: http://www2.mazda.com/en/publicity/release/archive/2007/200705/070531.html. [Accessed: 05-Sep-2015].

[114] I. Hirose, H. Kudo, T. Kihara, M. Yamakawa, and M. Hitomi, "MAZDA SKYACTIV-G 2.0L Gasoline Engine," in *1st Aachen Colloquium China 2011*, 2011.

[115] D. J. Haugen, P. L. Blackshear, M. J. Pipho, and W. J. Esler, "Modifications of a Quad 4 Engine to Permit Late Intake Valve Closure," in *SAE Technical Paper*,

1992, p. 921663.

[116] R. Wurms, R. Budack, M. Grigo, G. Mendl, T. Heiduk, and S. Knirsch, “The New Audi 2.0l Engine with innovative Rightsizing - a further Milestone in the TFSI Technology,” in *36. Internationales Wiener Motorensymposium 2015*, 2015.

[117] R. Budack, M. Kuhn, R. Wurms, and T. Heiduk, “Optimization of the Combustion Process as Demonstrated on the New Audi 2.0l TFSI,” in *24th Aachen Colloquium Automobile and Engine Technology 2015*, 2015.

[118] W. Demmelbauer-Ebner, H. Middendorf, A. Birkigt, M. Ganzer, D. Hagelstein, and K. Persigehl, “EA211 TSI®evo – The New 4-Cylinder Gasoline Engines from Volkswagen,” in *25th Aachen Colloquium Automobile and Engine Technology 2016*, 2016.

[119] F. Eichler, W. Demmelbauer-Ebner, J. Theobald, B. Stiebels, H. Hoffmeyer, and M. Kreft, “The New EA211 TSI® evo from Volkswagen,” in *37. Internationales Wiener Motorensymposium 2016*, 2016.

[120] J. Jablonski *et al.*, “The New 3.0l V6 TFSI Engine from AUDI – Key Mechanical Aspects of the Top-Of-The-Range V6,” in *25th Aachen Colloquium Automobile and Engine Technology 2016*, 2016.

[121] K. Akima, K. Seko, W. Taga, K. Torii, and S. Nakamura, “Development of New Low Fuel Consumption 1.8L i-VTEC Gasoline Engine with Delayed Intake Valve Closing,” in *SAE Technical Paper*, 2006, pp. 2006-01–0192.

[122] A. Yonekawa, M. Ueno, O. Watanabe, and N. Ishikawa, “Development of New Gasoline Engine for ACCORD Plug-in Hybrid,” in *SAE Technical Paper*, 2013, pp. 2013-01–1738.

[123] K. Kuzuoka, T. Kurotani, H. Chishima, and H. Kudo, “Study of High-Compression-Ratio Engine Combined with an Ethanol-Gasoline Fuel Separation System,” *SAE Int. J. Engines*, vol. 7, p. 1773–1780 (2014–01–2614), 2014.

[124] K. Ikeya, M. Takazawa, T. Yamada, S. Park, and R. Tagishi, “Thermal Efficiency Enhancement of a Gasoline Engine,” *SAE Int. J. Engines*, vol. 8, p. 1579–1586 (2015–01–1263), 2015.

[125] M. Wirth, U. Mayerhofer, W. F. Piock, and G. K. Fraidl, “Turbocharging the DI Gasoline Engine,” in *SAE Technical Paper*, 2000, pp. 2000-01–0251.

[126] P. E. Kapus and P. Poetscher, “ULEV and Fuel Economy - A Contradiction?,” in *SAE Technical Paper*, 2000, pp. 2000-01–1209.

[127] P. E. Kapus, D. Denger, and T. Holland, “Intelligent Simplification-Ways Towards Improved Fuel Economy,” in *SAE Technical Paper*, 2002, pp. 2002-01–0236.

[128] G. Fraidl, P. Kapus, and M. Neubauer, “Gasoline Engine 2020: 200 kW/l and 200 g/kWh?,” in *SIA Versailles 2015 International Powertrain Conference*, 2015.

[129] H. Sorger *et al.*, “AVL’s VCR System Modular and Cost Efficient CO2 Reduction,” in *25th Aachen Colloquium Automobile and Engine Technology 2016*, 2016.

[130] S. ADACHI and H. HAGIHARA, “The renewed 4-Cylinder Engine Series for Toyota Hybrid System,” in *33. Internationales Wiener Motorensymposium 2012*, 2012.

[131] T. Yamada, S. Adachi, K. Nakata, T. Kurauchi, and I. Takagi, “Economy with Superior Thermal Efficient Combustion (ESTEC),” in *SAE Technical Paper*, 2014, pp. 2014-01–1192.

[132] T. Shinagawa, M. Kudo, W. Matsubara, and T. Kawai, “The New Toyota 1.2-Liter ESTEC Turbocharged Direct Injection Gasoline Engine,” in *SAE Technical Paper*, 2015, pp. 2015-01–1268.

[133] E. Murase and R. Shimizu, “Innovative Gasoline Combustion Concepts for Toyota New Global Architecture,” in *25th Aachen Colloquium Automobile and Engine Technology 2016*, 2016.

[134] A. Cairns, A. Todd, H. Hoffman, P. Aleiferis, and J. Malcolm, “Combining Unthrottled Operation with Internal EGR under Port and Central Direct Fuel Injection Conditions in a Single Cylinder SI Engine,” in *SAE Technical Paper*, 2009, pp. 2009-01–1835.

[135] J. Taylor, N. Fraser, R. Dingelstadt, and H. Hoffmann, “Benefits of Late Inlet Valve Timing Strategies Afforded Through the Use of Intake Cam In Cam Applied to a Gasoline Turbocharged Downsized Engine,” in *SAE Technical Paper*, 2011, pp. 2011-01–0360.

[136] G. Vent, C. Enderle, N. Merdes, F. Kreitmann, and R. Weller, “The New 2.0l

Turbo Engine from the Mercedes-Benz 4-Cylinder Engine Family," in *21st Aachen Colloquium Automobile and Engine Technology 2012*, 2012.

[137] E. Rau, H. Kohler, G. Karl, K. Fieweger, J. Betsch, and B. Krutzsch, "Variabilities on Gasoline Engines and their Future Potentials," in *35. Internationales Wiener Motorensymposium 2014*, 2014.

[138] W. Gottschalk, U. Lezius, and L. Mathusall, "Investigations on the Potential of a Variable Miller Cycle for SI Knock Control," *SAE Technical Paper 2013-01-1122*. 2013.

[139] M. Riess, A. Benz, M. Wöbke, and M. Sens, "Intake Valve Lift Strategies for Turbulence Generation," *MTZ Worldw.*, vol. 74, no. 7, pp. 42–47, Jul. 2013.

[140] A. Benz, M. Rieß, M. Sens, M. Wöbke, and K.-G. Stapf, "Valve Train Variabilities on Gasoline Engines between Dethrottling and Turbulence Generation," in *SIA Versailles 2013 International Powertrain Conference*, 2013.

[141] M. Scheidt, C. Brands, M. Kratzsch, and M. Günther, "Combined Miller/Atkinson Strategy for Future Downsizing Concepts," *MTZ Worldw.*, vol. 75, no. 5, pp. 4–11, May 2014.

[142] M. Sens, S. Zwahr, and M. Günther, "Potential of the Variable Compression Ratio on a Fully "Millered'' Gasoline Engine," *MTZ Worldw.*, vol. 77, no. 4, pp. 50–55, Apr. 2016.

[143] M. Sens *et al.*, "Selecting a suitable stroke / bore ratio when combining variable compression and Early Intake Valve Closure (EIVC)," in *Internationaler Motorenkongress 2017: Mit Konferenzen Nfz-Motorentechnologie und Neue Kraftstoffe*, J. Liebl and C. Beidl, Eds. Wiesbaden: Springer Fachmedien Wiesbaden, 2017, pp. 65–100.

[144] A. Birckett, N. Engineer, P. Arlauskas, M. Shirley, and P. Neuman, "Mechanically Supercharged 2.4L GDI Engine for Improved Fuel Economy and Low Speed Torque Improvement," in *SAE Technical Paper*, 2014, pp. 2014-01–1186.

[145] K.-P. Ha, W. T. Kim, I. S. Ryu, and Y. S. Son, "Development of Continuously Variable Valve Duration (CVVD) Engine," in *25th Aachen Colloquium Automobile and Engine Technology 2016*, 2016.

[146] R. Osborne, K. Pendlebury, J. Stokes, J. Dalby, and C. Rouaud, "The Magma

Engine Concept – A Downsized Turbocharged Gasoline Engine with High Compression Ratio," in *JSAE Annual Congress 2015*, 2015.

[147] K. Pendlebury, R. Osborne, T. Downes, and S. O'Brien, "Development of the Magma Combustion System - A High Compression Ratio Miller Cycle Engine," in *JSAE Annual Congress 2016*, 2016.

[148] R. Osborne, T. Downes, S. O'Brien, K. Pendlebury, and M. Christie, "A Miller Cycle Engine without Compromise - The Magma Concept," *SAE Int. J. Engines*, vol. 10, p. 846–857 (2017–01–0642), 2017.

[149] R. Osborne, K. Pendlebury, T. Downes, and S. O'Brien, "A Miller cycle engine without compromise -- The Magma concept," in *17. Internationales Stuttgarter Symposium: Automobil- und Motorentechnik*, M. Bargende, H.-C. Reuss, and J. Wiedemann, Eds. Wiesbaden: Springer Fachmedien Wiesbaden, 2017, pp. 1507–1529.

[150] F. Söderberg and B. Johansson, "Fluid Flow, Combustion and Efficiency with Early or Late Inlet Valve Closing," in *SAE Technical Paper*, 1997, p. 972937.

[151] C. Wu, P. V. Puzinauskas, and J. S. Tsai, "Performance analysis and optimization of a supercharged Miller cycle Otto engine," *Appl. Therm. Eng.*, vol. 23, no. 5, pp. 511–521, Apr. 2003.

[152] B. Ribeiro, J. Martins, and N. Kothari, "Otto and VCR Miller Engine Performance during the European Driving Cycle," in *SAE Technical Paper*, 2006, pp. 2006-01–0440.

[153] B. Ribeiro and J. Martins, "Direct Comparison of an Engine Working under Otto, Miller and Diesel Cycles: Thermodynamic Analysis and Real Engine Performance," in *SAE Technical Paper*, 2007, pp. 2007-01–0261.

[154] P. A. Stansfield *et al.*, "Unthrottled Engine Operation using Variable Valve Actuation: The Impact on the Flow Field, Mixing and Combustion," in *SAE Technical Paper*, 2007, pp. 2007-01–1414.

[155] R. Patel *et al.*, "Comparison between Unthrottled, Single and Two-valve Induction Strategies Utilising Direct Gasoline Injection: Emissions, Heat-release and Fuel Consumption Analysis," in *SAE Technical Paper*, 2008, pp. 2008-01–1626.

[156] R. Patel *et al.*, "Un-throttling a direct injection gasoline homogeneous mixture

engine with variable valve actuation," *Int. J. Engine Res.*, vol. 11, no. 6, pp. 391–411, 2010.

[157] L. Miklanek, O. Vitek, O. Gotfryd, and V. Klir, "Study of Unconventional Cycles (Atkinson and Miller) with Mixture Heating as a Means for the Fuel Economy Improvement of a Throttled SI Engine at Part Load," *SAE Int. J. Engines*, vol. 5, p. 1624–1636 (2012–01–1678), 2012.

[158] Y. Li *et al.*, "Exhaust Gas Recirculation, Late Intake Valve Closure and High Compression Ratio for Fuel Economy Improvement in a MPI Gasoline Engine," in *SAE Technical Paper*, 2014, pp. 2014-01–1197.

[159] M. E. S. Martins and T. D. M. Lanzanova, "Full-load Miller cycle with ethanol and EGR: Potential benefits and challenges," *Appl. Therm. Eng.*, vol. 90, pp. 274–285, Nov. 2015.

[160] C. Schenk and P. Dekraker, "Potential Fuel Economy Improvements from the Implementation of cEGR and CDA on an Atkinson Cycle Engine," in *SAE Technical Paper*, 2017, pp. 2017-01–1016.

[161] D. Hancock, N. Fraser, M. Jeremy, R. Sykes, and H. Blaxill, "A New 3 Cylinder 1.2l Advanced Downsizing Technology Demonstrator Engine," in *SAE Technical Paper*, 2008, pp. 2008-01–0611.

[162] G. Lumsden, D. OudeNijeweme, N. Fraser, and H. Blaxill, "Development of a Turbocharged Direct Injection Downsizing Demonstrator Engine," *SAE Int. J. Engines*, vol. 2, p. 1420–1432 (2009–01–1503), 2009.

[163] Y. Zhang, "Experimental investigation of CAI combustion in a two-stroke poppet valve DI engine," Brunel University London, 2014.

[164] H. Zhao and N. Ladommatos, *Engine Combustion Instrumentation and Diagnostics*. SAE International, 2001.

[165] A. L. Randolph, "Methods of Processing Cylinder-Pressure Transducer Signals to Maximize Data Accuracy," in *SAE Technical Paper*, 1990, p. 900170.

Appendix

A.1 Fuel Flow Meter Validation

The Coriolis mass flow meter used in engine tests was calibrated by the manufacturer before delivery. The calibration was validated in a university laboratory by using an accurate scale before the flow meter was integrated into testbed system. In these validations, fuel flowed through the flow meter into a container whose dry weight was measured prior to each test. The container was sealed immediately after the fuel flow was cut-off and then weighted on the laboratory scale. The fuel mass in the container weighted by the scale was compared to the flow meter reading. The results were shown in the below table. The differences between two devices were 0.77~0.87%. The actual differences could be less than these values considering the loss of gasoline via evaporating while flowing into the container.

Table A.1 Flow Meter Measurement Compared to the Laboratory Scale

Round	Weight by Lab Scale (g)	Weight by Flow Meter (g)	Difference between Scale and Meter (%)
1	112.796	113.689	-0.79
2	93.690	94.515	-0.87
3	67.405	67.926	-0.77

The following figure shows the check on linearity of the flow meter measurement. The horizontal axis is current output signal from flow meter. Red dots are the measured mass fuel flow readings. The volume fuel flow was recorded through a burette installed in the fuel delivery loop, and then another mass fuel flow was calculated by using a fuel density value provided by the Coriolis flow meter, which are the green dots / line in the figure. These two curves did not perfectly match each other due to the tolerance of volume flow measurement by using burette, however both curves indicate a good linearity of measurement.

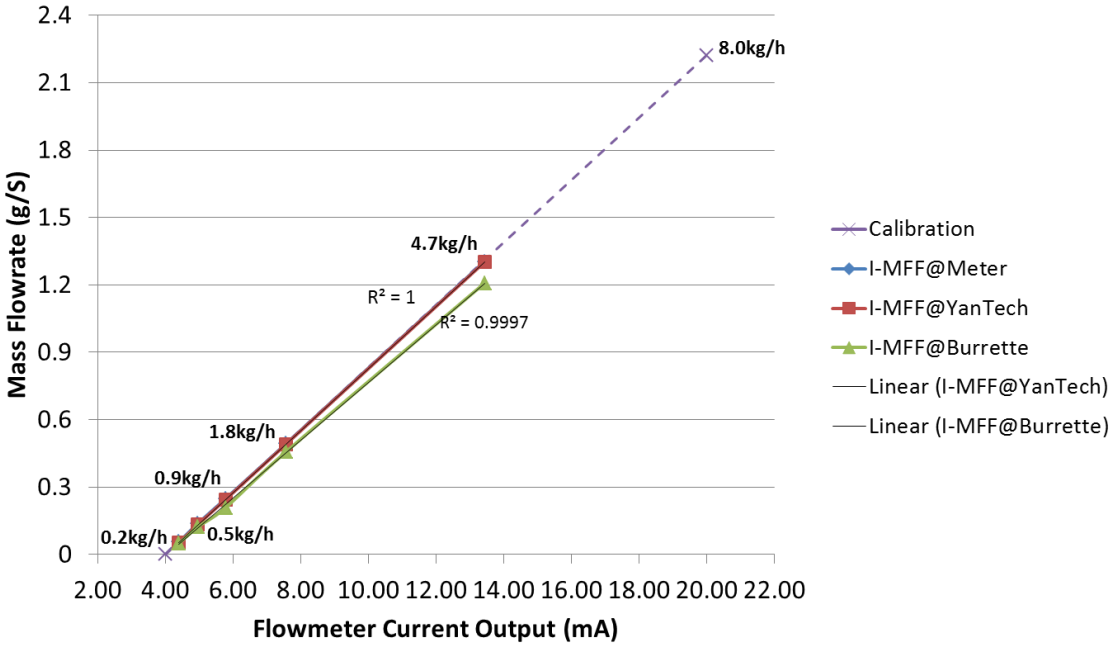

Figure A.1 Flow Meter Measurement Linearity Check